ABSTRACT

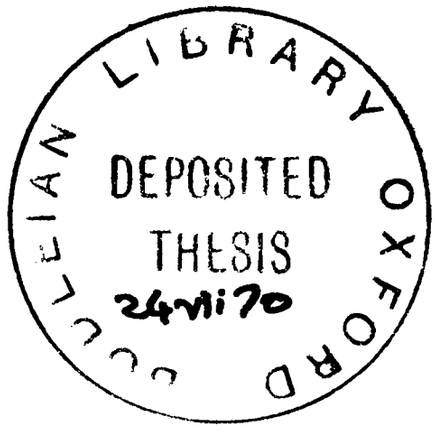
of

THESIS SUBMITTED FOR THE DEGREE OF DOCTOR

OF PHILOSOPHY IN THE UNIVERSITY OF OXFORD

SOME INVESTIGATIONS USING ATOMIC BEAMS

M.A. Player



Balliol College
Oxford

Trinity Term
1970

Clarendon Laboratory
Oxford

Abstract

We describe an atomic beam resonance experiment to search for an electric dipole moment in the $^3P_2$ metastable state in xenon. The experiment avoids the "$\underline{v} \times \underline{E}$" difficulty of earlier work by using an atomic state which has a high differential polarizability. Small residual effects of order five times greater than the experimental precision are cancelled by comparison between xenon and krypton. We obtain a null result for the electron edm.

We also present atomic beam resonance measurements of the differential Stark splittings in the $^3S_1$ metastable state of helium and the $^3P_2$ metastable states of the rare gases, together with a theoretical result for helium.

It is well known (see e.g. Schweber 1961) that the most general single-particle relativistic wave equation for a spin $\frac{1}{2}$ particle has, under certain general assumptions, only three types of terms in addition to those included in the Dirac equation. The lowest order terms represent an intrinsic Darwin interaction, an intrinsic or "anomalous" magnetic moment, and an intrinsic electric dipole moment (edm). There is particular interest in the search for an edm interaction because, as is well known, its existence would imply both P and T violation (Lee and Yang, 1957). So far the only clear evidence of T noninvariance appears from the CP forbidden decay of the long-lived K^o meson (Christenson et al., 1964), from which T violation may be deduced indirectly by the CPT theorem or directly, from a study of the phases involved (Casella, 1968, 1969).

It was first pointed out by Sandars (1964) that the edm of the neutral cesium atom should be of order 100 times greater than the electron edm and that therefore atomic beam resonance experiments using cesium or a similar heavy, highly polarizable, element should yield very precise data on the electron edm. This result relies on the relativistic nature of the atoms and so does not contradict the theorem of Schiff (1963). Many experiments of this type have been performed, but difficulty has been encountered from the motional magnetic field $\underline{B}^m = \underline{v} \times \underline{E}/c$ seen in the rest frame of the atoms as they move through an electric field $\underline{E}$ applied in the laboratory (Sandars and Lipworth, 1964). Unless the applied $\underline{E}$ and $\underline{B}$ fields are exactly parallel, $\underline{B}^m$ will have a component along $\underline{B}$ which will give rise to a shift linear in $\underline{E}$; this mimics an edm of magnitude $\simeq 3 \times 10^{-17}$ cm, which is very much greater than the limit of precision of the atomic beam experiments. Shapiro (1968) has reviewed the methods used to eliminate the "$\underline{v} \times \underline{E}$" effect. The most successful (Weisskopf et al., 1968) involves a comparison between the apparent dipole moments in Na and Cs as a function of the angle between $\underline{B}$ and $\underline{E}$; the results of this experiment have been

interpreted to set a 90% confidence limit on the edm of the free electron:

$$| d_{electron} | < 3 \times 10^{-24} \text{ e x cm}$$

It would appear to be extremely difficult to improve on this value by similar techniques.

Following a suggestion by Sandars (Player and Sandars 1966) we have avoided the "$\underline{v} \times \underline{E}$" effect by using an atomic state of high differential polarizability; this ensures that $\underline{B}^m$ is automatically perpendicular to the axis of quantisation, which is now essentially determined by $\underline{E}$, so that $\underline{B}^m$ cannot contribute to level splittings in lowest order. We have chosen to work with xenon in the $^3P_2$ metastable state; this has a high dipole enhancement factor (closely similar to that of cesium), and an adequate differential polarizability, but is unfortunately less suitable for high precision atomic beam work than cesium. Nonetheless, it seems to represent the best available compromise in fulfilling all requirements.

To avoid difficulty with the strong electric field dependence of transitions which change $| M_J |$, we have used the $M_J = +1 \rightarrow M_J = -1$ transition, excited by two-quantum magnetic resonance. The experiment consists of observing this resonance in parallel electric and magnetic fields, and looking for a change in transition frequency on reversal of the electric field.

We have constructed an effective Hamiltonian for the $| M_J | = 1$ sublevel in high electric field, and have used it to show that the higher order residual effects of $\underline{B}^m$ are of order 10^{-3} Hz at our working values of electric and magnetic fields. This is about four orders of magnitude smaller than the effect in the cesium ground state for the same misalignment of $\underline{B}$ and $\underline{E}$. We also use our Hamiltonian to give a simple discussion of the $M_J = +1 \rightarrow -1$ two-quantum transition. The method of treatment is in a sense complementary to that of Salwen (1955), and allows us to predict the approximate size of resonance

shifts dependent on the fourth power of the r.f. amplitude; these were not treated by Salwen.

The atomic beam apparatus used in this work was designed and built specifically for the edm experiment. In general, any atomic beam apparatus may be considered as a device for observing atomic transitions by use of a state selecting polariser and analyser relying on atomic deflections. Our apparatus uses this principle in a straightforward form. The atoms are excited to the metastable state in a discharge resembling a Heil ion source (Heil 1944) but working in a strong pressure gradient to improve extraction efficiency for the metastables. On leaving the source, the beam enters a standard 2-pole deflecting magnet A which removes from the beam all atoms with $M_J \neq 0$. The selected $M_J = 0$ atoms enter a region A′ of crossed electric and magnetic fields where they pass adiabatically and with 100% transition probability to the $M_J = +1$ state in high electric field. The A and A′ regions constitute the polariser. The beam next enters the resonance region where the $M_J = +1 \longrightarrow -1$ transition is excited in high electric field with parallel magnetic field. The Ramsey two-loop system (Ramsey 1956) is used, with a 1.2 m separation between the loops, which are wound round the electric field plates. The magnetic field is supplied by an analog of a 2-dimensional Helmholtz coil, with shimming, and the region is screened by a double mumetal shield. The analyser consists of a second deflecting magnet and a stop, so adjusted that only atoms with $M_J = +1$ are deflected to miss the stop and reach the detector surface. The detection is by Auger emission from a continuously sprayed alkali metal surface.

This set-up gives relative freedom from background from photons produced in the source, and, because the detected beam is deflected only after its passage through the electric field plates, optimum use can be made of the solid angle subtended at the source by the exit aperture of the field plates. The two-quantum resonance full width at half height in xenon is 80 ± 10 Hz, and the size is about

7×10^5 counts/sec.on a background of 5×10^5 counts/sec.

The basic technique for the observation of small shifts in resonance frequency is to set the radio frequency to the point of greatest slope on the resonance and look for changes in signal intensity. To avoid as many spurious effects as possible, to obtain the best signal to noise, and to enable calibration and locking of resonance drift to be performed at the same time as data collection, we have used digital techniques and have extended and adapted the multi-channel orthogonal square-wave analysis method of Angel (1967) for use with a PDP-8 computer. In this method, as many parameters of the experimental system as possible are switched in a complicated but cyclic fashion, and the desired components of the system response are extracted by the computer. We have controlled the electric and magnetic field directions, the sign of the resonance slope (by modulating the phase of the second r.f. loop) and have applied a calibration signal at the same time.

We have attempted to analyse the response of the analysis system to random but non-white noise, and find the waveform structure to be relatively unimportant; the basic period of the waveforms is important, and generally (though not always) greater speed gives greater freedom from noise, as with an ordinary phase-sensitive detector. Complexity in the waveforms guards against spurious shifts due to drifts (Harrison 1969) and transient effects.

Using these methods, we have observed and analysed or eliminated a number of spurious edm-like effects (none as serious as uncancelled "$\underline{v} \times \underline{E}$"). We have observed the expected behaviour of the residual "$\underline{v} \times \underline{E}$" effect, shown power shifts and other voltage dependent effects to be negligible at our normal working fields, and observed an effect due to slight rotation of electric field direction on reversal; of other shifts, the most important and least clearly defined seem to be certain magnetic field modulation effects.

We have taken edm data in the presence of a so far untraced dipole-like

shift of order 2 to 3 times 10^{-2} Hz; this fluctuates and reverses sign in an apparently random manner. Despite this effect we obtain a null result for the edm of the xenon atom:

$$| d_{Xe} | = (0.4 \pm 4.3) \times 10^{-22} \text{ e x cm.}$$

A more precise null result has been obtained by comparing the shift observed in Xe with that observed in Kr; this seems to cancel the residual effects, but it should not cancel any true edm effect since the edm enhancement factor in Kr is only of order 20. We get

$$| d_{Xe} - d_{Kr} | = (0.7 \pm 2.2) \times 10^{-22} \text{ e x cm}$$

We interpret this in terms of the electron edm:

$$| d_{electron} | = (0.7 \pm 2.2) \times 10^{-24} \text{ e x cm}$$

which confirms the result of Weisskopf et al. (1968). All these results are at 90% confidence limit.

The precision of these latter values is 2 to 3 times poorer than the ideal shot noise value, probably as a result of magnetic field noise caused by vibration. Since taking the above data, we have been able to observe strong peaks in the noise power spectrum of the beam intensity between 10 and 20 Hz.

Angel and Sandars (1968) have introduced a theoretical description of the quadratic Stark effect in atoms which is particularly suited to the treatment of differential effects within levels. One of the most interesting predictions of the theory is that relativistic effects produce a small quadratic splitting of the magnetic substates of the $^3S_1$ metastable state of He^4; any such splitting must be zero for an $L = 0$ state in pure LS coupling. It has been stated by Sandars (1966) that to order v^2/c^2 the only contribution to the splitting arises from the magnetic spin-spin interaction between the two electrons; Sandars has also given an approximate semi-empirical calculation of the size of the splitting. There is considerable interest in an accurate comparison between theory and experiment at this point because the effect gives a new method for investigating the two electron relativistic interaction.

In part II of this thesis we give an explicit derivation of the results of Angel and Sandars for this case using diagrammatic angular momentum techniques (see e.g. Brink and Satchler 1969), and calculate approximate corrections to the semi-empirical result of Sandars (1966) using third order perturbation theory and hydrogenic wavefunctions. Our final result agrees to within its accuracy with the more accurate value of Drake (1970) although there is an as yet untraced discrepancy in some intermediate quantities.

We have performed an atomic beam resonance measurement of the helium differential polarizability using the apparatus described above. The precision is limited to about 5% by uncertainty in the electric field. Our result

$$\alpha_t = +(3.38 \pm 0.13) \times 10^{-3} \text{ a.u.}$$

is in excellent agreement with that of Ramsey and Petrasso (1969) and with the theoretical value. We note that our apparatus is free of "filling factor" and end effects. We have studied other possible sources of error, including resonance distortions of the $M_J = 0 \rightarrow +1$ transition by the neighbouring $M_J = 0 \rightarrow -1$ transition (Ramsey, 1959), and conclude that the method may be extended to give

a precision of 1 part in 10^4.

We give also experimental results for the differential polarizabilities of the $^3P_2$ metastable states of the rare gases, obtained in both high and low electric fields. These results agree with the deflection measurements of Robinson et al. (1966) to within the accuracy of the latter.

Angel J.R.P. (1967) Thesis, Oxford University.

Angel J.R.P. and Sandars P.G.H. (1968) Proc.Phys.Soc. A305 , 125.

Brink D.M. and Satchler G.R. (1969) "Angular Momentum" (2nd ed.) O.U.P.

Casella R.C. (1968) Phys.Rev.Lett. 21, 1128.

Casella R.C. (1969) Phys.Rev.Lett. 22, 554.

Christenson J.H., Cronin J.W., Fitch V.L. and Turlay, R. (1964) Phys.Rev. Lett. 13, 138.

Drake G.W.F. (1970) Phys.Rev.Lett. 24, 765.

Harrison G.E. (1969) Thesis, Oxford University.

Heil H. (1944) Z.Phys. 120, 212.

Lee T.D. and Yang C.N. (1957) Brookhaven report BNL443 (T91)

Player M.A. and Sandars P.G.H. (1966) Clarendon Laboratory report (unpublished).

Ramsey A.T. and Petrasso R. (1969) Phys.Rev.Lett. 23, 1478

Ramsey N.F. (1956) "Molecular Beams" O.U.P.

Ramsey N.F. (1959) in "Recent Research in Molecular Beams" ed. I. Estermann, Academic Press.

Robinson E.J., Levine J. and Bederson B. (1966) Phys.Rev. 146, 95.

Salwen H. (1955) Phys.Rev. 99, 1274.

Sandars P.G.H. (1966) Clarendon Laboratory report.

Sandars P.G.H. and Lipworth E. (1964) Phys.Rev. Lett. 13, 718.

Schiff L.I. (1963) Phys.Rev. 132, 2194.

Schweber S.S. (1961) "An Introduction to Relativistic Quantum Field Theory" Row, Peterson and Co.

Shapiro F.L. (1968) Sov.Phys.Uspekhi 11, 345.

Weisskopf M.C., Carrico J.P., Gould H., Lipworth E., and Stein T.S. (1968) Phys.Rev.Lett. 21, 1645.

THESIS SUBMITTED FOR THE DEGREE OF DOCTOR

OF PHILOSOPHY IN THE UNIVERSITY OF OXFORD

SOME INVESTIGATIONS USING ATOMIC BEAMS

M.A. Player

Balliol College
Oxford

Trinity Term
1970

Clarendon Laboratory
Oxford

Acknowledgements

The author wishes to express his gratitude to the following people:

Professor B. Bleaney for providing the facilities of the Clarendon Laboratory.

The Science Research Council for financial support during most of the work.

Dr. G.E. Harrison and Dr. G.K. Woodgate for many helpful discussions.

The staff of the Clarendon Laboratory for technical assistance, and especially Mr. C. Sanders for much help in designing and building electronics.

Mr. M.A. Sheen for assistance in early design stages and for many helpful discussions.

Finally, to his supervisor Dr. P.G.H. Sandars for constant help and encouragement throughout the work.

Contents

General introduction		1
Part I	Electric dipole moment of $^3P_2$ state of Xe	2
Chapter 1.	Introduction	2
1.1	The purpose of the experiment	2
1.2	The atomic beam resonance method	7
1.3	Choice of system	10
Chapter 2.	Spectroscopy of the $^3P_2$ levels of the rare gases	13
Part I	General	13
2.1	The metastability of the levels	13
2.2	Effect of electric and magnetic fields	15
a)	General	15
b)	High electric field	17
c)	Low electric field	19
2.3	The "$\underline{v} \times \underline{E}$" effect	23
2.4	Effect of electric dipole moment	25
2.5	The odd isotopes of xenon	27
Part II	Magnetic resonance in high electric field	28
2.6	General formalism	28
2.7	Results	29
Chapter 3.	The atomic beam apparatus	34
3.1	General scheme	34
3.2	General mechanical details	38
3.3	The source	41
3.4	The deflectors	48
3.5	The A transition region	51

3.6	The resonance region	56
a)	The electric field system	56
b)	Radio frequency loops	57
c)	The magnetic field system	57
3.7	The detector	63
3.8	Summary of performance	69
Chapter 4.	Techniques of data collection	70
Part I	Basic method	70
4.1	Detection of small resonance shifts	70
4.2	A simple data analysis system	73
4.3	Method of orthogonal waveforms	76
4.4	Practical system	82
Part II	Computer hardware and instrumentation	84
4.5	The PDP-8 computer	84
4.6	Interfacing	89
4.7	The electric field system	92
4.8	The pulse counting system	98
4.9	C-field and r.f. system	101
Part III	Computer programming	104
4.10	Introduction	104
4.11	The "Updown counter" program	114
Chapter 5.	Spurious effects	119
5.1	The "$\underline{v} \times \underline{E}$" effect	124
5.2	Power shifts and other voltage magnitude dependent effects	127
5.3	Magnetic field effects	134
a)	Field magnitude effects	134
b)	Alignment effect	140

5.4 Other effects 143

Chapter 6. Experimental results 147

6.1 Procedure for experimental runs 147

6.2 Preliminary measurements 150

6.3 Runs without magnetic field reversal 158

6.4 Runs with magnetic field reversal 163

6.5 Analysis of results 165

6.6 Further discussion 170

Part II Quadratic Stark effects in the metastable states of He and the rare gases 172

Chapter 7. Introduction 172

7.1 Helium 172

7.2 The rare gases 174

Chapter 8. Theoretical treatment for He 175

8.1 Symmetry arguments 175

8.2 Perturbation treatment 177

a) The dominant term 179

b) The P contributions 181

c) The D contributions 185

8.3 Result and discussion 191

Chapter 9. Experimental results 193

9.1 Introduction and experimental method 193

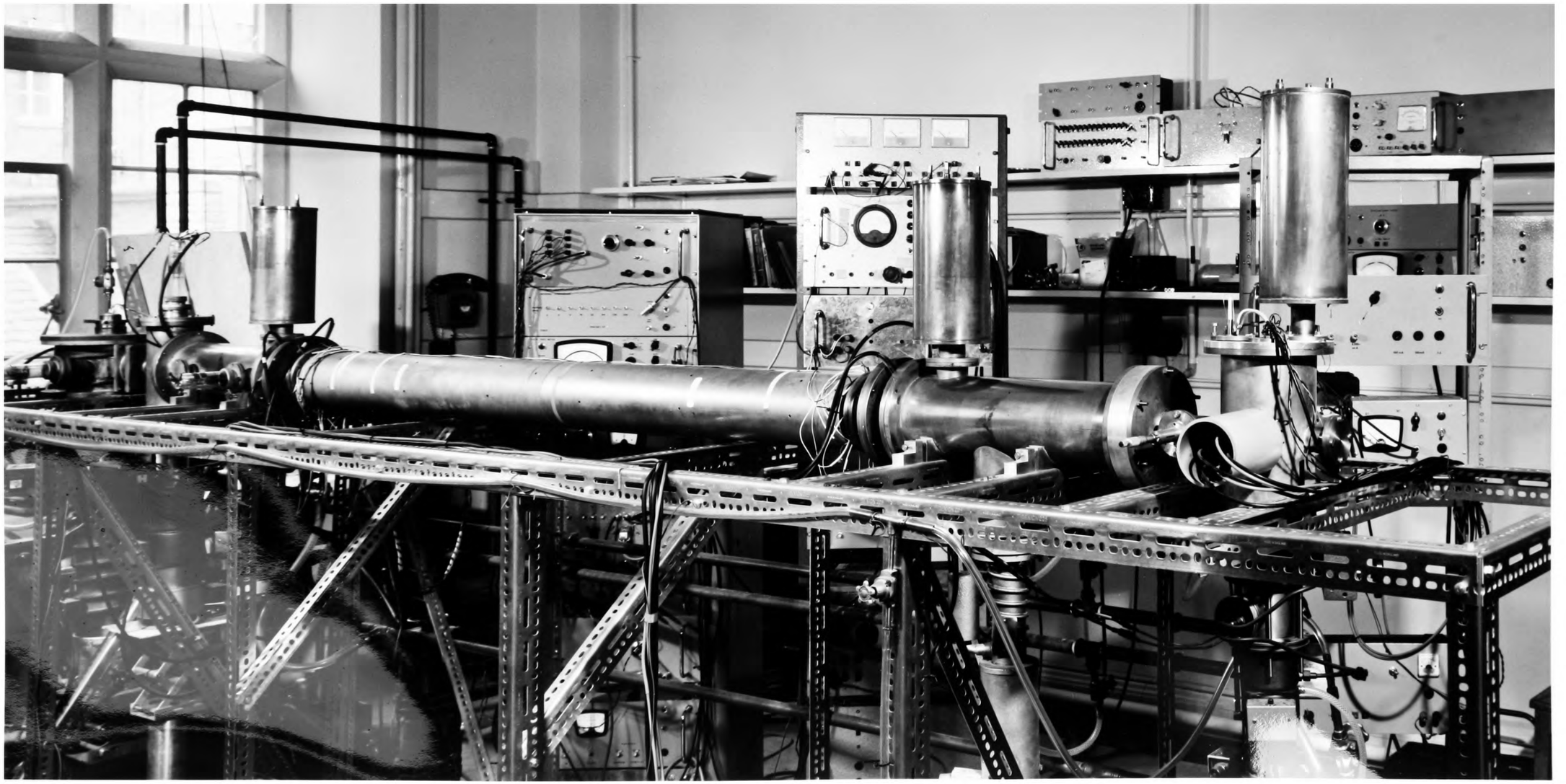
9.2 Sources of error 195

9.3 Helium 199

9.4 The rare gases 205

9.5 Future work 206

Appendix A.	Effective Hamiltonians	208
Appendix B.	Stark shift symmetry properties	215
Appendix C.	Time reversal, spectra, and electric dipole moments	220
Appendix D.	Assorted electronics	225
Appendix E.	"Updown counter" program	237
Bibliography		248



General Introduction

This thesis is divided into two parts. In part I we describe a new atomic beam resonance experiment to search for an electric dipole moment in the $^3P_2$ metastable state of xenon. In part II we describe measurements of the differential polarizabilities of the $^3S_1$ metastable state of helium, and of the $^3P_2$ metastable states of the rare gases, using the apparatus designed for the electric dipole experiment. The work represents a logical extension of past work of this group, which has for some time been concerned with electric field effects in atoms, and in particular electric dipole moment searches, using the atomic beam technique. In the thesis we describe the construction of the new machine and an extension of our data collection techniques to a new level of sophistication. We also have time for a little physics.

Part I. Electric dipole moment of $^3P_2$ state of Xe

Chapter I. Introduction

The purpose of this experiment is to search for an intrinsic electric dipole moment (edm) of the electron. We give first some reasons for undertaking such a search.

The dominant interaction between an electron and the electromagnetic field is described by the Dirac equation, which of course contains no edm term. Interactions over and above those included in the Dirac equation may be treated by a phenomenological approach without the full apparatus of quantum field theory. Foldy (1952; see also Schweber 1961) has considered the possible forms of interactions which are Lorentz covariant, gauge invariant, linear in the external fields, non-vanishing at zero momentum, and expressible in a multipole type expansion. He finds for the most general extension to the Dirac equation under these conditions:

$$[\gamma_\mu p_\mu - imc]u - \frac{1}{c}\sum_{n=0}^{\infty}\left[\epsilon_n \Box^n \gamma_\mu A_\mu + \frac{1}{2}\mu_n \Box^n \gamma_\mu \gamma_\nu F_{\mu\nu}\right] u = 0$$

The ϵ_n and μ_n are constants. The term in ϵ_0 is just the original Dirac interaction. The term in μ_0 represents the "anomalous" or "intrinsic" magnetic moment of the electron, and the term in ϵ_1 represents an intrinsic Darwin term. The effects are of course treated more fundamentally by quantum electrodynamics. The equation still shows no edm term.

The interactions considered by Foldy maintain covariance under all Lorentz transformations. If we only demand covariance under proper Lorentz transformations, a new series of interaction terms is allowed. The lowest (n = 0) member of this series has been given by Salpeter (1958) who writes as an addition to the Dirac Hamiltonian

$$H' = -\frac{1}{2c}\,\mu_0'\,\gamma_5\,\gamma_\mu\,\gamma_\nu\,F_{\mu\nu}$$

Schweber (1961), using a Langrangian formalism with quantised fields, has shown that this is the only n = 0 term introduced by the relaxed symmetry requirement; in particular the obvious contender

$$H' = -\frac{1}{c}\,\epsilon_0'\,\gamma_\mu\,\gamma_5\,A_\mu$$

does not maintain gauge invariance.

The term written by Salpeter represents an intrinsic dipole interaction. Its inclusion in the theory implies that both spatial inversion (P) and time reversal (T) are no longer valid symmetry operations.

This is a special case of the well known result that any edm in a non-degenerate system must be zero if either P or T is a valid symmetry. This basic theorem was first proved by Lee and Yang (1957), and has been extended by Sandars (1968); we give a variant of this treatment in appendix C. Much of the interest in the search for an electron edm centres on the connection with invariance properties, and we give now a brief description of the present state of knowledge on the discrete "symmetries" P, T and C (charge conjugation).

It is well known that P, T and C are related through the CPT theorem, which states that the combined operation CPT represents a symmetry even if the individual operations P, C, T do not. The theorem can be proved in any local, Lorentz covariant field theory constructed under very general rules (see e.g. Streater and Wightman, 1964) and also appears in S-matrix theory as a consequence of causality and Lorentz covariance (see e.g. Barut 1967). It is thus well woven into the structure of contemporary theory. However, the CPT theorem is the only strong theoretical assertion which can be made about C, P and T; there is no basic theoretical indication as to the status of each individually as a symmetry.

In 1957 Wu et al. showed experimentally that P is not a symmetry for the weak interaction; in fact P-violating and P-conserving processes are equally allowed by the weak interaction. In 1964 Christenson et al. observed apparent CP violation in the decays of long-lived K°-mesons; in contrast to the situation in P violation, this was a weak effect with "forbidden' decays occurring about 10^{-3} times less frequently than corresponding "allowed" decays. Further experiments and careful examination of possible explanations seem to confirm the original interpretation of CP violation with relatively small amplitude (see Kabir, 1968). So far, despite fairly intensive experimental activity, no clear cases of CP violation have been observed in any other system.

Large numbers of theoretical models for the origin of the CP violating interaction have been constructed (see e.g. Okun', 1967). Although some have been eliminated by experimental observations, a large amount of uncertainty remains. It is still not possible to say whether the breakdown occurs in electromagnetic, weak or some other interaction.

The breakdown of T symmetry is implied by CP violation through the CPT theorem. Also, Casella (1968, 1969) has shown that the K°data can be interpreted to give direct evidence of T violation without assuming the CPT theorem. There is no other definite evidence of T violation.

We now consider the likely size of an electron edm. Few of the theoretical models for CP violation directly involve leptonic interactions, so that there is a relative scarcity of firm predictions of the size of the electron edm. However, order of magnitude predictions are readily made.

The basic length involved is the electron Compton wavelength

$$\lambda_c = 3.8 \times 10^{-11} \text{ cm.}$$

With complete P and T violation in the electromagnetic interactions, we therefore expect an electron edm

$$d_e \simeq 10^{-11} \text{ e x cm.}$$

(the number represents the effective separation of positive and negative electronic charges, in centimetres).

With complete violation of P and T in the weak interactions, we introduce the weak coupling constant G, for which it is known that:

$$G m_p^2 \simeq 10^{-5}, \text{ or } G m_e^2 \simeq 10^{-11} \quad .$$

This gives

$$d_e \simeq 10^{-22} \text{ e x cm.}$$

The theory of Salzman and Salzman (1965), which attributes an intrinsic edm to the intermediate W boson, predicts essentially this value, supressed by one or two orders of magnitude.

The "milliweak" theories invoke a CP violating component of the weak interactions of order 10^{-3} times weaker than the CP conserving component. This implies

$$d_e \simeq 10^{-25} \text{ e x cm.}$$

This is the region of the experimental limit at the present time. Below this lie the predictions of models involving second order weak interactions and the "superweak" interactions (Hiida, 1965; Bég, 1969). A number of the more detailed models suggest that the CP violating interactions are limited to the hadrons, and they therefore predict a vanishing electron edm. This is the case with the theory of Lee et al. (1965), who take a total breakdown of C and T symmetry in the electromagnetic interactions of the hadrons as the source of CP violation.

This survey illustrates the potential importance of the discovery of an edm on the electron. On the other hand, it is clear that the non-observation

of an edm does relatively little to differentiate between theories. However, a non-observation may be viewed in a more positive light if it is accepted as a quantitative statement about the electron. From the point of view of the phenomenological theories presented at the beginning of this section, our measurement provides information about the one set of terms whose lowest member has not so far been observed. If the terms are absent, the structure of the theory is simpler. This is not an unwelcome state of affairs and it means that at least on one level the electron remains well understood - the only massive particle to be so.

1.2 The atomic beam resonance method

It is clearly easier to search for an edm in an electrically neutral system than in a charged system. It is therefore desirable to seek an atomic edm induced by an electron edm, rather than attempting direct observation of the electron edm.

However, Schiff (1963) has given a theorem which may be interpreted to show that in a non-relativistic theory an atom will not have an edm even if the electron has one. This result may be viewed as a consequence of the requirement that the average force on any atomic electron must be zero to maintain dynamic equilibrium; in a non-relativistic theory, this implies that the average value of electric field at any electron must be zero, so that there can be no interaction with an electronic edm. Happily, the situation is very different in a relativistic system; Sandars (1965, 1966a) has shown that for cesium, where the s-electron is highly relativistic, the atomic edm is actually of order 100 times greater than the electronic edm. This arises because the electrons are subject to magnetic as well as electrostatic forces so that the average electric field at the electron need not be zero. The enhancement factor has been confirmed by Foley (1969) and Sternheimer (1969), and by Ignatovich (1968), who also discusses the origin of the enhancement in detail. It is this enhancement factor which really makes electron edm experiments worthwhile.

Thus a search for an electron edm requires a technique for high precision spectroscopy on atoms in a high electric field. Because the frequency shifts sought are small, it is extremely important to avoid spurious systematic effects. These requirements are rather well met by the atomic beam resonance method, which provides a technique for high precision r.f. spectroscopy using essentially free atoms. In general, an atomic beam resonance apparatus consists of a source and detector of atoms, a state selecting polariser and analyser, and the

resonance region. The polariser and analyser almost always utilise magnetic deflection of the atoms. Because the atoms must traverse a flight path of several metres at thermal velocities, they must be in a metastable state or the ground state. The technique achieves its sensitivity because transitions are detected not by the absorption of r.f. power but by changes in beam flux at the detector. The precision of the method is determined by the particle counting statistics and by the resonance linewidth. Because relaxation is negligible, the linewidth is determined by the time spent by each atom under the influence of the r.f. field; this is determined by the length of the resonance region.

The setup in the resonance region required for the observation of an edm is as follows. All degeneracies in the atomic level concerned are raised by a magnetic field. The electric field is applied parallel to the magnetic field, and one looks for a shift in some resonance frequency on reversing the relative direction of electric and magnetic field. Any such shift must be zero in the absence of T and P violating effects (appendix C). In the presence of a permanent edm $\underline{D}$ directed along the atomic angular momentum, the shift of an energy level is

$$\delta W^{edm} = -\underline{D} \cdot \underline{E} .$$

To take the case with which we shall be concerned, if $\underline{E}$ is along the axis of quantisation and if there is no nuclear spin, we may use the Wigner-Eckart theorem to write for the relative edm shift between states JM_J and JM_J' :

$$\delta W^{edm}_{M_J} - \delta W^{edm}_{M_J'} = d_A(J) \frac{M_J - M_J'}{J} E$$

which reverses sign with $\underline{E}$ (or $\underline{B}$). This defines the atomic dipole moment, $d_A(J)$.

With present apparatus, shifts in resonance frequency down to 10^{-3} Hz can

be detected. The highest electric field which may conveniently be applied in vacuo is about 10^5 V/cm; using the above formula this implies that an atomic edm of order 10^{-22} e x cm, or an electronic edm of 10^{-24} e x cm, should be observable.

1.3 Choice of system

We now have to consider the choice of a suitable atomic state for use in an edm experiment. The first requirement is that the atom should have a high edm enhancement factor; this implies that it should have a large Z and also be highly polarizable (Sandars 1965, 1966). Most experiments up to the present have used cesium, in which these requirements are well satisfied. The cesium ground state has a low differential Stark effect, so that it is relatively easy to discriminate against quadratic electric field effects. It is easy to obtain high intensity cesium beams. However, the use of cesium suffers from a major difficulty: the "$\underline{v} \times \underline{E}$ effect" (Sandars and Lipworth 1964, Carrico et al. 1968). This arises from the motional magnetic field $\underline{B}^m = \underline{v} \times \underline{E}/c$ seen in the rest frame of the beam atoms as they move with velocity $\underline{v}$ through an electric field $\underline{E}$ applied in the laboratory frame. If the static magnetic field $\underline{B}$ is not exactly parallel to $\underline{E}$, $\underline{B}^m$ will have a component along $\underline{B}$, and this will lead to a Zeeman shift linear in $\underline{E}$. The effect therefore mimics an edm of magnitude

$$\theta \, \mu_0 \, v/c \simeq \theta \times 10^{-16} \text{ e x cm}$$

where θ is the (small) angle of misalignment between $\underline{E}$ and $\underline{B}$.

Because this shift is potentially so much larger than the limit of resolution of atomic beam experiments, elaborate cancellation procedures are necessary. A survey of the methods which have been used has been given by Shapiro (1968). The most successful is that of Lipworth and collaborators (Weisskopf et al., 1968) which involves plotting the apparent edm's of sodium and cesium as functions of θ, whose absolute value is unknown. In the absence of true edm's, the observed edm for both elements should vanish at the same value of θ. True edm's should be very different in sodium and cesium, and would be indicated by a difference in null angles for the two elements. No such difference has been observed, and a limit on the electron edm has been deduced:

$$|d_e| < 3 \times 10^{-24} \text{ e x cm.}$$

This procedure involves cancelling the $\underline{v} \times \underline{E}$ shift to a part in a million or so, and its extension to higher precisions appears to be very difficult. In this thesis we describe a technique which avoids the $\underline{v} \times \underline{E}$ effect. We have used an atomic state with a high differential Stark effect, so that in the resonance region the level splitting due to the electric field is much greater than that due to the magnetic field. Under these conditions the axis of quantisation is essentially determined by the direction of the electric field; the $\underline{v} \times \underline{E}/c$ field is automatically perpendicular to this, and its effect must vanish in first order. In a suitable atom, higher order effects can be made negligibly small (see chap. 2).

The choice of a suitable atom is therefore restricted by three conditions:

1) the atom must have a high edm enhancement factor.

2) the differential polarizability must be high.

3) the atom must be suitable for high intensity beam work.

The best compromise we have found is xenon in the $^3P_2$ state. Conditions 1) and 2) are well satisfied (see chap. 2); unfortunately condition 3) is less well satisfied.

In principle, as indicated in the last section, the edm could be found by looking for a shift of any resonance frequency on reversal of the electric field. In practice, transitions which change $|M_J|$ are unsuitable because of the high dependence of the resonance frequency on the magnitude of the electric field; this leads to inhomogeneous broadening of the resonance lines unless extreme care is taken, and also to spurious edm effects unless the electric field is reversed with enormous accuracy. It is therefore necessary to use a transition which keeps $|M_J|$ constant, when there is no electric field dependence to lowest order (see chap. 2). Although such transitions violate the $\Delta M_J = 0, \pm 1$ selection rule

for magnetic dipole radiation, they can be induced as "multiple quantum" transitions. This is easiest for $M_J = +1 \longrightarrow M_J = -1$, a two quantum transition, and we have used this in the present experiment.

In summary, we describe in this thesis an experiment sensitive to an edm on the electron, using the $M_J = +1 \longrightarrow -1$ transition in the $^3P_2$ metastable state of xenon. The experiment is insensitive to the major spurious effect of earlier work.

Chapter 2. Spectroscopy of the $^3P_2$ levels of the rare gases

Part I. General

2.1 The metastability of the levels

In each of the rare gases (except helium) the first excited state is the $^3P_2$ and it is metastable. No lifetimes for these states have been measured, but we can give a theoretical estimate which shows the lifetimes are adequate for our purposes.

The $^3P_2$ state has odd parity (P) while the ground state is of course even. Single photon decay to the ground state therefore requires a process in which $\triangle J = 2$, $\triangle P = 1$. The lowest order of multipole radiation for which such a process is allowed is magnetic quadrupole. This occurs with typical transition probability less than that for electric dipole radiation by a factor

$$\simeq \left(\frac{d_o}{\lambda}\right)^2 \alpha^2$$

For the rare gases $\lambda \simeq 10^3$ Å and the factor is $\simeq 10^{-10}$. The lifetime against fully allowed electric dipole radiation is of order

$$\tau \text{ (dipole)} \simeq e^2 a_o^2 \omega^3/c^3$$

$$\simeq 10^{-9} \text{ sec}$$

for $\lambda = 10^3$ Å. Thus the lifetimes of the $^3P_2$ states against magnetic quadrupole decay are of order 10 seconds.

A competing process may be two photon decay via a virtual intermediate state. In this case decay by one magnetic dipole and one electric dipole photon is allowed, and using the treatment of Akhiezer and Berestetskii (1965) we find

$$\tau \text{ (two-photon)} \simeq 10^3 \text{ sec}$$

for the $^3P_2$ states.

As the transit time for the atoms in the beam apparatus to be described is of order 10^{-2} sec we can ignore spontaneous radiative decay.

The metastability may of course be destroyed in collisions, either by transfer of energy to excite or ionise the colliding atom or by destruction of the $J = 2$ quantisation of the metastable atom allowing radiative decay via the $^3P_1$ state. Most such processes should have small cross sections; only resonant transfer of excitation to an atom of the same type, or ionisation of the colliding atom (Penning ionisation), have cross-sections comparable with momentum transfer cross-sections (Hasted, 1964, reviews the data on these points). We have observed pressure dependent attenuation of the beam over its 3m flight path at background pressures of order 10^{-5} torr; however, this is quite consistent with scattering rather than deexcitation.

Another possibility is the quenching of the metastability by admixture of $^3P_1$ state in static electric or magnetic fields. The lifetime of the $^3P_1$ state, τ_1, is of order 10^{-9} sec. It is straightforward to show that the lifetime of the $J = 2$, $M_J = +1$ state against mixing and decay in a magnetic field B is

$$\tau\,(\text{mixing}) = \tau_1 \left[\frac{\sqrt{3}/6\ \mu_B B}{W_1 - W_2} \right]^{-2}$$

where $W_1 - W_2$ is the $J = 1, 2$ energy difference. In argon, we find

$$\tau\,(\text{mixing}) \simeq 10/B^2 \text{ sec}$$

where B is in K Gauss. In argon and neon the effect may therefore be observable and might even be usable as the basis of a state selector; however, it is smaller in the heavier rare gases. We have not used fields sufficiently high to investigate it. Electric field induced mixing is much smaller at attainable fields.

2.2 Effect of electric and magnetic fields

a) General

In this section we shall consider only even isotopes, so that $I = 0$. We shall treat only fields sufficiently low that we may neglect the breakdown of J quantisation; such fields may be very high by laboratory standards since the "multiplet" separation of the $^3P_2$ level from the $^3P_1$ is of order .1 eV i.e. 10^{13} Hz (see also previous section).

We shall find it convenient to express the electric and magnetic perturbations on the states of the $J = 2$ level in terms of an effective Hamiltonian operating within the level. We write for the perturbing Hamiltonian

$$\hat{H}_{pert} = \hat{H}_M + \hat{H}_E$$

where

$$\hat{H}_M = + \mu_B g_J \hat{\underline{J}} \cdot \underline{B}$$

$$\hat{H}_E = -\sum_i e \underline{r}_i \cdot \underline{E} = - \underline{P} \cdot \underline{E}$$

Then to second order the required effective Hamiltonian may be written

$$\hat{H}_{eff} = \hat{H}_{pert} + \hat{H}_{pert} \lambda \hat{H}_{pert}$$

where

$$\lambda = \sum_{\alpha}{}' \frac{|\alpha\rangle\langle\alpha|}{W_0 - W_\alpha}$$

The sum over α spans all states other than those of the $^3P_2$ level; W_0 is the unperturbed energy of the level. This well-known form of effective Hamiltonian can be derived from a slight extension of techniques used in Brillouin-Wigner perturbation theory (see e.g. Davydov, 1965). These techniques involve manipulation of the secular determinant; $\hat{H}_{eff}$ can also be obtained by approximate

unitary transformations of the Hamiltonian, an approach which may be extended to time dependent problems (Appendix A).

On writing $\hat{H}_{pert}$ in full, certain parts of $\hat{H}_{eff}$ are seen to vanish by parity requirements and we obtain

$$\hat{H}_{eff} = \hat{H}_M + \hat{H}_E \lambda \hat{H}_E = \hat{H}_M + \hat{H}_S'$$

To proceed further, we note that the energy denominator in λ involve unperturbed, free atom energies, so that λ is independent of the direction of the axis of quantisation. This means that λ is a scalar in the space of the whole atom; this enables us to use standard tensor methods to recouple the tensors in the effective Stark interaction and obtain it in the form

$$\hat{H}_S' = e^2 \left\{ \underline{p} \, \lambda \, \underline{p} \right\}^{(0)} \cdot \left\{ \underline{E} \, \underline{E} \right\}^{(0)} + e^2 \left\{ \underline{p} \, \lambda \, \underline{p} \right\}^{(2)} \cdot \left\{ \underline{E} \, \underline{E} \right\}^{(2)}$$

(Angel, 1967). This recoupling is demonstrated diagrammatically in Appendix B. The first term in $\hat{H}_S'$ involves a scalar in the space of the atom; since this cannot contribute to splittings within a level of given J, we may ignore it and write for the effective Hamiltonian

$$\hat{H}_{eff} = \hat{H}_M + T^{(2)} \cdot \left\{ \underline{E} \, \underline{E} \right\}^{(2)} = \hat{H}_M + \hat{H}_S$$

where

$$T^{(2)} = e^2 \left\{ \underline{p} \, \lambda \, \underline{p} \right\}^{(2)} .$$

b) High electric field

We now consider the case where $\hat{H}_S$ gives rise to shifts much greater than $\hat{H}_M$. In the limit of zero $\hat{H}_M$, the spectrum of the $^3P_2$ level can be written

$$W_S(|M_J|) = -\tfrac{1}{2}\alpha_t E^2 \quad \frac{3M_J^2 - J(J+1)}{J(2J-1)}$$

where the axis of quantisation has been chosen parallel to the direction of E, and α_t the tensor polarizability is a constant. This form for the spectrum follows at once from evaluating the 3-j symbols which appear on applying the Wigner-Eckart theorem to the matrix elements of $\hat{H}_S$, which has the form of a rank 2 tensor in the space of the atom.

The spectrum consists of three sublevels corresponding to the three values of $|M_J|$, two of the sublevels being doubly degenerate. A magnetic field will raise this degeneracy. However, to first order only the component of $\underline{B}$ parallel to $\underline{E}$ will contribute to the splitting since the parts of H_M associated with other components have no matrix elements within the sublevels. For reasons explained in the introduction we shall be interested in the $|M_J| = 1$ sublevel; its lowest order splitting is

$$W_1 - W_{-1} = 2\mu_B g_J B_{||}$$

To treat higher order effects we again use an effective operator formalism; using the techniques of appendix A, we can write for the $|M_J| = 1$ effective Hamiltonian

$$\langle +1 | H^{eff} | +1 \rangle = \tfrac{1}{4}\alpha_t E^2 + \mu_B g_J B_{\parallel} + \frac{(\mu_B g_J B_{\perp})^2}{\tfrac{3}{4}\alpha_t E^2 - \mu_B g_J B_{\parallel}} + \frac{\tfrac{3}{2}(\mu_B g_J B_{\perp})^2}{-\tfrac{1}{4}\alpha_t E^2 + \mu_B g_J B_{\parallel}}$$

$$\langle +1 | H^{eff} | -1 \rangle = \langle -1 | H^{eff} | +1 \rangle = \frac{\tfrac{3}{2}(\mu_B g_J B_{\perp})^2}{-\tfrac{1}{4}\alpha_t E^2}$$

$$\langle -1 | H^{eff} | -1 \rangle = \tfrac{1}{4}\alpha_t E^2 - \mu_B g_J B_{\parallel} + \frac{(\mu_B g_J B_{\perp})^2}{\tfrac{3}{4}\alpha_t E^2 + \mu_B g_J B_{\parallel}} + \frac{\tfrac{3}{2}(\mu_B g_J B_{\perp})^2}{-\tfrac{1}{4}\alpha_t E^2 - \mu_B g_J B_{\parallel}}$$

The Hamiltonian may now be diagonalised to obtain the level splitting to second order:

$$W_1 - W_{-1} = 2\mu_B g_J B_{\parallel} - \frac{25}{9}(\mu_B g_J)^3 \frac{B_{\perp}^2 B_{\parallel}}{(\tfrac{1}{4}\alpha_t E^2)^2} + \frac{9}{4}(\mu_B g_J)^3 \frac{B_{\perp}^4}{(\tfrac{1}{4}\alpha_t E^2)^2 B_{\parallel}}$$

In these expressions, $B_{\parallel}$ denotes the component of $\underline{B}$ parallel to $\underline{E}$, $\underline{B}_{\perp}$ denotes the components perpendicular to $\underline{E}$.

We now insert some numbers for Xe. The measured value of α_t (see Part II of this thesis) is equivalent to -10×10^{-3} Hz/ $(V/cm)^2$; therefore at

$E = 10^5$ V/cm, a fairly convenient laboratory field, the Stark splitting between the sublevels $|M_J| = 1, 0$ is about 25 M Hz. This compares with a lowest order magnetic splitting

$$\frac{1}{h}(W_1 - W_{-1}) = 80 \text{ k Hz}$$

for $B_{||} = 20$ m Gauss, our usual resonance field. With these fields, the $|M_J|$ sublevels are clearly well separated as required in the effective Hamiltonian formalism, and we expect higher order terms in the $|M_J| = 1$ splitting to be small; in fact, for $B_\perp = B_{||}$, their contribution is of order 1 Hz.

c) Low electric field

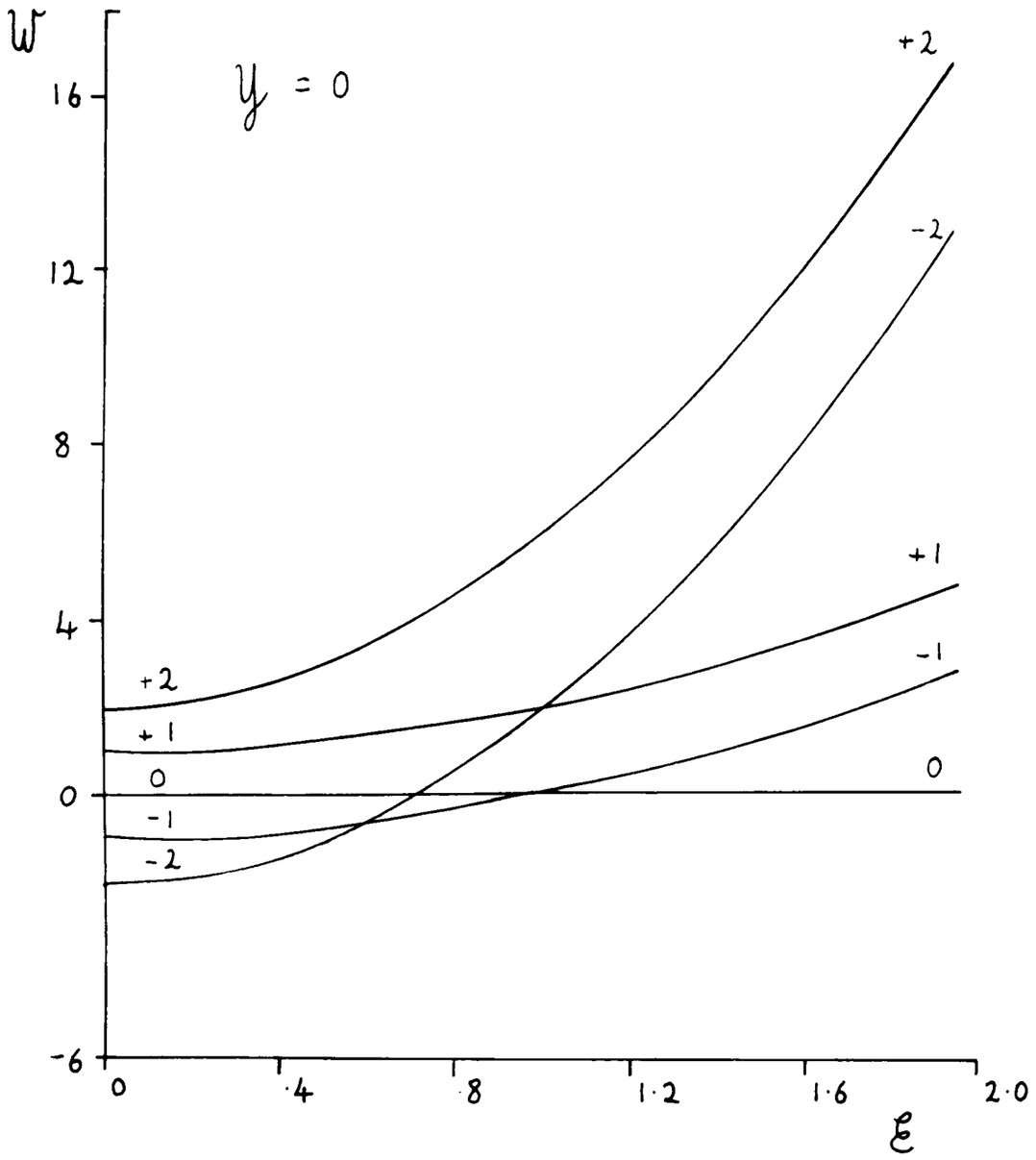
We now consider the case where the Zeeman and Stark splittings are comparable in size. This will be of interest in discussing the adiabatic transition technique used in our apparatus (chap. 3.5 below). To solve the problem, it is necessary to diagonalise the complete $J = 2$ effective Hamiltonian.

It is convenient to work in the high electric field representation, in which case the effective Stark operator H_E has only diagonal elements of form

$$\langle M_J | H_E | M_J \rangle = -\tfrac{1}{2} \alpha_t \frac{3M_J^2 - J(J+1)}{J(2J-1)} E^2$$

H_M has elements on the diagonal and elements for which $\Delta M_J = \pm 1$. This means that the full Hamiltonian can be written at once in triple-diagonal form, and may be diagonalised by the Sturm sequence technique (see Modern Computing Methods, 1961, p.31). A further feature of the matrix as written in this form is that none of the one-off-diagonal elements is zero for nonzero $B_\perp$; under these conditions it may be shown that the matrix has no degenerate eigenvalues, so we expect no crossing points in the energy level diagram.

Low E Energy Levels . 1



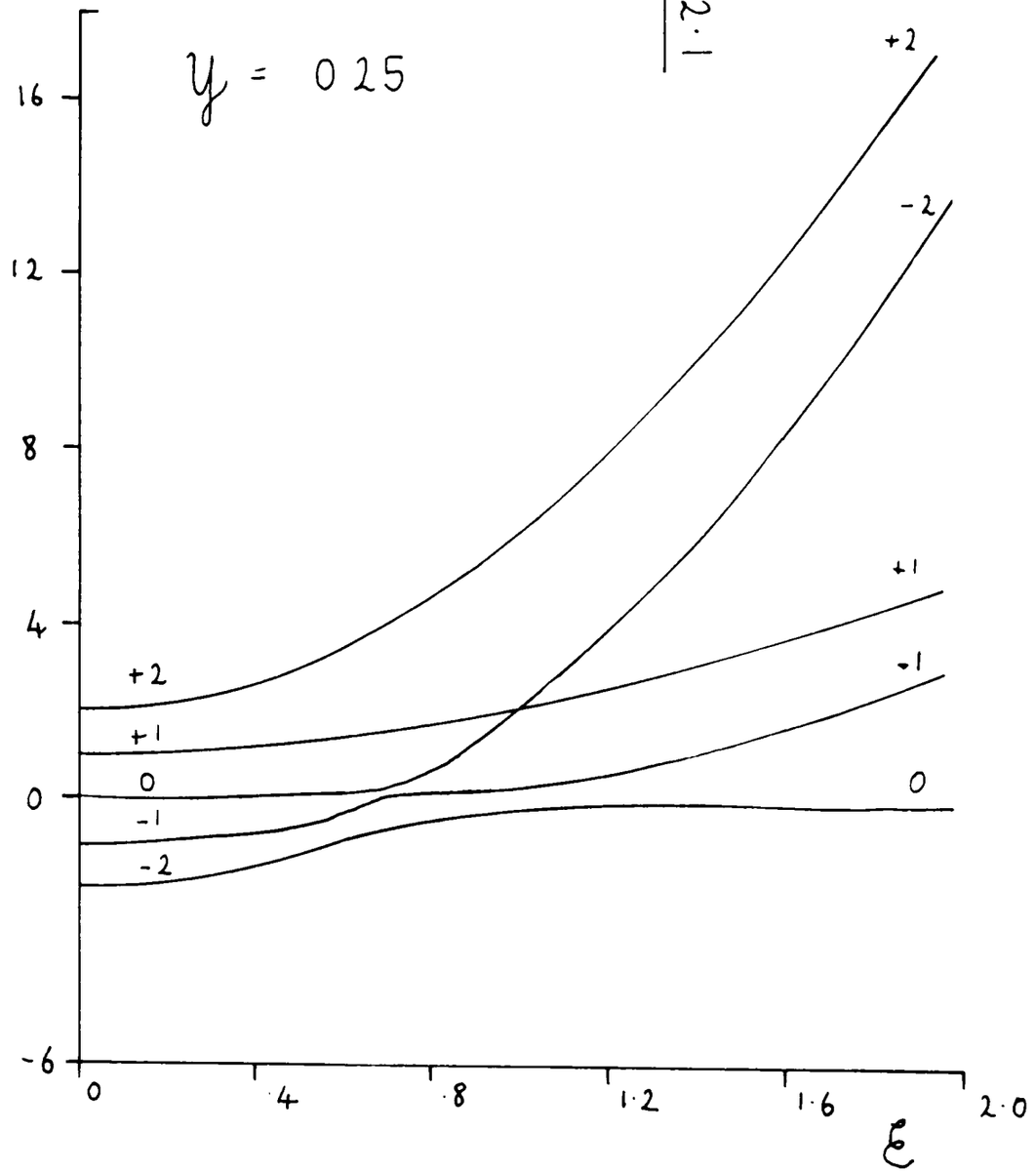
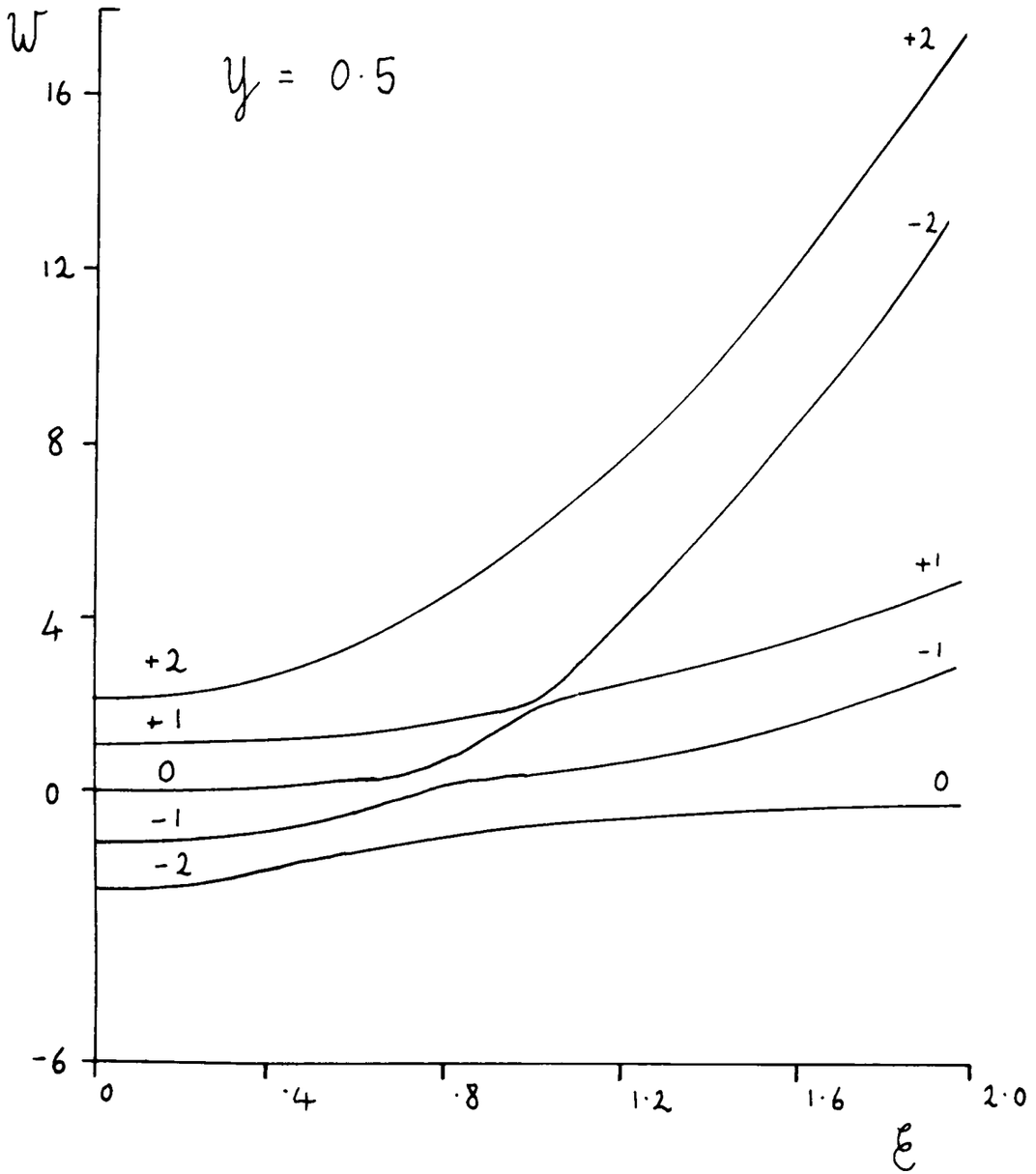


Fig 2.1

Low E Energy Levels . 2



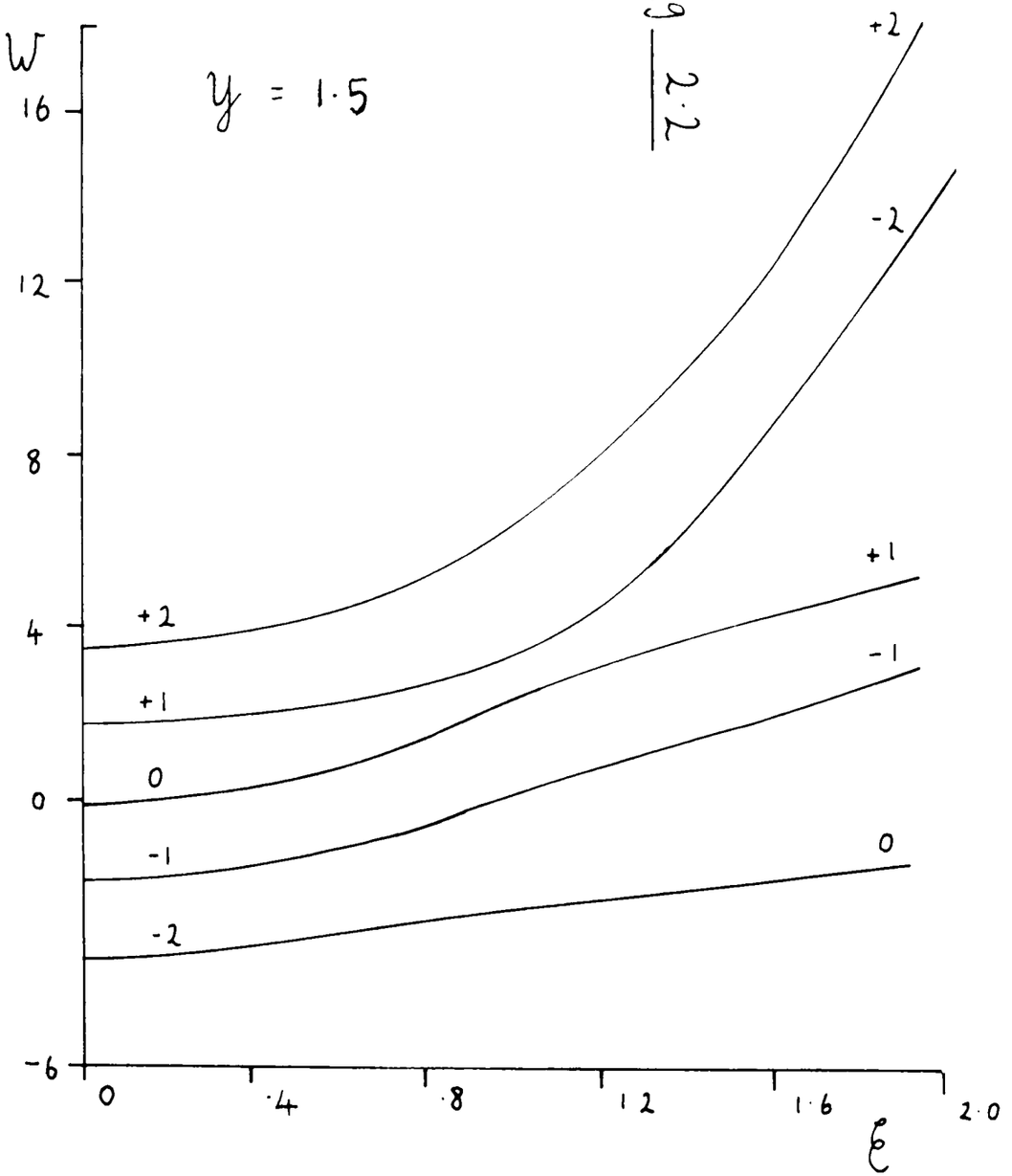


Fig 2.2

We show the energy level diagrams obtained in fig. 2.1 and 2.2. They are plotted in terms of dimensionless variables

$$\xi^2 = \left| \frac{1}{4} \frac{\alpha_t E^2}{\mu_B g_J B_{11}} \right|$$

$$W = \frac{W}{|\mu_B g_J B_{11}|} + 2\xi^2$$

with a parameter

$$Y = B_\perp / B_{11}$$

For Y = 0, the Hamiltonian matrix is already diagonal in the high electric field representation, and the diagram shows straightforward quadratic Stark shifts in the energy levels, with crossing points. For low Y, some crossing points remain to the accuracy which can be indicated on the diagram, but for Y = 2 the intermediate field region is grossly perturbed with no trace of crossing points, and with a new connection between low and high E quantisation. However, we note that even in this case the splittings $W_2 - W_{-2}$ and $W_1 - W_{-1}$ are approaching their high electric field values for ξ as low as 1.8.

The computer program used in this work was written in Fortran for use on our PDP-8 machine.

2.3 The $\underline{v} \times \underline{E}$ effect

Consider electric and magnetic fields $\underline{E}$ and $\underline{B}$ applied in the laboratory frame. In the rest frame of a beam of atoms moving with velocity $\underline{v}$ relative to the laboratory, the observed fields may be found by applying the Lorentz transformation to the field tensor constructed from $\underline{E}$ and $\underline{B}$ (see e.g. Jackson 1966, p.380). The result is

$$\underline{E}' = \underline{E} + \underline{v} \times \underline{B}/c$$
$$\underline{B}' = \underline{B} - \underline{v} \times \underline{E}/c$$

omitting terms of order $(v/c)^2$.

We consider first the effect on the atoms of the motional electric field $\underline{E}^m = \underline{v} \times \underline{B}/c$. In our beam of xenon, $v \simeq 2 \times 10^4$ cm/sec and, for B = 20 mGauss, we find that $E^m \simeq 10^{-5}$ V/cm approximately perpendicular to $\underline{E}$. The main effect of E^m is to produce a rotation of the axis of quantisation. For $E = 10^5$ V/cm, the angle of rotation $\phi \simeq 10^{-10}$ radians, which can lead to a maximum level splitting of order

$$g_J \mu_B B \phi \simeq 10^{-5} \text{ Hz}$$

This is two orders of magnitude too small to be observable in the present experiment. The effect has also been negligible in all previous work.

We turn now to consider the motional magnetic field $\underline{B}^m = \underline{v} \times \underline{E}/c$. In our xenon beam at $E = 10^5$ V/cm, this is approximately 0.2 mGauss in magnitude and is of course rigorously perpendicular to $\underline{E}$. Using the analysis of chap. 2.2 (b) above, this confirms that it does not contribute to the splitting $W_1 - W_{-1}$ to first order, but that it does contribute through higher order terms. If we suppose that $\underline{B}^m$ and $\underline{B}_\perp$ are parallel (worst case) and that $B_\perp < B_{||}$, it is easy to see that the dominant contribution to the splitting involving B^m is

$$\delta W^m_1 - \delta W^m_{-1} = -\frac{25}{9} (\mu_B g_J)^3 \frac{2 B_\perp B^m B_{||}}{(\frac{1}{4} \alpha_t E^2)^2}$$

We now suppose that there is a small misalignment θ between $\underline{B}$ and $\underline{E}$. Then we may write $B_\perp = B\theta$. If we again take xenon with B = 20 mGauss and $E = 10^5$ V/cm, then

$$\frac{1}{h}\left(\delta W_1^m - \delta W_{-1}^m\right) \simeq \theta \times 10^{-2} \text{ Hz}$$

This is to be compared with the case of the alkali ground states where the effect is of first order, leading to shifts of about $\theta \times 100$ Hz. We note also that in our case the motional shift is proportional to $1/E^3$, which allows a ready experimental separation from true electric dipole shifts.

This immense reduction in the size of the $\underline{v} \times \underline{E}$ effect is the central motivation for performing the present experiment. The use of an atomic state with high α_t was first suggested by Sandars (Player and Sandars, 1966).

2.4 Effect of electric dipole moment

We have already mentioned (chap. 1.2) that the change in splitting due to an edm between states $J\,M_J$, $J\,M_J'$ is

$$\delta W^{edm}_{M_J} - \delta W^{edm}_{M_J'} = d_A(J)\,\frac{M_J - M_J'}{J}\,E$$

where $\underline{E}$ is along the axis of quantisation and there is no nuclear spin. We may therefore write for the change in splitting of the $|M_J| = 1$ sublevel of the $^3P_2$ state in high electric field

$$\delta W^{edm}_{1} - \delta W^{edm}_{-1} = d_A\,E$$

This will lead to a shift in the observed frequency of the two-quantum transition $M_J = +1 \longrightarrow -1$

$$h\,\delta\nu^{edm} = \tfrac{1}{2}\,d_A\,E$$

(see chap. 2.7 for the factor $\frac{1}{2}$).

Sandars (1968) has discussed the more general case of $I \neq 0$, and uses dipole constants d_{kK} to parameterise the dipole interaction, where k refers to tensorial behaviour of the interaction in nuclear space and K to electron space. It is easy to show that in terms of this general treatment, we have $d_{01} = d_A$ with all other d_{kK} zero.

We now consider the size of d_A to be expected as a result of any intrinsic edm of the electron. This problem may be solved for the rare gases by reference to the results of Sandars (1966) for the alkalis, using the following argument. The $^3P_2$ metastable state for each rare gas has the configuration $(n-1)p^5\,ns$ where n is the same as the principal quantum number of the ground state s electron in the

neighbouring alkali. We therefore expect that the s electron orbitals are closely similar for the rare gas and its alkali neighbour; this is confirmed by the near equality of the measured polarisabilities (Robinson et al. 1966). Also, the $^3P_2$ state is a stretched state for electronic angular momentum, so that if the dipole moment of the incomplete p shell is negligible we may conclude

$$d_A \text{ (rare gas)} \simeq d_{01} \text{ (alkali)} .$$

In particular

$$d_A \text{ (Xe)} \simeq 130$$

$$d_A \text{ (Kr)} \simeq 20$$

The theory of Sandars suggests that the p shell contribution should indeed be negligible, because of the low polarisability of the shell, and because it is less highly relativistic than the s shell.

These results have recently been checked by Sandars by direct computation on the rare gases, with results in good agreement.

2.5 The odd isotopes of xenon

We consider briefly the odd isotopes of xenon, which are the only abundant isotopes with $I \neq 0$ among all the rare gases. These have not been used in any quantiative experiments, but have served to identify the working beam substance as xenon with absolute certainty.

The isotopes are Xe^{129} (abundance 26%, $I = \frac{1}{2}$) and Xe^{131} (21%, $I = 3/2$).

These states have high tensor polarizability, and offer the possibility of searching for an electric dipole moment in a system with an odd number of fermions, still avoiding the $\underline{v} \times \underline{E}$ effect, and without using two-quantum magnetic resonance. This is attractive, but low signals have made the experiments not feasible with our apparatus.

Chapter 2

Part II Magnetic resonance in high electric field

2.6 General formalism

As explained in the introduction, it is necessary for us to use a two-quantum magnetic resonance transition between the $M_J = +1, -1$ states of the $^3P_2$ level. Such transitions have been treated in the literature, notably by Salwen (1955) who uses a transformation to a rotating frame in which the applied r.f. field is stationary. This assumes the perturbing field is circularly polarised. Salwen takes his treatment to second order in r.f. amplitude.

We have adopted a different approach based on the effective Hamiltonian technique (appendix A). This is considerably less elegant than the method of Salwen in that approximations of varying degrees of severity are made throughout the treatment. However, it does give a straightforward account of two-quantum resonance, and it allows treatment of linearly polarised r.f. fields and separated r.f. regions (Ramsey 1956; see chap. 3.6).

The method consists in transforming the time dependent perturbation due to the r.f. field into the 2 x 2 submatrix for the $|M_J| = 1$ sublevel, as in the solution of the time independent problem (chap. 2.2 (b)). Since the transformations amount to small rotations in the space of the wavefunctions, the resonance behaviour in the sublevel is described by the transformed Hamiltonian rather than by the explicit effect of the transformation on the wavefunctions. This is in contrast with the approach using rotating coordinates, where the time dependence of the problem appears only in the transformation of the wavefunctions.

The problem is thus reduced to a standard two level problem, with a Hamiltonian formally indentical with that used in the time independent case (chap. 2.2 (b)).

2.7 Results

We now use the effective Hamiltonian, together with the standard treatment for the two level problem (Ramsey, 1956) to obtain a description of the two-quantum resonance process.

If we consider a perturbing r.f. field represented by

$$B = B_{r.f.} \sin \omega t$$

we obtain in our effective Hamiltonian an off-diagonal matrix element

$$\langle +1 | H^{eff} | -1 \rangle = \frac{\frac{3}{2} (\mu_B g_J B_{r.f.})^2 \sin^2 \omega t}{-\frac{1}{4} \alpha_t E^2}$$

This has both a static part and a periodic part proportional to sin $2\omega t$. This holds also for the diagonal elements.

Now, the transition probability for a two-level system subject to a perturbation

$$H_{12} = \hbar b e^{-i\omega t}$$

which is switched on at time t=0 and off at time t, is given by Ramsey as

$$P_{1,2} = \frac{(2b)^2}{(\omega_0 - \omega)^2 + (2b)^2} \sin^2 \left\{ \frac{1}{2} \left[(\omega_0 - \omega)^2 + (2b)^2 \right]^{1/2} t \right\}$$

where $\omega_0 = (W_1 - W_2)/\hbar$ and W_1, W_2 are the energy eigenvalues of the system in the absence of the perturbation. In order to apply this result to our system, we have to introduce certain assumptions.

First, we suppose that we can neglect the effect of periodic parts of the

diagonal elements. This assumption is discussed by Ramsey for the single quantum case; it is justified under normal circumstances. We also assume that the static terms involving $B_{r.f.}$ give rise to a shift in resonance frequency proportional to the differential shift in energy eigenvalues which would occur if the static part of the perturbation were applied alone, with no periodic perturbation. This assumption seems somewhat questionable, especially as regards the off-diagonal elements, but it should at least give the correct order of size for the shifts. To treat the off-diagonal periodic perturbation we resolve it into two oppositely circularly polarised components. One will be able to excite resonant transitions; we assume the other gives rise to a shift in resonance frequency in the usual way.

Making these assumptions, we can at once make use of Ramsey's formula for transition probability. We find for the two quantum transition probability

$$P_{1,2}\ (2\text{-quantum}) = \frac{(2b')^2}{(\omega_0' - \omega)^2 + (2b')^2} \sin^2 \left\{ \tfrac{1}{2} \left[(\omega_0' - \omega)^2 + (2b')^2 \right]^{1/2} t' \right\}$$

where

$$\hbar b' = \tfrac{1}{2} \times \frac{\tfrac{3}{8} (\mu_B g_J B_{r.f.})^2}{-\tfrac{1}{4} \alpha_t E^2}$$

$$t' = 2t$$

$$\omega_0' = \tfrac{1}{2} \omega_0 \qquad \text{(to lowest order)}$$

With these replacements, the transition probability is of the same form as in the single quantum case.

If we consider the widths of single and two-quantum resonances in the same beam moving through r.f. field regions of equal length, the appearance of $t' = 2t$ in the expression for $P_{1,2}$ (two-quantum) leads at once to the conclusion

that the observed two-quantum resonance width is half that for the single quantum case, if the perturbations b and b' are adjusted to give equal transition probabilities at exact resonance in the two cases.

We have thus reached the well-known conclusion that the two-quantum resonance has the usual structure, but with half the resonance frequency and half the width.

So far we have included only the on-resonance part of the off diagonal elements of the effective Hamiltonian, together with the lowest order static terms in the diagonal elements. To include the higher order effects, we write

$$\nu_0' = \frac{1}{2h}\left[\langle +1|H|+1\rangle - \langle -1|H|-1\rangle\right] + \delta\nu_1 + \delta\nu_2$$

where H is the unperturbed Hamiltonian. $\delta\nu_1$ arises from the static parts of the r.f. dependent terms in the diagonal elements of the effective Hamiltonian:

$$h\delta\nu_1 \simeq (\mu_B g_J)^3 \frac{B_{r.f.}^2 B_{||}}{(\frac{1}{4}\alpha_t E^2)^2}$$

and $\delta\nu_2$ from the static and off-resonance parts of the off-diagonal elements, whose effects are of the same order:

$$h\delta\nu_2 \simeq (\mu_B g_J)^3 \frac{B_{r.f.}^4}{(\frac{1}{4}\alpha_t E^2)^2 B_{||}}$$

To put numbers into the theory, we take a xenon beam moving at thermal velocity through a 5 cm long r.f. region with $E = 10^5$ V/cm, B = 20 mGauss. To obtain the optimum value of b', we use Ramsey's formula for a Maxwellian beam

(remembering the factor of two in t'):

$$4 b' \ell / \alpha = 1.2 \pi$$

from which we find

$$B_{r.f.} \text{ (optimum)} = 120 \text{ mGauss}$$

With this value, we obtain

$$\delta \nu_1 \simeq 3 \text{ Hz}$$

$$\delta \nu_2 \simeq 100 \text{ Hz}$$

From this, it seems we should consider higher order shifts. Although we have no theory for these, it is clear that the effects may be expressed in the form of power series, with dominant terms of the form

$$h \delta \nu_n \simeq \left[\frac{(\mu_B g_J B_{r.F.})^2}{\frac{1}{4} \alpha_t E^2} \right]^n \frac{1}{(\mu_B g_J B_{11})^{n-1}}$$

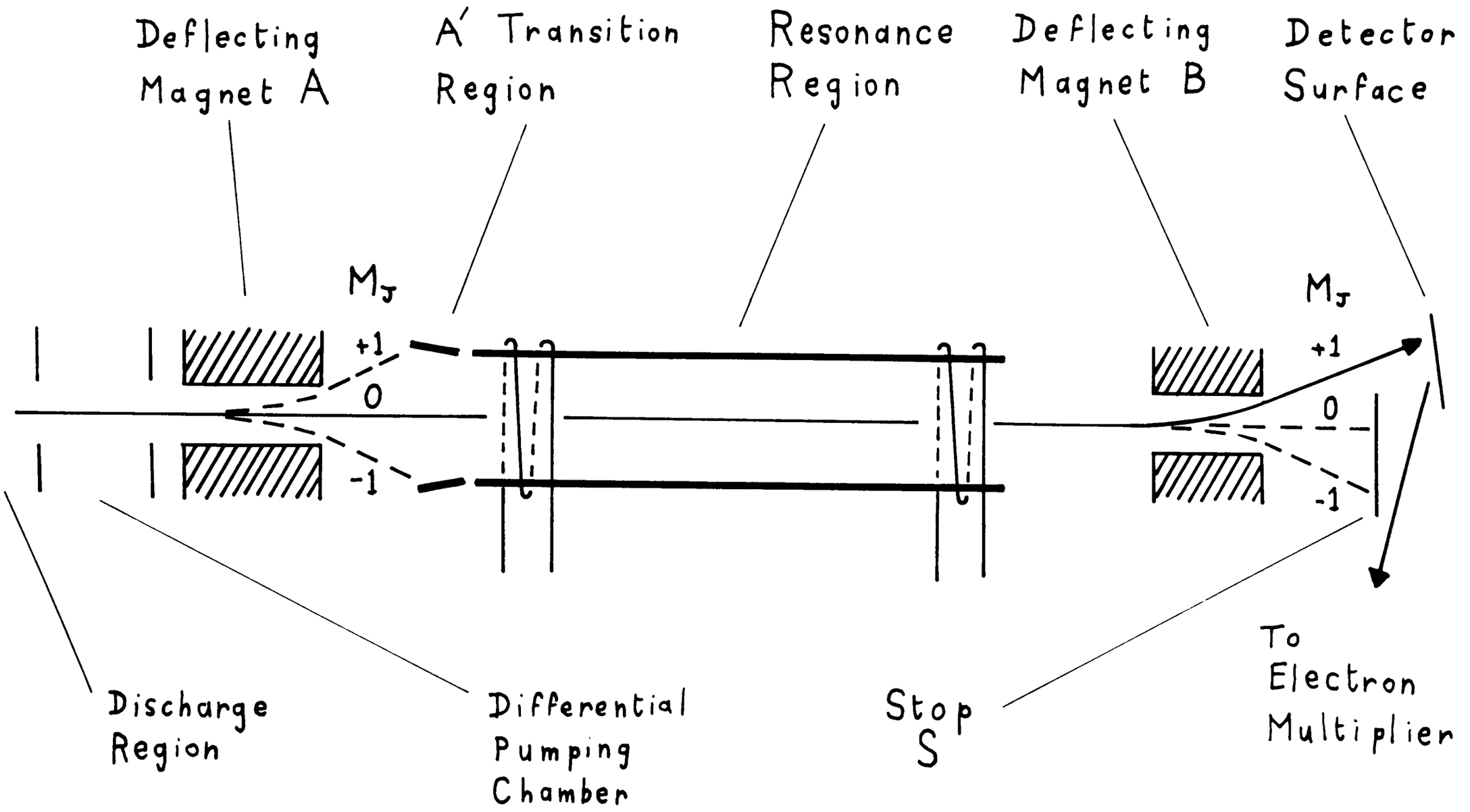
Our term $\delta \nu_2$ is the lowest member of this set. The next,

$$\delta \nu_3 \simeq 10 \text{ Hz}$$

All these results are readily extendable to the case of separated r.f. fields, and we shall introduce the required extensions as we need them. The power shifts are smaller with the separated field system. We shall show that they are relatively unimportant in the present experiment, despite the fact that they do introduce a dependence of resonance frequency on the magnitude of the electric field.

Fig 3.1

The Beam Apparatus



Chapter 3. The atomic beam apparatus

3.1 General scheme

The apparatus to be described was constructed specifically for the present experiment. As mentioned in the introduction, any atomic beam resonance apparatus may be considered as a device for observing atomic transitions by use of a state selecting polariser and analyser. Our apparatus, shown in fig. 3.1, uses this principle in a straightforward way.

On leaving the source, the beam enters a 2-pole deflecting magnet A of standard "two-wire" design (see Ramsey 1956). This has sufficient deflecting power that all atoms in states with $M_J \neq 0$ are deflected out of the beam. The selected $M_J = 0$ atoms enter a region A′ of crossed electric and magnetic fields where they pass adiabatically and with 100% transition probability to the $M_J = +1$ state in high electric field. The deflecting magnet A and transition region A′ constitute our polariser.

The beam next enters the resonance region C where the $M_J = +1 \rightarrow -1$ transition is excited in high electric field, with a parallel magnetic field. The Ramsey double-loop system is used, with the r.f. applied by solenoids wound round the field plates. Because the electric and magnetic fields are parallel, the atoms retain their quantisation when they leave the electric field region.

The analyser consists of the second deflecting magnet B and the stop S. These are so adjusted that only atoms with $M_J = +1$ are deflected to miss the stop and reach the detector surface. The detected beam is thus decreased when the $M_J = +1 \rightarrow -1$ transition is excited; in the jargon, the scheme gives a flop out on flop in signal.

This setup has an important advantage over the more usual refocussing scheme: because the detected beam is deflected only after its passage through

the electric field plates, optimum use can be made of the solid angle subtended at the source by the exit aperture of the field plates. Also, because the detector can be positioned well off axis, there is relative freedom from background from photons produced in the source. Alignment is less critical than with refocussing arrangements, which simplifies mechanical design of the apparatus.

We now discuss some features of the general design of the machine - why it has the shape it does.

The beam intensity depends on the entrance width of the B magnet or the electric field plate spacing, whichever is smaller, on the beam height, the distance between the source and the end of the field plates or start of the B magnet, and the source intensity. For high intensity, the B magnet width should be not much less than the field plate spacing, which should be large. However, it is desirable to use as high an electric field as possible, and this is about 10^5 V/cm nearly independent of field plate spacing; since the highest potentials which may be conveniently switched are of order 10^4V, the field plate spacing must be no more than a few mm. We chose 2 mm. The width of the B magnet is actually only 1 mm, because of the difficulty of obtaining sufficient deflection in a 2 mm beam; even so, relatively little precision is lost.

The beam height is also largely determined by difficulties in designing the deflectors and, in this case, the source; also partly by the difficulty in achieving vertical alignment sufficiently accurate to enable utilisation of a beam much higher than 10 times its width. We have chosen a height of 1 cm, fairly arbitrarily.

Having set the width and height of the beam, we consider the optimum length. We have to achieve adequate deflections in the A and B magnets with limited magnetic field strength, and in our design this requires a length of about 0.5 m for each deflector. There is additional length contributed by the differential pumping chamber and various coupling regions; the total beam path

without resonance region is about 1.5 m. It is clearly desirable to have the resonance region of length comparable or longer; we have used an overall length of 2 m for the magnetically shielded region, the resonance region itself occupying about 1.2 m. If the length ℓ of the resonance region is made much greater, the intensity I becomes nearly proportional to $1/\ell^2$; assuming ideal counting statistics this implies the overall precision, which is proportional to $\sqrt{I}/\Delta\omega$, will become independent of ℓ, since the linewidth $\Delta\omega \propto 1/\ell$.

The design of the source is determined more by the requirement of high production efficiency for metastables than by geometrical considerations; happily a 1 cm x 1 mm source aperture is quite convenient.

We note that our design is largely determined by the gapwidth, a , of the electric field plates, which we set to give the highest possible E with fairly conveniently reversible applied potentials. We now examine the effect of increasing a. First, E will fall, introducing a factor 1/a into the precision for a dipole measurement. Then, the required optimum magnet gapwidth and deflections both rise proportional to a. Assuming the magnetic field in the deflectors is fixed (we are at present not very far from the limit of saturating the iron), the length of the magnets must increase; if we assume all lengths are scaled up together, this has no direct effect on precision. However, the source and detector areas may both be scaled up proportional to a^2, and this gives a factor a^2 in the overall precision.

The precision therefore actually increases proportional to the gapwidth a if full advantage is taken of the possibility of scaling up the apparatus size. However, this may well be illusory if (as is likely) the size of the source cannot be scaled, or if there is a limit on precision other than counting statistics (an effect we have encountered in the present experiment). The larger machine would of course be much more difficult (and costly) to build; to ensure success

from an expansion in size, it would seem necessary first to improve the high voltage technology.

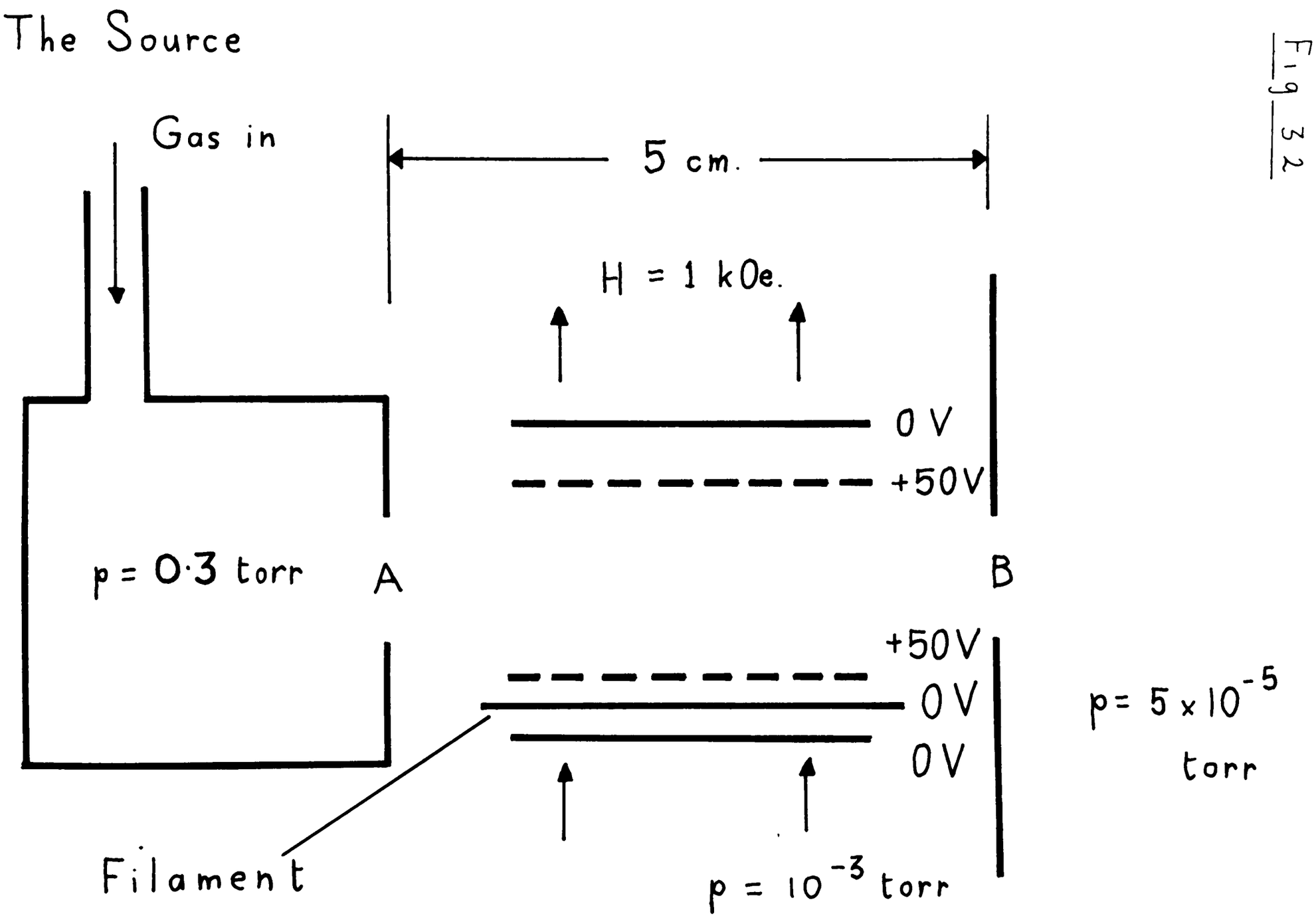
3.2 General mechanical details

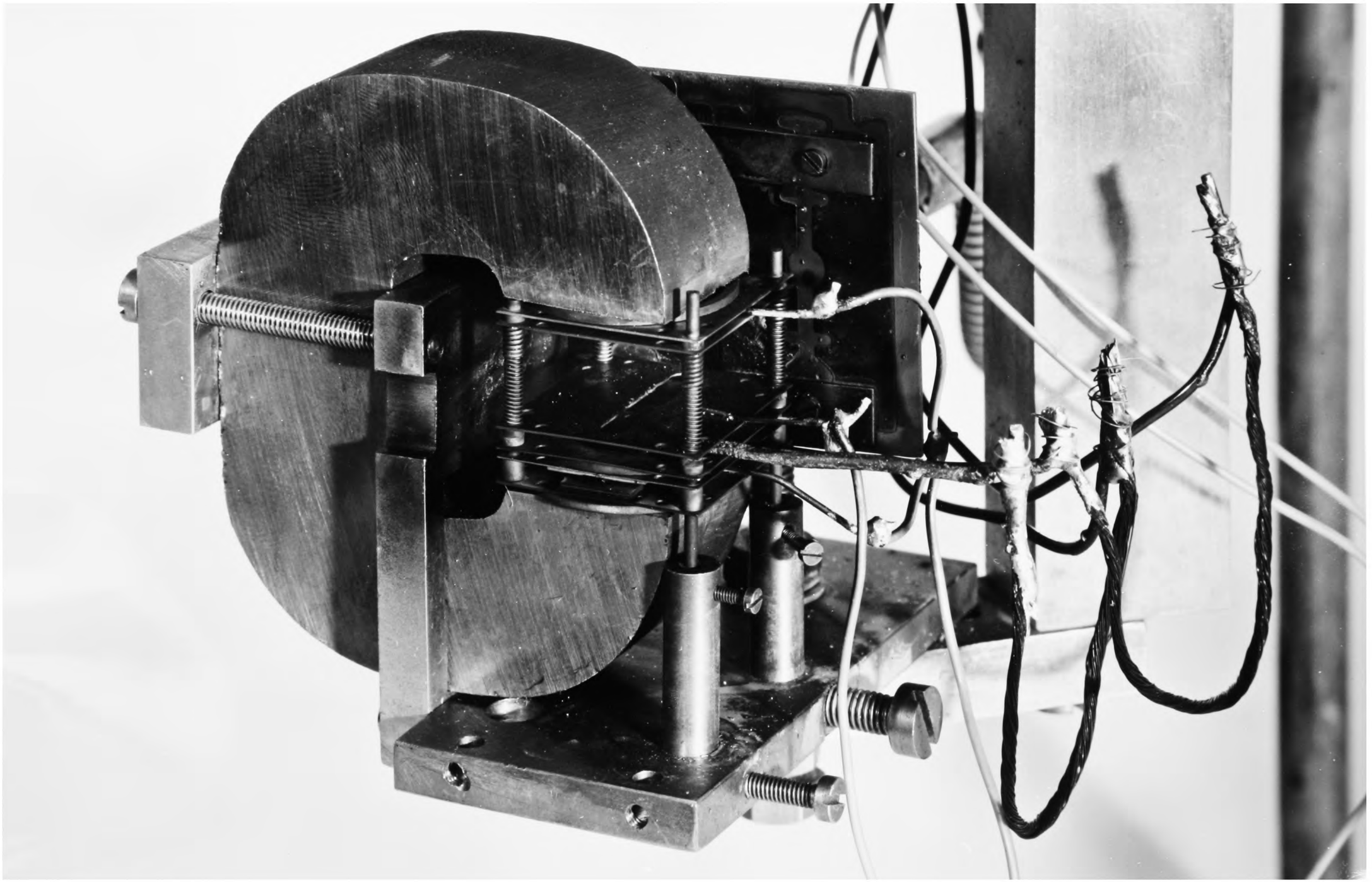
The vacuum system is constructed almost entirely of brass with hard-soldered joints. All pumping is by oil diffusion pumps, each provided with a thermo-electrically cooled baffle. The source is provided with a 6" pump for reasons discussed below. A differential pumping chamber isolates the source with its poor pressure from the main vacuum system; the differential pumping chamber is 10" long and is pumped by a 4" pump. The A and B deflectors are housed in 6" diameter tubes each provided with a 2" pump and a liquid nitrogen trap with a substantial refrigerated surface protruding into the main vacuum can. A 4" diameter tube contains the resonance region; this has no separate pumps, but is pumped from the A and B chambers. The detector has a separate chamber with a 2" pump and liquid nitrogen traps. With liquid nitrogen, pressures of a few times 10^{-7} torr are reached in the main apparatus.

Support is provided by an aluminium alloy Dexion framework.

The alignment is adjustable as follows. The A and B magnets can be moved within their chambers for initial adjustment before assembly. Coupling between the deflector cans and resonance region tube is accomplished by o-rings which seal onto the outer surface of the tube; this permits slight bending motion between the three regions. The coupling flanges also permit slight transverse motion. Thus final lineup between A and B deflectors and the field plates is accomplished by moving the chambers by external pushers. The source, differential pumping exit slit and the stop S in front of the detector are all externally movable. The detector surface is broad and needs only approximate alignment before assembly.

Fig 32


The Source
Gas in
5 cm.
H = 1 kOe.
0 V
+50V
p = 0·3 torr
A
B
+50V
0 V
0 V
p = 5 x 10^-5 torr
Filament
p = 10^-3 torr



3.3 The source

A schematic diagram of the source is shown in fig. 3.2, and a photograph in fig. 3.3. Metastables with high excitation energies may be produced in a discharge or by electron bombardment of a ground state beam. Our source was initially constructed to operate as an electron bombardment gun.

To obtain as high an efficiency as possible, magnetic collimation of the electron beam is used, with "oscillating electron" electrode geometry. This means that electrons leaving the filament, which lies below and parallel to the atomic beam, spiral up the magnetic lines of force through the electrode shown as a grid in fig. 3.2, pass through the interaction region, through the second grid, and are then reflected back by an electrode at filament potential. This geometry is well known in ion sources, following the work of Heil (1944). The electrons are supposed to oscillate up and down several times before falling onto one of the grids, which serve as the anode. If emission from the filament is space charge limited, this technique should increase the electron density in the interaction region, and hence the production efficiency for metastables.

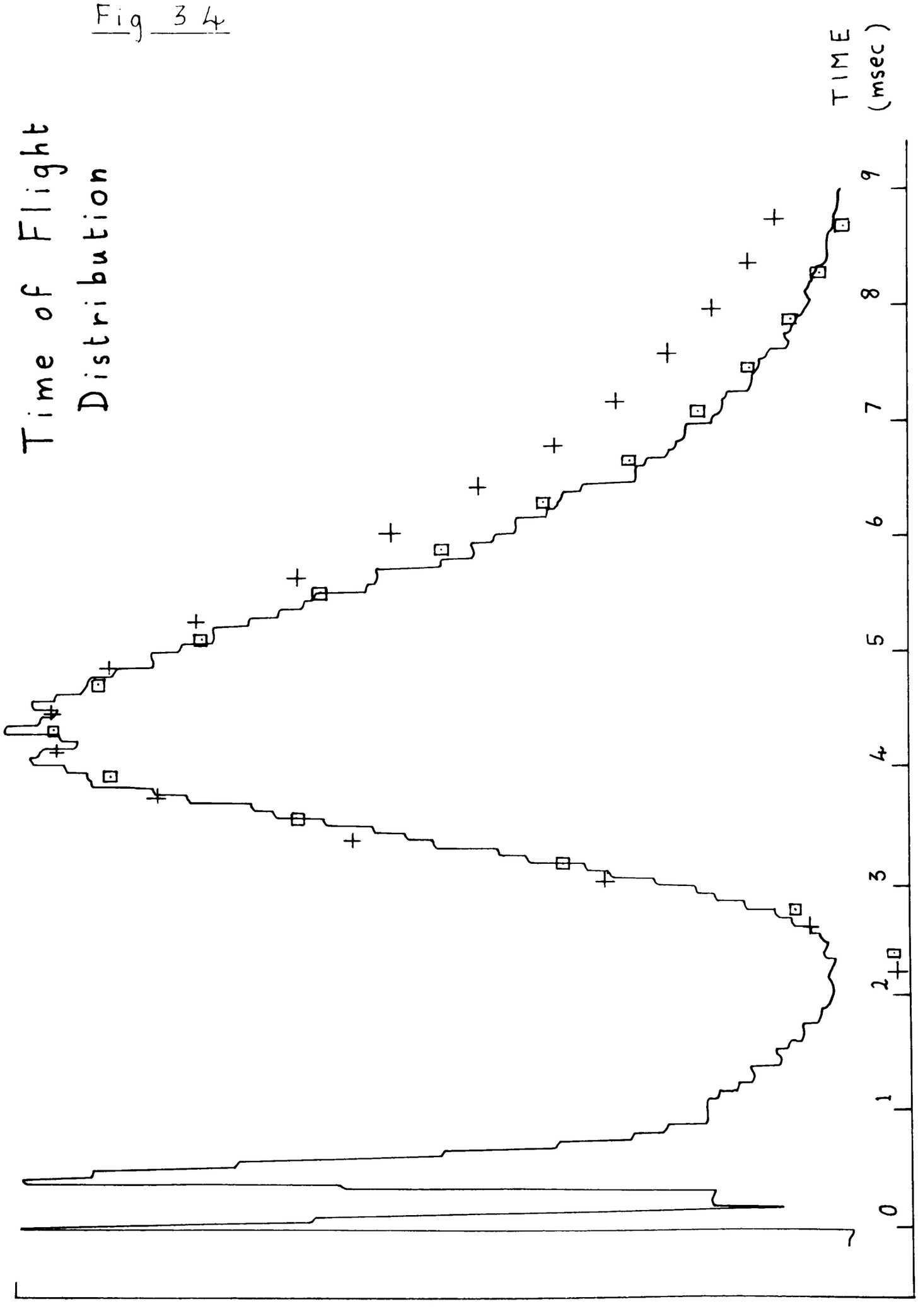
The electron gun was constructed from the "EAI kit" supplied by the Nuclide Corporation. The electrodes are stainless steel; the "grids" shown in fig. 3.2 are actually steel plates with slit apertures about 0.1 in wide. The filament is a thoriated tungsten wire 10 thou in diameter, spot welded to stainless steel supports. All insulators are alumina. In fig. 3.2 the gas source aperture A is a slit 1 cm by .25 mm wide, and the aperture B leading into the differential pumping chamber is 1 cm by 1 mm. The collimating magnetic field is about 1 kGauss and is supplied by a permanent magnet.

A fairly good performance is given by the source acting in the conventional "gun" mode. About 10 mA anode current is obtained, and using argon at a pressure of about 20 micron behind the source slit a full beam of about 10^6 metastables per second may be observed with a detector subtending about 10^{-6}

steradians at the source. The pressure in the source chamber is about 5×10^{-5} torr under these conditions. However, we have discovered that for a pressure of around 300 microns behind the source slit, a discharge occurs in the gun and the flux of metastables rises by at least ten times. The measured source chamber pressure is about 10^{-3} torr. This discharge is of the "hot-cathode, low-voltage" type, and the phenomena involved are similar to those in a hot cathode mercury vapour rectifier tube. Most of the electronic current is supplied by thermionic emission from the filament, but positive ions in the plasma neutralise the usual filament space charge so that the full temperature limited current is available. The discharge voltage is of order the gas ionisation potential. In our case the voltage is about 50 V. Metastable production rises nearly linearly with discharge current up to about 50 mA, then saturates rather rapidly; this saturation value is highest at the lowest source pressure consistent with the maintenance of the discharge. The photon flux is about 10 times greater than the metastable flux at 50 mA, and rises linearly with current. Operation of the source depends critically on the fact that the discharge runs in a pumped chamber. If the 6" pump is throttled and the gas flow reduced to maintain the same source chamber pressure, the flux of metastables drops rapidly; it essentially vanishes if the pump is closed. The pressures and potentials for the discharge are shown in fig. 3.2.

It is difficult to make a good estimate for the production efficiency of the source because the detector efficiency is unknown, and because the position of the effective source aperture is uncertain. If we assume continuum flow up to the entrance aperture of the differential pumping chamber, and use the observed pressure in this chamber to estimate the gas flow rate in the beam, the estimated ground state flux at the detector is of order 10^{11} atoms/sec. The full beam of argon metastables is of order 10^{7} atoms/sec; assuming 10% detection efficiency, the production efficiency is of order 10^{-3}. This seems to be comparable with the

Fig 34


Time of Flight
Distribution
TIME (msec)
0
1
2
3
4
5
6
7
8
9
INTENSITY (arbitrary units)

best electron gun type sources, and better than previous discharge sources, though quantitative specifications are not easy to find. For a review of sources, see Hasted (1964) or Hughes and Schultz (1967).

The reasons for this good performance seem fairly straightforward. The features of our gun which gave it good electron collimation performance allow it to run at a relatively high electron temperature in the discharge regime; this is why similar geometries are used in ion sources. The population of metastables may be expected to reach several percent in such a discharge. The low density and high density gradients in the source region might be supposed to lead to a "freezing" of this population as the gas expands and passes from continuum to free molecular flow. The extraction efficiency is also helped by the closeness of the discharge to the differential pumping chamber inlet aperture.

In order to obtain a little more information about the source, we have measured the time of flight distribution for the metastables. Such a distribution is shown in fig. 3.4 for the straight-through beam in argon over a 360 cm flight path. This was obtained using our PDP-8 computer in an on-line mode. The machine was programmed to pulse on the discharge for about 100 μsec, and perform a multichannel analysis of the detector count rate in subsequent 100 μ sec intervals, averaging the results of repeated pulsings and time sweeps. The zero of the time scale is marked by a sharp peak due to photons.

The main peak of the distribution corresponds to metastables at thermal velocities. One might expect a Maxwellian distribution in the discharge and v x Maxwellian in the beam. In fact, only a poor fit is obtainable even with a v^2 x Maxwellian distribution (crosses in fig. 3.4) in which α ,the most probable velocity, is taken as adjustable. A better fit is obtained (squares in fig. 3.4) with the distribution

$$f(v) = \exp(-v_o/v) \times v \times v^2 \exp(-v^2/\alpha^2)$$

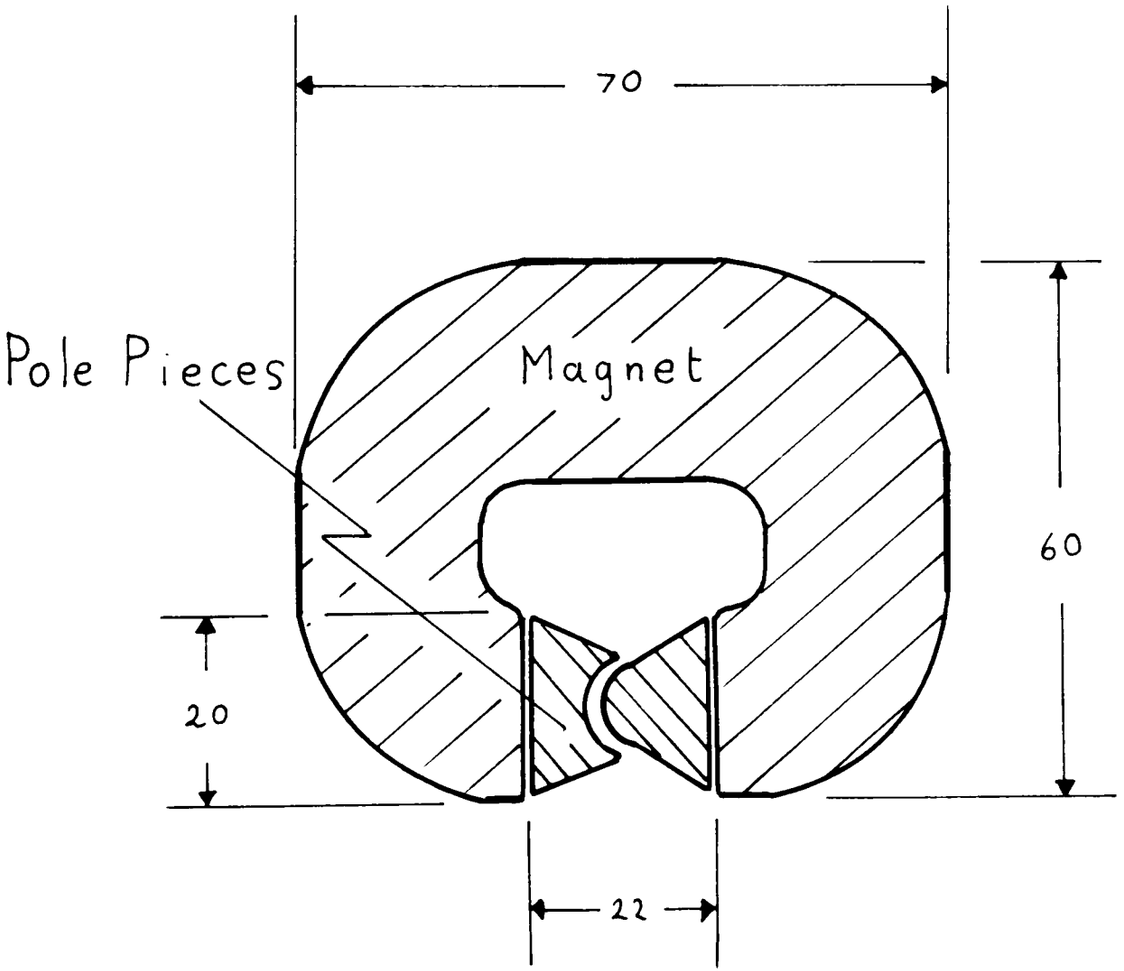
which corresponds to a suppression of slow atoms. Since both α and v_o must be taken as adjustable (the source temperature is unknown), the fit is less impressive than it might be. However, the value of α used corresponds to a temperature of 180°C, which is reasonable in view of a filament dissipation of 40W with no specific cooling provided for the source. The value of v_o is $0.34\,\alpha$. If the fit is accepted as meaningful, and if the implied de-excitation of slow atoms occurs in the source and not later, then the extraction efficiency for the source is still quite low, with about 10% of the metastable population contributing to the beam. The form of the distribution also implies that the mean free path against de-excitation for the metastables at the edge of the discharge is inversely proportional to their velocity.

One quite interesting feature of the time of flight curve is the subsidiary peak at less than 1 msec delay. Ions at these velocities would be unable to pass through the A and B magnets. The peak disappeared when the pressure rose to 10^{-4} torr in the main can; this is typical of metastables. It therefore appears that the fast peak represents metastables produced by ionic recombination. The kinetic energy of these metastables is about 2 eV.

Xenon is an expensive gas (£5 /l at STP) and we have used a simple recirculating system to economise. We have found it adequate to recirculate via the Edwards helium sealed backing pump which serves the oven chamber, without cleaning. About 100 cc (STP) of Xe, corresponding to $\simeq$ 60 torr pressure in the recirculating system, lasts for up to 40 hours of running.

Fig 35

A Magnet



Dimensions in mm. Scale 1x

B Magnet

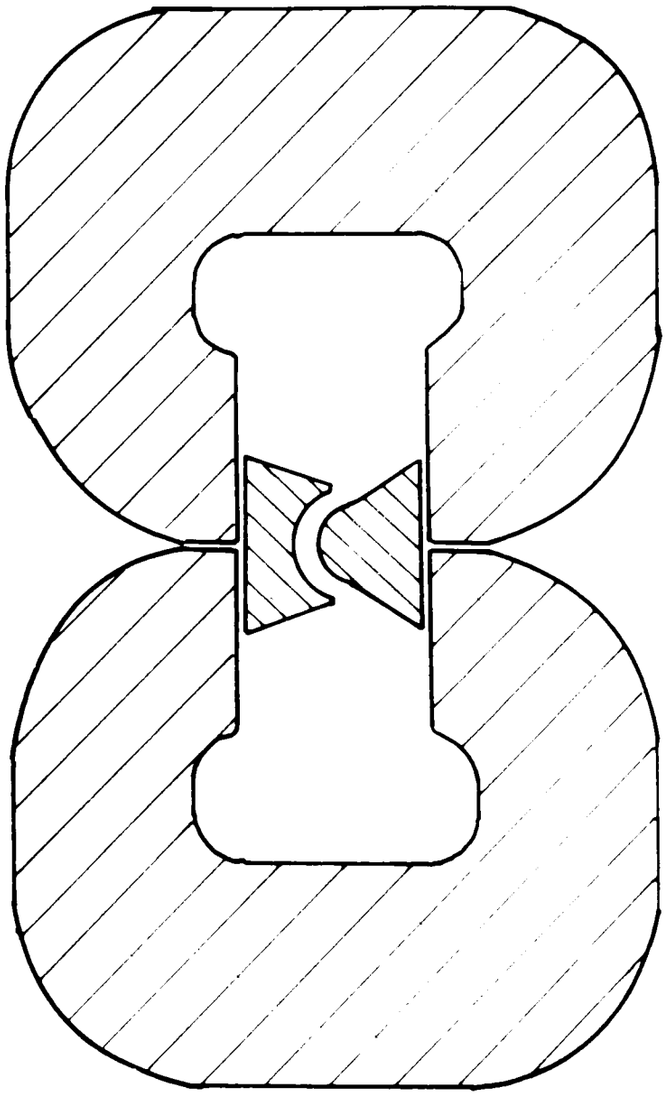
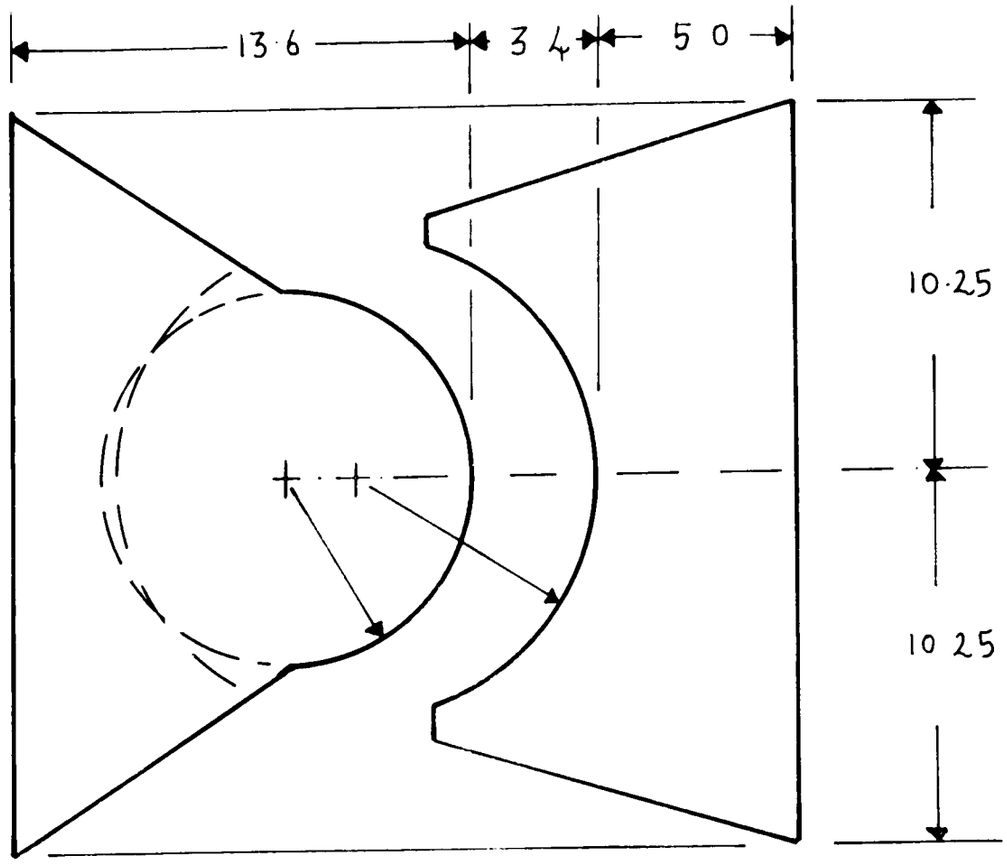
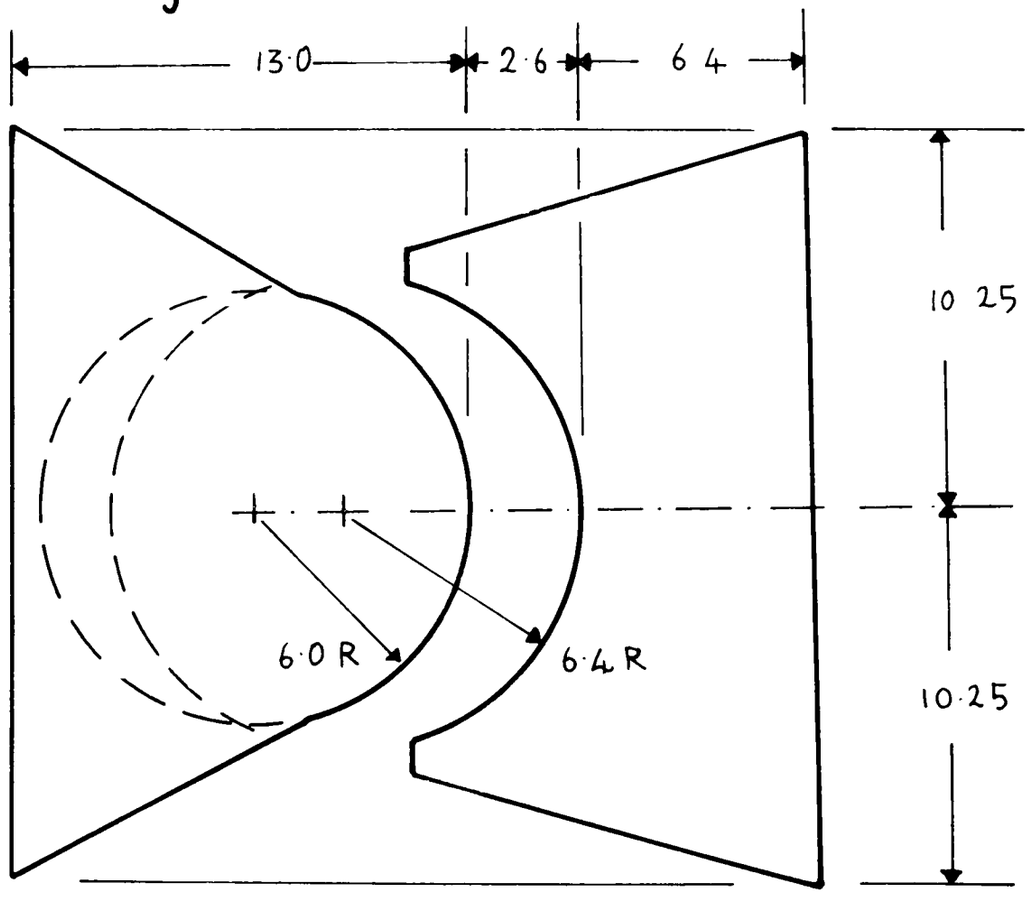


Fig 36

A Magnet Pole Pieces



B Magnet Pole Pieces



All dimensions in mm Scale 4x

3.4 The deflectors

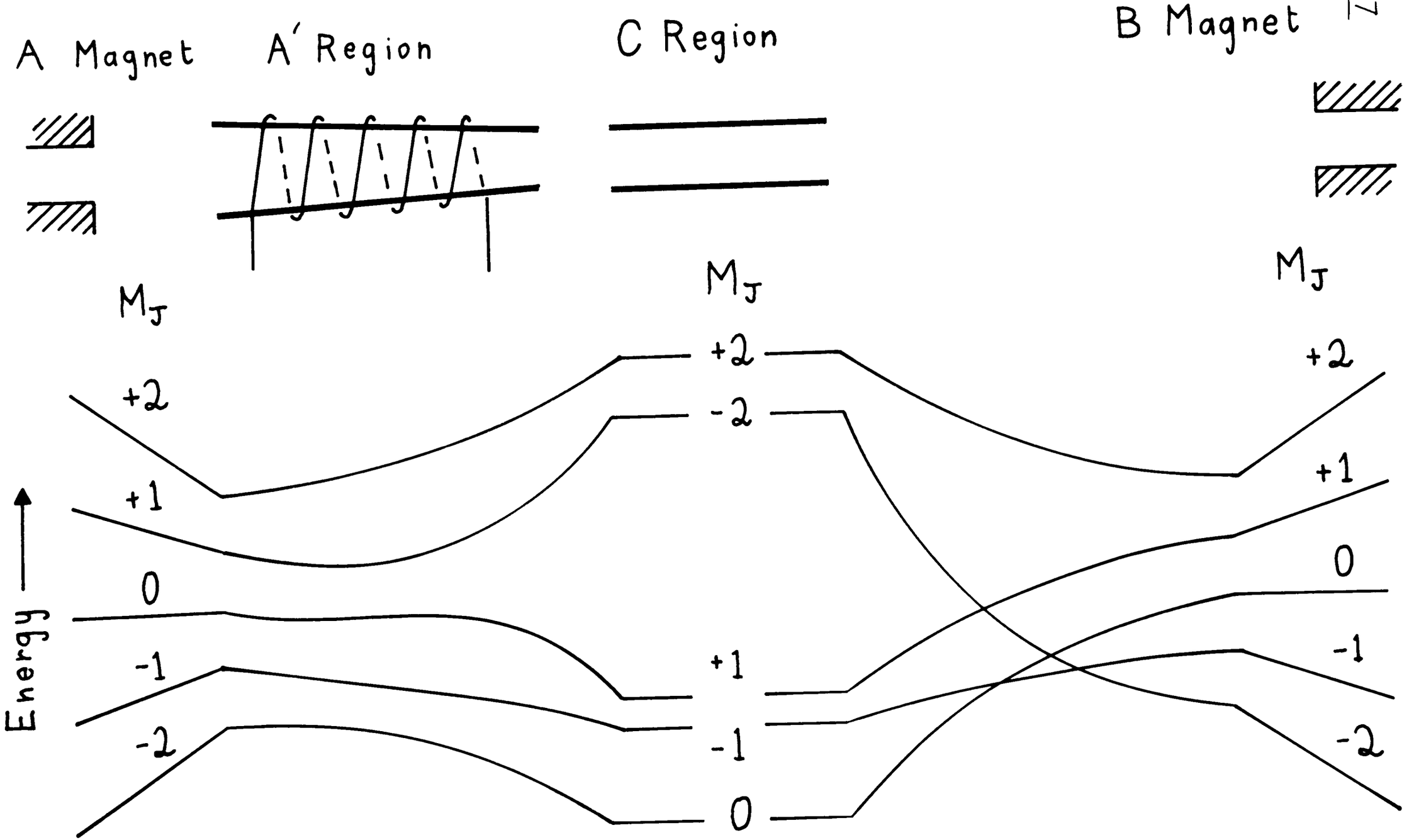
The deflectors are energised by permanent magnets of Alcomax III made by Jessop-Saville Ltd. Fig. 3.5 shows end views of the magnet assemblies. The individual permanent magnets are 2 cm long, and numbers of them are stacked in line along continuous polepieces to give an extended deflector. With the single row arrangement of the A magnet, a field of about 7 KGauss is obtainable in a 3 mm gap; to produce this field over the total length of our deflectors by use of electromagnets would be much less straightforward.

The design of the A magnet polepieces is straightforward. The shape must give a compromise between achieving a high field gradient and allowing a large aperture for the undeflected beam; design was by trial and error. A cross-section of the polepieces is shown in fig. 3.6. The length of the magnet is 32 cm, and the field gradient is $\simeq$ 13 kG/cm. Deflections at the far end of the magnet for atoms with $M_J \neq 0$ are of order 5 mm, and the aperture accommodates a beam 1 cm by 1 mm.

The design of the B magnet is complicated by the requirement that a large entrance aperture must be provided for a beam which is to be deflected. If we attempt to obtain large deflections by using a long magnet, the deflected beam atoms will strike the polepieces unless a large gap is used with consequent loss of deflecting power. The magnet length must therefore be considered in the design compromise. For a given total length of deflection region, it appears that a fairly short magnet is desirable. This gives the atoms angular deflection but little sideways deflection so the gap can be narrow; angular deflection is converted to lateral distance deflection over the remainder of the flight path. The polepieces are shown in fig. 3.6; the magnet is 16 cm long, and the flight path from the end of the magnet to the stop S is 30 cm. The field in the gap is $\simeq$ 9 kGauss and the field gradient $\simeq$ 14 kG/cm. At the stop S, deflections of order 2 mm are obtained, with an estimated transmission efficiency of about

70% for the $M_J = +1$ state. This state is deflected towards the concave polepiece; one expects and finds a better transmission efficiency for this than for $M_J = -1$. This is the reason why we choose to detect $M_J = +1$ atoms.

The Adiabatic Transition Technique



3.5 The A′ transition region

The action of the A′ region may be understood by reference to fig. 3.7, which shows in schematic form the $^3P_2$ energy levels as a function of position along the beam apparatus. In the A′ region, a relatively large magnetic field is applied perpendicular to the electric field, and the perturbation from this is sufficiently large to ensure that there are no level crossing points as the electric field increases through the region. If the adiabatic condition is well satisfied throughout the A′ region, then atoms traversing the region will pass from their initial to final states along the energy level lines of the diagram. As we discuss below, the adiabatic condition requires that the passage from low to high electric field occur in a time long compared with the inverse frequency splitting between levels; this is satisfied by applying the field by means of plates about 15 cm long, with a spacing decreasing from 2 cm to 2 mm. Once the electric field is high enough to make the Stark splitting a few times greater than the Zeeman splitting, the axis of quantisation is nearly parallel to the electric field and a rapid transition can be made to the much higher electric field of the resonance region without violating the adiabatic condition or losing quantisation. Thus the overall effect of the region is to induce the transition $M_J = 0 \rightarrow +1$ with 100% transition probability in those atoms leaving the A magnet with $M_J = 0$.

There is no similar region at the other end of the resonance section; electric and magnetic fields are kept as closely parallel as possible, and the adiabatic condition is violated at crossing points, so that the atoms retain their high electric field quantum numbers on passing to the B magnet.

The condition for the applicability of the adiabatic approximation (see Schiff 1955) is

$$\frac{\langle \psi_k(t) \left| \frac{\partial H}{\partial t} \right| \psi_m(t) \rangle}{\hbar \omega_{km}^2} \ll 1$$

for all k, m, where

$$H(t)\,\psi_k(t) = W_k(t)\,\psi_k(t)$$

$$\omega_{km} = W_k(t) - W_m(t)$$

To obtain an order of magnitude estimate, we put, dropping subscripts

$$H \simeq \alpha E^2 + \mu B$$

$$\frac{\partial H}{\partial t} \simeq \alpha E \frac{dE}{dt}$$

$$\simeq \frac{\hbar\omega}{E} \cdot \frac{dE}{dt}$$

$$\simeq \frac{\hbar\omega}{a} \cdot \frac{da}{dl}\, v$$

where a is the plate separation, l the distance along the plates, and v the beam velocity. The adiabatic condition is then

$$\frac{\omega a}{v} \cdot \frac{L}{a} \gg 1$$

where L is the plate length and a the change of separation. This gives

$$\omega \gg 10^4$$

which corresponds to a transverse magnetic field

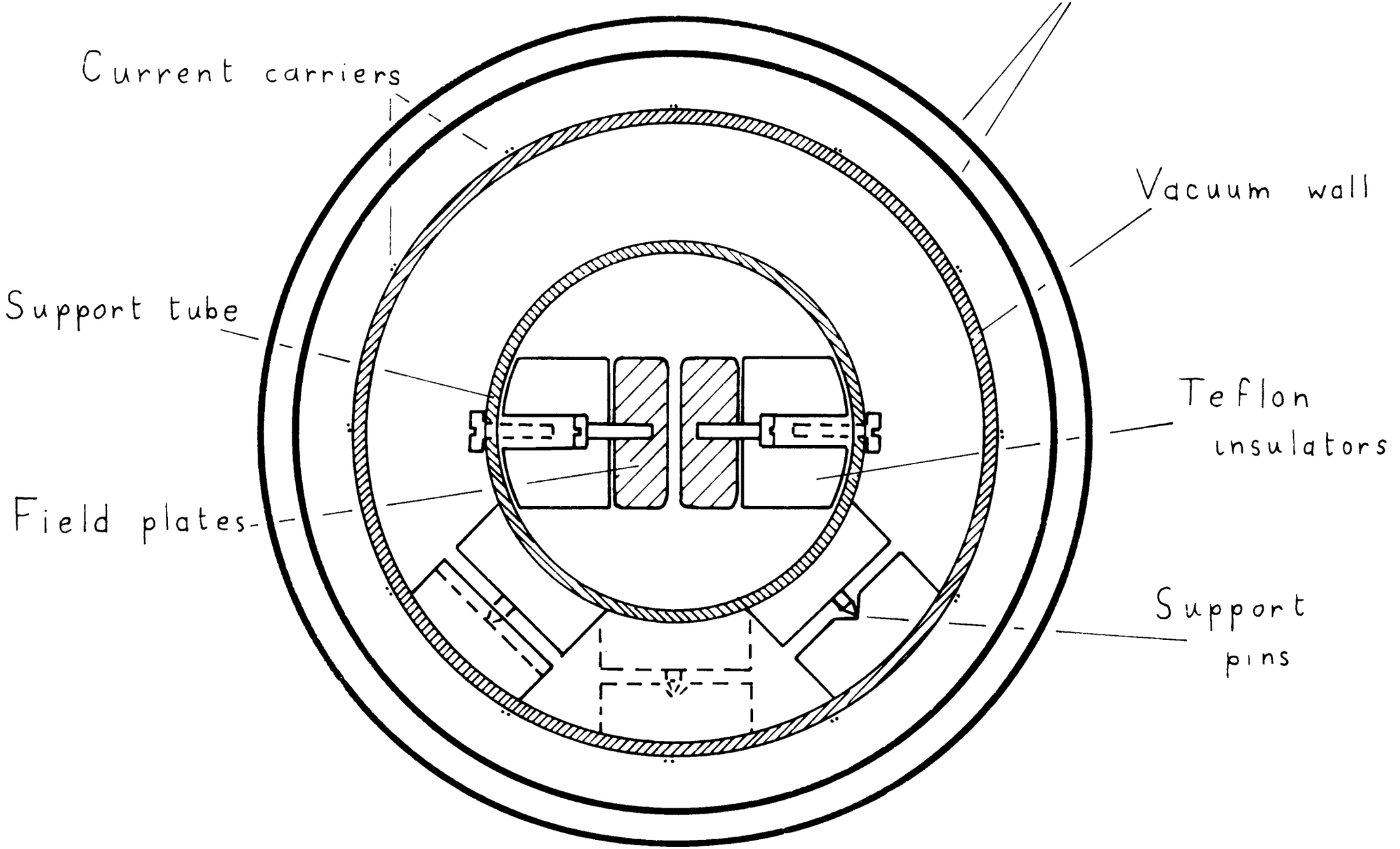
$$B_\perp \gg 10 \text{ mGauss.}$$

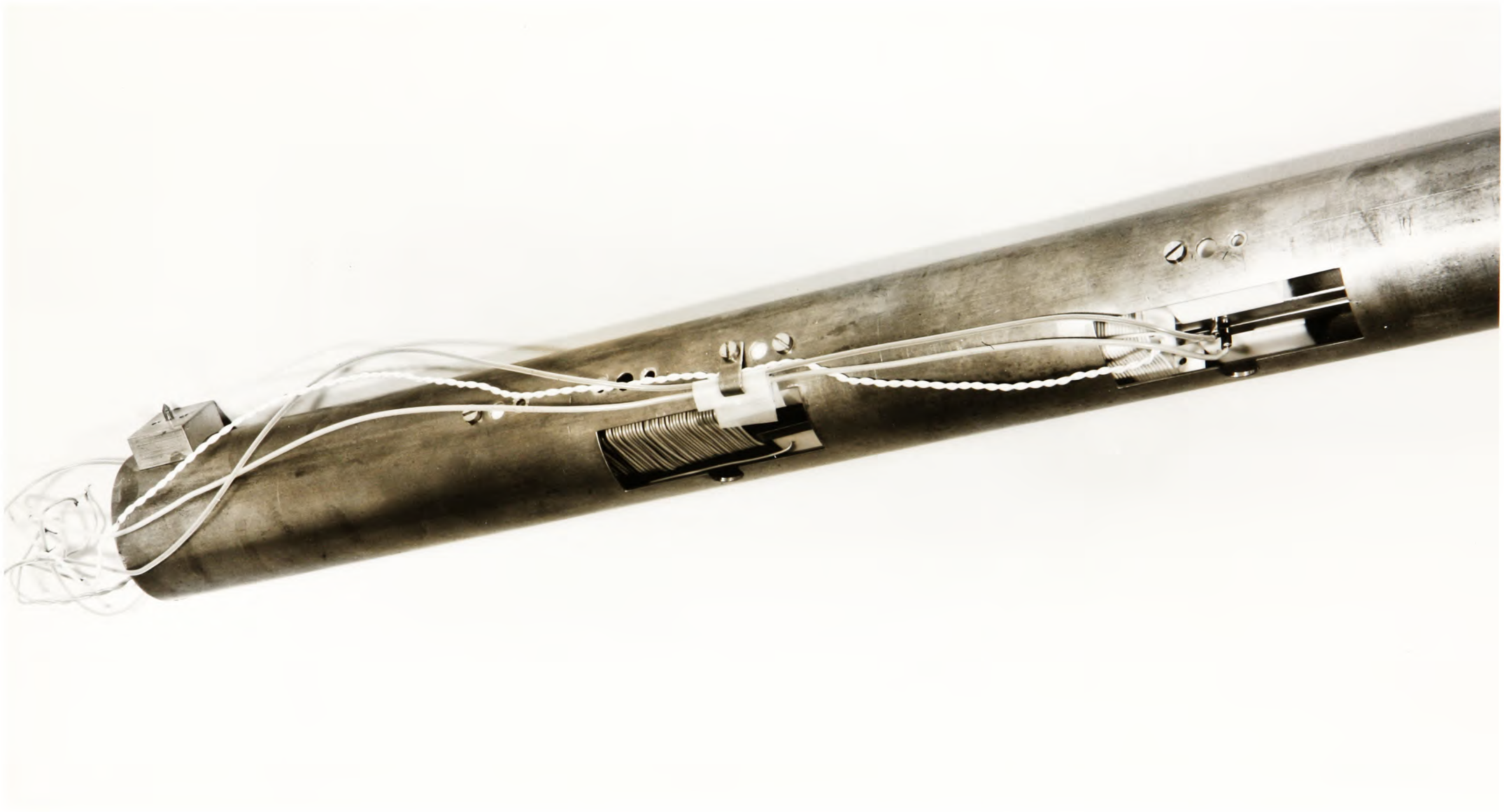
However, this is a serious underestimate, since we have assumed the character of the wavefunctions changes more or less uniformly over the whole level crossing region. Looking at fig. 2.2, we see that the states $M_J = 0, +1$ at low E pass into the states $M_J = +1, -2$ respectively at high E, and do so fairly rapidly. This will involve a large change in $\langle \psi_k(t) | \mu B | \psi_m(t) \rangle$,

and may occur in about 10% of the total electric field range. We conclude we may need $B_{\perp} >> 100$ mGauss. The field actually required is of order 500 mGauss in xenon, the electric field varying between 10^3 and 10^4 V/cm. The magnetic field is applied by a solenoid wound in PTFE insulated wire on the field plates.

We point out that this technique is essentially the well-known method of "adiabatic fast passage" much used in NMR work, though at zero frequency. (See Bloch, 1946; Bloch et al., 1946; and for a theoretical discussion Daniels, 1964). The method also has clear affinities with the "level-crossing" technique of atomic spectroscopy.

Resonance Section





3.6 The Resonance region

A sectional view of the resonance region assembly is shown in fig. 3.8, and a photograph in fig. 3.9.

a) The electric field system

The electric field plates consist of two dural strips each 135 cm long and 2.5 cm high, and each supported by five PTFE insulators 5 cm long. The plates are attached to the insulators by nylon screws, and the insulators are bolted to the brass support tube; there are no spacers between the plates. Pumping speed into the field plate region is increased by providing the support tube with large holes at frequent intervals. The assembly rests on three pins, and may be removed as a complete part.

Lineup is achieved by shimming; a telescope is used to check for straightness by sighting on targets inserted into the gap at various positions. The gap width is about 2 mm.

Performance of the plates seems to depend on their surface finish in an unpredictable manner. Mechanical buffing to a mirror finish leads to low values of breakdown field, while hand polishing using Brasso gives much improved behaviour. With this finish, 10^5 V/cm can be sustained with less than about 10^{-8} A leakage current (as measured by timing the discharge of the interplate capacitance). This occurs only after some initial flashover; we find flashover always occurs after the apparatus has been open to air (see also Fraser 1968). We have also found, with Fraser, that leakage current may be reduced by allowing flashover to occur in a poor vacuum, about 10^{-4} torr of air; but this conditioning is not always needed for 10^5 V/cm. Performance has at times been limited by nonuniform gap width, and by lack of cleanliness in assembly: particles of metal may produce discharging if they find their way onto one of the plates. The PTFE insulators have performed reliably after ultrasonic cleaning in petrol ether, followed by hand cleaning with acetone.

b) Radio frequency loops

The r.f. loops are solenoids of about 50 turns of PTFE covered wire would on PTFE formers supported from the field plates. An r.f. current of about 10 mA is required to give the necessary r.f. field $\simeq$ 100 mGauss. The coils are 5 cm long, and are spaced 120 cm apart.

Extending the treatment of chap. 2.7, the resonance width for a two-quantum double loop pattern should be half that for the corresponding single quantum case. Using the usual formula for a v x Maxwellian velocity distribution (Ramsey 1956)

$$\Delta\nu = \tfrac{1}{2} \times 0.65 \, \alpha \, /L$$

where L is the loop separation and $\Delta\nu$ the full width at half intensity. For a xenon beam at a source temperature of 180°C, we find

$$\Delta\nu = 73 \text{ Hz}$$

while the observed value is 80 ± 10 Hz. This agreement may seem surprising in view of the fact that the velocity distribution is not v x Maxwellian. However, the position of the velocity distribution peak varies by only about 10% between the ideal and actual distributions at the same temperature, and so we may expect a relatively weak dependence of resonance width on the structure of the distribution.

c) The magnetic field system

The magnetic field must have a homogeneity equivalent to $\simeq$ 10 Hz over the beam height in order to avoid degrading the resonance shape. The lowest usable transition frequency is $\simeq$ 50 kHz, as below this power shifts may become important (see chap. 5 below); the magnetic field required is therefore $\simeq$ 20 mGauss with a homogeneity $\simeq$ 10 μGauss over a 1 cm height. We consider first the shielding, then the production of a uniform field.

We use two coaxial mumetal (Permally C) shields made to our design by Magnetic Shields Ltd. The shields are 160 cm long, with radii 6.5 cm and 7.0 cm,

and 1 mm thickness. The design is a matter of standard 2 dimensional potential theory. We find for a single shield of radius b, thickness d and permeability μ

$$R_1 = H_{ambient} / H_{internal} \simeq \frac{\mu d}{2b}$$

The value for two shields is

$$R \simeq R_1^2 \ (1 - b^2/c^2)$$

where c is the radius of the outer shield. We expect in our case $R \simeq 10^3$. We have been unable to measure residual fields when the ambient field is just the earth's field, but $H_{internal} < 1$ mGauss. The inner shield is provided with a 12 turn toroidal defluxing winding which saturates the mumetal at about 40A; current is provided by two Variacs connected in cascade to ensure smooth control down to low currents. Defluxing has been needed intermittently during the life of the system.

The ends of the shields are open, but end effects are in fact rather unimportant as may be seen from the following argument. The general solution of Laplace's equation in cylindrical coordinates, finite at r = 0, has the form

$$e^{\pm kz} \left\{ \begin{matrix} \cos \\ \sin \end{matrix} \right\} m\theta \ J_m (kr)$$

We take z = 0 as the end of the cylinder. We assume the mumetal cylinder may be treated as a magnetic equipotential $\phi = 0$. Well inside the cylinder $\phi = 0$ everywhere. The form of field at z = 0 is not known, but if we take m = 0 the potential corresponds to a uniform field at small r, and we may equate this to the external field as an order of magnitude estimate. Then we must have $J_o (k\,b) = 0$ where b is the cylinder radius. Using this value of k, the external field is reduced to $\simeq 10^{-5}$ its value at z = 0 for $z \simeq 4b$. Other components fall off more rapidly.

We now consider the production of the field. Consider a distribution of

current on the surface of a cylinder of radius a. The current flows parallel to the axis, and the current $I(\theta)\, d\theta$ flows in the segment of surface between θ and $\theta + d\theta$. We first suppose there is no mumetal cylinder, and look for solutions of Laplace's equation for the magnetic scalar potential ϕ_1 inside the current cylinder and ϕ_2 outside. ϕ_1 is single valued, and so is ϕ_2 if we consider only cases for which $\int_0^{2\pi} I(\theta)\, d\theta = 0$. Then we must have

$$\phi_2 \longrightarrow 0 \qquad r \longrightarrow \infty$$

$$\text{finite} \qquad r \longrightarrow 0$$

$$\left.\frac{\partial \phi_2}{\partial r}\right|_a - \left.\frac{\partial \phi_1}{\partial r}\right|_a = 0$$

$$\left.\frac{\partial \phi_2}{\partial \theta}\right|_a - \left.\frac{\partial \phi_1}{\partial \theta}\right|_a = 4\pi I(\theta)$$

where we are specialising to a 2 dimensional case. We attempt to find solutions in terms of cylindrical harmonics

$$\log r\,, \quad r^{-m} \left\{ \begin{matrix} \sin \\ \cos \end{matrix} \right\} m\theta\,, \quad r^{m} \left\{ \begin{matrix} \sin \\ \cos \end{matrix} \right\} m\theta$$

Suppose we take $I(\theta) = I^{(n)} \sin n\theta$. Then suitable solutions are

$$\phi_1 = A_1 r^n \cos n\theta$$

$$\phi_2 = A_2 \frac{1}{r^n} \cos n\theta$$

with

$$A_1 = \frac{2\pi I^{(n)}}{n} \frac{1}{a^n}$$

$$A_2 = -a^{2n} A_1$$

If $n = 1$, ϕ_1 corresponds to a uniform field in the x (i.e. $\theta = 0$) direction, ϕ_2 to the field produced by a dipole at the origin oriented along the x direction.

Using these results, we may solve for a more general distribution using Fourier analysis. We consider a system of N wires equispaced round the cylinder, starting at $\theta = 0$, carrying currents $i = i_o \sin\theta$. We write

$$I(\theta) = i_o \sin\theta \sum_{n=0}^{N-1} \delta\left(\theta - 2\pi \frac{n}{N}\right)$$

$$= \frac{N i_o}{2\pi} \sin\theta - \frac{N i_o}{2\pi} \sin(N-1)\theta + \ldots$$

We retain only these two terms, as the second provides the lowest order inhomogeneity. Using this to get ϕ_1, we see that the field near the origin is given by

$$\underline{H} = \underline{H}_o + \Delta \underline{H}$$

where $$\underline{H}_o = \frac{N i_o}{a} \hat{\underline{x}}$$

$$\Delta H \simeq H_o \left(\frac{r}{a}\right)^{N-2}$$

The same order of magnitude is obtained if the wires are at $\theta = (n + \frac{1}{2}) \frac{2\pi}{N}$.

For N = 6, we have a 2 dimensional Helmholtz coil with 4 wires at $\theta = 60^\circ$, 120° etc (at $\theta = 0$ the wires carry no current) or a less conventional 6 wire arrangement with wires at $\theta = 30^\circ$, 90°, 150° etc. We have had to use nothing more elaborate than these systems, but it is to be noticed that better arrangements can be set up with little more effort; it was in designing such a coil for another experiment that the above solution was adopted.

The effect of the mumetal shield must now be considered. We take a continuous current distribution $I(\theta) = I^{(1)} \sin\theta$ and assume the mumetal to be a perfect equipotential. We neglect end effects for the moment and still use a 2

dimensional formalism. In the absence of mumetal

$$\phi_2 = -2\pi I^{(1)} \frac{a}{r} \cos\theta$$

which may be considered to be produced by a dipole at the origin

$$\underline{d} = -2\pi I^{(1)} a \hat{\underline{x}}$$

The image of such a dipole is simply deduced from the image of a linear charge (Bleaney 1957). If the centre of the shield lies at Y along the y axis, the image dipole lies on the y axis at $Y_{im} = b^2/Y$ and has a moment

$$\underline{d}_{im} = \underline{d} \frac{b^2}{Y^2}$$

The field at the origin due to the image is

$$\underline{H}_{im} = -\frac{\underline{d}_{im}}{Y_{im}^2} = 2\pi I^{(1)} \frac{a}{b^2} \hat{\underline{x}}$$

with a gradient

$$\frac{\partial \underline{H}_{im}}{\partial y} = 2\underline{H}_{im} \frac{Y}{b^2}$$

This vanishes at Y = 0. Using a potential treatment, it can be shown all higher gradients vanish also. For an N wire field we have at the origin, therefore

$$\underline{H} = \frac{N i_o}{a} \left(1 + \frac{a^2}{b^2}\right) \underline{x}$$

with a first gradient $\simeq H \frac{Y a^2}{b^4}$. The importance of making the shield coaxial with the current cylinder, and also truly cylindrical, is clear.

The end effects for the system are negligible by the same discussion as given for the shielding. This is a very positive benefit of the mumetal.

The practical field production setup utilises 12 equispaced grooves about 0.5 mm wide cut in the surface of the cylindrical vacuum chamber (a = 5.5 cm). These are used to position double cotton covered wires (two wires per groove) which are secured by Durofix. The wires must be within 0.1 mm of their nominal position to obtain the required homogeneity. This is also the requirement on the positioning of the shield, which is supported on the vacuum chamber by accurate annular dural spacers. The arrangement of wires allows one main N = 6 coil to produce horizontal field (1 wire at 30°, 150°, 2 at 90° etc., all in series), a Helmholtz coil to produce a vertical field, a coil to provide field modulation for calibration purposes, and four wires at $\theta = 60^{\circ}$, 120° etc all passing current in the same sense; this provides shimming for residual vertical inhomogeneity.

The main coil provides up to about 200 mGauss at a field to current ratio of about 450 mGauss/A. An 80 Hz Ramsey resonance is not visibly distorted at 50 kHz transition frequency if about 1 mA shimming current is provided, corresponding to an inhomogeneity of about 2×10^{-5} G/cm. Long term drifts in resonance frequency are of order 100 Hz i.e. 10^{-4} G.

3.7 The detector

As is well known, metastable atoms are able to eject electrons on collision with a suitable metal surface. This forms the basis of our detector.

The physics of such processes have been discussed by many authors (notably Hagstrum 1956) and a summary is given by Kaminsky (1965). The basic description is as follows. We represent the atom by A, its first ion by A^+ with ionisation potential I, and its metastable state by A*, excitation energy M. The metal work function is ϕ and the N electrons in the metal are represented by e_m^-. Then as the atom A* approaches the surface, two nonradiative processes may become possible:

a) $$A^* + N e_m^- \longrightarrow A + e^- + (N-1)\, e_m^-$$

which can occur for $M > \phi$; this is Auger deexcitation.

b) $$A^* + N e_m^- \longrightarrow A^+ + (N+1)\, e_m^-$$

which can occur for $I - M < \phi$; this is resonance ionisation. In this case, the ion A^+ may escape or it may suffer Auger neutralisation:

c) $$A^+ + (N+1)\, e_m^- \longrightarrow A + e^- + (N-1)\, e_m^-$$

if $I - 2\phi > 0$.

Hagstrum (1956) has shown that the two-stage process of b) followed by c) is most favoured for rare gas metastables incident on a refractory metal surface.

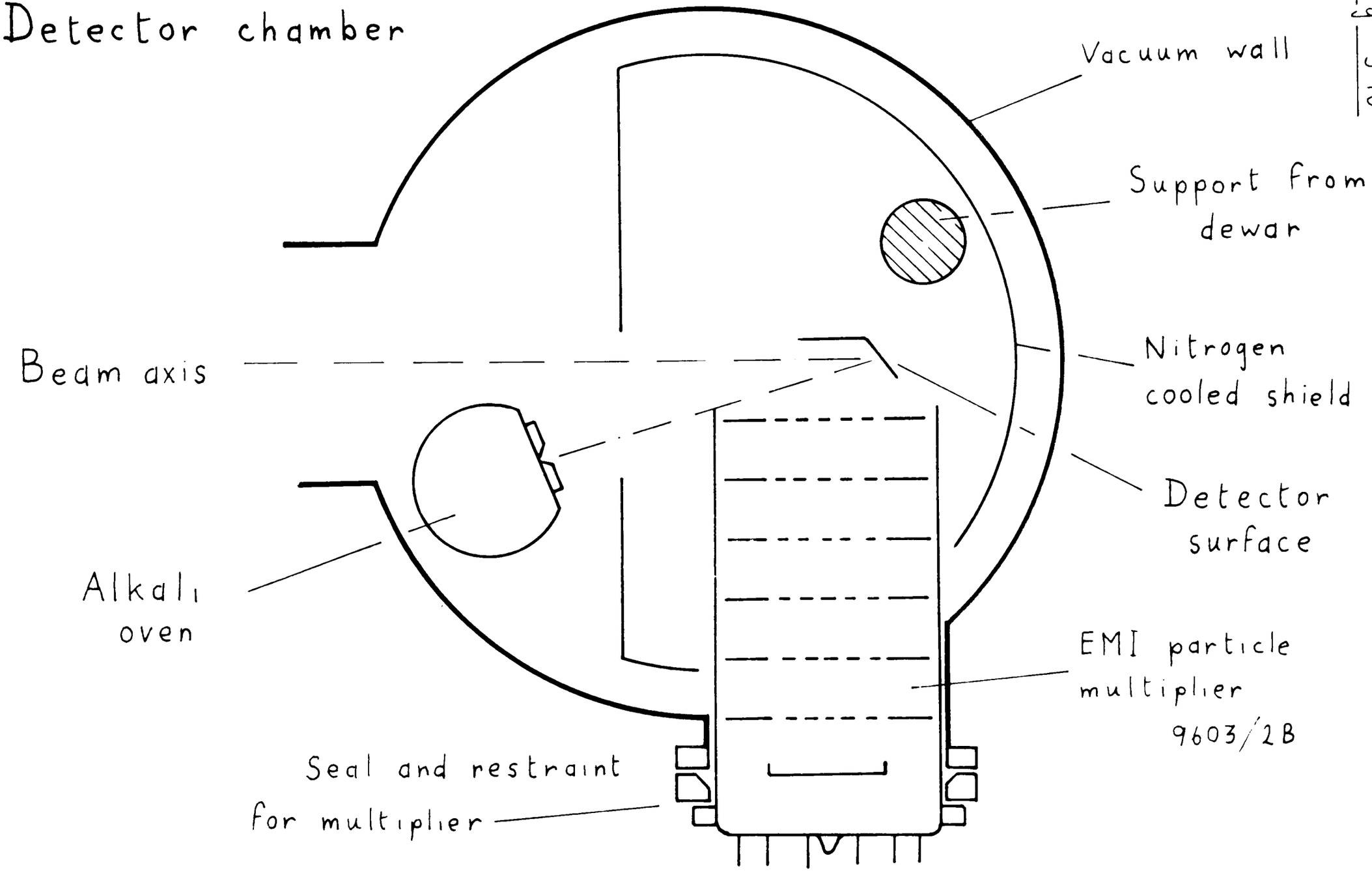
Our first detector was simply the first BeCu dynode of an EMI "venetian blind" electron multiplier type 9603/2B. This gave good performance with argon, but the detected beam of xenon was about 50 times smaller, despite the fact that $I - M < \phi$ and $I - 2\phi > 0$ are both well satisfied for both elements:

A	: $I = 15.8$ eV	$M = 11.6$ eV	$I - M = 4.2$ ev
Xe	: $I = 12.1$ eV	$M = 8.5$ eV	$I - M = 3.6$ eV

$$\phi \simeq 4.5 \text{ eV}$$

Fig 2.10

Detector chamber



We were unwilling to believe the discharge source gave much poorer performance in Xe than in A, and supposed that positive ions of Xe might be produced with greater efficiency at a tungsten detector (Varney, 1968). We were however unable to detect any positive ion emission of argon or xenon from tungsten or oxygenated tungsten.

With this matter unresolved, we turned to the well-known technique of using a continuously-sprayed alkali metal surface to achieve a low ϕ . In this way we obtained about a factor of 50 improvement in beam intensity in Xe, with a slight increase in A.

The detector chamber is shown in fig. 3.10. The detector surface is cooled to liquid nitrogen temperature to ensure that the sprayed alkali adheres well and does not emit thermionic electrons. The geometry and the liquid nitrogen shielding are designed to prevent alkali reaching and ruining the electron multiplier dynodes. No deterioration in multiplier performance has been noticed after running times $\simeq$ 100 hours. The nitrogen shield and dewar are electrically insulated from the vacuum chamber, and the detector surface is supported from the shield by a sapphire rod (which is an electrical insulator with a high phonon thermal conductivity at liquid nitrogen temperature). The alkali oven is essentially identical with the oven described by Harrison (1969). It is heated by a temperature controlling supply (appendix D).

The first arrangement of potentials tried was: shield earthed, detector earthed, first dynode $\simeq$ + 500 V. Pulses from the multiplier anode, which is at about + 3kV, are preamplified and transformer coupled out for counting (see chap. 4). This setup gave a large background count of thermionic electrons from the oven. We then tried first dynode earthed, detector surface $\simeq$ -500 V, shield variable. Using cesium, a large background ($\simeq 10^7$ counts/sec) was observed, independent of shield potential. At this stage we received a private communication from Lurio, who attributed the effect to chemical reaction of oxygen with the cesium

surface, the energy of reaction being sufficient to eject electrons. This was verified by the observation of a beam of ground state air using the cesium surface as detector. This effect is almost completely absent with potassium, while the detection efficiency for Xe metastables is close to that using cesium; we have used potassium throughout following this observation.

Fig 3.11

Ramsey Pattern

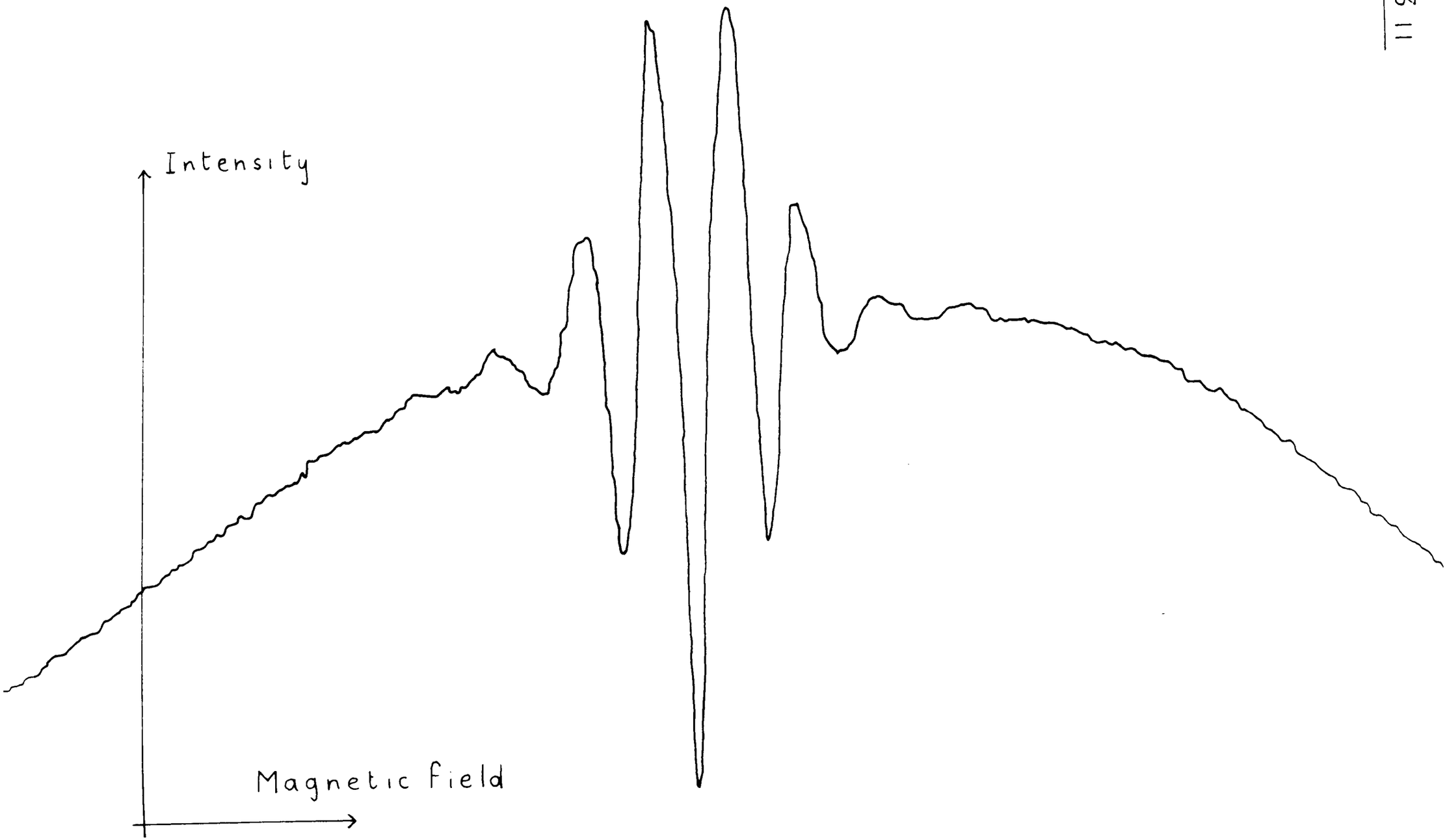
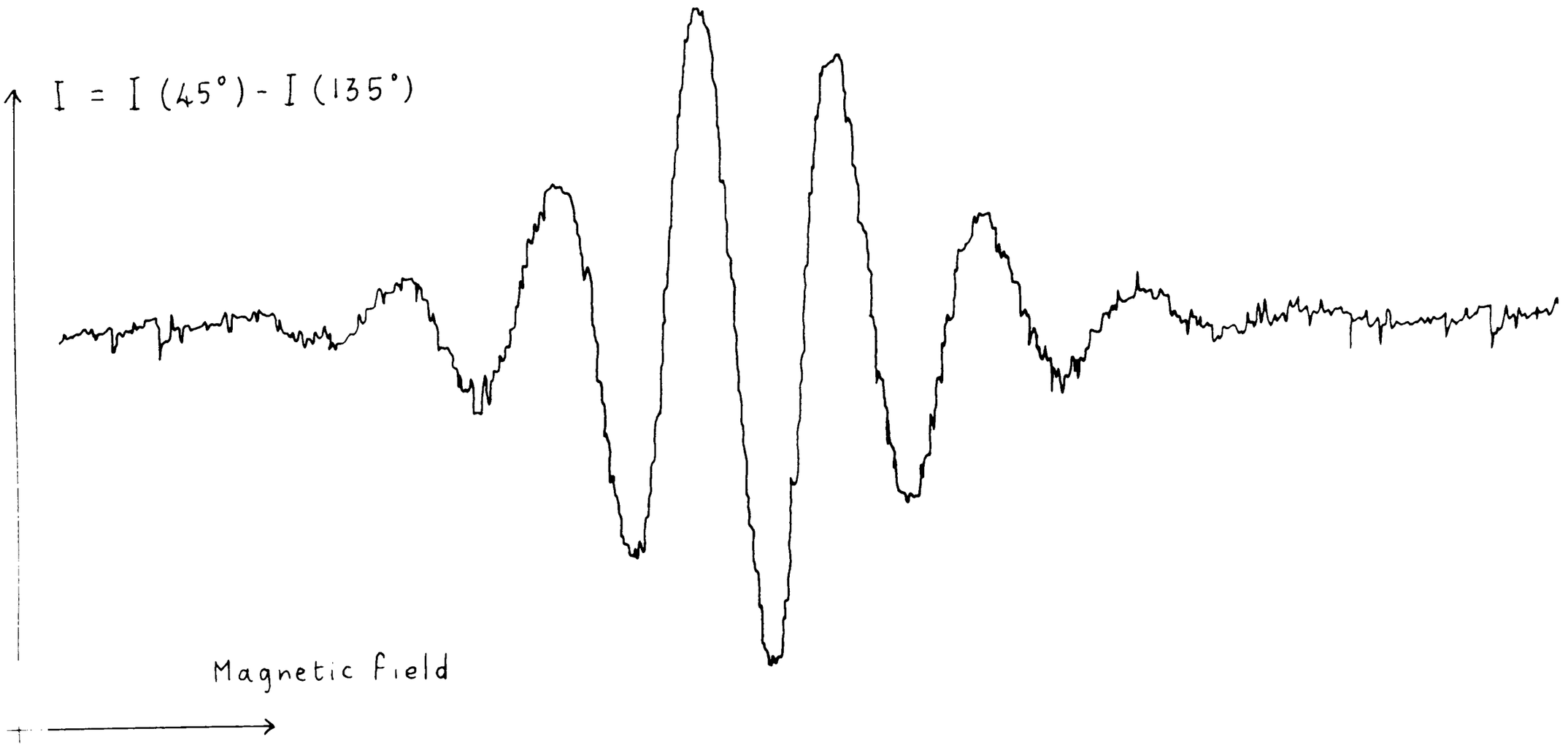


Fig 3.12

Phase-switched Two-quantum Ramsey



3.8 Summary of performance

The observed Ramsey resonance width for the $M_J = +1 \longrightarrow -1$ transition in xenon is

$$\Delta \nu = 80 \pm 10 \text{ Hz}$$

(full width at half intensity). The width increases inversely with square root of mass for lighter elements. Typical Ramsey patterns in argon are shown in fig. 3.11 and 3.12. Both figures are the result of several sweeps, using a signal averaging program on the PDP-8 (Harrison, 1969). Fig. 3.12 actually shows the difference in intensity for different relative phases of the r.f. currents in the two loops. As the frequency sweep was made, the relative phase was at each point switched between 45° and 135° and the difference in signal stored. These values of phase correspond to 90° and 270° for a single quantum Ramsey, and lead to a dispersion type curve.

The detected resonance intensity is 7×10^5 counts/sec on an equal background in Xe, improving to 1.5×10^6 counts/sec on 1×10^5 counts/sec background in Kr and A. The background in A and Kr is almost entirely photons. In Xe it is mainly atoms; presumably these belong to odd isotopes and are insufficiently deflected by the A-magnet. Using Ne, the source chamber pump is insufficiently fast and the signal falls to 10^5 counts/sec. The $^3S_1$ state of He can be obtained, with an $M_J = 0 \longrightarrow +1$ resonance of about 10^4 counts/sec on 10^5 counts/sec background.

Apparatus running time is limited mainly by destruction of the source filament by positive ion bombardment. The lifetime using Xe or Kr is $\simeq$ 20-30 hours, and is shorter in A.

Chapter 4. Techniques of data collection

Part I. Basic method

4.1 Detection of small resonance shifts

We wish to observe shifts in resonance frequency arising from an edm interaction. The basic technique for the observation of small shifts is to set the radio frequency to the point of greatest slope on the resonance and look for changes in signal intensity; in the case of a dispersion-type Ramsey resonance, this point is the centre of the resonance pattern. If the change in count rate of the detected signal between top and bottom of the resonance is I_{res}, and the resonance width is $\Delta\nu$, a shift $\delta\nu$ in frequency leads to a change in count rate

$$\delta I \simeq \delta\nu \frac{I_{res}}{\Delta\nu}$$

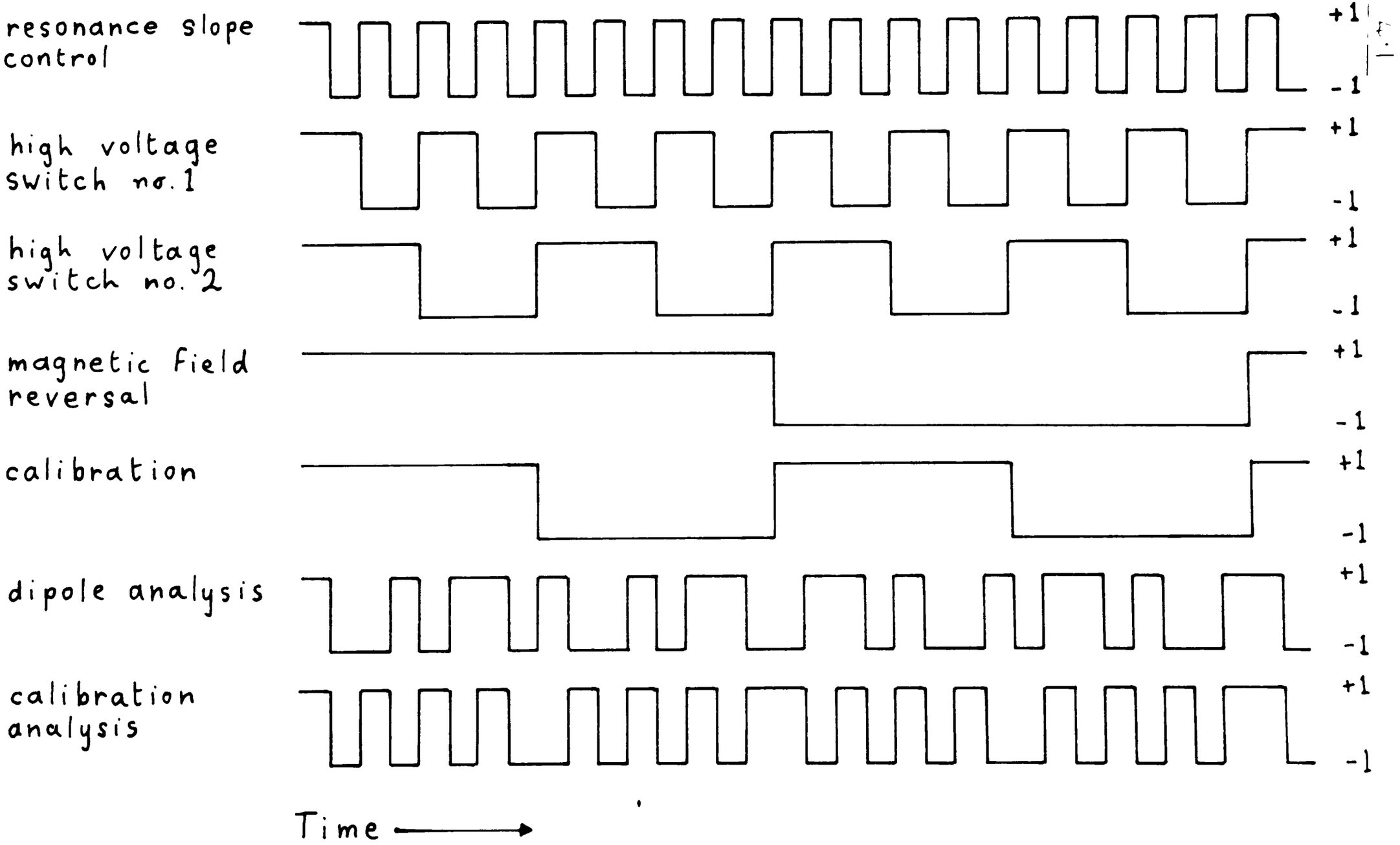
In an ideal system, the smallest detectable change δI should be limited by particle counting statistics. It is well known (see e.g. Parzen, 1960) that the arrival of particles at the detector is, if the arrivals are truly random, described by a Poisson distribution which tends to a Gaussian distribution for large numbers of detected counts. If one detects for a time T a mean count rate I_{av}, the expected number of counts $N = I_{av}T$ is subject to an expected standard deviation $\sqrt{N}$. Therefore in the time T one should be able to detect changes in I of order $\sqrt{(I_{av}/T)}$, and thus resonance shifts

$$\delta\nu \text{ (minimum)} \simeq \frac{\Delta\nu}{I_{res}} \times \sqrt{\frac{I_{av}}{T}}$$

It is clear from these facts that to observe a small shift it is necessary to integrate data over long times. Also, the electric dipole shifts are likely to be obscured by various systematic effects, and for this reason it is desirable to use a fairly complicated data collection system. This has led to the use of a PDP-8

computer which allows a system of suitable sophistication to run automatically for many hours. Because the signal is collected and handled in digital form, there is no degradation of information nor introduction of spurious instrumental effects over the longest integration times.

Simple Control and Analysis Waveforms



4.2 A simple data analysis system

We now describe a somewhat simplified version of the data analysis system in use.

If an edm interaction is present, a shift in resonance frequency and hence a change in detected signal intensity should occur on reversing the electric field. However, a change will also occur if the overall beam strength depends on the electric field direction. To separate these effects, we must collect data with the sign of the resonance slope reversed, and use the fact that the change in signal due to a frequency shift reverses sign with the resonance slope, while pure intensity effects remain unaltered.

It is easy to take this further and eliminate other spurious effects by reversing more parameters of the system. One spurious effect can arise from inaccurate reversal of the electric field, which leads to an edm-like shift if the resonance frequency has any dependence on the electric field magnitude; However, any such shift is independent of magnetic field direction, in contrast to a true edm effect, and so it may be eliminated by collecting data with both signs of magnetic field. Similarly, spurious shifts associated with the switch used to reverse the electric field may be eliminated by periodically reversing the high voltage connections to it with a second switch; true edm effects will change sign, while magnetic field and other shifts associated with the first switch remain unaltered.

We show in fig. 4.1 a set of switching waveforms which could be used in an automatic system based on these ideas. The top four waveforms are used respectively to reverse the resonance slope, the two high voltage switches, and the direction of the magnetic field. Consider the analysis required to extract from the signal at the detector any component due to an edm shift. By the discussion given above, any such shift will lead to a modulation of the signal proportional to the product of these four switching waveforms. Hence, if we multiply the incoming

signal with an analysis waveform equal to this product, we shall obtain a signal whose steady component is proportional to the edm shift. This analysed signal will also contain periodic components arising from the various shifts which we are trying to avoid, and, of course, from the analysis waveform itself. All these periodic components may be eliminated by taking the average of the signal over a whole number of periods of the slowest switching waveform. This average will give the required steady component with, of course, noise.

To find the absolute size of the edm shift, we use the calibration waveform shown in fig. 4.1 to modulate the magnetic field by a small, known amount; an analysis waveform constructed from the product of calibration and resonance switching waveforms will extract a signal whose steady component is proportional to the resulting resonance Zeeman shift. The size of the edm shift can be obtained by comparing the two signals.

One very important feature of these waveforms is an orthogonality property. Consider the dipole analysis waveform; it is orthogonal, over a complete period of the slowest waveform, to all the control waveforms and to all products of them (except the one used to construct it). It is this basic feature which leads to the cancellation of spurious effects. It also means that, for instance, the calibration modulation does not affect the output obtained by use of the dipole analysis waveform; thus the dipole and calibration analyses can proceed simultaneously. This can be extended to further parameters; for example, we have monitored the dependence of the resonance frequency on the magnitude of the electric field by modulating the field magnitude with a waveform orthogonal to the field reversal waveforms.

One further signal, very important in practice, is obtained by analysing with a waveform identical to that used for switching the resonance slope. This gives an output whose steady component is zero only if the resonance is set correctly, so that on average the reversal of slope does not alter the beam intensity.

A non-zero output can be fed back to the magnetic field coil supply to maintain the optimum resonance position despite long term drifts in the magnetic field strength or oscillator frequency. Again, one must average over a complete number of analysis waveform periods to obtain the feedback signal, and the average should extend over a complete number of cycles of the control waveform for a particular parameter if shifts associated with the parameter are not to be cancelled out. It is best to feed back the integral of the error signal so that no static error in resonance position occurs however large the drifts.

4.3 Method of orthogonal waveforms

One can introduce control and analysis waveforms of a more complicated general type than those used in the above example. If we write $S_Q(t)$ for such a waveform, where Q denotes a set of positive integers, then

$$S_Q(t) = \prod_n \delta_n(t)$$

where n is a member of the set Q, and $\delta_n(t)$ is a square wave of period $\tau_n = 2^n \times \tau$ where τ is a basic period. Thus

$$\delta_n(t + \tau_n) = \delta_n(t)$$

$$\delta_n(t) = +1 \quad 0 \leq t < \tau_n/2$$

$$= -1 \quad \tau_n/2 \leq t < \tau_n$$

$$\tau_n = 2^n \times \tau$$

Thus the waveform consists of a product of square waves, each possible member of the set of square waves having twice the period of the preceding member. We specify the set Q by a bracket like (1011011) where a 1 in the n^{th} position from the right denotes the presence of n in the set Q. If we have a number of such waveforms with the same basic period τ, and the longest period involved is τ_N, then over the period τ_N all the waveforms are mutually orthogonal and have average value zero. These are just the properties required in an analysis system of the type described above. They were first introduced by Angel (1967). The use of such waveforms gives some advantages over the use of simple square waves, as we now describe.

First, the additional complexity reduces the probability of spurious effects arising from switching transients. To see this, suppose that whenever high voltage switch no.2 changes from state +1 to -1 the beam intensity is momentarily reduced; with the simple waveforms of fig. 4.1, this always occurs when the resonance switch has just reached the +1 state, and high voltage switch 1 is in the +1 state,

so that there is a systematic beam modulation occurring for one particular sign of resonance slope and electric field - i.e. an apparent edm effect. Such an effect is likely to be only partially cancelled by magnetic field reversal, but clearly it is eliminated by periodic phase reversals of the waveforms involved; such reversals will occur using the more general control waveforms.

The other properties of these waveforms concern the noise performance of the system. It is fairly straightforward to see that for pure random shot noise the periods and structure of the analysis waveforms have no influence on the noise performance (Angel, 1967). However, in any practical system there are additional sources of noise: we distinguish between random noise, whose statistical parameters we shall suppose are time independent, and non-random noise such as slow drifts due to some systematic change in some part of the system, or 50 Hz pickup.

Consider random noise. We express the noise output from the detector in terms of a variable y(t) with a power spectrum w(f). For shot noise, y(t) ideally consists of infinitely sharp pulses occurring at random times and, as is well known, it follows that w(f) is a constant (see e.g. Robinson, 1962). For other types of random noise such as source or detector fluctuations, magnetic field noise, or noise induced by vibrations of the apparatus, this is not so. In general, we may make the connection between frequency spectrum and displacement using a theorem of MacDonald (1949, 1962): if

$$Y(T) = \int_t^{t+T} y(t)\, dt$$

then
$$\langle Y^2(T) \rangle = 2 \int_0^\infty \frac{w(f)}{4\pi^2 f^2} (1 - \cos 2\pi f T)\, df$$

or
$$\frac{\partial}{\partial T} \langle Y^2(T) \rangle = 2 \int_0^\infty \frac{w(f)}{2\pi f} \sin 2\pi f T\, df$$

The pointed brackets denote the ensemble average, or statistical expectation value.

Now, if we know w(f) for the noise from the detector, then we may find W(f) for the power spectrum of the noise after multiplication by an analysis waveform S(t), and hence find the expected integrated or averaged signal due to noise in the relevent analysis channel after some time T. It is straightforward to find for W(f)

$$W(f) = \tfrac{1}{4} \sum_n a_n^2 \quad \{ w(f_n - f) + w(f_n + f) \}$$

where a_n and f_n are the amplitude and frequency of the n^{th} Fourier components of the analysis waveform. We note that $[S(t)]^2 = 1$, and so by averaging over a complete period we obtain the relation

$$1 = \tfrac{1}{2} \sum_n a_n^2$$

Now, suppose w(f) = w, a constant. Then

$$W(f) = \tfrac{1}{4} \times \sum_n a_n^2 \times 2w$$

$$= w$$

Using MacDonald's theorem, we obtain

$$\langle X^2(T) \rangle = \tfrac{1}{2} wT$$

where X(T) is the integrated value of the signal after multiplication by the analysis waveform. This agrees with our remark that shot noise is unaffected by the waveform structure.

As another special case we consider a $1/f$ type noise spectrum, which characterises much low frequency noise. Writing

$$w(f) = K/f$$

we find

$$\langle X^2(T) \rangle = \tfrac{1}{4} \sum_n a_n^2 \frac{2K}{f_n} \times T$$

if T is a complete number of periods of the analysing waveform. We see at once from this that high frequency analysis waveforms reduce the effect of low frequency noise.

To consider other types of noise spectrum it is only necessary to integrate using MacDonald's theorem. Such integrations are best performed by contour integration (see e.g. Phillips, 1940). For those familiar with these methods, we give the following discussion. The form of the integral depends on the poles of W(z) where z is a complex variable. If W(z) has no poles on the real axis, then the contributions of the poles to the integral fall off exponentially for sufficiently long T. The value of the integral then depends only on the value of the integrand at the origin, where $\frac{1}{z} W(z)\, e^{2\pi i z T}$ has a simple pole. This is not surprising as $\frac{1}{f}\sin 2\pi fT$ approaches a δ-function as $T \longrightarrow \infty$. For the more singular case where W(z) has poles on the real axis this result does not hold so obviously. However, if the singularities in W(f) correspond to singularities in w(f) at the origin, which is the only physically possible case, then the effects of the poles cancel if T is a complete number of periods of S(t). This just means that w(f) is allowed to have a value at f = 0 corresponding to a finite steady value of y(t), which will be cancelled by analysis only if integration is over a whole number of periods. This is the case for the $\frac{1}{f}$ spectrum. We conclude that

$$< X^2(T) > \;=\; \tfrac{1}{2} \sum_n a_n^{\,2}\; w\,(f_n)\; x\, T$$

for T much longer than any relaxation times associated with the noise sources. Unfortunately this result is not very easy to apply as our $S_Q(t)$ have a rather complicated Fourier expansion in general. However, consider the case of a square wave having N periods (N even) in a time T. Most of the contribution to $< X^2(T) >$ comes from the fundamental $f_n = \frac{N}{T}$ if w(f) has no marked peaks at higher harmonics. If $S_Q(t)$ is now taken as the product of this square wave

with one of frequency $\frac{1}{T}$, the fundamental is now at frequency $\frac{1}{T}$ but it is easy to show that its amplitude is $\simeq \frac{1}{N}$ times that for the original square wave fundamental. Most of the power of $S_Q(t)$ is concentrated at frequencies $\frac{N \pm 1}{T}$. Thus even for a $\frac{1}{f}$ spectrum, the introduction of a new product square wave in S_Q makes little difference to the noise performance; this conclusion may be expected to hold unless w(f) shows very sharp peaks. We expect then

$$< X^2(T) > \simeq \tfrac{1}{2} w(f_o) \times T$$

where f_o is of order the fastest square wave frequency in the analysis waveform:

$$f_o \simeq 1/\tau$$

These results are now very rule of thumb, and are likely to be particularly inaccurate if w(f) shows sharp peaks. In any case, we expect that the basic period τ of the waveform will have more effect on the noise performance than any changes of waveform structure, but this is again only rule of thumb.

These unfortunately vague results do not suggest any advantage for complicated analysis waveforms in dealing with random noise. The position is more clear cut for non-random noise. Harrison (1969) has proved the following theorem for slow drifts: for each basic square wave period included in the product waveform, one more successive term in the Taylor expansion of the noise is eliminated. It is also readily shown, using a Taylor expansion, that decreasing τ improves the rejection of slow drifts as may be expected. Harrison's theorem demonstrates a distinct advantage for complicated waveforms, especially in the presence of exponentially time dependent drifts. A simple square wave will give a steady output in the presence of a steady linear drift and is therefore particularly dangerous.

For non-random noise of higher frequency, one expects little effect unless

the frequency is very close to a Fourier component of the analysis waveform.

We note here that the digital techniques used for signal processing introduce negligible noise.

4.4 Practical system

We now give an outline of the actual system used to implement these techniques, before describing some aspects of it in greater detail.

The signal from the detector consists of pulses and so is already in essentially digital form. After amplification and shaping, the pulses are counted into an input buffer whose contents may be read into the computer. The counting and reading cycle is controlled by a crystal clock, which also provides a timebase for the control and analysis waveforms. A gate, also clock controlled, is used to ensure that no data is collected while switching is actually occurring, so that transient effects may be avoided; it is particularly important to avoid charging current effects associated with electric field reversal. We note that this is very difficult with a sine-wave type of phase sensitive detection system. The logic for the production of the control and analysis waveforms is supplied by the computer, which also analyses the incoming signal.

Analysis is performed as follows. For each channel associated with an analysis waveform $S_Q(t)$, the input signal is added to a store in the computer during times for which $S_Q(t)$ is positive, and subtracted during times for which $S_Q(t)$ is negative. This store therefore contains in digital form the integral of the signal multiplied by $S_Q(t)$. In 4.2 we discussed the operation of the system in terms of average levels; in practice it is quite convenient to retain the signals in integrated form, although averaging would present no difficulty.

The analysed, integrated signals are periodically printed out on a Teletype under computer control; this must occur only after a whole number of analysis periods. Also printed out at this time are the total number of detected counts N and the expected standard deviation of the analysis results, $\sqrt{N}$; this gives a comparison between ideal and actual noise performance.

The control waveforms and resonance locking feedback signal are output

from the computer into buffers whose contents are externally available. Each control waveform involves just a single digital bit, while the feedback signal is a twelve bit digital word which must be decoded to an analog signal.

All timing periods and waveform structures may be controlled by the operator from the Teletype keyboard.

Part II. Computer hardware and instrumentation

4.5 The PDP-8 computer

The computer is extensively described in the handbooks of the manufacturer, the Digital Equipment Corporation. We give here a brief outline of its organisation and operation, viewed from the user's standpoint.

The computer consists of two main sections: the memory and the processor. The memory is capable of storing 4096 twelve bit words, and is used to store both program and data. The processor contains the system logic and several registers, the main ones being the program counter (PC), memory address (MA), memory buffer (MB) and accumulator (AC). These are all 12 bit registers. The PC is used to control the execution of the program. Its contents specify the address of the memory word which will constitute the next program instruction. The MA is used to reference the actual location in the memory whose contents are to be used or modified. The MB acts as an interface between the memory and processor; words read from the memory or words to be written into the memory are contained in the MB. The AC is the main arithmetic register; addition, negation and various shifts can be performed using it. A second arithmetic register, the multiplier quotient (MQ), is used in multiplication, division and various shift operations. The basic arithmetic is 2's-complement binary.

When the machine is in operation, the contents of the PC are used to bring a word into the MB from the memory. This is viewed as an instruction and is decoded by the logic of the computer . The available instructions fall into several types: they may specify operations to be performed on the contents of the AC or MQ; logical or arithmetic operations to be performed jointly on the contents of the AC and a memory location specified by part of the instruction code; or they may act as "decision" instructions in which the contents of the PC (and hence the subsequent program operation) are altered according to the status of the AC or a specified memory location; they may also transfer control to program

starting at a specified location. Following the execution of one instruction, the contents of the PC are normally incremented and the next instruction fetched. The transfer of a word to or from memory occurs in 1.5 μsec; the complete execution of an instruction typically 3 or 4 times this.

The PDP-8 is designed to operate in an "on-line" system; that is, it has features which allow it to interact readily with its environment of peripheral equipment. This involves both the transfer of data into and out of the computer and an "interrupt" system whereby a piece of peripheral equipment can request attention from the computer. Data may be transferred directly into and out of the memory ("data-break" facility) while the program execution is momentarily halted but not otherwise modified, or it can be transferred into or out of the AC under program control. We have used the latter method. The 12 output and 12 input lines are available to all peripherals.

Transfer of data is accomplished by a special type of program instruction known as an input/output (IO) instruction which contains an address which references a particular peripheral. This address is available to all peripherals on lines connected to the MB; its utilisation will be described in the next section. Also available externally are three "IO" pulses, whose generation is controlled by the IO instruction. These are used to effect the actual transfer of data. They are also used to check the status of a peripheral (e.g. whether or not it is ready to transfer data) by means of the skip line. This line is available to all peripherals and when suitably pulsed it increments the contents of the PC by one, causing the next sequential program instruction to be skipped.

The interrupt system also uses a single line available to all peripherals; when this line is grounded, the computer program is interrupted and control transferred to memory location number one, with the address at which program control ceased stored in location zero to permit later return to the main program. The peripherals can be interrogated to see which caused the interrupt by means of

10 instructions, using the skip line.

This system is extremely flexible in that the physical connection of a peripheral device involves coupling it to a number of lines already available, rather than modifying the structure of the computer in any way. The correct operation of all the peripherals is a matter more of programming than of sophisticated hardware.

Interface Output Section

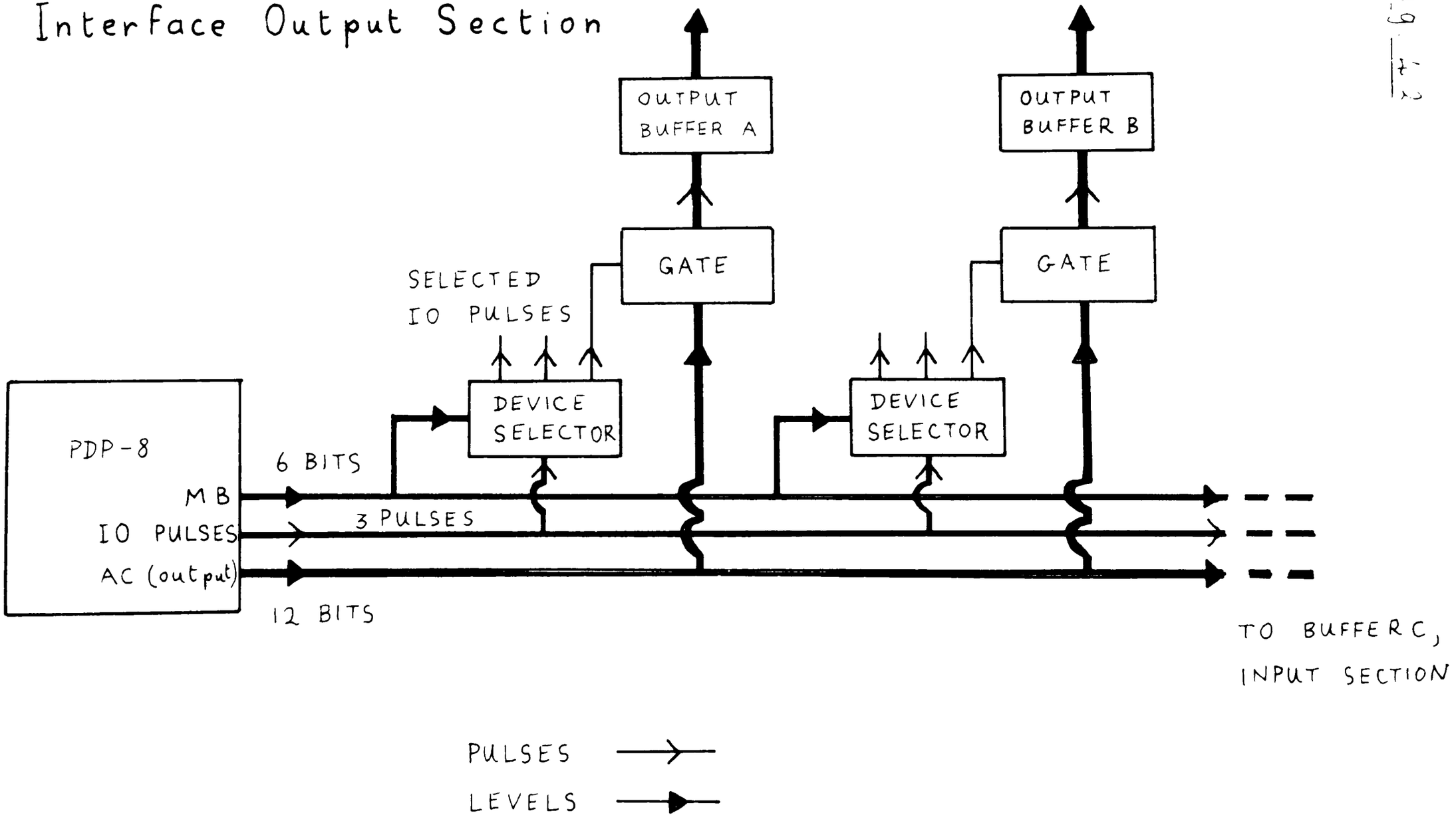
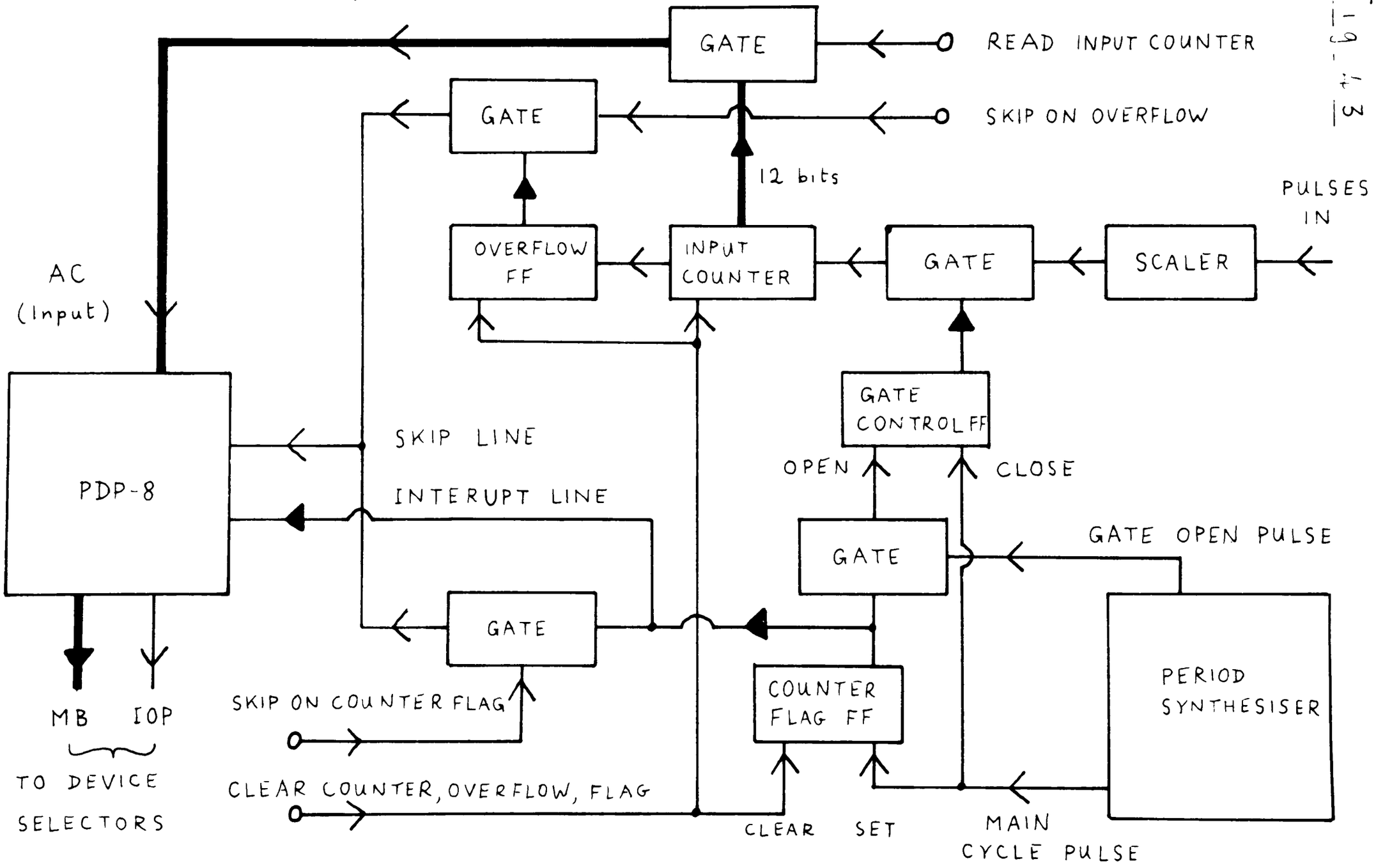


Fig. 9

Interface Input Section



4.5 Interfacing

The system of peripheral equipment used to couple the computer to the experimental apparatus and its instrumentation is known as the interface. The interface used in our system is described by Harrison (1969); we give here a short account. Schematic diagrams are given in figs. 4.2 and 4.3.

The output section (fig. 4.2) is quite straightforward. When it is required to transfer data from the AC to one of the three output buffers, an IO instruction is given. This instruction contains a 6 bit address which appears on the external MB lines. The address enables gates in one of the device selectors, each of which is prewired to recognise one address code. The device selector gates then transmit the input/output pulses generated under the control of the IO instruction. One of the selected IO pulses then enables gates between the AC output lines and the output buffer associated with the addressed device selector.

This sets the buffer (a 12 bit flip flop register) equal to the AC, and these contents are retained until the next loading instruction. They are externally available in suitably buffered form.

The input section contains two interconnected parts, the period synthesiser and the input counter, together with associated status flip flops. The period synthesiser is driven by a crystal clock, and produces a main timing pulse at a repetition rate controlled via a switch register by the user; it also produces a second pulse following the main pulse by a similarly controlled delay time. The input counter is provided with a 10 MHz $\div$ 8 prescaler, and a 2 MHz scaler with a division ratio switchable from 1 to 512 in powers of two; the scalers are followed by a gate, and then a binary counter and an overflow flip flop.

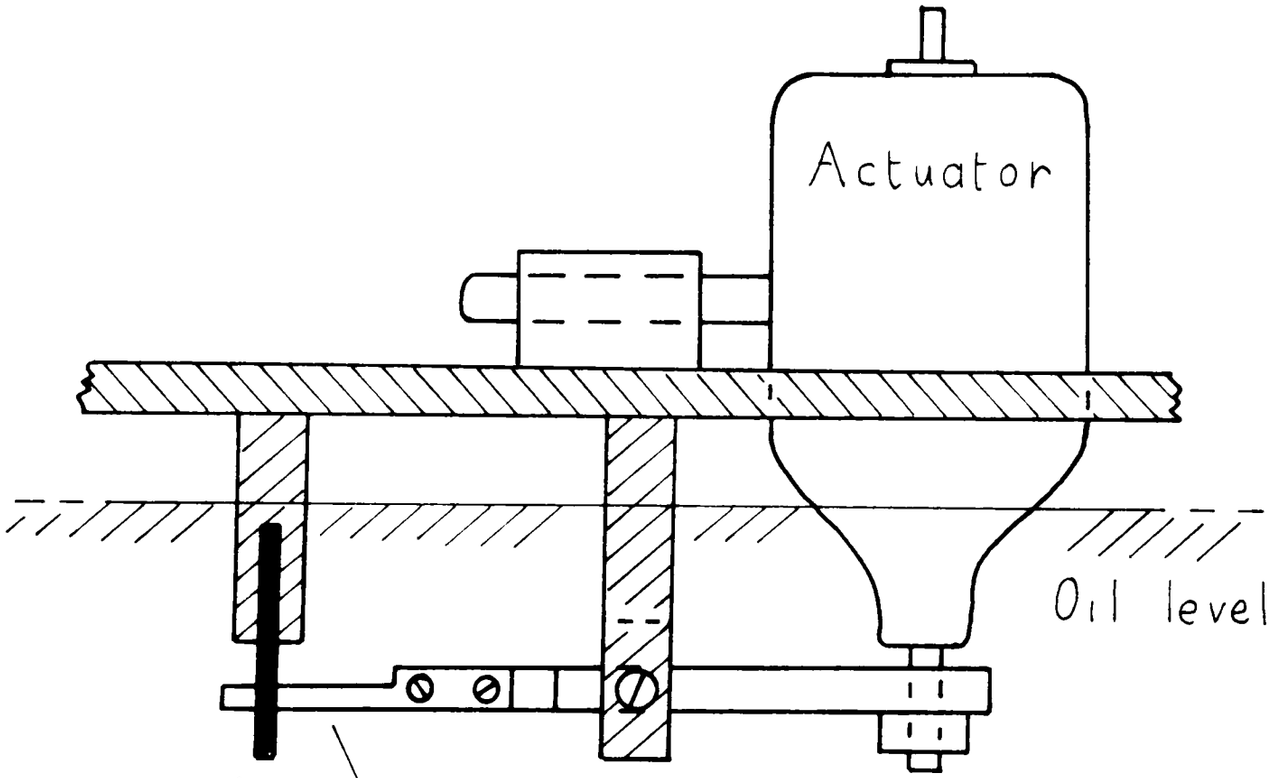
The main timing pulse is used to set the gate control flip flop to close the gate, and also to set the counter status flip flop, or "flag". This causes a program interrupt, and opens a gate which is then able to pass pulses to the skip line; a pulse can be applied via a device selector using the requisite IO instruction, which

we may label "skip on counter flag". The computer may respond to this interrupt by interrogating the flag, and having determined the source of the interrupt it may load the contents of the input counter into the AC using essentially the reverse of the outputting process. The overflow flip flop may also be checked, using the skip line. A further IO instruction may be used to clear the input counter, overflow flip flop and flag. This enables the second pulse from the period synthesiser to set the gate control flip flop to open the gate; if the flag has not been cleared, this action is inhibited and the gate remains closed. Thus one may say the setting of the flag informs the computer that data is ready for transfer into the AC; clearing of the flag by the computer informs the interface that its data has been accepted, and it may continue collecting counts at the correct point in the timing cycle.

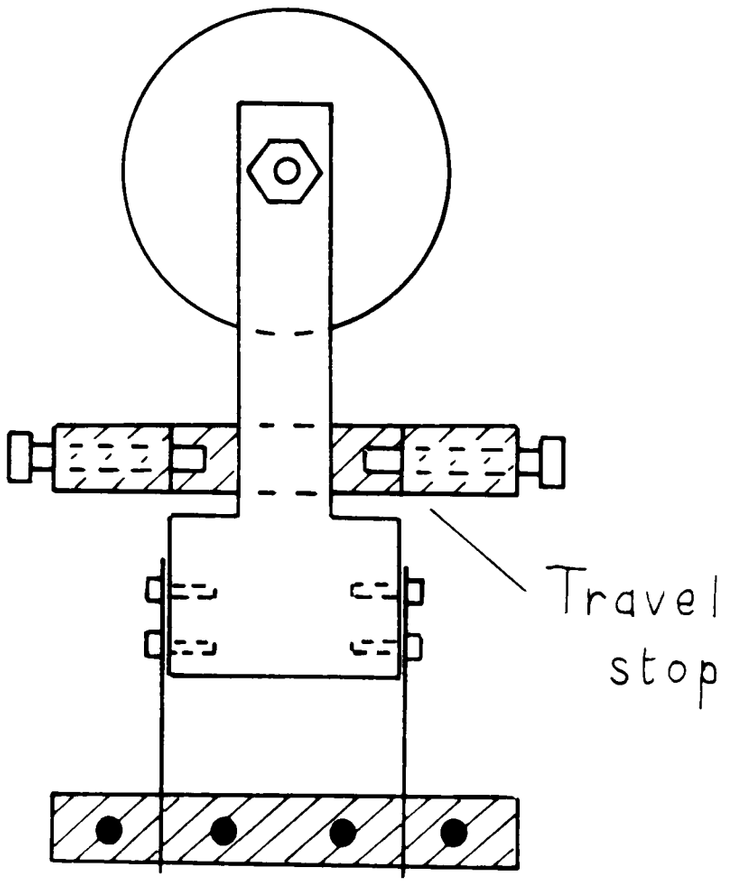
EHT Switch

Fig 444

Side view



Bottom view



All insulating parts Perspex

Scale approx 1·1

4.7 The electric field system

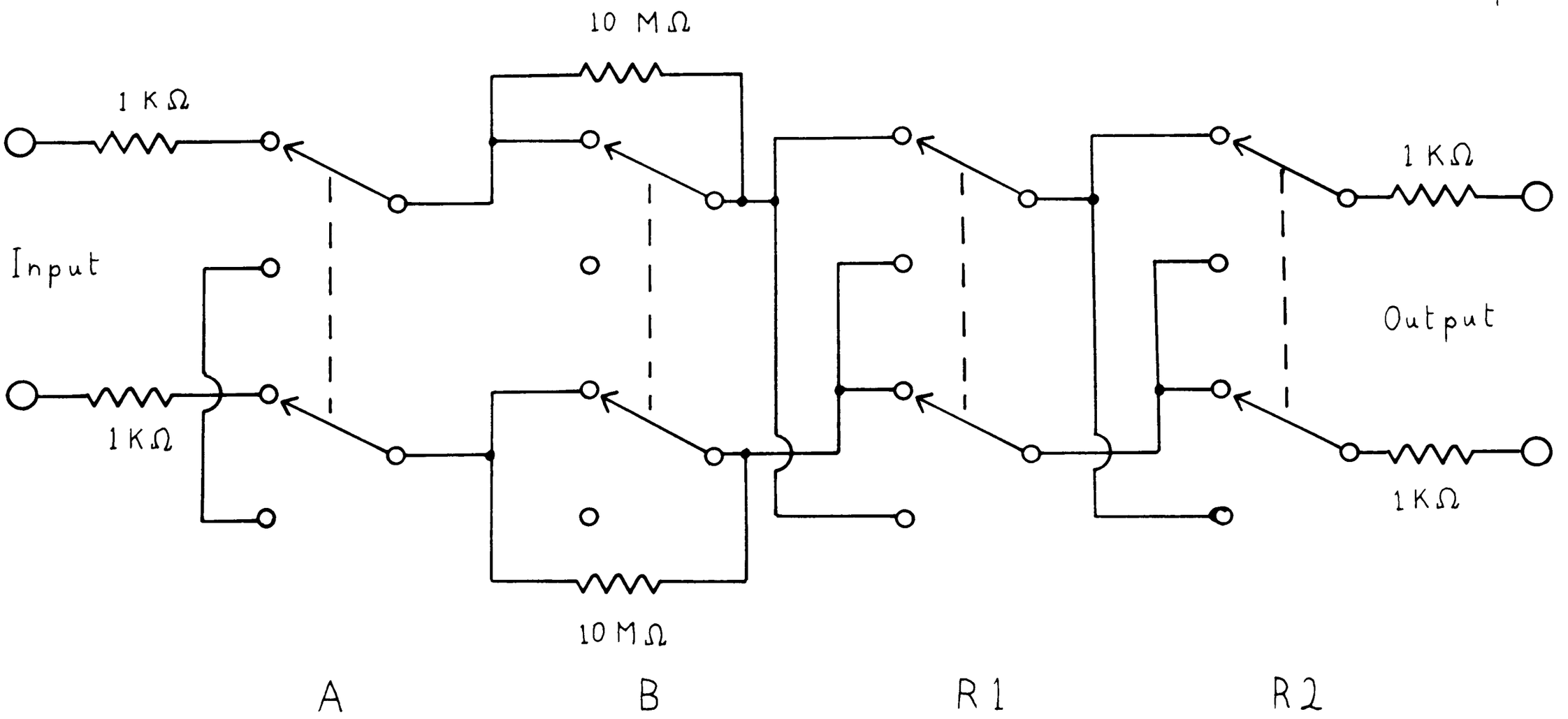
The measured field plate gap after assembly was found to be approximately 2.5 mm. To obtain the design field of 10^5 V/cm we require supply voltages $\simeq \pm 12.5$ kV. The voltages should have equal and opposite values to avoid spurious effects associated with motion of the plates (see chap. 5 below); this also eases the switching problems. The requirements of the switching system are that it should reverse the EHT accurately (better than 1 part in 10^4 - see chap.5) to avoid spurious effects, that the switching speed should be as high as possible to avoid low frequency noise in the data analysis, that the switching should produce little electrical interference, and that it should be reliable. So far we have not found a system which completely fulfils all these requirements at once.

Our first system employed thermionic emission tubes, and well fulfilled all requirements except that of accuracy; we feel this is not a fundamental limitation, but further development requires time and money. The circuits evolved are given in appendix D. The second attempt utilised vacuum reed relays manufactured by Hamlin Inc. and rated to switch 20 kV. Apart from the slightly inadequate voltage rating, these switches suffered very badly from electrostatic sticking, making them impossible to turn on. The switches have since been re-designed but we have not yet tried them. This system is also discussed in appendix D.

The system used during final data collection employs mechanical switches designed and built in the laboratory. A single switch is shown in fig. 4.4 and a schematic of the system in fig. 4.5. The system achieves its voltage rating (it reverses ± 15 kV and holds ± 20 kV) by immersion in transformer oil. Each switch is a double pole, double throw type, and is actuated by a slightly modified Miller bicycle dynamo. These give a relatively high output torque when a current of order 1A is passed through the stator coil; to reverse the switch position one must reverse the current supplied. The switches reverse in 15 msec, followed by 30 msec contact bounce.

Fig 45

EHT Switching System



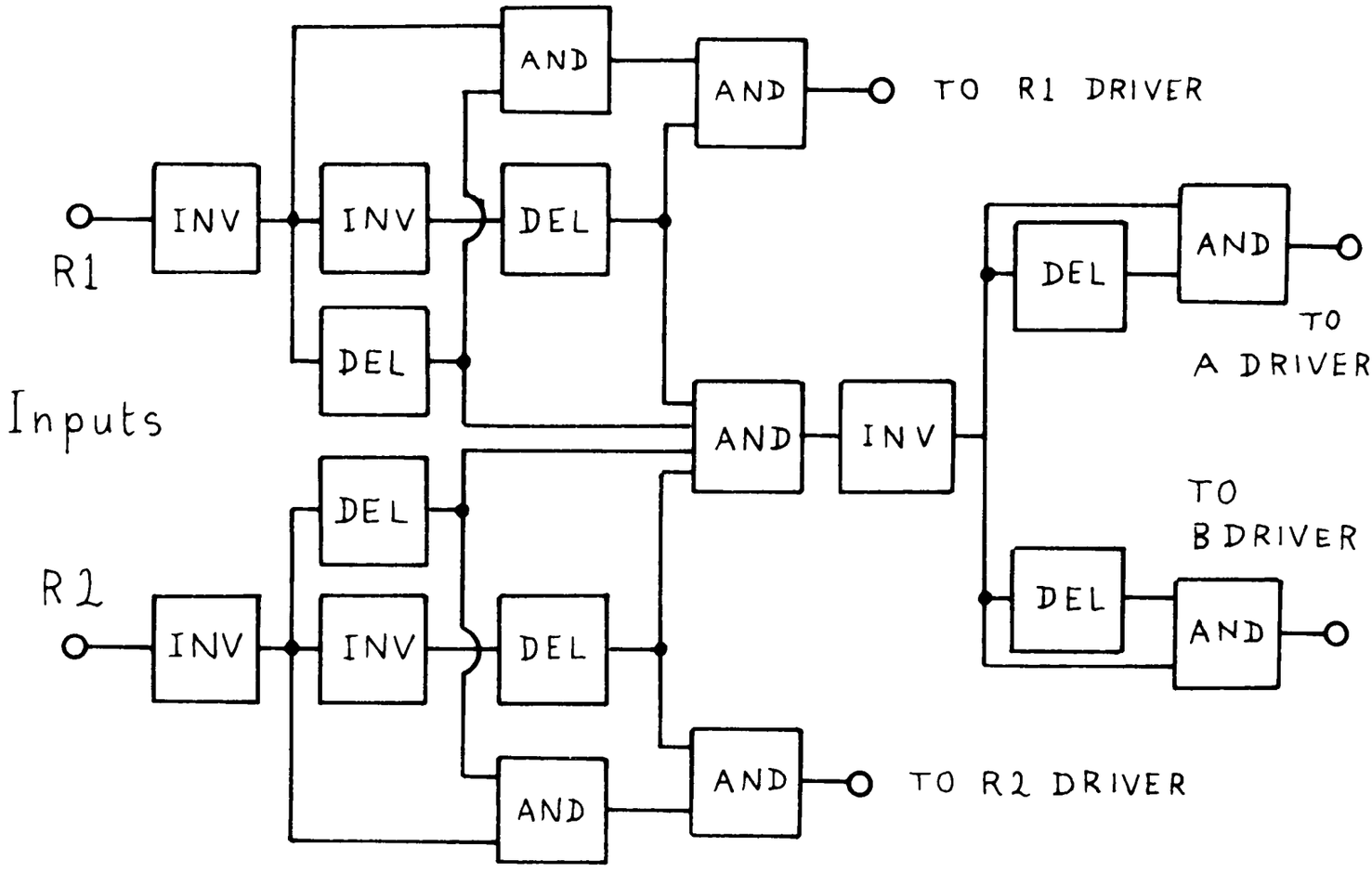
The connections shown in fig. 4.5 correspond to a static state. When one of the reversing switches R1 or R2 is to be switched, the first thing that occurs is that switches A and B go over; when B is open, the two 10 M Ω current limiting resistors are put into circuit, and when A moves to its second state the plate capacitance (about 10^3 pF) can discharge through the resistors. After a short delay, R1 or R2 is operated as required, and A then returns to its normal position. When the plates have charged nearly to the full supply voltage, B closes; this completes the switching cycle. The time occupied is about 150 msec in all. The logic required for the switching control is shown in fig. 4.6.

It is found that electrical interference from the switches is very greatly reduced by the 1 K Ω resistors shown. These apparently act as r.f. suppressors, lowering the efficiency for radiation from the connecting cables of r.f. generated in switching sparks. The 10 M Ω current limiting resistors reduce sparking and interference, and prolong switch life, but by themselves do not provide adequate noise suppression. The switch A is needed for the following reason. Suppose R1 were to be reversed with A in its normal position, and suppose one plate (which we label 1) is initially at + 10 kV. Plate 2 will be -10 kV. If R1 is so constructed that plate 2 is connected after switching marginally before plate 1, plate 2 will be switched to +10 kV and, assuming the voltage across the plate capacitance remains constant, plate 1 will momentarily reach + 30 kV. This effect has been observed; it can lead to breakdown of the vacuum leadthroughs. We may point out that all these difficulties were considerably more apparent in the present experiment than in previous work in the group both because of the higher voltages and the higher plate capacitance.

The switch system is accurate, and its interference production is adequately low. The switching speed is really too low, and the reliability only moderate. Sparking destroys the switch contacts and produces a tarry substance from the oil.

A second pair of switches is used for the A′ plates; no special precautions

Fig 46 EHT Switching Logic



Truth tables

INV

IN	OUT
H	L
L	H

AND

IN	OUT
ANY INPUT H	L
ALL INPUTS L	H

DEL

IN	OUT
L, H	NORMALLY L
L → H	NO CHANGE
H → L	L → H ; DELAY THEN H → L

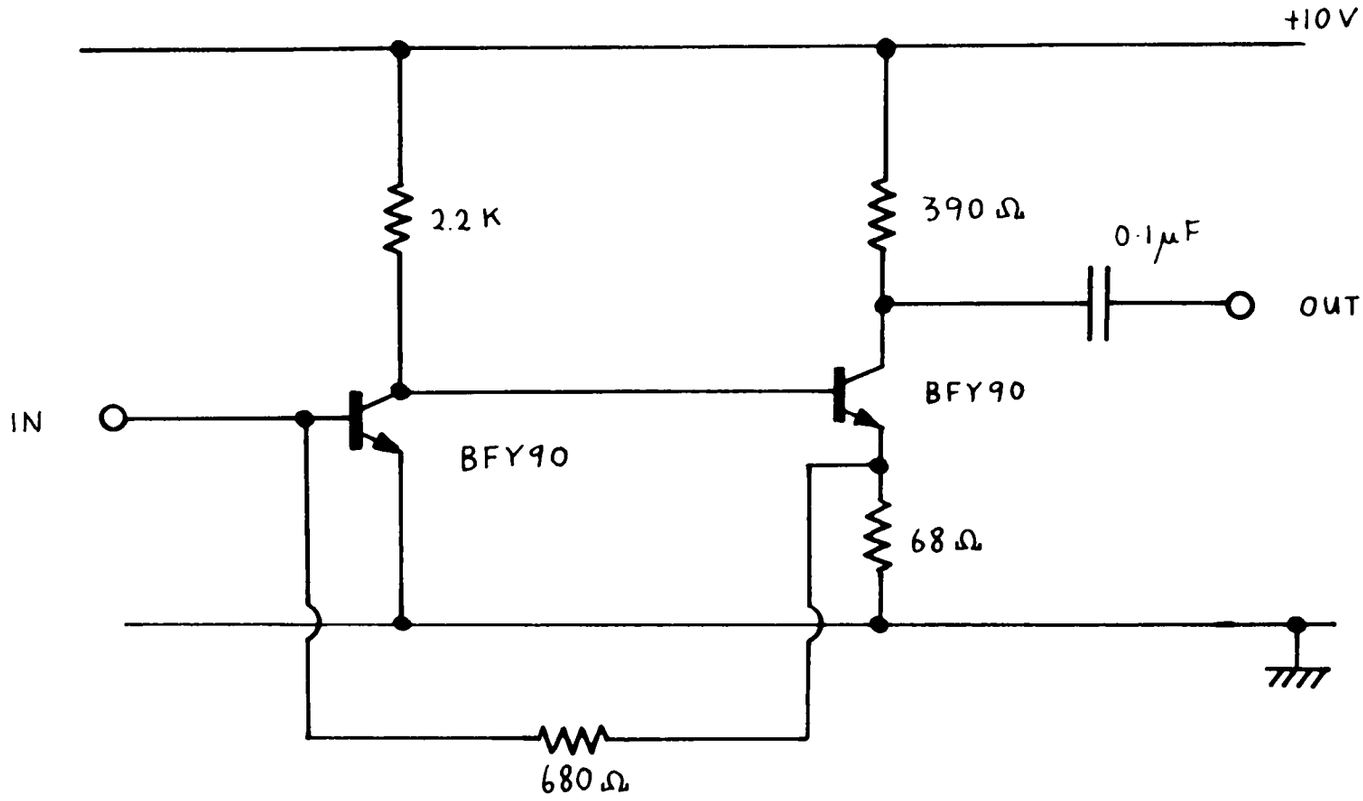
H CORRESPONDS TO -10 V
L CORRESPONDS TO 0 V

for spark suppression are needed.

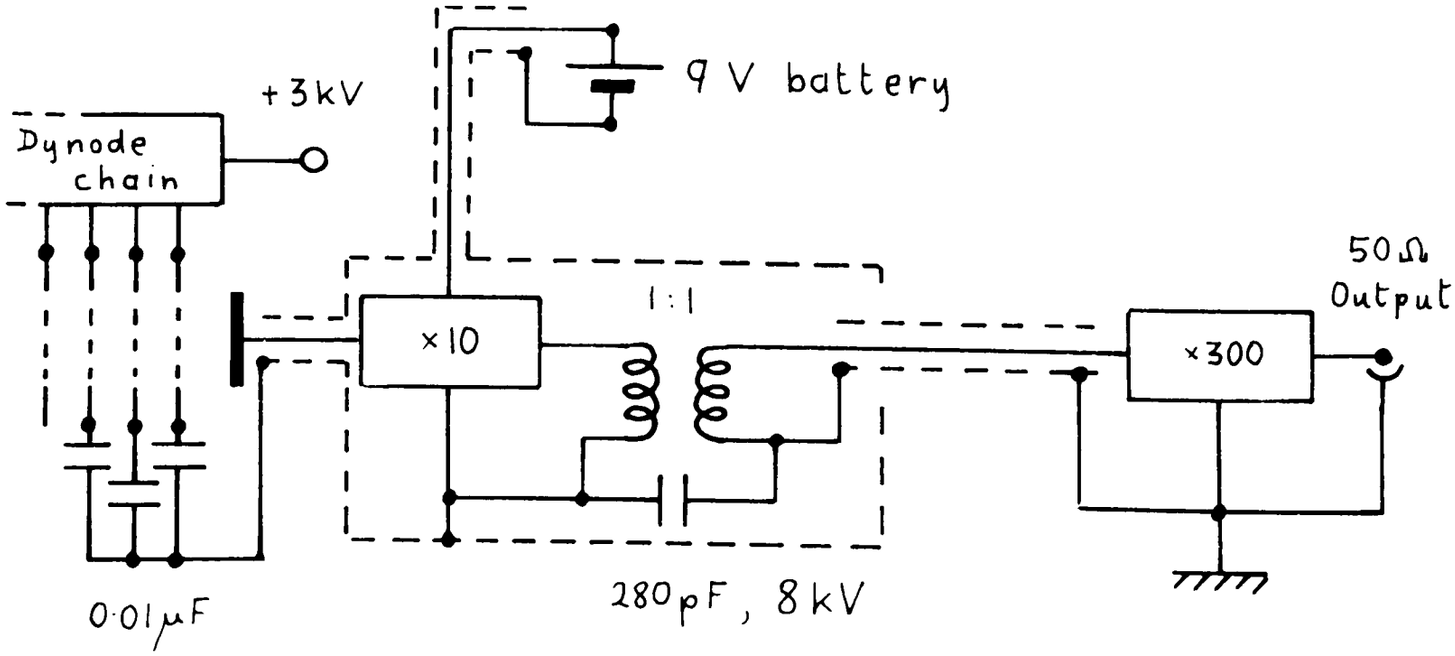
Pulse amplifier

Fig 47

Basic amplifier



System



Multiplier Preamplifier Main amplifier

4.8 The pulse counting system

The pulse counting system is based on broad band amplifiers described in Texas Instruments Application Report B1/22. The circuit of a single amplifier is shown in fig. 4.7; it has a nominal gain of 10 (50 Ω source and load) with useful gain to above 200 M Hz.

The maximum available gain with the EMI 9603/2B electron multiplier is about 10^6, so that each electron detected produces a pulse of size about 10^{-13} coulombs at the anode. The pulse lasts about 10 n sec. The first amplifier stage therefore has a fairly difficult job. In our system the preamplifier consists of a single Texas x 10 amplifier unit built on to the multiplier socket and very well shielded. To reduce r.f. pickup at the multiplier anode the last three dynodes are decoupled to the ground plane of the amplifier. The amplifier is built on a $\frac{1}{4}$ in thick sheet of aluminium, in the manner described by Brooker (1969), to improve earthing and screening. It has a low input impedance ($\simeq$ 10 Ω) and this should be shunted by a low capacitance because of its physical closeness to the multiplier anode. We hope this avoids degradation of the pulse shape at the anode, and thereby improves the time resolution of the system and the signal to noise in a pulse. The preamplifier floats at the + 3kV anode potential and is battery operated; output is taken via a transformer consisting of a few turns of PTFE insulated wire wound on a Mullard ferrite pot core type FX 2236, which is not designed to work at VHF but does so rather well. The r.f. earth line is continued past the transformer through a capacitor.

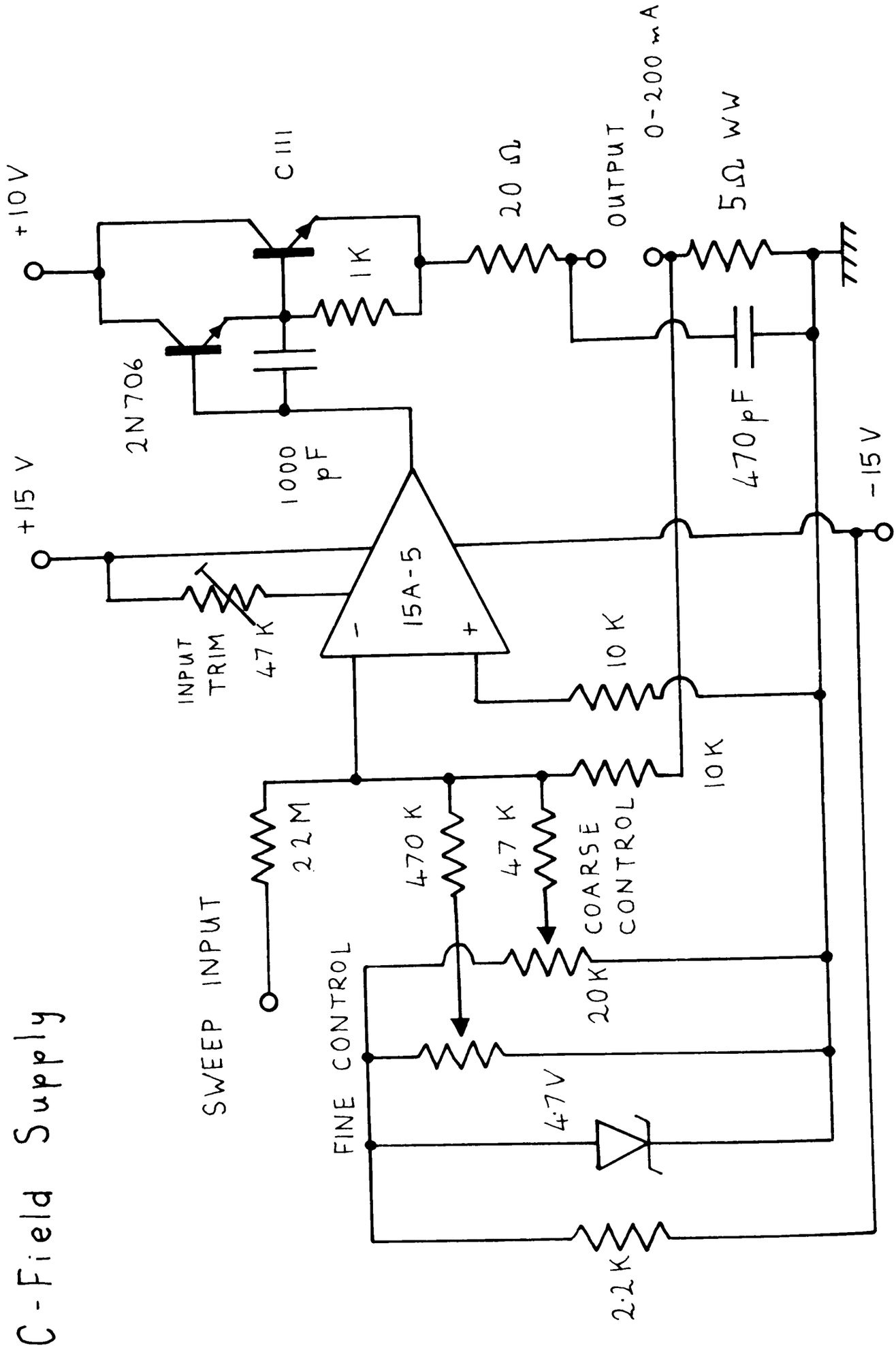
The main amplifier consists of three x 10 units on a single aluminium sheet, with a preset input attenuator. A small attenuation factor is needed to obtain overall stability of the system. The output pulses are fed to a pulse rate meter (appendix D) and the computer installation. Here they are amplified by a x 10 amplifier of the type described by Warrington (1968); this is normally overloaded by the pulses and acts as a shaper. The shaped pulses operate the 10 M Hz

interface scaler. No advantage is found in including a threshold discriminator in the system. The system is shown in fig. 4.7.

The output pulses before shaping, with a multiplier gain of about 10^6, have about 0.5 V amplitude and are 20 n sec long with about 7 n sec rise time; rather faster pulses are observed after the preamplifier alone. The amplitude is normally greater than ten times the baseline "noise" which consists largely of pickup from the local BBC VHF transmitter. This pickup can increase erratically at times, and the system has sometimes become unstable for no clear reason; apart from this it performs well.

The maximum counting rate we have used is about 3×10^6 cps, with no apparent nonlinearity due to pulse overlap. The maximum possible rate should be limited by pulse overlap to around 10^7 cps; a statement by Angel (1967) that the electron multiplier anode current is limited to 10^{-7} A, in which case the maximum count rate might be limited by input amplifier noise, seems to be untrue. The true limitation is $\simeq 10^{-4}$ A for continuous stable operation.

Fig 48


C-Field Supply
+10 V
+15 V
C111
2N706
1K
1000 pF
20 Ω
OUTPUT
0-200 mA
5Ω WW
470 pF
-15 V
15A-5
INPUT TRIM
47 K
10 K
10K
SWEEP INPUT
22M
470 K
47 K
COARSE CONTROL
FINE CONTROL
20K
47V
2.2K

4.9 C-field and r.f. system

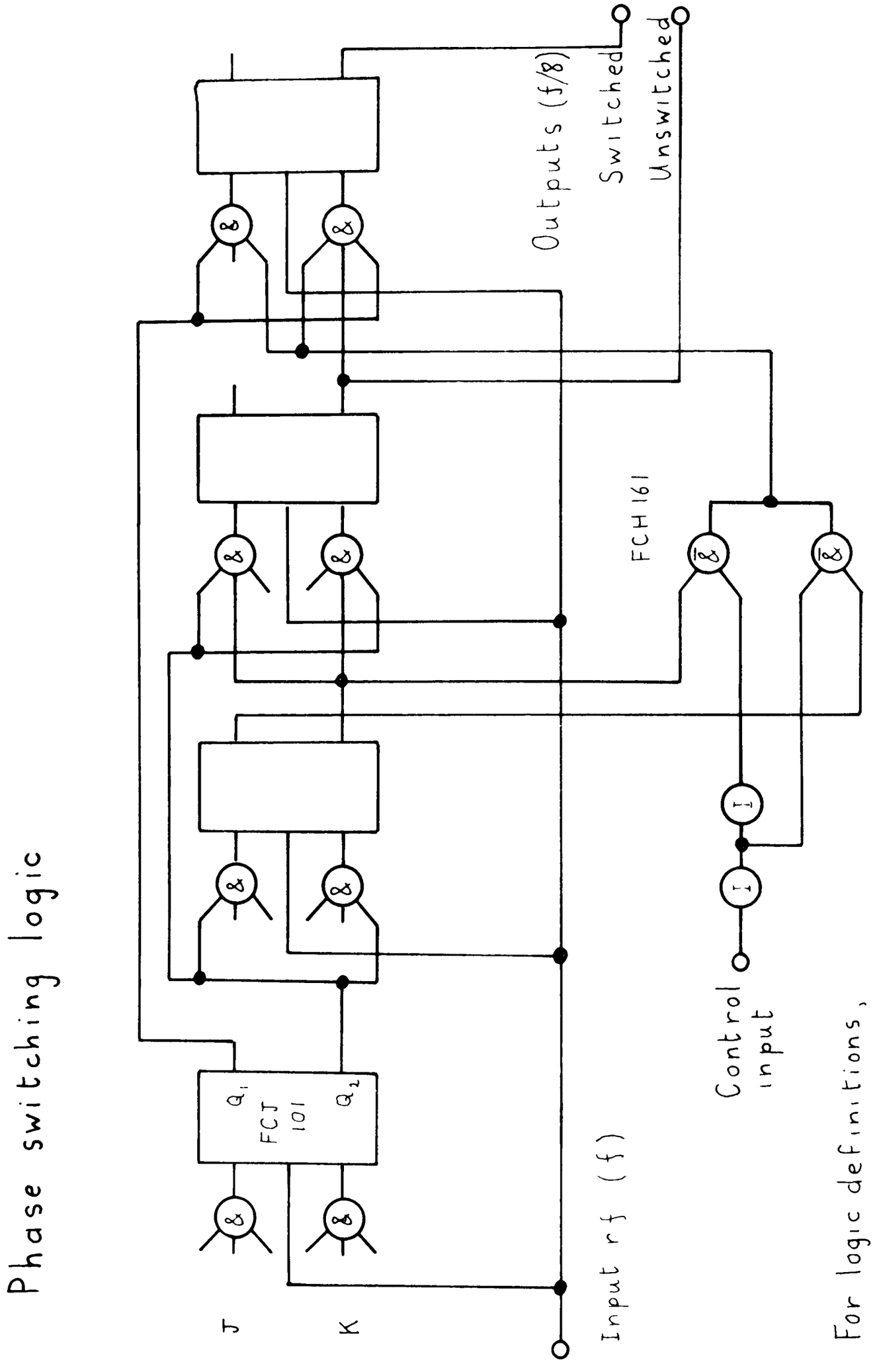
The resonance region requires a stable, noise-free current for the main field coil, a stable radio frequency, and supplies for the various subsidiary magnetic field coils. Either fields or radio frequency must be modulable to provide correction for drifts, calibration, and reversal of sign of resonance slope. The magnetic field must be reversible.

The main field coil is supplied from a constant current source designed round an operational amplifier, Ancom type 15A5. A schematic is shown in fig. 4.8. The noise voltage across the 5 ohm current sensing resistor is measured to be less than 0.1 μV in a bandwidth of about 2 Hz at 20 Hz, using a General Radio tuned amplifier; this corresponds to fluctuations in resonance position of less than 10^{-2} Hz, for 1 Hz observation bandwidth. Since the precision limit from shot noise for 1 second observation time is 10^{-1} Hz for xenon in our system, this suggests that magnetic field noise due to the current source should be negligible. Mains pickup is typically 50 μV across the current sensing resistor, corresponding to 5 Hz modulation of resonance position; this and rather larger effects due to hum currents in the frame of the machine are cancelled by modulating the current source from a 50 Hz supply of variable phase and amplitude. The "sweep" input of the supply is used for feedback modulation to correct drifts. Drifts due to the supply are less than 100 Hz.

The various subsidiary coils need less stable sources of cruder design. Calibration is applied to a separate coil using a simple electronic switch feeding the coil through a suitable resistor.

When the main field is reversed, one must also reverse the vertical inhomogeneity shimming coil and adjust the magnitude of the main field current to keep the resonance position unaltered. The hum cancellation condition is changed by the reversal, and two "hum-bucking" circuits are provided, preset for each sign of field. All switching is performed by mechanical relays. The

Fig 49


Phase switching logic
Outputs (f/8)
Switched
Unswitched
FCH 161
Q1
FCJ
101
Q2
J
K
Input rf (f)
Control
input
For logic definitions,
see Mullard handbooks

resonance position is reproducible to about 10 Hz after repeated reversals.

The sign of the resonance slope is reversed by switching the phase of the second r.f. loop with respect to the first, the required phases being 45^{o} and 135^{o}. Compared with a method using resonance position modulation, this gives slightly better signal to noise, ensures better symmetry between the two signs of slope, and requires no setting up. The main advantage, however, is that the system takes less time to respond to the phase switching so that more frequent reversal and hence better signal to noise can be achieved. The response time for a change in resonance position is the transit time for atoms to pass through the whole resonance region and reach the detector; if the second loop is phase switched, the relevent transit time is just that between second loop and detector. The transient effect on beam intensity should also be much less.

Phase switching is performed digitally to ensure accuracy of phasing. The system is shown in fig. 4.9. Control of the two output amplitudes is obtained by varying the common power supply to the last switching stages of the two sides of the system, before final power amplification.

The r.f. oscillator is an Airmec type 304A. It does not need to be modulated in any way.

Part III. Computer programming

4.10 Introduction

The basic feature of programming for an on-line system is that the programmer must take explicit care of the interactions between the computer and its particular environment of peripheral devices. For this reason it is difficult to introduce a program structure of sufficient generality to act as the basis of a higher-order language to control all on-line situations. To obtain flexibility, it seems to be necessary to employ machine code at least in those sections of program directly concerned with external interactions.

The structure of any on-line program is dominated by the idea of the priority of peripherals. In a system such as ours one usually has a "main" or "background" program which runs while no peripheral is demanding attention, perhaps performing calculations on previously accumulated data, or perhaps merely waiting. This is interrupted by the peripherals, which are then "serviced" by different sections of program. Each peripheral is assigned a priority; the top priority peripheral will be serviced as soon as it interrupts even if the computer is already servicing another device, the second priority will receive immediate attention unless the top priority service is in progress.

In the PDP-8 system, where all peripherals are connected to common "bussed" interrupt, skip and data lines, the assignment and structure of priorities is entirely a matter of programming. Interrupt programming works roughly as follows. On receipt of the interrupt, the address at which the computer was about to operate is automatically stored in location 0 ; control must be returned to this section of program when the interrupt has been serviced. The first section of interrupt program must store the contents of all processor registers used jointly by background and interrupt programs; it may also remove the return address from location 0 and store it elsewhere. The program then checks the peripherals to see which interrupted, using the skip line. The priorities are assigned by

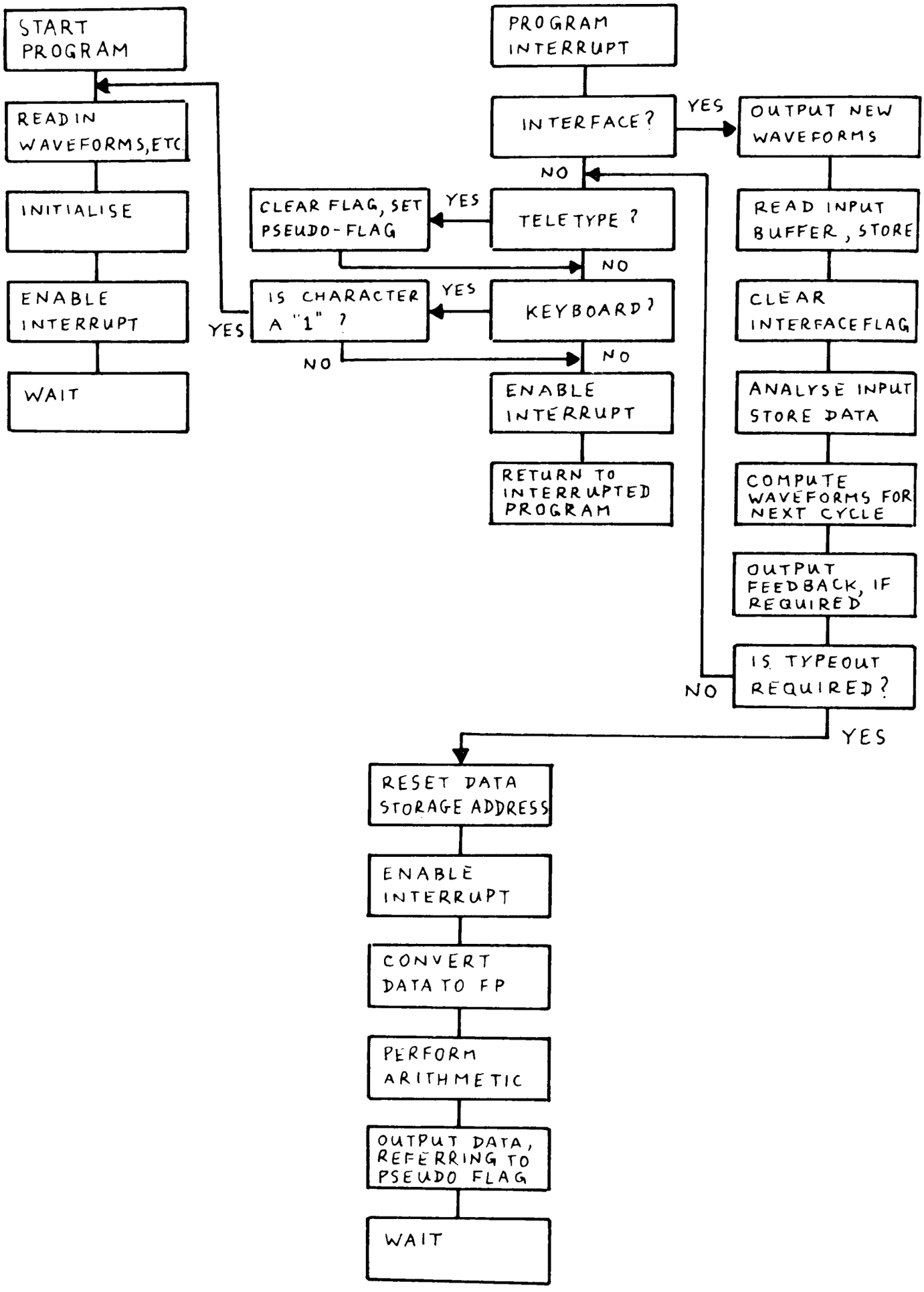
making the program check the status registers (flags) of the peripherals sequentially in the desired order of priority. The priorities may clearly be reassigned by any level of program.

One has at this point a choice of structure. The hardware interrupt line is disenabled following receipt of an interrupt (to avoid multiple interrupts causing confusion before processor registers have been stored), and the line may either be kept inactive throughout the interrupt service, or it may be enabled immediately after the computer has acknowledged receipt of interrupt from the peripheral by clearing its flag. The first choice leads to locking out even of high priority devices while servicing occurs, and is acceptable only if low priority services are short. The second choice leads to faster response, but entails storage of processor registers and return address in a push-down list, where the last data put in is the first to be retrieved. In this way the program avoids confusion under a barrage of interrupts, even with a device interrupting its own service routine. To maintain priority order, the program must set up "pseudo flags" which inform the initial interrupt service that a high priority service is being performed, should a low priority device interrupt it. One usually mixes the two systems, the highest priority service having the interrupt disenabled throughout. Whatever choice is made, one must ensure that the flag of the device causing an interrupt is cleared before the interrupt is re-enabled.

These are the rules of the game, very roughly; the fun is in the playing.

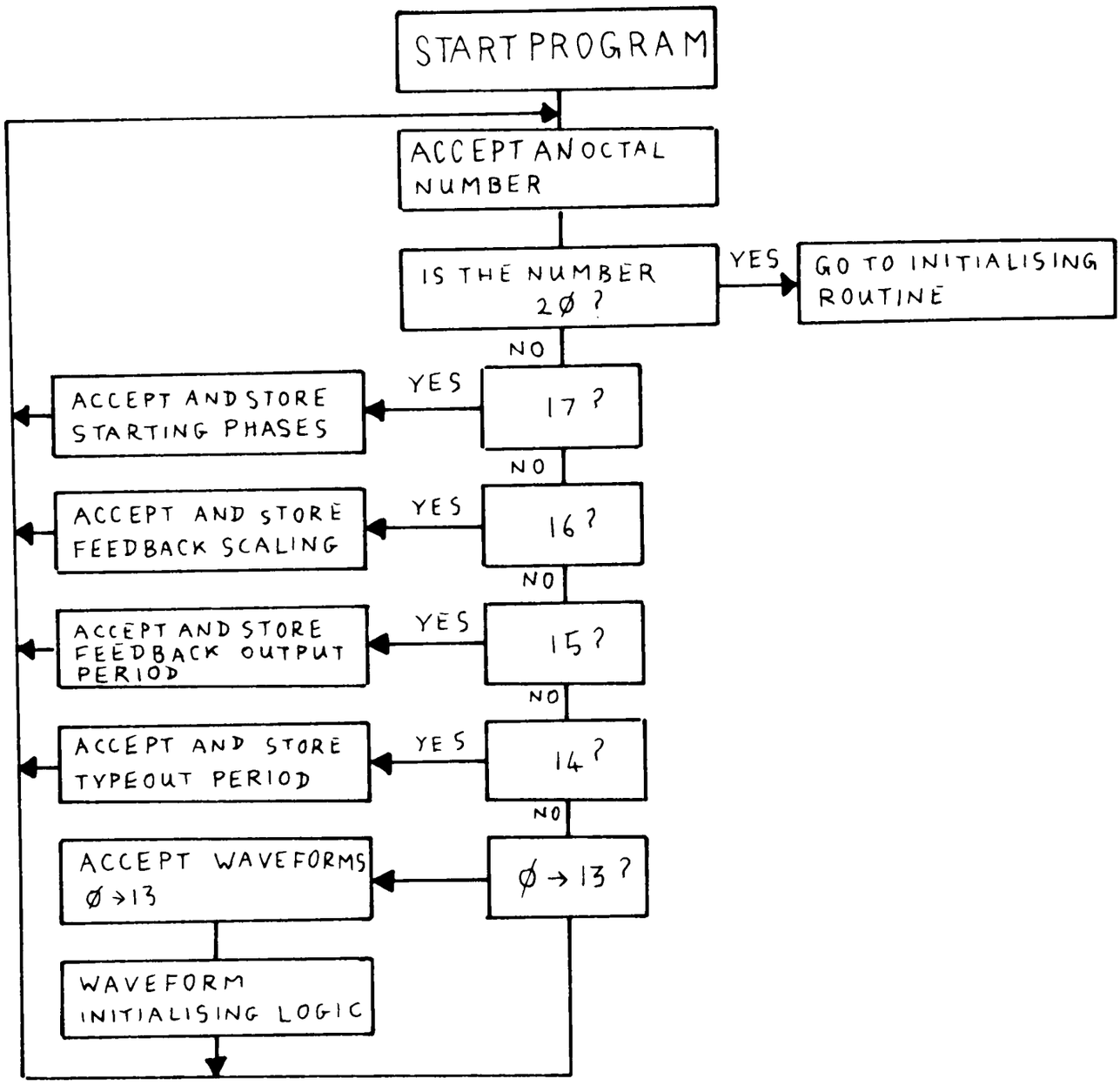
MAIN FLOW CHART

Fig 4·10



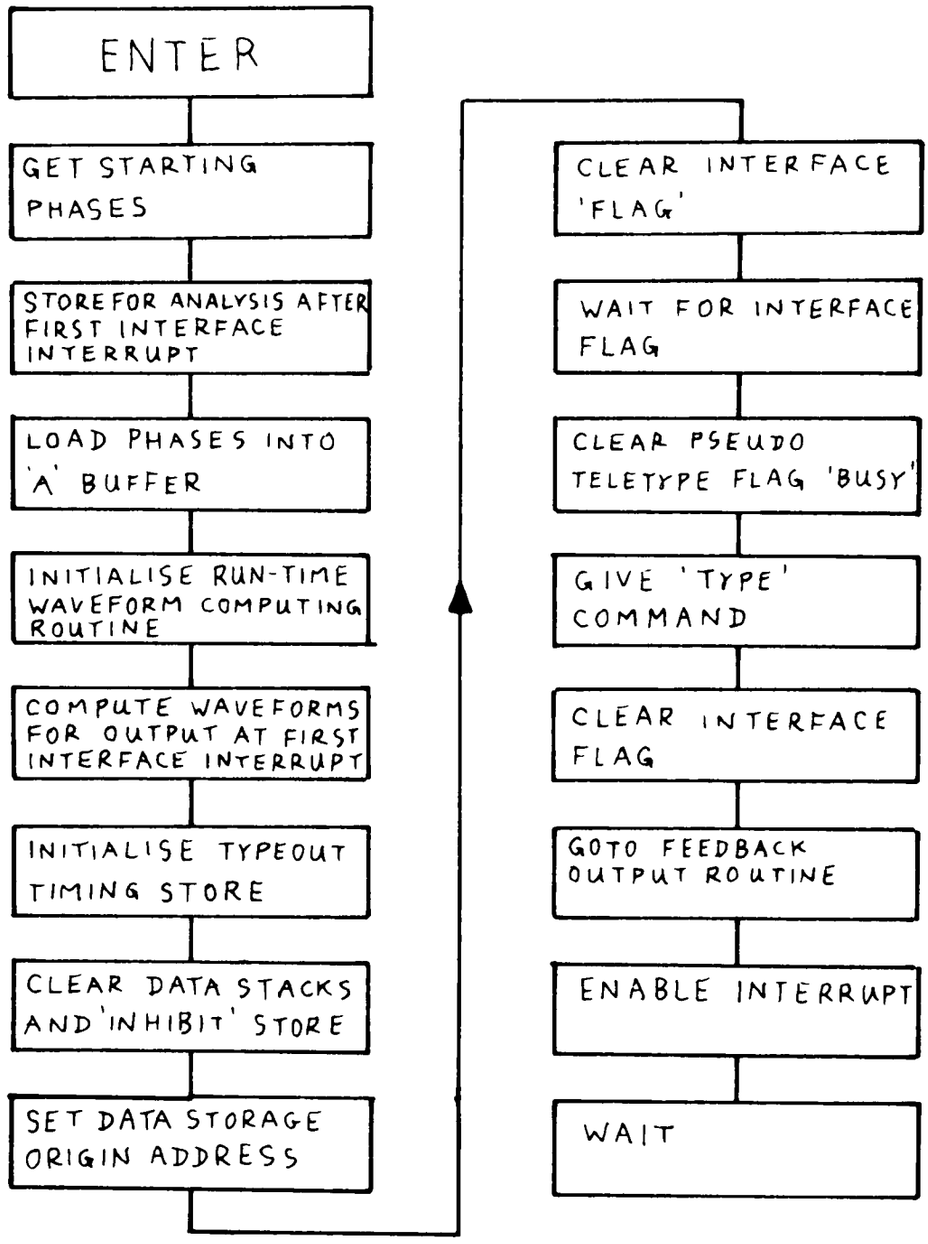
COMMAND INPUT SECTION

Fig 4·11



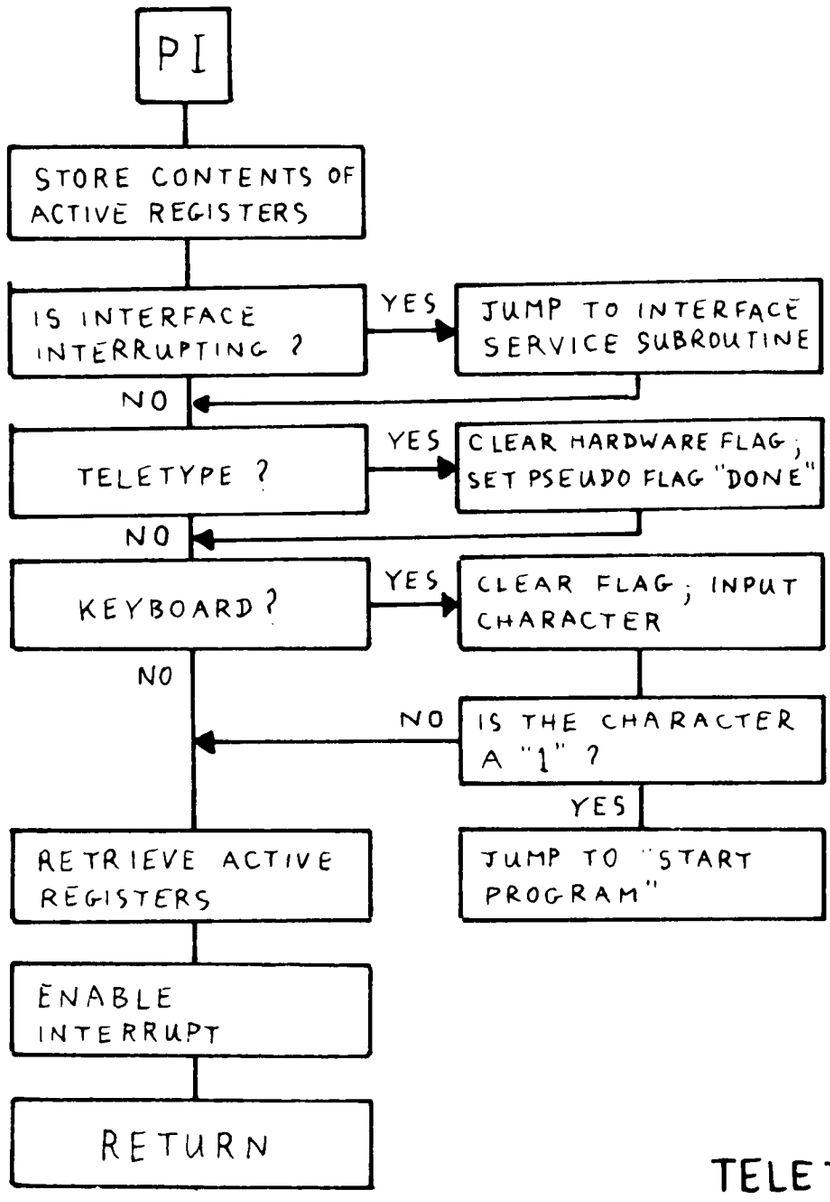
INITIALISING ROUTINE

Fig 4.12

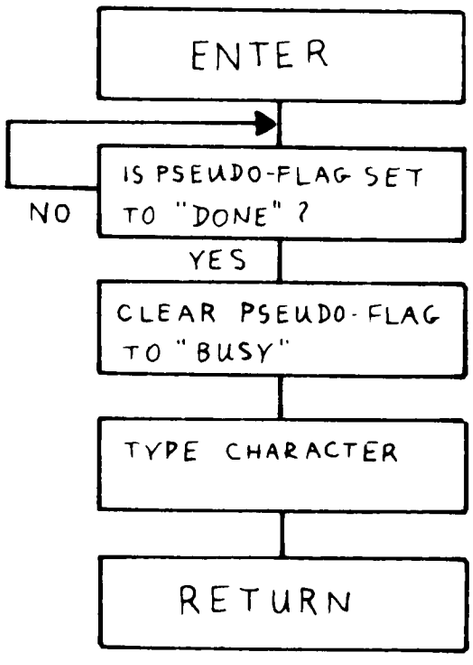


PROGRAM INTERRUPT SERVICE

Fig 4.13

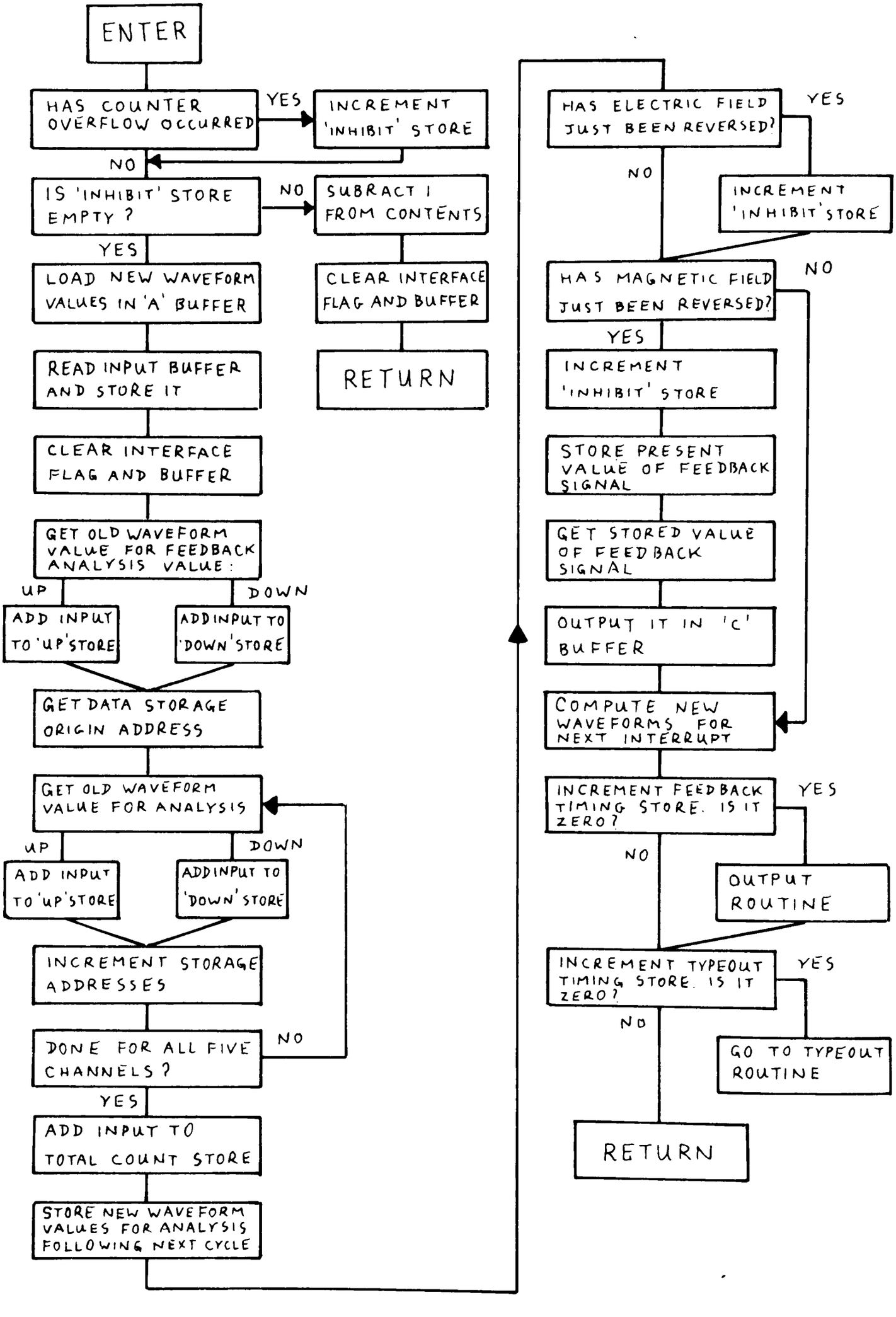


TELETYPE OUTPUT SUBROUTINE

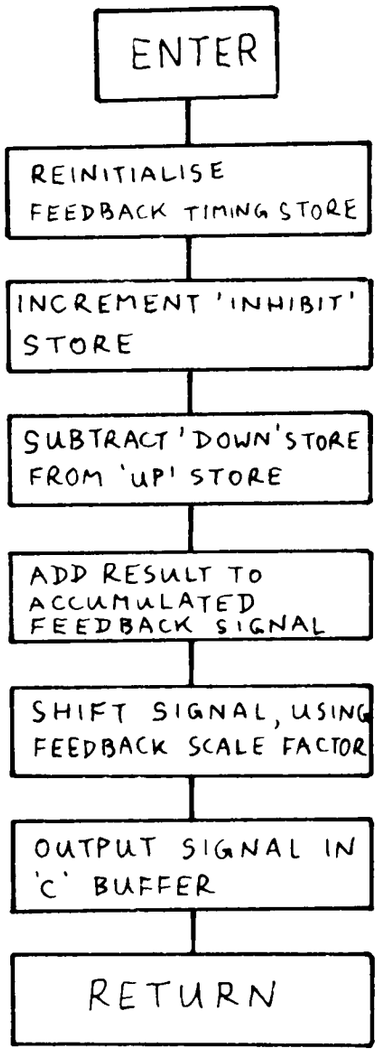


INTERFACE SERVICE SUBROUTINE

Fig 4.14



FEEDBACK OUTPUT SUBROUTINE Fig 4.15



TYPEOUT ROUTINE

Fig 4.16

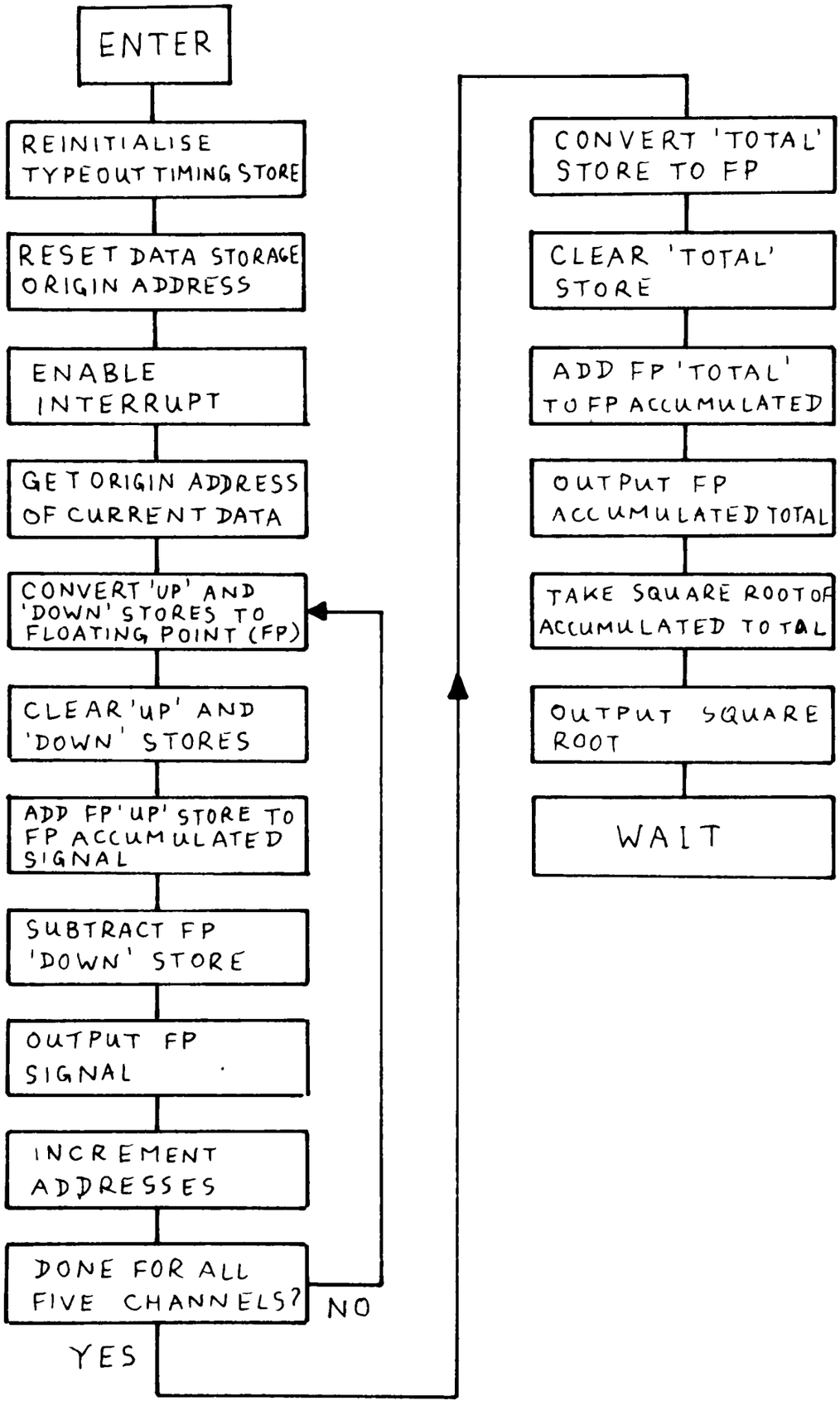


Fig 4.17

TELETYPE CONTROLLED UPDOWN COUNTER WITH MAGNETIC FIELD REVERSAL

STARTING ADDRESS 200Ø

TYPE IN THE FOLLOWING INFORMATION:

14(OCTAL) MODES
TYPEOUT PERIOD
ANALOG FEEDBACK READOUT PERIOD
READOUT SCALING BINARY EXPONENT
INITIAL PHASES OF MODES

THIS IS DONE BY TYPING AN OCTAL NUMBER (TERMINATED BY /) TO SPECIFY WHICH PIECE OF INFORMATION IS BEING SUPPLIED:

MODES Ø THROUGH 13
TYPEOUT PERIOD 14
READOUT PERIOD 15
READOUT SCALE 16
INITIAL PHASES 17

FOLLOWED BY A BINARY NUMBER IN THE CASE OF MODES, PERIODS AND PHASES, AND AN OCTAL NUMBER FOR THE READOUT SCALE. THE BINARY FORMAT IS A MANTISSA FOLLOWED OPTIONALLY BY AN (OCTAL) EXPONENT, THE MANTISSA BEING TERMINATED BY ; AND THE COMPLETE NUMBER BY A CARRIAGE RETURN.

THE MODES APPEAR IN BUFFER A, THE ANALOG READOUT IN C.

THE ANALOG READOUT IS THE ACCUMULATION OF THE CHANNEL CONTROLLED BY MODE Ø.

MODES 1 THROUGH 5 CONTROL THE CHANNELS WHOSE ACCUMULATIONS ARE TYPED OUT (IN ORDER) EVERY TYPEOUT PERIOD. ALSO OUTPUT ARE THE TOTAL NUMBER OF COUNTS AND ITS SQUARE ROOT.

MODE 7 IS THE MAGNETIC FIELD REVERSAL MODE.

MODES 6 AND 1Ø HALT DATA ACCUMULATION FOR 16 BASIC PERIODS WHEN THEY CHANGE, MODE 7 FOR 32 BASIC PERIODS. THESE CONSTANTS ARE IN LOCATIONS 3Ø13, 3Ø61 RESPECTIVELY.

DATA ACQUISITION IS INITIATED BY TYPING 2Ø/

DATA ACQUISITION IS HALTED AND CONTROL RETURNED TO THE INITIALISATION SECTIONS BY TYPING A 1 (NO TERMINATOR).

4.11 The "Updown counter" program

The program to be described has been used in nearly all the data collection discussed in the next two chapters. Its title derives from a previous technique for analysis by orthogonal waveforms, using reversible ("updown") binary counters (Angel, 1967).

A listing of the available facilities is given in fig. 4.17; basically the program provides 12 waveforms for control and analysis of which five can be used for data analysis and one for analysis in the analog feedback channel. The fastest basic period for counting and waveform generation is about 1 msec, and the minimum interface gating period about 100 μ sec. The waveform structure is specified by a binary number (as in chap. 4.3) which may be up to 24 bits long. Special provision is made for the control waveforms used to reverse electric and magnetic fields. Reversal of the electric field halts data accumulation for (normally) 16 basic periods to avoid switching transients. Reversal of the magnetic field is complicated by drift in external fields, which will cause a shift in resonance position on field reversal even if the field supply is set up to give no shift initially. This is taken into account by keeping two accumulated feedback signals, one for each sign of field. Magnetic field reversal halts data accumulation for 32 periods.

The main flow chart of the program is given in fig. 4.10. More detailed flow charts are given in figs. 4.11 through 4.16. A listing of the program, which is written in a mnemonic form of machine code (PAL III), is given in appendix E. We give a survey of the main flow chart, with some remarks on a few more specific points.

On starting the program, the command section is entered, and waveform structures and other variables may be read in. On the command to start data collection, the program initialises all the run-time sections, outputs the initial values of the control and analysis waveforms, and computes the next values of the waveforms ready for the first interface interrupt. It then waits for the start of

an interface timing cycle (by checking the interface flag) before enabling the interrupt, and waiting.

Normally, the first device to interrupt will be the interface, which has highest priority to ensure steady running of the data collection cycle. On interface interrupt, the interrupt service routine transfers control to the interface service subroutine.

The interface subroutine first checks the interface counter overflow flag and the "inhibit" store, of which more below. If all is well, it at once outputs the new waveform values (which have been computed either by the initialisation section or the previous interface service), reads the input buffer, and then clears the buffer and interface flag; in this way minimum time elapses before the counter gate can be opened to restart data collection. The input data is now analysed, using the waveform values of the cycle just finished; to save time, no arithmetic is performed and the analysis at this stage consists in adding the new input to an "up" or a "down" store (one each for each channel) according to the value of the analysis waveform. New waveforms are now computed ready for output at the start of the next cycle, and the present values are stored for use in analysis after the start of the next cycle.

At this stage the program checks whether the electric or magnetic field has just been reversed. If either has, the "inhibit" store is incremented by 16 or 32 respectively. If this store is not empty when checked at the start of the subroutine, the subroutine is redirected to ignore input data, leave the output waveform values unchanged, and subtract 1 from the contents of the "inhibit" store before clearing the interface flag and returning to the interrupt service routine. Thus the output will be static and input will be ignored for 16 or 32 periods following a field reversal. If the magnetic field has been reversed, the current value of analog feedback signal is stored, and the value reached at the previous reversal is put in its place. The new value is output.

The subroutine now checks if it is time to output analog feedback. If it is, the relevant "up" and "down" stores are respectively added to and subtracted from a running total whose new value, suitably scaled, is output. The "up" and "down" stores are cleared ready for more data acquisition; if these are allowed to accumulate continuously they eventually overflow.

If it is not time for data typeout, control now returns to the interrupt routine which checks further flags (see below) and, if they are clear, restores the stored processor registers, enables the interrupt, and returns to the interrupted program. If typeout is required, the typeout routine is entered. This constitutes the "background" program. Its task is similar to that of the feedback output subroutine, but it is convenient to do storage, analysis and output using floating point format for the numbers. All manipulations can then be performed using Digital Equipment Corporation's floating point subroutines. The floating point format avoids overflow problems. However, conversion of the "up" and "down" stores to floating point is slow, and new data coming in must be put elsewhere while the old data is processed; therefore, immediately after entry to the typeout routine, the input data storage origin address is reset so that new data is put in a block of locations which have been cleared by the previous typeout routine. The position of the storage block used by the interface service routine therefore alternates under control of the typeout routine. When the origin address has been reset, the interrupt can be enabled. The output then goes at its own rate while new data is being accumulated. When all data is output, the typeout routine simply waits.

The teletype, onto which typeout occurs, is also connected to the interrupt line, and interrupts whenever it is ready to type. It is assigned a priority below the interface. When it interrupts, a "pseudo-flag" is set and the teletype flag is cleared. The printing subroutine used by the background program refers to this pseudo flag to find when the teletype is ready, and clears the pseudo flag after output.

Also on the interrupt is the keyboard, on the lowest priority; this is used to enable the operator to return control to the start of the program (by typing a "1"). Both teletype and keyboard routines are so short that no time is lost using a simple interrupt service, with the interrupt disenabled throughout.

A complete account of the logic used for the generation of the control and analysis waveforms is given by Harrison (1969). We illustrate the algorithm used by reference to an example. Suppose we wish to produce the waveform corresponding to (1 0 1 1) where we use the notation of 4.3. We keep a count, in binary, of the number of elapsed basic periods. The first (i.e. least significant) bit of the count will change every basic period, the second after every second period, the n^{th} after every n^{th} period. These are just the times when the basic square waves in the product waveform change. Suppose now that, on updating the count, only the first bit changes; then the waveform corresponding to (1) changes sign, but those corresponding to (1 0) and (1 0 0 0) do not, and so our waveform corresponding to the product (1 0 1 1) will change sign. If now the first two bits of the count are found to change (if one bit changes when the count is incremented by one, all less significant bits must also change), both the waveforms (1 0) and (1) change sign, the waveform (1 0 0 0) does not, and so the waveform (1 0 1 1) does not. Similarly, it does not if the first three bits change, it does if the first four or more change. The rule in general is as follows: find the most significant bit to change in the count. If it is in the n^{th} place from the right, the waveform value will change only if the binary representation of the waveform contains an odd number of ones in the first n places from the right. We may construct from the binary representation a second number representing this eveness or oddness; for our example it is all ones except the last few digits: ... 1 1 1 0 0 1. In this number, the "mode parity", the n^{th} position from the right contains a one if there are an odd number of ones in the first n places from the right in the binary representation of the waveform.

On reading in the waveform representations, this parity is computed in each case. The results are stored in a list in the memory, so that the n^{th} member of the list contains the n^{th} bit of the mode parity for each waveform. The list has only 24 members, since the count is only kept to 24 bits. On run time, it is necessary only to find the position of the most significant bit change in the count, and use it to reference the computed parity list. The waveform generation is therefore very fast.

Chapter 5. Spurious effects

We turn at last to discuss the experiments performed with the system described above. It will be recalled that the experiment was devised to avoid effects which might mimic an edm interaction; nonetheless the history of the experiment has largely been a process of tracing and eliminating such effects. We review in this chapter all the effects we have observed, thought of, or dealt with. None of these effects seems to hold much intrinsic interest; in each case we have simply tried to obtain sufficient information to ensure the minimum interference from the effect.

The usual method of analysing a spurious effect is to check its behaviour on altering all available parameters of the system. A true edm shift reverses sign with reversal of $\underline{E}$ and $\underline{B}$ (see appendix C), is linear in electric field strength and essentially independent of all other parameters. Accordingly, dipole-like shifts are often categorized by their behaviour under manual reversal of electric field plate connections and magnetic field coil connections, manual reversal being a process as free as possible of instrumental effects. Unfortunately, a number of shifts behave in an ill-defined way under these operations; this is true of those dependent on transverse magnetic field for instance, since this is usually changed when $\underline{B}$ is reversed. One cay say, however, that by and large all purely instrumental effects tend to remain unchanged upon reversal of connections, effects dependent on the size of electric field fail to reverse with reversal of $\underline{B}$, and magnetic field modulation effects reverse with both (and therefore cannot be cancelled from the dipole analysis).

Apart from reversal of $\underline{B}$ and $\underline{E}$, the parameters we have most usually varied in investigating shifts are transverse magnetic field, electric field strength, r.f. amplitude, and frequency.

Where we quote frequency shifts, these are shifts in observed two-quantum resonance frequency; a dipole-like shift is the shift obtained on reversing the EHT.

Spurious shifts

Table 51

Shift	Size	B rev.	E rev	V dep	$B_\perp$ dep.	r f dep	ν dep
$\underline{v} \times \underline{E}$	$\sim 10^{-3}$	?	YES	$\propto 1/V^3$	$\propto B_\perp$	NONE	$\propto \nu$
power	$< 10^{-3}$	NO	?	NONE	NONE	$\propto B_{r.f}{}^4$	$\propto 1/\nu$
power	$< 10^{-3}$	NO	?	$\propto 1/V^2$	NONE	$\propto B_{r.f}{}^2$	$\propto \nu$
V dependent	$< 10^{-3}$	NO	?	$\propto 1/V^4$	$\propto B_\perp^2$	NONE	$\propto \nu$
EHT relays	$< 10^{-3}$	YES ?	NO	NONE	NONE	NONE	NONE
leakage current	$< 10^{-4}$	YES	YES	?	NONE	NONE	NONE
charging current	$< 10^{-4}$	YES	YES	?	NONE	NONE	NONE
hysteresis	$< 10^{-3}$?	YES	YES	?	NONE	NONE	NONE
mech. mod.	?	YES	?	?	NONE	NONE	NONE
r.f. pickup	?	?	?	?	NONE	NONE	NONE
alignment	$\sim 10^{-3}$	?	YES	?	$\propto B_\perp$	NONE	$\propto \nu$
50 Hz	$< 10^{-3}$	?	YES	?	NONE	NONE	?
volts chopping	$\sim 10^{-4}$	?	YES?	?	?	?	?
drifts (various)	$< 10^{-3}$	?	?	NONE	NONE	NONE	NONE
transients	$\lesssim 10^{-3}$	?	?	?	NONE	NONE	?

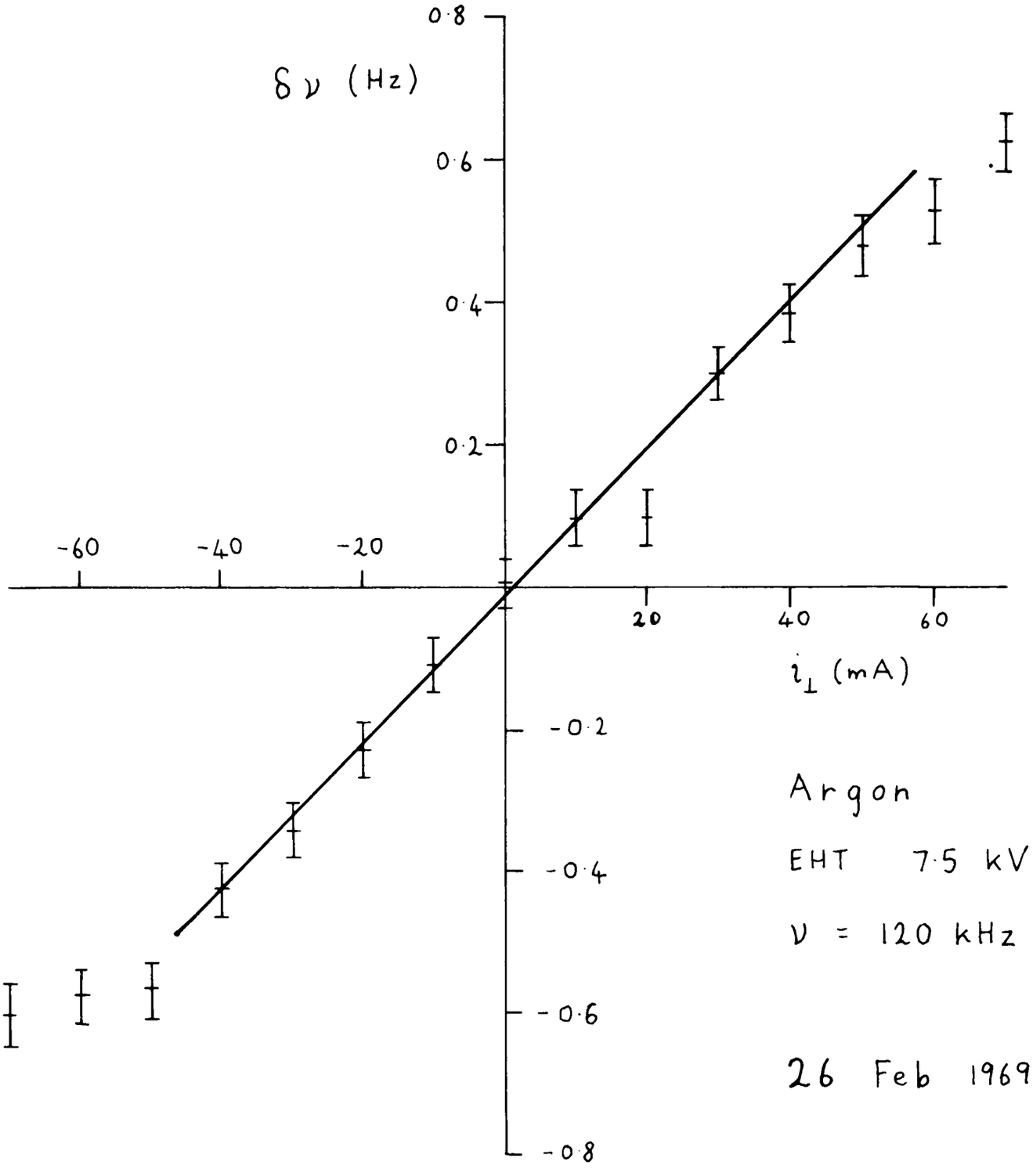
shifts in mHz, at working field values

V dependence of power shifts given for optimum r.f setting

size of power and V dependence shifts given before cancellation

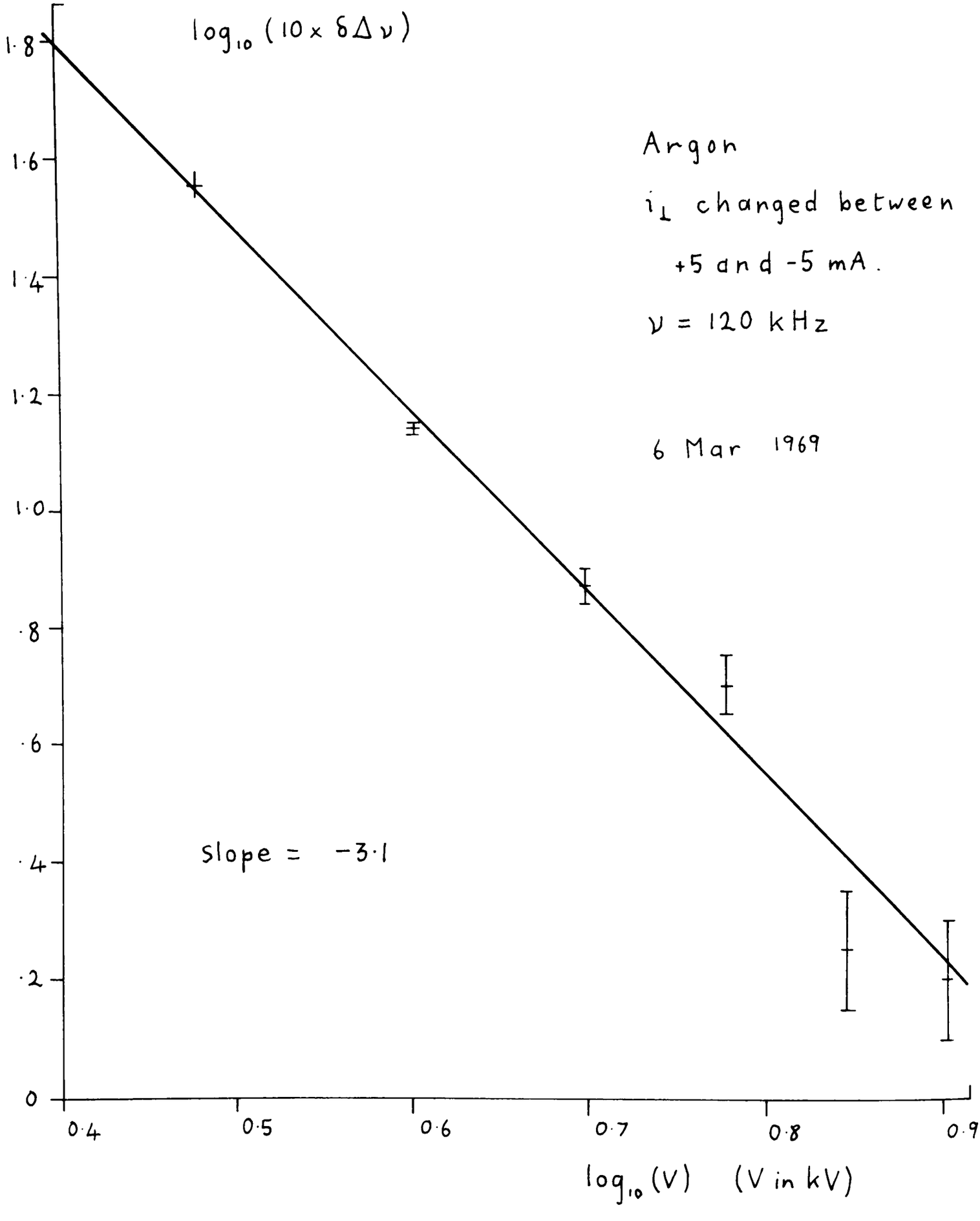
We summarise the results of this chapter in table 5.1.

Dipole-like shift vs. $B_\perp$ Fig 51



Change of dipole-like shift on reversing $B_\perp$, vs. E

Fig. 52



5.1 The "$\underline{v} \times \underline{E}$" effect

In chap.2 we gave a theoretical discussion of the residual $\underline{v} \times \underline{E}$ effect to be expected in the $^3P_2$ levels. This effect has not so far been troublesome, but it has been observed. We show in fig. 5.1 a plot of the dipole-like shift observed in argon as a function of current in the transverse magnetic field coil; the shift is defined as the change in observed resonance frequency obtained on reversing the applied electric field. In fig. 5.2 we give on a log-log plot the change in dipole-like shift on reversing the direction of $\underline{B}_\perp$, as a function of applied EHT. It will be seen that the shift behaves as a $\underline{v} \times \underline{E}$ effect, being linear in $B_\perp$ and proportional to $1/E^3$.

We may calculate the expected size of the shift using the results of chap. 2. We have

$$B_\perp = 0.21\, i_\perp$$

($B_\perp$ in Gauss, $i_\perp$ in A) where $i_\perp$ is the current in the transverse field coil, and in argon we take

$$v_{beam} = 8 \times 10^4 \text{ cm/sec}$$
$$\tfrac{1}{4}\alpha_t E^2 = 12.2 \text{ MHz at } E = 10^5 \text{ V/cm}$$

where the velocity taken corresponds to the peak of the velocity distribution given in chap. 3, and α_t comes from measurements to be described in Section II of this thesis. From these we get

$$B^m = 8.9 \times 10^{-4} \text{ G at } E = 10^5 \text{ V/cm in A.}$$

The data of fig. 5.2 was taken with $i_\perp = 5$ mA, and at an observed transition frequency of 120 kHz; the expected change in dipole-like shift on reversing $i_\perp$ is, under these conditions:

$$\Delta\delta\nu^m = 3.7 \times 10^{-2} \text{ Hz} \quad \text{at } E = 10^5 \text{ V/cm}$$

Taking a field plate gap of 2.5 mm, this gives

$$\Delta\delta\nu^m = 2.7 \text{ Hz} \quad \text{at EHT of 3 kV}$$

(corresponding to $E = 2.4 \times 10^4$ V/cm), while the measured value under these

conditions is 3.6 Hz. In view of the number of imprecisely known factors, especially the effect of the velocity distribution, this seems to be fair agreement. We conclude that the dominant effect at low values of E and moderate values of $B_\perp$ is the residual $\underline{v} \times \underline{E}$ effect, which behaves as predicted.

The effect has also been observed in krypton and xenon. At an observed transition frequency of 40 k Hz (our usual running frequency), and at 3kV EHT, the observed values of $\Delta \delta \nu^m$ are about 0.6 Hz and 0.2 Hz respectively, on reversing $i_\perp$ = 10 mA. The calculated values are 0.7 Hz and 0.3 Hz.

It is observed that for $i_\perp = 0$ the remaining shifts at 3 kV are about 1/10 the size of these. If we suppose that $\underline{v} \times \underline{E}$ effects are dominant so that the vanishing of the observed shift corresponds to the vanishing of $B_\perp$, this implies that at $i_\perp = 0$ there is a misalignment θ between $\underline{E}$ and $\underline{B}$ of 10^{-2} radians. Using this value, we find $\delta \nu^m$ equal to about 10^{-3} Hz at E = 10^5 V/cm in Kr, and 0.3×10^{-3} Hz in Xe. These values are below our present experimental limits. Because θ is sufficiently low without additional cancellation, no trouble from the $\underline{v} \times \underline{E}$ effect should arise when the magnetic field is automatically reversed. This will not be the case, however, if the experimental precision should be significantly increased in the future.

We note again that these results assume the dominance of $\underline{v} \times \underline{E}$ effects at low E. However, the shifts observed at low E are very much larger than those at high E so that any effect comparable in size with the $\underline{v} \times \underline{E}$ effect at low fields must also depend inversely on E. Now, if this hypothetical effect falls off less rapidly than $1/E^3$, it will dominate $\underline{v} \times \underline{E}$ at high E, and again we may neglect $\underline{v} \times \underline{E}$ at least until the "new" effect has been traced. To make uncancelled $\underline{v} \times \underline{E}$ a problem, there must therefore exist some other shift, larger than $\underline{v} \times \underline{E}$ at small E, and falling off more rapidly with increasing E. This seems implausible physically, and as we have seen there is no evidence for any such shift in the observed dependence of shift on electric field.

We note that under usual conditions the sign of the $\underline{v} \times \underline{E}$ effect depends in an ill-defined way on the sign of $B_{||}$, since reversal of $B_{||}$ usually completely changes $B_{\perp}$; this is why the $\underline{v} \times \underline{E}$ effect must be small before automatic magnetic field reversal is useful. However, if $B_{\perp}$ is sufficiently large not to be greatly disturbed by reversing $B_{||}$, the $\underline{v} \times \underline{E}$ effect will be independent of the sign of $B_{||}$. One usual way of checking shift behaviour is to observe the effect of manual reversal of connections to the electric field plates; clearly the sign of the $\underline{v} \times \underline{E}$ shift reverses under this operation. This has been observed.

5.2 Power shifts and other voltage magnitude dependent effects

In chap. 2 we discussed a two-quantum resonance in a single r.f. region, and produced an order-of-magnitude estimate of the r.f. dependent resonance shifts to be expected. In a Ramsey two-loop system, the r.f. perturbation which causes the shifts is of course present within the loops only, and under these conditions it is well known that the overall shift of the Ramsey resonance is of order ℓ/L times smaller than the shift of a single loop resonance, where ℓ is the length of a loop, and L the separation of the loops (see e.g. Ramsey, 1956). In Xe, the dominant shift for a single loop is

$$h\,\delta\nu_2^{(s)} \simeq (\mu_B g_J)^3 \frac{B_{r.f.}^4}{(\frac{1}{4}\alpha_t E^2)^2 B_{||}}$$

$$\therefore \quad \delta\nu_2^{(s)} \simeq 100 \text{ Hz}$$

at $\nu = 40$ k Hz, $E = 10^5$ V/cm. In our machine $\ell/L = 1/20$, so we expect for the shift in the Ramsey resonance

$$\delta\nu_2 \simeq 10 \text{ Hz}.$$

We note again that this by itself does not constitute a dipole-like shift because it is independent of the sign of the electric field. However, any change δE in field magnitude which occurs on reversal of the field will lead to a dipole-like shift

$$\delta\nu_2(\text{dipole-like}) \simeq 10 \times 4 \frac{\delta E}{E} \text{ Hz}.$$

If we rewrite $\delta\nu_2$ in terms of the effective transition matrix element b':

$$\delta\nu_2 \simeq \frac{h(b')^2}{(\mu_B g_J) B_{||}}$$

we see that $\delta\nu_2$ should be independent of electric field if b' is kept constant. In general b' will be kept constant at around the value for optimum

transition probability if any deliberate change in E is made. Without such a deliberate change in b', we have of course $\delta\nu_2 \propto 1/E^4$.

The situation becomes more complicated at low electric field and high $B_{||}$, since under these conditions $\delta\nu_1$ may become important. We write

$$h\delta\nu_1 \simeq (\mu_B g_J)^3 \frac{B_{rf}^2 B_{||}}{(\frac{1}{4}\alpha_t E^2)^2} \frac{\ell}{L}$$

$$\simeq b' \times \frac{(\mu_B g_J) B_{||}}{(\frac{1}{4}\alpha_t E^2)} \frac{\ell}{L}$$

$$\therefore \quad \delta\nu_1 \simeq 0.3 \text{ Hz}$$

at $\nu = 40$ k Hz, $E = 10^5$ V/cm. More generally, then, we have for Xe (at constant transition probability, or b')

$$\delta\nu^{\text{r.f.}}(\text{dipole-like}) \simeq 4 \frac{\delta E}{E} \times \left| 10 \times \frac{40}{\nu} - .3 \times \frac{\nu}{40} \times \frac{10^{10}}{E^2} \right| \text{ Hz}$$

where ν is in k Hz and E in V/cm, and b' is at its optimum value. The relative sign of the two terms is the same as for the case of static perturbations.

A further level shift dependent on the magnitude of E is that due to a static $B_\perp$. This gives a dipole-like shift

$$h\delta\nu^{(B_\perp)}(\text{dipole-like}) = \frac{25}{9} (\mu_B g_J)^3 \frac{B_\perp^2 B_{||}}{(\frac{1}{4}\alpha_t E^2)^2} \times 4 \frac{\delta E}{E} \times \frac{1}{2}$$

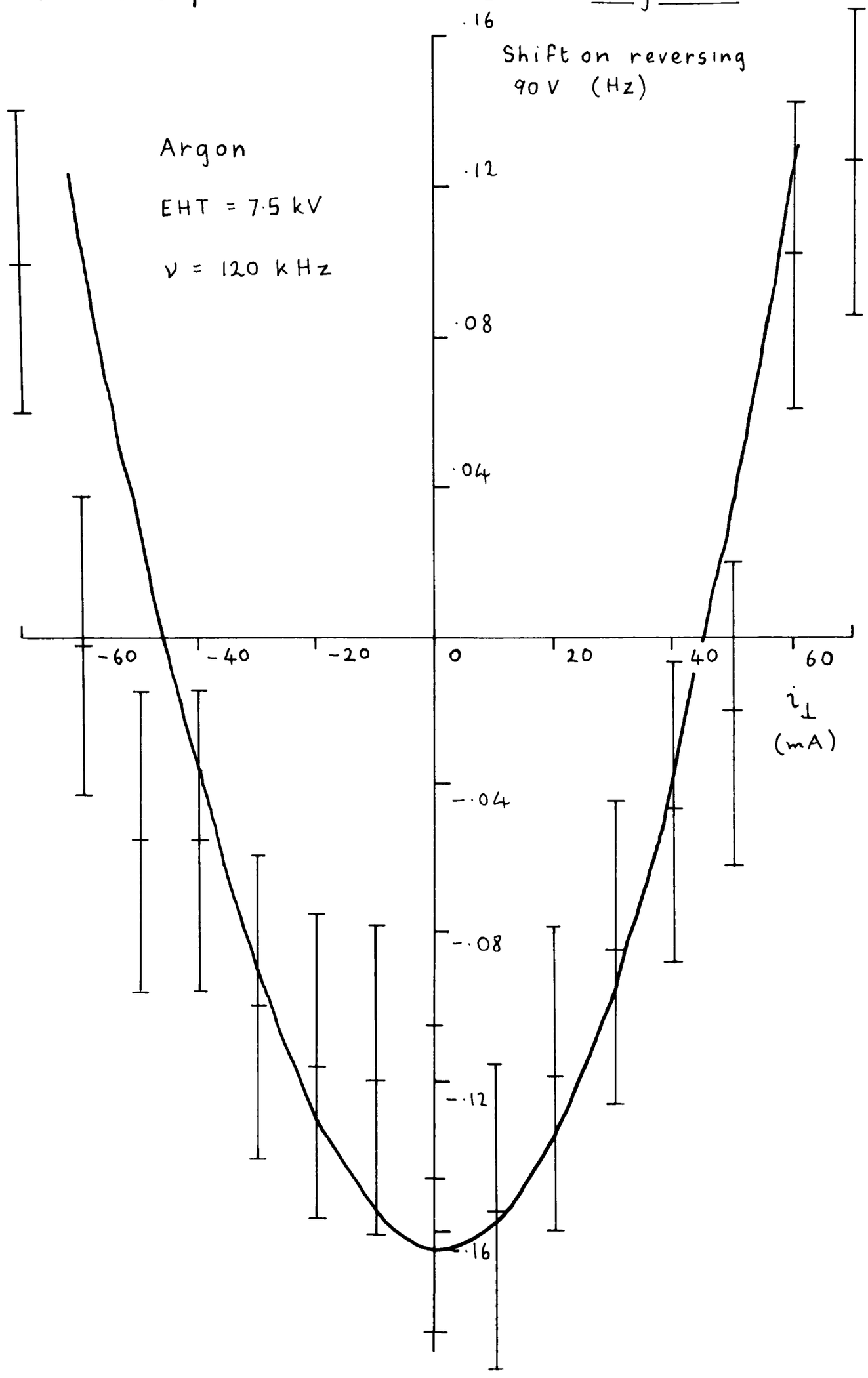
In Xe, taking $E = 10^5$ V/cm, $\nu = 40$ k Hz, $B_\perp = 1$ m G ($i_\perp \simeq 5$mA), this gives

$$\delta\nu^{(B_\perp)}(\text{dipole-like}) \simeq 3 \times 10^{-3} \frac{\delta E}{E} \text{ Hz}$$

which is negligible; however, at $\nu = 120$ k Hz, $E = 2.5 \times 10^4$ V/cm,

Field dependence vs. $B_\perp$

Fig 53



$$\delta \nu^{(B_\perp)} \text{(dipole-like)} \simeq 3 \frac{\delta E}{E} \quad \text{Hz}$$

which is comparable with the r.f. effects.

Experimentally, the field dependence of the resonance frequency can be measured directly by observing the frequency shift obtained on reversing a small voltage in series with the main high voltage supplies to the field plates. We show in fig. 5.3 a graph of measured resonance E dependence against $i_\perp$, taken in Argon at 120 k Hz and 7.5 kV EHT; the shift plotted is that obtained on reversing a 90 V battery in the lead from one EHT supply. It will be seen that the plot has a parabolic shape, with a nonzero voltage dependence at $i_\perp = 0$. It may be verified that the order of magnitude of the shifts is accounted for by the discussion given above; the parabola drawn is in fact calculated from the expression for $\delta \nu^{(B_\perp)}$.

The dependence of the voltage-dependent shift on r.f. amplitude has been observed in Xe, under conditions where $\delta \nu_2$ should dominate. In measurements taken on 15 Aug. 1969, at 6 kV EHT and $\nu = 28$ k Hz, we found the following dependences on r.f. amplitude:

r.f. amplitude	shift on reversing 90 V (Hz)	dipole-like shift (Hz)
optimum	$0.4 \pm .03$	$+0.02 \pm .03$
.7 optimum	$0.2 \pm .03$	$+0.00 \pm .03$
1.3 optimum	$1.1 \pm .02$	$-0.01 \pm .03$

We note the expected rapid increase in voltage dependence on increasing r.f. amplitude, and the complete lack of correlation between dipole-like shift and voltage dependence. No increase in voltage dependence was found on reducing the EHT to 3 kV, although a dependence on transverse magnetic field was observed at 3 kV and $\nu = 130$ k Hz; the largest voltage-dependence shift observed with optimum r.f. amplitude was $1 \pm .03$ Hz, at 130 k Hz with $i_\perp = 20$ mA. At no

stage in any of these measurements was any correlation between dipole-like and voltage-dependence shifts observed.

It seems, then, that under normal operating conditions in Xe or Kr we may put for the dipole-like shifts arising from voltage dependence of the resonance:

$$\begin{aligned} & \delta\nu^{\text{v.d.}}(\text{dipole-like}) \\ \simeq\ & \delta\nu^{\text{r.f.}}(\text{dipole-like}) \\ \simeq\ & 10 \times 4\,\frac{\delta E}{E}\ \text{Hz}\ . \end{aligned}$$

The question remains as to how large δ E may be on reversing E. Such a change in E can arise from two sources: a change in applied voltage, and a change in plate separation. The first effect should be small; we have measured the change in output voltage from the Brandenburg EHT supplies on reversing the field, and find it to be less than 1 V. Voltage drop across the switches should be much less than this, giving

$$\delta\nu^{\text{v.d.}}(\text{dipole-like}) \lesssim 10^{-3}\ \text{Hz}$$

from voltage changes. It is in fact difficult to see how any systematic supply voltage changes can occur on reversal, especially since in later data collection we have buffered the Brandenburg outputs by adding 0.1 μF capacitors. More serious effects could arise from plate movement, about which we have no direct information; such effects would be particularly likely to occur for unequal positive and negative EHT supplies. To check directly for these effects, we have observed the dipole-like shifts as a function of r.f. amplitude. These measurements were made using the mechanical switch system described in chap. 4, at full operating voltage, when it unfortunately became impracticable to include circuitry for direct field dependence measurements. Results in Kr on 17 Sept. 1969, at 12 kV EHT and 40 k Hz, were

r.f. amplitude (mV)	dipole-like shift (Hz)
18	$-0.029 \pm .01$
36	$-0.033 \pm .02$
36	$-0.025 \pm .02$
18	$-0.032 \pm .01$

and similarly on 13 Sept. :

r.f. amplitude (mV)	dipole-like shift (Hz)
12	$+0.01 \pm 0.02$
28	0.00 ± 0.02
28*	-0.02 ± 0.03

* this measurement was taken with EHT supplies at 11 kV and 13 kV. Normally the supplies are set equal to better than 100V. Similar results have been taken on other occasions, and no evidence of any power-dependent shifts has appeared. Since a factor 2 increase in r.f. amplitude increases $\delta\nu_2$ by 16 times, the above results imply that power-dependent dipole-like shifts are at most of order 10^{-3} Hz. The observations also render unlikely another possible source of trouble, mechanical movement of the r.f. coils on reversing the EHT.

Probably the most important point about all these shifts is that they do not behave like an edm shift under magnetic field reversal. It will be seen below that there is no significant difference between shifts observed with and without reversal of magnetic field. We conclude that voltage dependent shifts are small and, if they ever should appear, may be easily cancelled.

One final possibility is that the effect induced by a static $B_\perp$, $\delta\nu^{(B_\perp)}$, which has a $1/E^4$ dependence, might lead to spurious cancellation of the $\underline{v} \times \underline{E}$ effect at low E. However, the size of the effect seems to be far too small, and

the fact that it depends on $B_{\perp}^{2}$ means it must vanish at $B_{\perp} = 0$ anyway.

We note that the behaviour of the power and other voltage-dependent shifts under manual reversal of field plate connections depends on the source of the change of field, δE. If δE is due to some asymmetry in the field plate system, the shifts will change sign. If δE should be due to voltage changes associated with leakage currents in the EHT switches, for instance, this would not be so.

5.3 Magnetic field effects

We shall report in the next chapter our most recent set of data actually taken to obtain a limit on the electron edm; the final precision is about 5×10^{-3} Hz. The change in magnetic field required to give a resonance shift equal to this is about 2×10^{-9} Gauss, corresponding to a few μ Gauss outside the magnetic shields. Moreover, most magnetic field changes correlated with electric field reversals are such that the shifts they induce change sign under reversal of $B_{||}$, like true edm shifts. The potential importance of magnetic field shifts is clear.

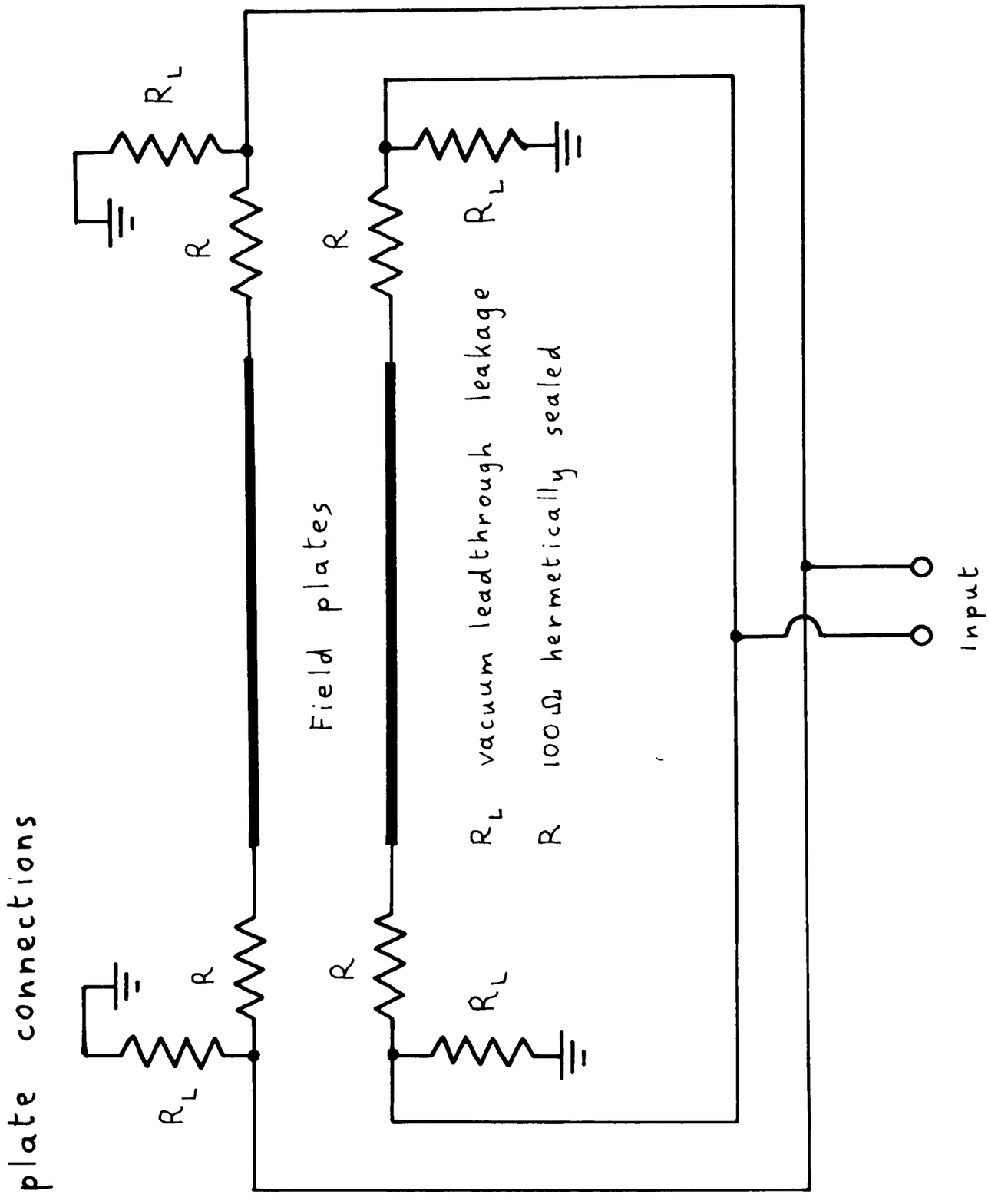
In our system, it is changes in $B_{||}$, the component of $\underline{B}$ parallel to $\underline{E}$, which are important and these can arise both from changes in B and from changes in the alignment of $\underline{B}$ and $\underline{E}$; we discuss these cases separately.

a) Field magnitude effects

The mechanical relays responsible for electric field reversal produce magnetic fields of about 5 Gauss at a distance of 5 cm. The relays are located at about 4 m from the resonance region, giving an expected field of order 10^{-5} Gauss at the magnetic shields, or 10^{-8} Gauss inside; this corresponds to a shift $\simeq 4 \times 10^{-2}$ Hz on reversal. The observed shift is about 10^{-1} Hz. The method of cancelling such shifts by the use of two banks of switches has been described in chap. 4. The completeness of such cancellation depends on the linearity of the resonance shape near the operating point; in view of the smallness of the shifts, we expect very small nonlinear effects, so that shifts due to non-cancellation should be negligible. This has been checked by running with the relays operating but with the field plates connected directly to the EHT supplies; under these conditions no significant dipole-like shifts have been observed, even with the relays positioned 1.5 m from the resonance region.

The magnetic effect of leakage current from the field plates is difficult to estimate since if the plates were plane and the current density uniform the magnetic field produced should be precisely perpendicular to $\underline{E}$, and first order effects should vanish. We have, however, directly measured the effect of passing

Fig 54


Field plate connections
R_L
R
R
R_L
R
R
R_L
R_L
Field plates
R_L vacuum leadthrough leakage
R 100Ω hermetically sealed
Input

current down the plates (which are provided with vacuum leadthroughs at each end) and find a current of 100 μA gives a shift of about 1 Hz on reversal. As mentioned in chap. 3, the actual plate current at full running voltage is measured at less than 10^{-8}A by timing the discharge rate of the interplate capacitance; this figure has also been checked by measuring the flow of current from one plate at ground potential while the other is at 12 kV. It appears from this that dipole-like shifts from leakage currents should be less than 10^{-4} Hz. However, it is suspected that the vacuum leadthroughs used, which are standard glass-to-metal seals, may be rather unreliable, and as a precaution we have attempted to eliminate the effects of any leakage currents in the seals by using the setup of fig. 5.4, where the plates are fed from both ends. The 100 ohm resistors inside the vacuum chamber prevent hum currents flowing round the closed loop formed by a plate and its feed wires.

We have mentioned the use of an extended gating period to avoid effects from transient charging currents. We have usually worked with a gating period 16 times a basic clock period of about 30 msec, i.e. 480 msec gating; this allows $\simeq$ 300 msec settling period after the completion of switching. This is very much greater than any time constants associated with the switching, with one possible exception: it is observed that if the transient reduction in output voltage from the Brandenburg EHT supplies is sufficiently severe following switching, the recovery to full voltage is rapid ($\simeq$ 10 msec) except for the last few tens of volts, which show a "creep" over about 1 second. However, even this creep can induce a charging current only of order 10^{-8}A, which is again too small to be troublesome. To check these effects, we have halved the gating period, with no significant change resulting. As a further precaution, we have added the 0.1 μF buffer capacitors mentioned above in connection with power shifts; these should greatly reduce transient disturbance of the Brandenburgs.

A further possibility associated with charging currents is an effect due to

hysteresis in the mumetal shields "remembering" some fraction of the current. The size of such an effect is difficult to estimate, but no increase in dipole-like shift is observed on reducing the EHT switching current-limiting resistors from 10 Mohm to 100 kohm.

One difficulty which has been encountered in previous experiments is modulation of the magnetic field through mechanical coupling of the magnetic field coils to the electric field plates. We have attempted to eliminate this possibility by the nature of the mechanical design; since the only contact between the electric field assembly and the coils is through 3 pins which are positioned at the ends of the resonance section, where it joins the deflector cans, it is difficult to see how there can be any coupling at all. A more serious possibility is suggested by the observation that the resonance frequency is rather sensitive to mechanical motion of the apparatus, apparently as a result of relative movement between the deflecting magnets and the resonance region. It may be that electrostatic forces on the EHT lead-in wires are sufficient to provide significant shifts through this mechanism. We have tried to reduce this effect as far as possibly by arranging long hanging loops in the lead-in wires, so that forces between them are not easily transmitted to the apparatus.

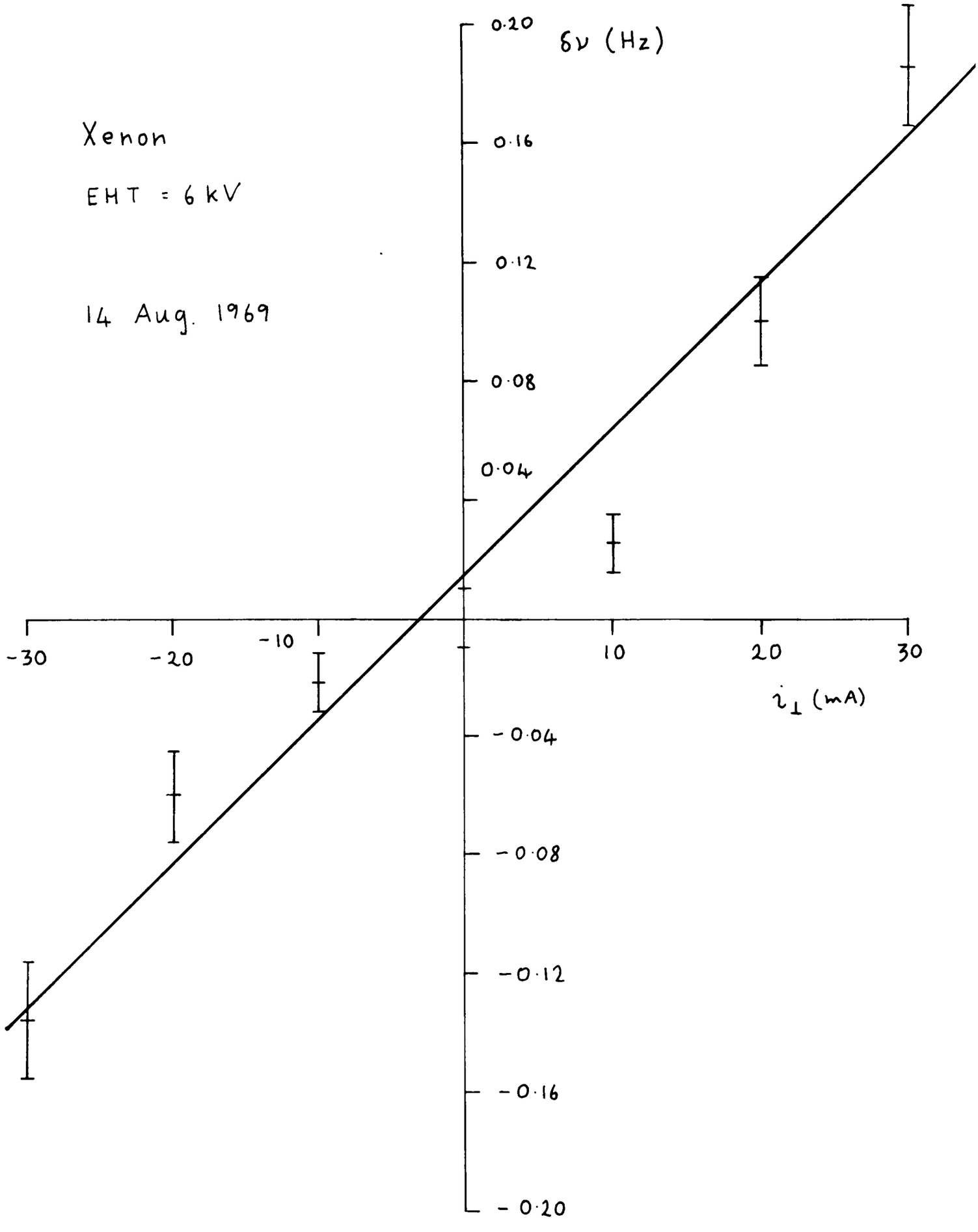
One further effect in this class is a possible modulation of the magnetic field current supply via r.f. interference from the switching relays. To produce a shift of the relevant size, a current modulation of a few parts in 10^7 is required. We have not been able to measure the current to this precision. It seems that there will be at least some transient modulation of the supply, but all instruments used in an attempt to observe this have proved more sensitive to r.f. interference than the current supply. It is difficult to see how any modulation could be correlated with the sign of electric field, but the required effect is so small it is not possible to be fully confident on this point.

We note that all these effects reverse sign with $B_{||}$, with the possible

exception of EHT switch effects and r.f. modulation of the field supply. The shifts involving leakage or charging currents will also reverse sign under manual reversal of the field plates; switching effects will not do so, and the behaviour of the other effects is ill defined.

Plate-twisting shift

Fig. 5·5



b) Alignment effect

Suppose there is a component of magnetic field $B_\perp$ perpendicular to $\underline{E}$ and to the beam axis. If $\underline{E}$ rotates in a plane perpendicular to the beam axis, $B_{||}$ will be changed by

$$\delta B_{||} = B_\perp \delta\theta$$

to first order in $\delta\theta$. This will contribute to a dipole-like shift if there is any twisting of the field plates on reversal of $\underline{E}$. The size of such an effect is difficult to estimate.

When data was first taken in Xe at moderately high EHT, under circumstances where all the shifts we have so far discussed should be small, a shift approximately proportional to $i_\perp$ was indeed observed. We give a plot of observed dipole-like shift vs $i_\perp$, obtained on 14th Aug. 1969, in fig. 5.5. The size of shift observed, $\simeq$ 0.1 Hz at $B_\perp \simeq$ 6 mGauss, corresponds to $\delta\theta \simeq 10^{-5}$ radians. We note that this effect reverses sign if $B_{||}$ is reversed while $B_\perp$ is kept the same, in distinction to the residual $\underline{v} \times \underline{E}$ effect. This behaviour has been observed; on 15th Aug. 1969 we obtained the following results in Xe at ν = 70 k Hz :

EHT = 3 kV

$i_{||}$ (mA)	$i_\perp$ (mA)	dipole-like shift (Hz)
+35	-20	+0.15 ± 0.04
+35	+20	-0.06 ± 0.04
-35	+20	-0.70 ± 0.10
-35	-20	+0.55 ± 0.03

EHT = 6 kV

+35	-20	-0.06 ± 0.03
+35	+20	+0.19 ± 0.03
-35	+20	-0.19 ± 0.10
-35	-20	+0.20 ± 0.03

Although the signal to noise is rather poor, these are certainly indicative of a shift which reverses sign with $B_{||}$ at high E. It seems that the shift persists at low E, where it is only slightly smaller than the $\underline{v} \times \underline{E}$ effect.

A large increase in shift was observed on unbalancing the positive and negative EHT supplies; a 1 kV imbalance at 6 kV gave about a 1 Hz shift at $i_{\perp} = 30$ mA, and the shift changed sign when the sign of the imbalance was reversed. This suggested all the shift might be due to lack of careful balancing; however, on setting the supplies equal to about 10 V, using Fluke precision potential dividers, a shift of the same size as those given in the table still remained. It appears that there are two different mechanisms for the origin of $\delta\theta$, one not requiring voltage asymmetry.

At about this time, the oil-filled relays were brought into operation (the above data were taken using reed relays), the EHT was increased to 12 kV and the plates promptly broke down. On removing the plates for repolishing (the causes of the breakdown was a piece of metal swarf stuck to a plate), it was found that most of the nylon assembly screws were loose, presumably having shifted under the mechanical stress of repeated field reversals. Having reassembled the plates as tightly as possible, it was found that the plate-twisting effect was at least ten times smaller than previously. At 12 kV, no $B_{\perp}$ -dependent shift has been subsequently observed, except with the EHT supplies unbalanced (at 11 kV and 13 kV) when shifts of -0.04 ± 0.02 Hz and $+0.06 \pm 0.02$ Hz were observed at $i_{\perp} = +10$ mA and -10 mA respectively (18th Oct. 1969).

We conclude that the plate twisting effect should be negligible in all measurements following the reassembly of the field plates, which includes the data of the next chapter, as long as the EHT supplies are balanced to the usual 100 V, with $i_{\perp}$ less than a few mA. This is particularly fortunate because it is difficult to employ automatic magnetic field reversal in the presence of a shift

with large $B_\perp$ dependence. Our conclusion assumes the field plate assembly has remained tight; for this reason rather frequent searches for any $B_\perp$ dependence have been made during data collection.

Clearly the situation outlined is less than fully satisfactory, and any future modification to the apparatus must include redesign of the field plates to reduce the risk of twisting.

5.4 Other effects

We have mentioned the effect of nonlinearities in resonance shape in connection with shifts arising from the EHT switches. One can conceive of similar mixing effects involving other shifts. The only shifts significantly larger than the uncancelled EHT switch effect are the calibration shift, and shifts due to 50 Hz mains pickup. It is difficult to see what the calibration could mix with to produce breakthrough into the dipole analysis channel; at various stages in the experiment we have increased the calibration shift to 10 Hz from its normal 1 Hz value, and reversed it, never with any observable effect on any analysis channels besides the calibration channel itself. 50 Hz pickup can modulate the resonance frequency by up to 10 Hz; however, this shift cannot interact with any of the control and analysis waveforms unless some harmonics virtually coincide. At one stage we had sufficiently good coincidence to observe slow beats on the pulse rate meter monitoring beam intensity, but even under these conditions no effect was observed in any analysis channel.

Another possibility involving hum pickup is interaction between background 50 Hz magnetic fields and fields arising from charging currents between the EHT plates caused by 50 Hz ripple on the EHT supplies. These fields might add for one sign of electric field and partially cancel for the other; this might produce a dipole-like shift if the 50 Hz modulation of the resonance were rectified by nonlinearity of the resonance. This rectification has been observed, and amounts to about 1 Hz shift for a 100 Hz modulation amplitude. However, the ripple on the EHT supplies is low, about 10 V peak to peak, which gives only $\simeq 1 \mu A$ charging current or a fraction of 1 Hz modulation of resonance position. To check the effect, we injected about 100 V 50 Hz ripple in series with one of the EHT supplies; no dipole-like shift was observed with any of several settings of resonance field "hum-bucking".

If there exists some modulation of the overall beam intensity on reversing

the electric field ("volts-chopping"), this may give rise to a dipole-like signal if the size of the effect changes when the sign of the resonance slope is reversed. "Volts-chopping" of about 10^{-3} times the full resonance intensity has been observed on reversing 10^{5} V/cm. However, the resonance shape is very little changed on reversing the slope (the calibration signals for the two signs of slope are equal to about 1%), and the average beam intensity is kept constant under reversal of slope by the feedback locking the resonance position; in view of this it is difficult to see how the "volts-chopping" can depend on the sign of the slope. The size of the "volts-chopping" alters spontaneously from time to time; no correlation between this behaviour and any dipole-like signal has been observed.

It is possible that steady drifts could give rise to spurious shifts, although these are unlikely to be specifically dipole-like. The largest effects are drifts in resonance frequency. Drifts observed under normal running conditions are usually less than 100 Hz per hour, or 3×10^{-2} Hz/sec; it is unusual for any drift to remain steady for as long as an hour. Even with a simple square-wave analysis waveform with 1 second period (about the basic EHT switching period), this can contribute an apparent shift of only 3×10^{-2} Hz. We have always used a dipole analysis waveform of very much greater complexity, and it seems most unlikely that there are any coherent drift effects capable of giving recognisable spurious shifts. No signals correlated with drifts have ever been observed in the dipole channel or any other channel, even when we have deliberately swept the resonance frequency at rates much greater than those normally encountered. This also seems to rule out less straightforward effects of drift, in which drift might contribute to a breakdown of orthogonality between analysis channels. A possible exception to this is mentioned in chap. 6.3, where simple waveforms not differing much from the calibration analysis waveform were used. Unfortunately we have no direct check on this. The effect is of order 10^{-2} Hz; no such simple waveforms were subsequently used.

Another class of possible shifts arises from transient effects. We have already discussed the case of charging currents, which give rise to transient frequency shifts which are essentially edm-like; we discuss here the slightly different case where the effect is not edm-like, but may still give a signal in the dipole analysis channel by the sort of process described in chap. 4.3. These effects, like the mixing effects, represent a breakdown of the orthogonality on which the analysis system is based. There are two lines of defence against such effects: the use of adequate gating periods, and the use of waveforms with structures designed to reject any transients remaining. The charging current effects are essentially independent of waveform structure. We note also that transient effects of the type to be discussed will generally lead to signals not just in the dipole channel but in any channel whose analysis waveform has a constant phase relation with the change causing the transient.

Transient effects due to reversal of resonance slope have been observed. If the resonance switching waveform corresponds to (1 1) in the notation of chap. 4, and on analysis waveform (1) is used (this is always negative just after the waveform (11) changes sign), a steady signal of about 1% of the full resonance intensity is observed when a 10 msec interface gating period is used. This effect practically vanishes for a 30 msec gating period. No such signal is obtained using more complicated analysis waveforms, nor has any effect on dipole-like shifts been observed when the gating period is changed.

We expect that transient effects following EHT switching, of the sort used as an example in chap. 4.3, should be adequately allowed for by the long gating period. In some runs, additional protection has been provided by arranging the resonance slope switching waveform to have a phase reversal after a complete cycle of EHT switching. No dependence of dipole shift on waveform structure has been observed, and, as mentioned during the discussion on charging currents, no effect is observed on halving the gating period.

The normal gating period following magnetic field reversal is 960 msec. Although no protection against transients was built in to the waveforms used with magnetic field reversal, no evidence of shifts has appeared in channels orthogonal to the dipole channel but still sensitive to the field reversal transients. Other indirect evidence of the unimportance of these effects will be presented below; nonetheless any future experiments should use better constructed waveforms.

It is clearly difficult to predict the behaviour of any of these shifts, if they escape cancellation, under reversal of magnetic field or electric field plate connections.

Chapter 6. Experimental Results

6.1 Procedure for experimental runs

Despite the precautions taken against spurious effects, there remains at the present time a dipole-like shift of about 10^{-2} Hz at high electric field in Kr and Xe. Before the data to be presented in this chapter were taken, attempts were made to analyse the behaviour of this residual shift. The shift seems to have no strong dependence on transverse magnetic field, but apart from this no clear results were obtained, and it became obvious that the shift was changing its size and sign erratically and apparently spontaneously. This behaviour is also demonstrated in the data to be presented. For this reason it is clear that the effect does not represent a genuine edm interaction.

It was decided to attempt to cancel the effect by comparing the shifts observed in Xe with those in Kr. As has been pointed out, a true edm effect should be about 6 times greater in Xe than in Kr; almost all other shifts should be of the same order of magnitude in the two elements, and in particular magnetic field effects should be equal to the extent that the magnetic moments are the same. The cancellation appears to be effective. Further discussion of the residual shift will be given later.

We describe in this chapter three sets of runs, the first two without automatic reversal of the magnetic field and the third with. In each case, a complete run consists of a run in Kr, a run in Xe lasting twice the time, and a final run in Kr. The procedure for such a run is as follows. All background instrumentation is switched on and the "up-down counter" program read into the computer; the desired waveform structures and other variables are read in. The source recirculating system is evacuated, then closed off and krypton let in. The gas flow rate into the discharge is adjusted for optimum signal, and the r.f. amplitude and resonance hum-bucking are adjusted. The effect of the hum-bucking is observed by viewing the output from the pulse-rate meter on an

oscilloscope. By adjusting the magnetic field, the resonance is set approximately to the point of greatest slope; if automatic magnetic field reversal is to be used, this adjustment and the hum-bucking must be performed for both signs of field. All control inputs are now connected to the computer output terminal, and data collection by the "up-down counter" program is initiated.

Data collection is allowed to proceed for a predetermined time (usually a few hours), with interruptions or further adjustments being required only exceptionally. At the end of the period, data collection is terminated, the krypton is evacuated from the recirculating system and replaced by xenon. The adjustments mentioned are remade and data collection restarted. The change-over takes less than five minutes; the apparatus is disturbed as little as possible at this time.

After the final krypton run, the correct operation of the data collection system may be checked by observing the $\underline{v} \times \underline{E}$ shift at low E and high $B_{\perp}$.

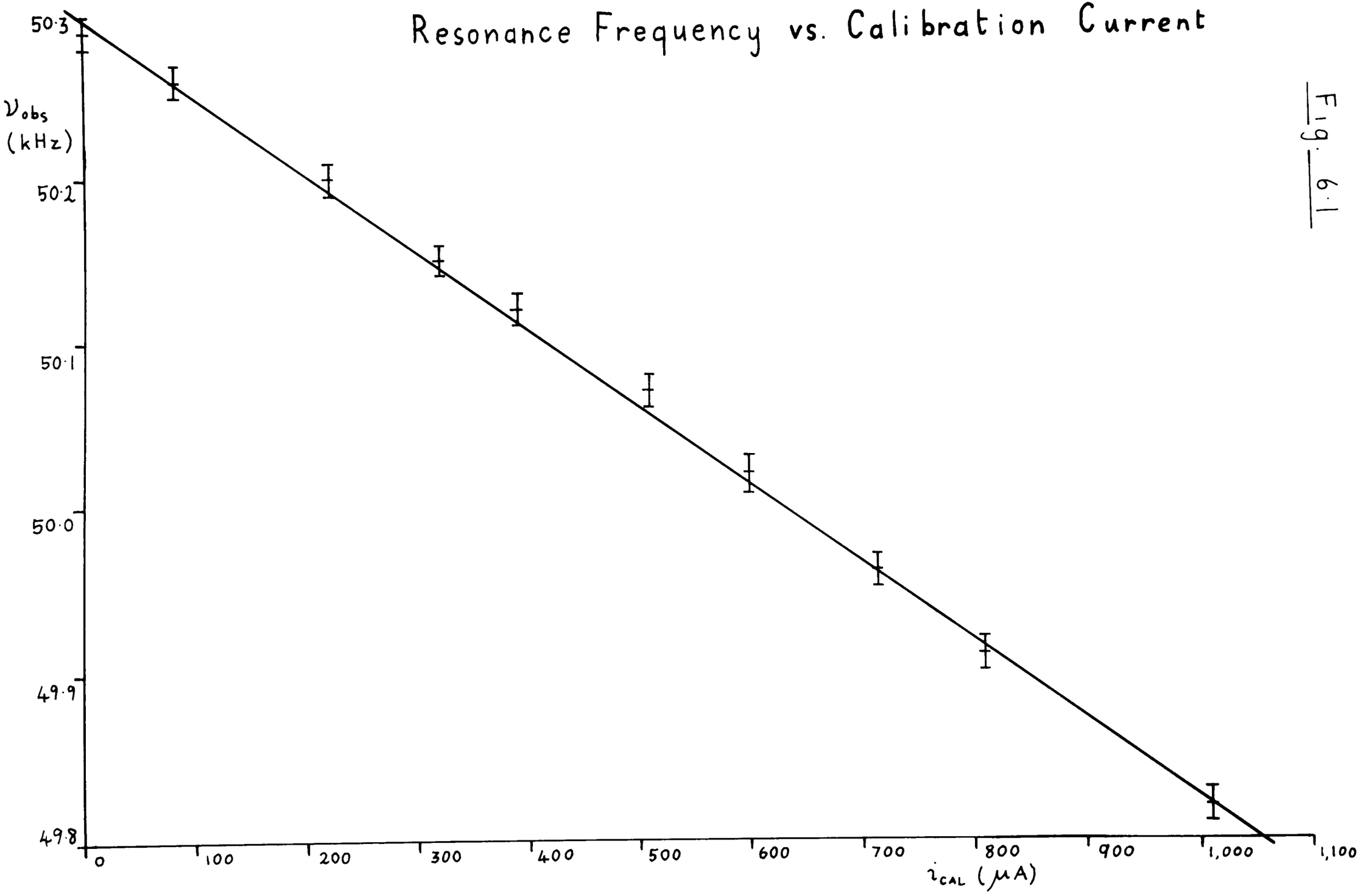

Resonance Frequency vs. Calibration Current
ν_{obs} (kHz)
50·3
50·2
50·1
50·0
49·9
49·8
0
100
200
300
400
500
600
700
800
900
1,000
1,100
i_{CAL} (μA)

Fig. 6.1

6.2 Preliminary measurements

We briefly mention all measurements directly relevent to the interpretation of the data to be presented. We require in particular the size of the calibration shift and of the electric field, and information sufficient to determine the sign of any dipole interaction.

The calibrating magnetic field is supplied by a Helmholtz coil. Using the dimensions of the coil and the mumetal shields, we find

$$\delta\nu_{obs} = (0.45 \pm 0.02)\, i_{cal} \text{ MHz} \quad (i_{cal} \text{ in A})$$

where $\delta\nu_{obs}$ is the change in observed transition frequency of the $M_J = +1 \longrightarrow -1$ transition. We have measured $\delta\nu_{obs}$ vs. i_{cal} directly by manually resetting the r.f. oscillator to the peak of the Ramsey pattern for various i_{cal}. The results are plotted in fig. 6.1; the slope of the graph gives

$$\delta\nu_{obs} = (0.471 \pm 0.005)\, i_{cal} \text{ MHz} \quad (i_{cal} \text{ in A})$$

Now, the measured current change on switching the calibration current supply used in all data collection is $2.15 \pm .005\ \mu$A, giving a calibration shift

$$\delta\nu_{cal} = 1.01 \pm .03 \text{ Hz}$$

in the observed resonance frequency. In the following, we shall express all outputs from the "up-down counter" program as equivalent shifts in the observed resonance frequency, by comparing them with the calibration output and taking the calibration value to be exactly 1 Hz for convenience.

The field plate gap a_{gap} has been measured at all accessible points (see section II of this thesis). It is found to vary over about 10% along the plates; we require the averaged value of electric field, and hence the average

value of $^1/a_{gap}$. We find

$$(^1/a_{gap})^{-1} = 2.70 \pm .04 \text{ mm.}$$

The applied EHT during all the data collection was measured as ± 12.5 kV, but the meters used read about 500 V too low. The average electric field is therefore

$$E = (0.96 \pm .04) \times 10^5 \text{ V/cm.}$$

All the data was taken at a resonance frequency of 40 k Hz, with no applied transverse field.

We shall quote as positive all frequency shifts which give a positive accumulation in the output from the "up-down counter" program. We have always used initial phases of control and analysis waveforms set so that the control outputs start in the logical 0, or low, state and analysis waveforms start at -1. It is found that when the resonance slope control is in the 0 state, an increase in transition frequency gives a fall in intensity when the resonance is correctly set. The connections of the electric field plates and the magnetic field coils are designated RR(red-to-red) and RB (red-to-black). For both electric and magnetic fields connected RR (or both RB), and with all switches in the 0 state, the electric and magnetic fields are observed to be in opposite senses, defining electric field direction as from positive to negative potential and magnetic field by right-hand corkscrew rule, with conventional current. This holds also for runs where the magnetic field is not automatically reversed. Thus if there is a dipole interaction such that the resonance frequency is increased when the electric and magnetic fields are antiparallel (as defined), a positive accumulation will occur in the dipole analysis channel.

This is all the information needed to find the sign of any edm detected in the data. However, we shall only be interested in relative signs, and we do not discuss the conventions needed to define an absolute edm sign.

For such a discussion see, e.g., Tinker (1967).

Fig 6·2

DATA COLLECTION PARAMETERS. SET 1.

BASIC PERIOD: 1024+512 ON 10 MICROSEC. RANGE.
INTERFACE GATING PERIOD: 512 ON 10 MICROSEC. RANGE.
EHT GATING: 32 TIMES BASIC PERIOD.
INPUT SCALING FACTOR: 8.

CONNECTIONS: FIELD PLATES RR
MAGNETIC FIELD RR
CALIBRATION (1 HZ) RB OR RR.

WAVEFORMS:

13/100000011	RESONANCE SLOPE REVERSE
12/101;5	CALIBRATION CONTROL
11/0	
10/10000;5	EHT SWITCH 2
7/0	
6/100111;5	EHT SWITCH 1
0/100000011	FEEDBACK ANALYSIS
1/1	DRIFT ANALYSIS
2/110110011	NOISE 1 ANALYSIS
3/1010100011	NOISE 2 ANALYSIS
4/11111100011	DIPOLE ANALYSIS
5/110100011	CALIBRATION ANALYSIS
14/1;15	
15/1;13	
16/12	
17/0	

Results. Set 1

Table 6·1

7·9·69

Run \ Channel	NOISE 1	NOISE 2	DIPOLE
Kr 1	+17·5	+ 6·8	+39·0
Xe 1	+15·9	+12·0	+47 9
Xe 2	+24·0	+17·5	+31·6
Kr 2	+18·0	+22·6	+20·4
Mean	+18·9	+14·7	+34·6
Standard deviation	3 1	5·9	10·1
Mean Xe - mean Kr	+ 2 2	+ 0·5	+10·0

7·9·69

Run \ Channel	NOISE 1	NOISE 2	DIPOLE
Kr 1	+ 7·1	+ 8·6	+17·1
Xe 1	+11·4	- 5·2	+ 4·5
Xe 2	+ 7·8	- 0·5	- 0 3
Kr 2	+ 8·1	- 9·9	+ 1·9
Mean	+ 8·6	- 1·8	+ 5·8
Standard deviation	1 6	6·8	6·7
Mean Xe - mean Kr	+ 2·0	- 2·2	- 7·4

All outputs expressed as shifts, in mHz

Fig. 6·3

DATA COLLECTION PARAMETERS. SET 2.

BASIC PERIOD: 2048+1024 ON 10 MICROSEC. RANGE.
INTERFACE GATING PERIOD: 1024 ON 10 MICROSEC RANGE.
EHT GATING: 16 TIMES BASIC PERIOD.
INPUT SCALING FACTOR: 16.

CONNECTIONS: FIELD PLATES RR
MAGNETIC FIELD RR
CALIBRATION (1 HZ) RB.

WAVEFORMS:

13/10001111	RESONANCE SLOPE REVERSE
12/101;4	CALIBRATION CONTROL
11/0	
10/10000;4	EHT SWITCH 2
7/0	
6/100111;4	EHT SWITCH 1
0/10001111	FEEDBACK ANALYSIS
1/1	DRIFT ANALYSIS
2/110111111	NOISE 1 ANALYSIS
3/1010111111	NOISE 2 ANALYSIS
4/1111111111	DIPOLE ANALYSIS
5/11011111	CALIBRATION ANALYSIS
14/1;14	
15/1;6	
16/12	
17/0	

Results. Set 2 Table 6·2

17·9·69

Run \ Channel	NOISE 1	NOISE 2	DIPOLE
Kr 1	-8·9	+5·8	-31·6
Xe 1	+4·2	-3·4	-30·5
Xe 2	+1·2	+15·1	-51·6
Kr 2	-5·8	-7·7	-41·5
Mean	-2·3	+2·5	-38·8
Standard deviation	5 3	8 9	8·5
Mean Xe - mean Kr	+10·0	+6·8	-4·5

19 9 69

Run \ Channel	NOISE 1	NOISE 2	DIPOLE
Kr1	-1·3	+12·6	-16·2
Xe1	-4·2	+5·2	-38·0
Xe2	+9·9	+4·8	-25·7
Kr2	-1·5	+14·0	-23·8
Mean	+0·7	+9·1	-25·9
Standard deviation	5 4	4·3	7 8
Mean Xe-mean Kr	+4 3	-8·3	-11·9

22 9 69

Run \ Channel	NOISE 1	NOISE 2	DIPOLE
Kr1	-4·4	+7·6	+25·2
Xe1	-0 2	+6·8	+15 1
Xe2	-1·2	+5·3	+28·0
Kr2	-10·1	+0·2	+25·9
Mean	-4·0	+5·0	+23·5
Standard deviation	3·9	3·3	5·0
Mean Xe-mean Kr	+6 6	+2·2	-4·0

All outputs expressed as shifts, in mHz.

Results. Set 2 (cont.)

Table 62 (cont.)

23·9 69

Run \ Channel	NOISE 1	NOISE 2	DIPOLE
Kr 1	+1·5	+2·7	+15·5
Xe 1	-1·4	-8·7	+30·1
Xe 2	-8 2	0·0	+26·5
Kr 2	-2·6	+0·5	+19·6
Mean	-1 4	-1·4	+22·9
Standard deviation	4 2	4 4	5·7
Mean Xe - mean Kr	-6 9	-6·0	+10·7

23 9 69

Run \ Channel	NOISE 1	NOISE 2	DIPOLE
Kr 1	-4·1	0·0	+13·0
Xe 1	+9·0	-4·0	+ 7·6
Xe 2	-10·0	+6·0	+12·5
Kr 2	+ 2·9	+5·6	+26·4
Mean	- 5·5	+1 9	+14·9
Standard deviation	8·8	4·1	7·0
Mean Xe - mean Kr	+1·0	-1·8	- 9·7

All outputs expressed as shifts, in mHz.

6.3 Runs without magnetic field reversal

We give in fig. 6.2 the waveform structures and other relevant parameters for the first two runs, and in fig. 6.3 those used in the next five runs. We give the results obtained in tables 6.1 and 6.2.

The first two runs, both made on 7th Sept. 1969, each lasted 8 hours (2 hours in Kr, 4 hours in Xe, and 2 hours in Kr). If noise were due simply to counting statistics, we should expect for each 2 hour run a standard deviation

$$\sigma \text{ (shot noise, 2 hours)} = 2.5 \text{ m Hz}$$

In table 6.1 we give the standard deviations as estimated from the four results for each analysis channel for each run. The r.m.s. value of these standard deviations, which we may use as a measure of the true standard deviation, is

$$\sigma \text{ (observed, 2 hours)} = 6.3 \text{ m Hz}$$

It is more meaningful to assign confidence limits to the value of σ using the χ^2 distribution (see e.g. Hoel, 1954). In this case we find we may put

$$10.1 > \sigma(\text{observed, 2 hours}) > 5.8 \text{ m Hz}$$

with 90% confidence.

The next five runs, made between 17th Sept. and 23rd Sept. 1969, each lasted 4 hours (1 hour in Kr, 2 hours in Xe, 1 hour in Kr). Here we find

$$\sigma \text{ (shot noise, 1 hour)} = 3.5 \text{ m Hz}$$

$$\sigma \text{ (observed, 1 hour)} = 6.6 \text{ m Hz}$$

with 90% confidence limits:

$$9.3 > \sigma(\text{observed, 1 hour}) > 6.5 \text{ m Hz}$$

These standard deviations are strictly meaningful if the variability of the data did not alter over the time of running. This may be checked by using standard deviations calculated from individual data typeouts. We have not done

this in all cases, but where checks have been made the standard deviations do not lie significantly outside the confidence limits given. However, there is some evidence of slight variability among the standard deviations calculated in this way; while this is too small to affect the conclusions we shall draw from the data, it does suggest the noise source, whatever it is, varies somewhat in intensity. We shall discuss this a little more later.

Of more direct interest is the behaviour of the means. It is clear that in the first two runs both the noise channels and the dipole channel show non-statistical behaviour. The noise channel analysis waveforms are rather simple, and both are similar to the calibration analysis waveform; we suspect a break-down of orthogonality involving drift, but we have no clear evidence. In the later runs, we see no evidence of non-statistical behaviour in the noise channels, which now have more elaborate waveform structures, but the dipole channel still shows a fluctuating shift. However, in all cases the average of the Xe shifts minus the average of the Kr shifts (which we call $\Delta\delta\nu$) shows no significant difference between the various channels or runs, and is consistent with zero, using the quoted standard deviations (we note that the expected standard deviation for $\Delta\delta\nu$ is equal to the standard deviation on a single quarter run).

It appears that the data collection system is operating as expected apart from the non-ideal noise but that there remains a dipole-like shift which is stable over periods of hours if the apparatus is undisturbed, but otherwise fluctuates.

Fig. 6·4

```
DATA COLLECTION PARAMETERS. SET 3.

BASIC PERIOD: 2048+1024 ON 10 MICROSEC. RANGE.
INTERFACE GATING PERIOD: 1024 ON 10 MICROSEC. RANGE.
EHT GATING: 16 TIMES BASIC PERIOD.
MAGNETIC FIELD GATING: 32 TIMES BASIC PERIOD.
INPUT SCALING FACTOR: 16.

CONNECTIONS: FIELD PLATES RB
             MAGNETIC FIELD RR
             CALIBRATION ( 1 HZ ) RB.

WAVEFORMS:

13/10001111          RESONANCE SLOPE REVERSE
12/101;4             CALIBRATION CONTROL
11/0
10/10000;4           EHT SWITCH 2
7/1;12               MAGNETIC FIELD REVERSE
6/100111;4           EHT SWITCH 1

0/10001111           FEEDBACK ANALYSIS
1/10110111111        NOISE ANALYSIS
2/110111111          UNCANCELLED CALIBRATION
3/1111111111         UNCANCELLED DIPOLE
4/11111111111        DIPOLE ANALYSIS
5/10011011111        CALIBRATION ANALYSIS

14/1;13
15/1;6
16/17
17/0
```

Results. Set 3

Table 63

15·10·69

Run \ Channel	NOISE	UNCANCELLED CALIBRATION	UNCANCELLED DIPOLE	DIPOLE
Kr 1	+7·3	-19·3	+1·1	-7·7
Xe 1	-3 3	- 0·2	-7·5	-12·2
Xe 2	-7·7	- 3·0	-2·5	-22·2
Kr 2	+7·5	-11·5	+7·5	- 9·6
Mean	+0·9	-8·5	-0·4	-12·9
Standard deviation	6·6	7·5	5·5	5 8
Mean Xe - mean Kr	-13·0	+13·8	- 9·4	- 8·6

18·10·69

Run \ Channel	NOISE	UNCANCELLED CALIBRATION	UNCANCELLED DIPOLE	DIPOLE
Kr 1	+3·0	-6·1	-1·8	+14·9
Xe 1	- 6·9	-18·5	+2·6	+ 8·5
Xe 2	- 6·6	+ 7·4	+2·0	- 6·9
Kr 2	-15 2	- 21·2	- 3·1	+14 3
Mean	- 6·4	- 9·6	- 0·8	+ 7·7
Standard deviation	6·5	11·3	2 5	9·0
Mean Xe - mean Kr	- 6·5	+8 2	+4·8	- 13·8

24 10 69

Run \ Channel	NOISE	UNCANCELLED CALIBRATION	UNCANCELLED DIPOLE	DIPOLE
Kr 1	+4 2	-19·1	- 3·3	+17·7
Xe 1	+ 3 1	-10·5	- 8·2	+17·0
Xe 2	- 0·5	-13 7	-12·7	+34·1
Kr 2	+0·8	-15·9	- 2·9	+19·6
Mean	+1·9	-14·8	- 6·8	+22·1
Standard deviation	1·8	3·0	4 1	6·7
Mean Xe - mean Kr	-1 2	+5 4	-7·4	+ 6·9

All outputs expressed as shifts, in mHz

Results. Set 3 (cont.)

Table 6·3 (cont)

Run \ Channel	NOISE	UNCANCELLED CALIBRATION	UNCANCELLED DIPOLE	DIPOLE
Kr 1	+8·5	-4·9	+8·1	+4·5
Xe 1	+11·5	+10·0	+13·0	+44 7
Xe 2	-4 1	+10·4	-19·1	+19·1
Kr 2	+15·6	-9·8	+18·9	+30·7
Mean	+7·9	+1·4	+5·3	+24·8
Standard deviation	7·4	9·0	14·7	14·8
Mean Xe - mean Kr	-8·3	+17·5	-16·5	+14 3

All outputs expressed as shifts, in mHz

6.4 Runs with magnetic field reversal

In a further effort to clarify the nature of the residual shift and to collect more valid edm data, we performed four further runs using automatic magnetic field reversal. These runs each lasted 8 hours, with the same pattern of 2 hours in Kr, 4 hours in Xe, 2 hours in Kr, as previously. The data collection parameters are given in fig. 6.4 and the results in table 6.3. In these results, the channels labelled "uncancelled calibration" and "uncancelled dipole" have analysis waveforms constructed to pick out signals like the calibration and dipole signals in all respects except that they do not reverse sign with the magnetic field.

The observed standard deviation for this set of runs is rather poorer than previously. We find from the r.m.s. value of the individual standard deviations quoted

$$\sigma \text{ (observed)} = 8.2 \text{ m Hz}$$

or using the χ^2 distribution

$$11.4 > \sigma \text{(observed)} > 8.2 \text{ m Hz}$$

at 90% confidence limits. This compares with an expected value of about 2.5 m Hz for a 2 hour run. In this connection we remark that the mechanical support of the apparatus was slightly altered, in an attempt to improve its rigidity, before this data was taken; this will be discussed later.

It will be observed that in the first two runs of the set, none of the channels produced mean outputs significantly different from zero. However, in the last two runs the dipole channel again shows non-statistical behaviour while the others are relatively quiet. In particular, the noise channel and "uncancelled dipole" are statistical throughout, with the possible exception of the last run where the dipole shift seems to have changed size in mid-run. The "uncancelled calibration" shows results consistent with a slight ($\simeq 1\%$) change in resonance slope for the two signs of magnetic field, but it is quiet.

We conclude that the spurious dipole shift is still present, and that it reverses sign under magnetic field reversal like a true edm effect.

6.5 Analysis of results

In order to combine the above dipole data, we have simply averaged the results for the difference of dipole shift between Xe and Kr, $\Delta\delta\nu$ (dipole). We must take into account the fact that the runs with automatic magnetic field reversal were taken with the opposite sense of field plate connections to the earlier runs, so that $\Delta\delta\nu$ (dipole) in the later runs must be changed in sign before averaging. The likely error on the mean has been assessed from the variability of the results, using Student's t-distribution (see e.g. Hoel, 1954). This takes into account the uncertainty in the standard deviation as found from the r.m.s. value of the results being combined; because the only information on their variability is taken from the results themselves, the method gives a conservative estimate of the precision.

The procedure of taking a simple average might be objected to on the grounds that the variability of the data changed somewhat during the course of the runs. However, this effect is small and probably not relevent because the variability of the dipole data depends somewhat on changes in the residual spurious shift. We consider that a simple average is the most meaningful combination of results under the circumstances; also, no other combination could lead to a significantly different final answer.

We find, then,

$$\Delta\delta\nu(\text{dipole}) = \delta\nu_{Xe}(\text{dipole}) - \delta\nu_{Kr}(\text{dipole})$$

$$= 1.8 \pm 5.4 \text{ mHz}$$

at 90% confidence limit, where $\delta\nu$ (dipole) is the shift in observed resonance frequency on reversing the applied electric field. Using the quoted value of this field, and the formulae of chap. 2.4, we find for the difference in atomic edm's

$$|d_{Xe} - d_{Kr}| = (0.7 \pm 2.2) \times 10^{-22} \text{ e x cm.}$$

If we assume that

$$(d_{Xe} - d_{Kr}) = 100\, d_{electron}$$

we find

$$| d_{electron} | = (0.7 \pm 2.2) \times 10^{-24} \text{ e x cm}$$

at 90% confidence limit.

We may also calculate the means of the shifts observed in Xe and in Kr individually. Again using Student's t-distribution to obtain 90% confidence limits, we find

$$| \delta\nu_{Xe}(\text{dipole}) | = 1.1 \pm 10.2 \text{ m Hz}$$

$$| \delta\nu_{Kr}(\text{dipole}) | = 0.3 \pm 8.3 \text{ m Hz}$$

$$| d_{Xe} | = (0.4 \pm 4.3) \times 10^{-22} \text{ e x cm}$$

$$| d_{Kr} | = (0.1 \pm 3.4) \times 10^{-22} \text{ e x cm}$$

These are lower than any previous limits obtained without recourse to comparison between elements.

The separate results for $| d_{Xe} - d_{Kr} |$, $| d_{Kr} |$, and $| d_{Xe} |$ seem to render most unlikely the hypothesis that our null results are caused by cancellation of an edm shift by some other shift; this cancellation would have to occur both in Kr and in Xe to explain the null results.

One further number we should like to obtain from our results is the ratio of the sizes of the residual spurious shift in Xe and in Kr. The best estimate would be obtained by a least squares procedure, taking account of the errors in both shifts. We have taken a cruder measure which we feel to be adequate for our purposes, as follows. Consider pairs of measurements in Kr and in Xe made in successive quarter-runs; if in both cases $\delta\nu$ (dipole) is greater than 10 m Hz, we have calculated the ratio of the shifts. There are 14 such pairs in the data;

we have averaged the 14 ratios and obtained their variance in the usual way for normally distributed values, without weighting. This avoids small values of the shifts, which give little information on the ratio, and also avoids attaching too much significance to the two or three particularly large shifts. In this way we get

$$\delta\nu_{Xe}/\delta\nu_{Kr} = 1.23 \pm 0.25$$
$$\delta\nu_{Kr}/\delta\nu_{Xe} = 0.99 \pm 0.23$$

The quoted errors correspond to 90% confidence values, although of course their derivation makes their interpretation less certain.

Fig. 6·5

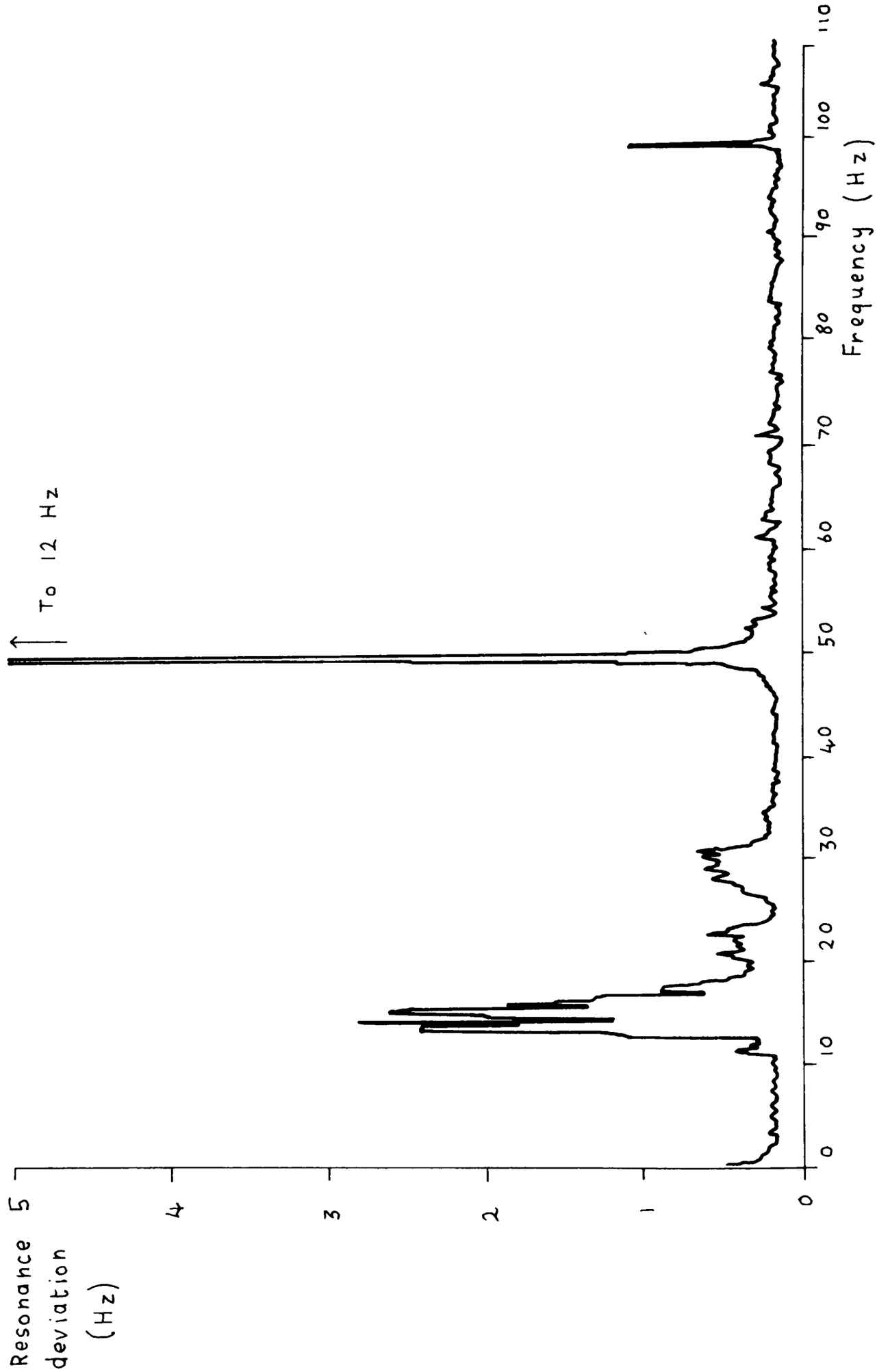
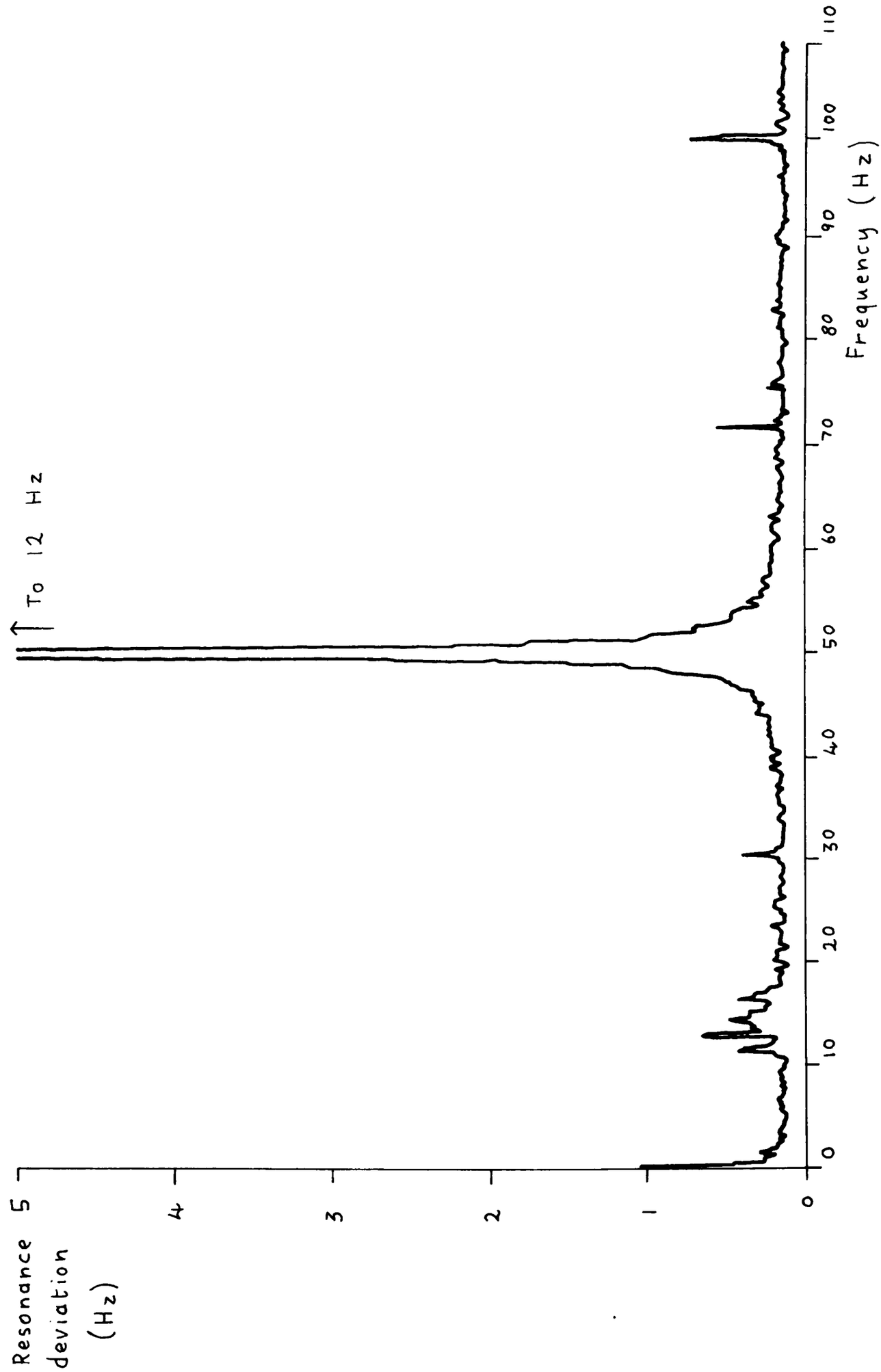

Noise Power Spectrum
Resonance deviation (Hz)
5
4
3
2
1
0
To 12 Hz
0
10
20
30
40
50
60
70
80
90
100
110
Frequency (Hz)

Fig 66


Noise Power Spectrum
Resonance deviation (Hz)
5
4
3
2
1
0
To 12 Hz
0
10
20
30
40
50
60
70
80
90
100
110
Frequency (Hz)

6.6 Further discussion

The results given above demonstrate why we have been unable to analyse fully the residual dipole shift: it is little larger than the disappointingly large errors, and it fluctuates in an almost statistical fashion. However, we can draw some conclusions about the shift. The fact that it appears to show the same behaviour with or without magnetic field reversal seems to render unlikely as an explanation a voltage dependence effect, or any effect depending on transverse magnetic field. The behaviour is consistent with a magnetic field modulation effect, or an instrumental effect. By direct checks, instrumental effects which do not depend on the direction of the electric field in the resonance region seem to be small; we therefore tentatively conclude that the shift is due to magnetic field modulation.

The difficulty in analysing the spurious shift is really due to the poor noise performance of the apparatus. This has also degraded our dipole limit both directly and indirectly, because of the necessity of intercomparison of elements, which quadruples the data collection time required to reach a given precision. Since taking the data presented above, we have found what seems to be the cause of the trouble. It was known before the data was taken that with the clock period used (about 30 msec) beam intensity noise, with no resonance, was close to the shot noise ideal; we supposed that the poor noise performance was due to low frequency magnetic field fluctuations, which can be serious because of the low frequency with which the EHT is reversed. The new information comes from the use of a program which computes the noise power spectrum of the signal input to the computer. This program has been recently written by Dr. G.E. Harrison; it uses a fast Fourier transform routine written by Rothman (1968) , and based on the Cooley-Tukey algorithm (1965). Noise power spectra for our apparatus, set to the point of greatest resonance slope, are shown in figs. 6.6 and 6.5. A peak at 50 Hz is obvious; also unpleasantly obvious in fig.6.5

are broad peaks between 10 and 20 Hz. These were induced by someone walking in the corridor outside the apparatus room. The main peak is still visible in fig. 6.6, where we attempted to keep mechanical excitation to a minimum, although it is much reduced. This noise can clearly get into the data collection through relatively high frequency "windows" in the Fourier spectrum of the analysis waveforms. The nature of the results at once provides explanations for the high noise level, its variability, and the increase after altering the mechanical support of the apparatus - which probably raised the resonant frequencies involved. We note that apart from the peaks the noise spectrum is flat, as expected for shot noise; it seems to be about the expected value. Apart from the size of the vibration peaks, the form of the spectrum is quite reproducible.

We feel that these noise peaks probably arise from relative motion between the deflecting magnets and the resonance region; they may presumably be eliminated by improving magnetic shielding and by arranging the apparatus support to raise the dangerous resonances to a safer frequency.

Another imperfection in the experimental apparatus whose source has recently been traced is the 50 Hz hum modulation of the resonance frequency. We have mentioned that we considered this to be due mainly to hum currents flowing in the resonance region vacuum chamber. This effect was observed to worsen midway through the last set of runs. Subsequent investigation has shown that the cooling water pipes appear to be acting as a 50 Hz source; isolating the detector end pumps by the use of plastic water piping almost completely removes the hum. Residual effects are consistent with power supply ripple. The worsening of the effect seems to have coincided with the installation of new water meters in the main laboratory supply.

Part II Quadratic Stark effects in the metastable states of He and the rare gases.

Chapter 7. Introduction

We shall describe in this section of the thesis measurements of the differential polarizabilities of the 2^3S_1 state in He^4 and of the $^3P_2$ states of the rare gases. We also give an approximate theoretical calculation for helium.

7.1 Helium

The effective operator formalism for the treatment of differential Stark effects has already been touched upon in chap.2. Introducing and using this theory, Angel and Sandars (1968) predicted that relativistic effects should produce a small quadratic Stark splitting of the magnetic substates of the 2^3S_1 state of He^4; any such splitting must be zero for an $L = 0$ state in pure LS coupling. In fact to order v^2/c^2 the only contribution to the quadratic Start splitting comes from the presence in the free atom Hamiltonian of the magnetic spin-spin interaction between the electrons. The differential polarizability therefore holds considerable interest as a test of wavefunctions or ultimately, with sufficiently good wavefunctions, as a test of the form of the two-electron relativistic interaction.

We shall find below that the differential Stark effect gives rise to a splitting of the $M_J = 1$ and $M_J = 0$ levels of about 13 k Hz at 10^5 V/cm. Clearly we should be able to measure an effect of this size with very high precision. Our present result for the differential polarizability is limited to about 5% accuracy by uncertainty in the electric field strength; however, we see no reason why ultimately an accuracy of 1 part in 10^4 should not be obtained, and our description of the experimental work (chap. 9) will be given with such an improvement in mind.

At the present level of precision, agreement between experimental and

theoretical values is good.

7.2 The rare gases

The rare gas metastable states have nonzero orbital angular momentum, so that the differential polarizability is not "forbidden" and might be expected to be of order a_o^3. This is found. No theoretical calculations of the polarizabilities are available; however, a qualitative discussion of the source of the effects has been given by Robinson et al. (1966). They show that in fact the direct contribution from the p-state core is small ($\simeq$ 1% of the total differential polarizability) and that the differential effects arise partially from coupling of the outer s-electron to the core (which can occur through electrostatic or magnetic interactions) and probably mainly from mixing in of configurations of higher l.

One rather practical use for measurements of these differential polarizabilities may be to calibrate electric fields used in measurements of smaller Stark effects. We at present envisage the use of such a technique in a precision measurement on the helium $^3S_1$ state.

Chapter 8. Theoretical treatment for He

8.1 Symmetry arguments

With a slight change of notation we can follow Angel and Sandars (1968) and write the Stark splitting of the magnetic levels of the $J = 1$ state of He^4 in the form

$$\delta W = -\tfrac{1}{2} \alpha_t \left(\tfrac{3}{2} E_z^2 - \tfrac{1}{2} E^2\right) \frac{3M_J^2 - J(J+1)}{J(2J-1)}$$

This is similar to the form used in chapter 2, but the situation differs here in that we assume the Stark splitting is small compared with the magnetic Zeeman splitting of the levels, so that the axis of quantisation is defined by the magnetic field (which is taken to be in the z-direction). We wish to calculate α_t, the tensor polarizability.

In the absence of relativistic effects the stationary states of an atom are eigenstates of S and L. Since the interaction with the external electric field acts in coordinate space any Stark splitting must be independent of M_S. Hence in an L=0 state one would expect no quadratic Stark splitting. However, if we take relativistic effects into account this argument breaks down because spin and orbit are no longer uncoupled.

To go further, we note again that the expression for δW has the form of the expectation value of a second rank spherical tensor operator. If we consider the relativistic effects as perturbations on the SL scheme this implies that the combined effects of the electric field and the relativistic interactions must behave like a tensor of rank two in spin space in order to produce any differential splitting in the ^3S state of He^4. Since the electric field interactions act in coordinate space this in turn means that the relativistic interaction must act in spin space as a tensor of rank two. Only the magnetic spin-spin interaction has this property, so it only will contribute to the splitting.

This result is derived explicitly in appendix B, using angular momentum diagrams (see e.g. Brink and Satchler, 1969). In the appendix we also show that the spin-spin interaction only contributes to the splitting of the levels, not to their overall shift. It follows from these two results that we can write α_t in terms of the energy shift of the stretched state $M_J = J$:

$$\delta W(M_J = J) = -\tfrac{1}{2} \alpha_t E^2$$

where δW is that part of the quadratic Stark shift involving the magnetic spin-spin interaction.

8.2 Perturbation treatment

We now calculate $\delta W(M_J = J)$ by a perturbation approach.

The contribution to the shift of the stretched state which is first order in the magnetic spin-spin interaction H^{SS} and quadratic in the electric field has the form:

$$\delta W = E^2 \times \sum_{J'\gamma\gamma'} \frac{\langle {}^3SJJ|\sum z_i|\gamma\,{}^3PJ'J\rangle\langle\gamma\,{}^3PJ'J|H^{SS}|\gamma'\,{}^3PJ'J\rangle\langle\gamma'\,{}^3PJ'J|\sum z_i|\,{}^3SJJ\rangle}{(W_{3S} - W_{\gamma\,{}^3P})(W_{3S} - W_{\gamma'\,{}^3P})}$$

$$+ E^2 \times 2\sum_{J'\gamma\gamma'} \frac{\langle {}^3SJJ|H^{SS}|\gamma\,{}^3DJJ\rangle\langle\gamma\,{}^3DJJ|\sum z_i|\gamma'\,{}^3PJ'J\rangle\langle\gamma'\,{}^3PJ'J|\sum z_i|\,{}^3SJJ\rangle}{(W_{3S} - W_{\gamma\,{}^3D})(W_{3S} - W_{\gamma'\,{}^3P})}$$

where we use atomic units. $\sum z_i$ is the z component of the electric dipole operator and H^{SS} is given by Judd (1963):

$$H^{SS} = \alpha^2 \sum_{i>j} \left[\frac{\underline{s}_i \cdot \underline{s}_j}{r_{ij}^3} - \frac{3\,(\underline{r}_{ij}\cdot\underline{s}_i)(\underline{r}_{ij}\cdot\underline{s}_j)}{r_{ij}^5} \right]$$

In the following we shall find it convenient to represent the states by their central field quantum numbers n l ; this will not always imply the use of the central field approximation. We shall also sometimes make use of the $L\,M_L\,S\,M_S$ representation in summing over intermediate states.

It will appear that the term with $\gamma = \gamma' = 1s2p$ is dominant in the perturbation sum, because of the near degeneracy of the states involved. We therefore find it convenient to divide our discussion and to treat separately:

1) δW_1 the contribution from the dominant term.
2) δW_2 the contribution from $\gamma = 1s2p$, $\gamma' \neq 1s2p$.
3) δW_3 the contribution from other ^3P states

4) δW_4 the contribution from ^3D states.

a) The dominant term

We need δW_1 to considerable accuracy to achieve a useful final result. Fortunately this is possible since we can use a semi-empirical approach and relate the spin-spin matrix elements to the measured $1s2p\ ^3P$ fine structure and the dipole matrix elements to the accurately computed f-values.

We write

$$\langle 1s2p\ ^3P,\ JM_J \mid H^{ss} \mid 1s2p\ ^3P,\ JM_J \rangle = V^{ss}(J)$$

with a similar definition involving H^{LS} the spin-orbit interaction. The J dependence of both $V^{ss}(J)$ and $V^{LS}(J)$ may be represented by

$$(-1)^{J+2} \begin{Bmatrix} 1 & K & 1 \\ 1 & J & 1 \end{Bmatrix}$$

with K = 1 for V^{LS} and K = 2 for V^{ss} (see e.g. Judd, 1963). Using this result we may at once relate $V^{ss}(J)$ to the observed fine structure, obtaining

$$V^{ss}(2) = \frac{1}{36}(2\Delta_1 - \Delta_2)$$

$$V^{ss}(1) = -\frac{5}{36}(2\Delta_1 - \Delta_2)$$

and

$$V^{ss}(0) = \frac{10}{36}(2\Delta_1 - \Delta_2)$$

where Δ_1 and Δ_2 are the J = 0, 1 and J = 1, 2 fine structure splittings of the ^3P level:

$$\Delta_1 = W(J=1) - W(J=0) \qquad \Delta_2 = W(J=2) - W(J=1)$$

We also need

$$\langle 1s2p\ ^3P,\ JM_J = 1 \mid \sum z_i \mid 1s2s\ ^3S,\ J = M_J = 1 \rangle = V^z(J)$$

These elements can be related to the matrix elements in the uncoupled representation

$$z_{ps} = \langle 1s2s\ \ L=0\ M_L=0 \mid \sum z_i \mid 1s2p\ \ L=1\ \ M_L=0 \rangle$$

where z_{ps} is related to the oscillator strength f_{ps} by

$$f_{ps} = 2 (W_{2^3S} - W_{2^3P}) | z_{ps} |^2$$

We find, using a 6 - j symbol to relate the matrix elements in the coupled and uncoupled representations,

$$V^z(1) = \frac{1}{\sqrt{2}} z_{ps}$$

$$V^z(2) = -\frac{1}{\sqrt{2}} z_{ps}$$

Substituting these relations and summing over J, we find

$$W_1 = E^2 \times \left| \frac{f_{sp}}{4 \Delta W_{sp}} \right| \times -\frac{4}{36} (2\Delta_1 - \Delta_2) \times \frac{1}{(\Delta W_{sp})^2}$$

where

$$\Delta W_{sp} = W_{2^3S} - W_{2^3P}$$

To evaluate this expression, we have used numerical values as follows:

f_{sp} = 0.5391 (Schiff and Pekeris, 1964)

ΔW_{sp} = 0.04208 (Moore, 1949)

Δ_1 = 4.501×10^{-6} (Pichanick et al., 1968)

Δ_2 = 3.482×10^{-7} (" " " ")

These values are all in a.u. ; we note that in the system we are using 1 a.u. of energy = 2 Rydbergs. From these values we get

$$\delta W_1 = -1.739 \times E^2 \times 10^{-3} \text{ a.u.}$$

and α_t(dominant term only) = 3.478×10^{-3} a.u.

which should be accurate to the quoted number of significant figures. This result was first obtained by Sandars (1966).

b) The P contributions

We have now to calculate the effect of the other ^3P states. At first sight it seems attractive to use a Sternheimer technique to transform the perturbation sums into the solution of a suitable inhomogeneous Schrödinger equation. However, this approach has not met with success, essentially because of the near degeneracy of the 1s2s and 1s2p levels. Even if one attempts to project out the 1s2p ^3P state from the perturbed function, the results are extremely sensitive to slight changes in wavefunction and are in complete disagreement with a straightforward summation approach; the difficulty seems to be that projecting out a simple 1s2p ^3P function leaves in some of the true ^3P function, which gives a large contribution to α_t.

We have therefore summed certain terms in the series, and estimated others, using computed f-values to obtain matrix elements of $\sum z_i$ and hydrogenic functions to calculate the matrix elements of H^{ss}. We have further approximated by neglecting exchange and the finite extent of the core, which enables us to write

$$H^{ss} = -\alpha^2 \times \sqrt{6}\ \underset{\sim}{C}^{(2)} \cdot \left\{ \underline{s}_1 \underline{s}_2 \right\}^{(2)} \times \frac{1}{r^3}$$

where $\underset{\sim}{C}^{(2)}$ and $1/r^3$ are taken to act only on the outer electron. (See Judd, 1963, for the recoupling leading to this form for H^{ss}).

For convenience we introduce the notation

$$\epsilon_{npn'p} = \sum_{J'} \frac{\langle {}^3SJJ | \sum z_i | np^3PJ'J\rangle\langle np^3PJ'J | H^{ss} | n'p\,{}^3PJ'J\rangle\langle n'p^3PJ'J | \sum z_i | {}^3SJJ\rangle}{(W_{3S} - W_{np^3P})(W_{3S} - W_{n'p^3P})}$$

We may obtain a simpler form for $\epsilon_{npn'p}$ by taking intermediate states in the uncoupled $LM_L SM_S$ representation, since only states with $M_L = 0$, $M_S = 1$ contribute and each $\epsilon_{npn'p}$ consists of a

single term. The relevent angular factors for the matrix elements of H^{ss} can then readily be written down, and we obtain

$$|\epsilon_{npn'p}| = \frac{\alpha^2}{10} \times \frac{f_{2snp}^{1/2}}{(\Delta W_{2snp})^{3/2}} \times \frac{f_{2sn'p}^{1/2}}{(\Delta W_{2sn'p})^{3/2}} \times \int_0^\infty R_{np} \frac{1}{r^3} R_{n'p} r^2 dr$$

The sign of $\epsilon_{npn'p}$ depends on the relative signs of the matrix elements of $1/r^3$ and $\sum z_i$; these are obtained by performing hydrogenic calculations of the matrix elements of r. As a check on this expression, we have calculated ϵ_{2p2p} and obtain

$$\epsilon_{2p2p} = -1.594 \times 10^{-3} \text{ a.u.}$$

$$\text{or } \alpha_t(2p2p \text{ only}) = 3.188 \times 10^{-3} \text{ a.u.}$$

which seems to constitute good agreement in view of the approximations involved.

The largest contributions after the dominant term are expected to come from the series ϵ_{2pnp}. The results for the first few terms are shown in table 8.1. We have used the f-values of Dalgarno and Kingston (1958). After n = 5, the sign of the terms ceases to alternate, and the size falls off roughly as $1/n^3$; the truncation error in neglecting these higher terms should be about equal to the error in the leading term. We find

$$\delta W_2 = E^2 \times 2 \sum_{n=3}^{5} \epsilon_{2pnp}$$

$$= (1.83 \pm 0.2) \times 10^{-4} \; E^2 \text{ a.u.}$$

which is about 10% of the dominant term. This result neglects altogether the case where one state γ' lies in the continuum; this is one of the major

sources of uncertainty in our treatment.

We have estimated various other ^3P contributions, constituting δW_3, without attempting accurate calculations; all these terms are sufficiently small that we may safely neglect them without seriously degrading the accuracy of our result, which is limited by uncertainties in δW_2 and δW_4. The terms with $\gamma = \gamma' = 1snp$ may be found in a manner similar to that used for the dominant term, or from a hydrogenic calculation; using the latter, we find

$$\begin{aligned} \epsilon_{3p3p} &\simeq 6 \times 10^{-6} \text{ a.u.} \\ &\simeq 4 \times 10^{-3} \epsilon_{2p2p} \end{aligned}$$

Higher terms of this class should fall off as $1/n^6$. Terms with and $n, n' \geq 3$ will be still smaller.

The contributions from doubly excited states are probably not given accurately by our treatment, because we have neglected exchange and the finite size of the core; also, it is unclear whether it is consistent to treat core excitations in one order of perturbation theory alone. However, we expect to be able to obtain an order of magnitude estimate. We find

$$\begin{aligned} \epsilon_{2s2p,\, 2s2p} &\simeq 2 \times 10^{-8} \text{ a.u.} \\ &\simeq 10^{-5} \epsilon_{2p2p} \end{aligned}$$

in an obvious notation; a larger contribution might occur for states with $\gamma = 1s2p$, $\gamma' = 2snp$, but even assuming the off-diagonal matrix element of H^{ss} to be as large as the diagonal, we find

$$\begin{aligned} \epsilon_{1s2p,\, 2s2p} &\simeq 6 \times 10^{-6} \text{ a.u.} \\ &\simeq 4 \times 10^{-3} \epsilon_{2p2p} \end{aligned}$$

We therefore expect to be able to set

$$\begin{aligned} \delta W_3 &\lesssim E^2 \times 10^{-5} \text{ a.u.} \\ &\lesssim 10^{-2} \delta W_1 . \end{aligned}$$

Table 8.1. The P state contributions

γ	γ'	$\epsilon_{\gamma\gamma'}$(a.u.)
1s2p	2s2p	-1.739×10^{-3}
1s2p	1s3p	$+6.65 \times 10^{-5}$
1s2p	1s4p	$+1.73 \times 10^{-5}$
1s2p	1s5p	$+7.70 \times 10^{-6}$
1s3p	1s3p	6×10^{-6}
1s2p	2s2p	6×10^{-6}
1s2p	2s2p	2×10^{-8}

c) The D contributions

In the case of the D state contributions a Sternheimer technique becomes more feasible because there is no large term to be projected out. It is in fact virtually essential to use such an approach because the convergence properties of the series sums are poor.

We have again used hydrogenic wavefunctions and the simplified approximate form for H^{ss}. Using the $L M_L S M_S$ representation for the intermediate states it is straightforward to show that

$$\epsilon^{(D)} = \sum_{J'\gamma\gamma'} \frac{\langle {}^3SJJ|H^{SS}|\gamma\,{}^3DJJ\rangle\langle\gamma\,{}^3DJJ|\sum z_i|\gamma'\,{}^3PJ'J\rangle\langle\gamma'\,{}^3PJ'J|\sum z_i|{}^3SJJ\rangle}{(W_{3S} - W_{\gamma\,{}^3D})\ (W_{3S} - W_{\gamma'\,{}^3P})}$$

$$= -\frac{\alpha^2}{15} \sum_{n\,n'} \frac{\int R_{2s}\frac{1}{r^3} R_{nd}\, r^2 dr \int R_{nd}\, r\, R_{n'p}\, r^2 dr \int R_{n'p}\, r\, R_{2s}\, r^2 dr}{(W_{2s} - W_{nd})\ (W_{2s} - W_{n'p})}$$

in our approximation. We rewrite this

$$\epsilon^{(D)} = -\frac{\alpha^2}{15} \times M_R \ .$$

The first plausible method for evaluating M_R is to consider only those terms involving the 2p state, since the small energy denominator $W_{2s} - W_{2p}$ should make this series large. To sidestep the summation, we introduce the function

$$\rho_2' = r \sum_n \frac{R_{nd} \int R_{nd}\ r\, R_{2p}\ r^2 dr}{W_{2s} - W_{nd}}$$

which satisfies the radial Sternheimer equation

$$(W_{2s} - H_R)\,\rho_2' = r^2 R_{2p}$$

where

$$H_R = -\tfrac{1}{2}\frac{d^2}{dr^2} + \frac{3}{r^2} - \frac{1}{r}$$

$$W_{2s} = -\frac{1}{8}$$

in our approximation, setting all hydrogenic Z = 1.

From this we find

$$\rho_2' = -\frac{1}{2\sqrt{6}}\,(r+6)\,r^3 e^{-r/2}$$

and we obtain

$$M_R = \int R_{2s}\,\frac{1}{r^3}\,\rho_2'\,r\,dr$$

$$= +17.8 \text{ a.u.}$$

This value may be improved by adding a few more terms from the perturbation sum, using hydrogenic functions. One group of terms with large values is that with $n = n'$, since the matrix element $\mathcal{R}_{np}^{nd} = R_{nd}\,r\,R_{np}\,r^2 dr$ is large. If we add the terms n = 3, 4, we increase the value of M_R to

$$M_R = 22.8 \text{ a.u.}$$

However, for large n we expect both $\mathcal{R}_{np}^{2s}$ and $R_{2s}\,\frac{1}{r^3}\,R_{nd}\,r^2 dr$ to fall off as $1/n^{3/2}$, while $\mathcal{R}_{np}^{nd}$ rises as n^2; hence terms with $n = n'$ fall off as $1/n$ and the sum of the series does not converge. There are of course other comparable terms with n close to n', so the complete expansion need not be divergent; however, the value of M_R just obtained is scarcely convincing.

To improve on the reliability of this value, we have used the P state

$$\rho_1 = r \sum_n \frac{R_{np} \int R_{np}\, r\, R_{2s}\, r^2 dr}{(W_{2s} - W_{np})}$$

where P_1 satisfies

$$(W_{2s} - H_R)\rho_1 = r^2 R_{2s}$$

with

$$H_R = -\tfrac{1}{2}\frac{d^2}{dr^2} + \frac{1}{r^2} - \frac{Zp}{r}$$

$$W_{2s} = -\frac{Z_s^2}{8}$$

This equation is soluble only if $Z_s \neq Z_p$, since otherwise the 2s and 2p functions have degenerate eigenvalues and ρ_1 contains an indeterminate amount of 2p. We use $Z_s = 1.18$, $Z_p = 1.03$, which reproduce the measured energies, and find

$$\rho_1 = (0.4029\, r^2 + 1.494\, r + 19.92)\, r^2 e^{-1.18\, r/2}$$

We expect this to be a rather poor approximation to the true first-order polarised 2s state, but it should at least give answers correct to a few tens of percent; it gives a value for the 2^3S polarizability about 30% too high. From this we have calculated the Sternheimer D state

$$\rho_2 = r \sum_{n\,n'} \frac{R_{nd} \int R_{nd}\, r\, R_{n'p}\, r^2 dr \int R_{n'p}\, r\, R_{2s}\, r^2 dr}{(W_{2s} - W_{nd})(W_{2s} - W_{n'p})}$$

$$= r \sum_n \frac{R_{nd} \int \rho_1\, r\, R_{2s}\, r\, dr}{(W_{2s} - W_{nd})}$$

The method is just the same as for ρ_2', and we obtain

$$\rho_2 = (-0.1584\, r^3 - 1.736\, r^2 - 23.52\, r - 91.27)\, r^3 e^{-1.18r/2}$$

Using this, we find

$$M_R = R_{2s} \frac{1}{r^3} \rho_2 \, r dr$$

$$= 20.0 \text{ a.u.}$$

in surprising agreement with our first estimate.

As a further check, we have attempted to calculate the Sternheimer D function from the perturbation $1/r^3$ on R_{2s}:

$$\rho_3 = r \sum_n \frac{R_{nd} \int R_{nd} \, 1/r^3 \, R_{2s} \, r^2 \, dr}{(W_{2s} - W_{nd})}$$

which satisfies

$$(W_{2s} - H_R)\, \rho_3 = \frac{1}{r^3} \, r \, R_{2s}$$

One can object to this procedure on the grounds of the singular nature of the perturbation. However, we may justify the technique by a plausibility argument: the true perturbation is not singular, but resembles our approximation over most of space; we expect our solution to resemble the true solution over most of space if we consider it to be obtained by integrating inwards from large r (see also Sternheimer, 1951).

This Sternheimer equation has a solution

$$\rho_3 = (0.3375\, r^{-1} + 0.4779\, r^{-2})\, e^{-1.18r/2}$$

which is clearly somewhat objectionable on the grounds of its behaviour at the origin. However, the integrals obtained do not diverge. Evaluating

$$\sum_{n=2}^{5} \frac{\int \rho_3 \, r \, R_{np} \, r \, dr \int R_{np} \, r \, R_{2s} \, r^2 \, dr}{(W_{2s} - W_{np})}$$

we find

$$M_R = 20.5 \text{ a.u.}$$

and evaluating

$$\int \rho_3 \, r \, \rho_1 \, dr$$

we get

$$M_R = 19.4 \text{ a.u.}$$

Another solution seems to exist if we set $Z_d = Z_s$ in the Sternheimer equation:

$$\rho'_3 = \frac{Z^{3/2}}{72\sqrt{2}} (-24 + 4Zr + Z^2 r^2) \, e^{\frac{-Zr}{2}}$$

If we use this, setting $Z = 1$, we obtain values from the above expression of

$$M_R = 23.4$$

and

$$M_R = 20.2$$

respectively.

Considering the wide range of rather crude approximations made in these various methods, the agreement is quite surprising. We take a value

$$M_R = 20 \pm 5 \text{ a.u.}$$

giving

$$\epsilon^{(D)} = -(7.10 \pm 0.18) \times 10^{-5} \text{ a.u.}$$

$$\delta W_4 = -E^2 \times (1.42 \pm 0.36) \times 10^{-4} \text{ a.u.}$$

which is again about 10% of δW_1. The uncertainty attached to this value largely reflects the uncertainty in our numerical techniques and does not take separate account of the basic approximations in the form of H^{ss} and the wavefunctions. However, we may reasonably expect these to have an effect similar to the 10% error observed in the hydrogenic calculation for ϵ_{2p2p}. The treatments given all include some of the continuum contributions; the calculations from $\int \rho_3 \, r \, \rho_1 \, dr$ and $\int R_{2s} \, r \, \rho_2 \, r \, dr$ should include them all.

8.3 Result and discussion

Combining the contributions calculated above, we obtain

$$\alpha_t = +(3.40 \pm 0.10) \times 10^{-3} \text{ a.u.}$$

We note that this is close to the value of the dominant term alone, the remaining P state contributions being cancelled by the D state contributions.

Since these results were obtained the tensor polarizability has been calculated with much greater accuracy by Drake (1970), who uses correlated variational wavefunctions and finds

$$\alpha_t = +(3.48 \pm 0.01) \times 10^{-3} \text{ a.u.}$$

Drake also obtains a cancellation between D and P contributions, his value for the dominant contribution alone being $\alpha_t = 3.49 \times 10^{-3}$ a.u. in excellent agreement with the semiempirical value. However, his D and P contributions are close to twice the size of ours; we find $2 \epsilon^{(D)} = -2.67\alpha^2$ a.u. while his value for $\epsilon^{(D)}$ is $-3.32\alpha^2$ a.u. We have tried to trace the source of this discrepancy by making various tests and comparisons. The hydrogenic f-values for the 2s-2p transition and 2p-3d transition are respectively 0.659 and 0.694 (using $Z_s = 1.18$) instead of accurate values 0.539 and 0.609 respectively (see Wiese et al., 1966), which constitutes the expected sort of agreement. Our hydrogenic value for $\langle 2^3P_2 \mid H^{ss} \mid 2^3P_2 \rangle$ is $4.17 \times 10^{-3}\alpha^2$ a.u. which compares well with the value $4.4831 \times 10^{-3}\alpha^2$ a.u. obtained by Drake. The discrepancy appears, as we might expect, when comparing our value of $\mid \langle 2^3S_1 \mid H^{ss} \mid 3\,^3D_1 \rangle \mid$ with that of Drake; we obtain $1.88 \times 10^{-3}\alpha^2$ a.u. while Drake's value is $4.395 \times 10^{-3}\alpha^2$ a.u. We have checked the angular factors involved in this matrix element, and find no discrepancy between our own treatment and that of Drake.

A number of surprising inconsistencies will be observed in this situation. We have not so far been able to resolve them. We are at present in communication with Drake in an attempt to clarify the matter. It is not easy to see a numerical

mistake in either treatment, and it may be that the hydrogenic calculations are in fact less reliable than we have supposed.

A value 3.5×10^{-3} a.u. for α_t corresponds to a frequency shift of the $M_J = 0, +1$ separation of 13.06 k Hz (towards lower frequency) at an applied electric field of 10^5 V/cm.

9. Experimental results

9.1 Introduction and experimental method

We have used the apparatus described in section I of this thesis to observe the quadratic electric field dependence of the $M_J = 0 \rightarrow +1$ transition in the metastable states of helium and the rare gases. In helium, the small differential polarizability means that the Stark shifts are smaller than the Zeeman splittings, and we measure the shift of a Ramsey resonance on applying the electric field. In the rare gases, the highest electric fields available produce Stark splittings of many MHz, and we have performed measurements both at low electric field using a Ramsey setup and at high electric field, where field inhomogeneity necessitates the use of a single hairpin resonance.

In none of these cases does the precision of measurement of the resonance frequency limit the accuracy of the final result; even in helium the observed shifts are up to ten times the linewidth, so that setting to $^1/10$ of the linewidth gives 1% precision in the shift measurements. Sources of error larger than this are discussed below. We have therefore adopted the simple procedure of applying an electric field and measuring the resulting resonance frequency by hand setting the r.f. oscillator to the centre of the resonance pattern.

This is adequate even in helium where the resonance flop-in signal is about 10^4 counts per sec. on an equal photon background. We note that our discharge source is inefficient in helium, apparently because of insufficient available pumping speed. The oscillator frequency is measured with a digital counter.

The applied electric potentials have been measured using Fluke precision potential dividers and either a digital voltmeter or a Farnell precision differential voltmeter (which is an all-inclusive potentiometer setup), except on the first run in helium when the internal meters of the Brandenburg power supplies were used. This was done because no digital voltmeter was available, and it was felt that

the time spent operating the potentiometer might introduce trouble from long term resonance drifts. In fact no drifts greater than about 50 Hz have been observed over the times involved, about $\frac{1}{2}$ hour per run. The Brandenburg meters have been calibrated to better than 100 V using the precision potentiometers.

The spacing of the electric field plates, which is about 2.5 mm, has been measured at the only 5 accessible points by use of feeler gauges. The accuracy of gap measurement at each point is about 1%, but the spacing varies by about 10% over the length of the plates. We require the average of the square of the electric field along the resonance region, and so we have calculated the quantity

$$a_{eff} = \left(\overline{1/a_{gap}^{2}} \right)^{-\frac{1}{2}}$$

Because the variation of spacing is smooth, our average should give a fairly reliable estimate for a_{eff}. We take 2% as a reasonable estimate for the final error.

9.2 Sources of error

As we have mentioned, the main source of error is in the measurement of electric field plate separation. We now discuss some other sources of error which may become important in higher precision work.

We note first one class of errors which our setup eliminates: because our electric field plates extend throughout the resonance region, we are not concerned with "filling factors" or field plate end effects, or with associated resonance distortions. This has not been the case in most previous work with electric fields. There seems no reason why this arrangement need be altered in future work.

There is one potentially important resonance distortion arising from the presence of the $M_J = 0 \longrightarrow -1$ transition, which is nearly degenerate with the $M_J = 0 \longrightarrow +1$ transition at low electric field. This problem has been discussed by Ramsey (1959) who shows that a nearby resonance can shift the desired resonance peak by at most about 10% of the Ramsey pattern linewidth. Such a shift depends on the spacing of the two resonances and on the r.f. amplitude. We have so far been unable to detect any deviation from quadratic behaviour in the shift, and variation of r.f. amplitude over a factor 6 gives no detectable resonance shift at 10^5 V/cm in helium (i.e. the shift is less than 100 Hz). Moreover, we shall see there is no significant disagreement between high and low electric field measurements in the rare gases. Nonetheless, in future work in helium it may be necessary to take more careful account of this effect.

Additional error will arise in the low field measurements if the electric and magnetic fields are not sufficiently parallel. From our measurements of the "$\underline{v} \times \underline{E}$" effect (chap. 5) we know that with no applied vertical magnetic field

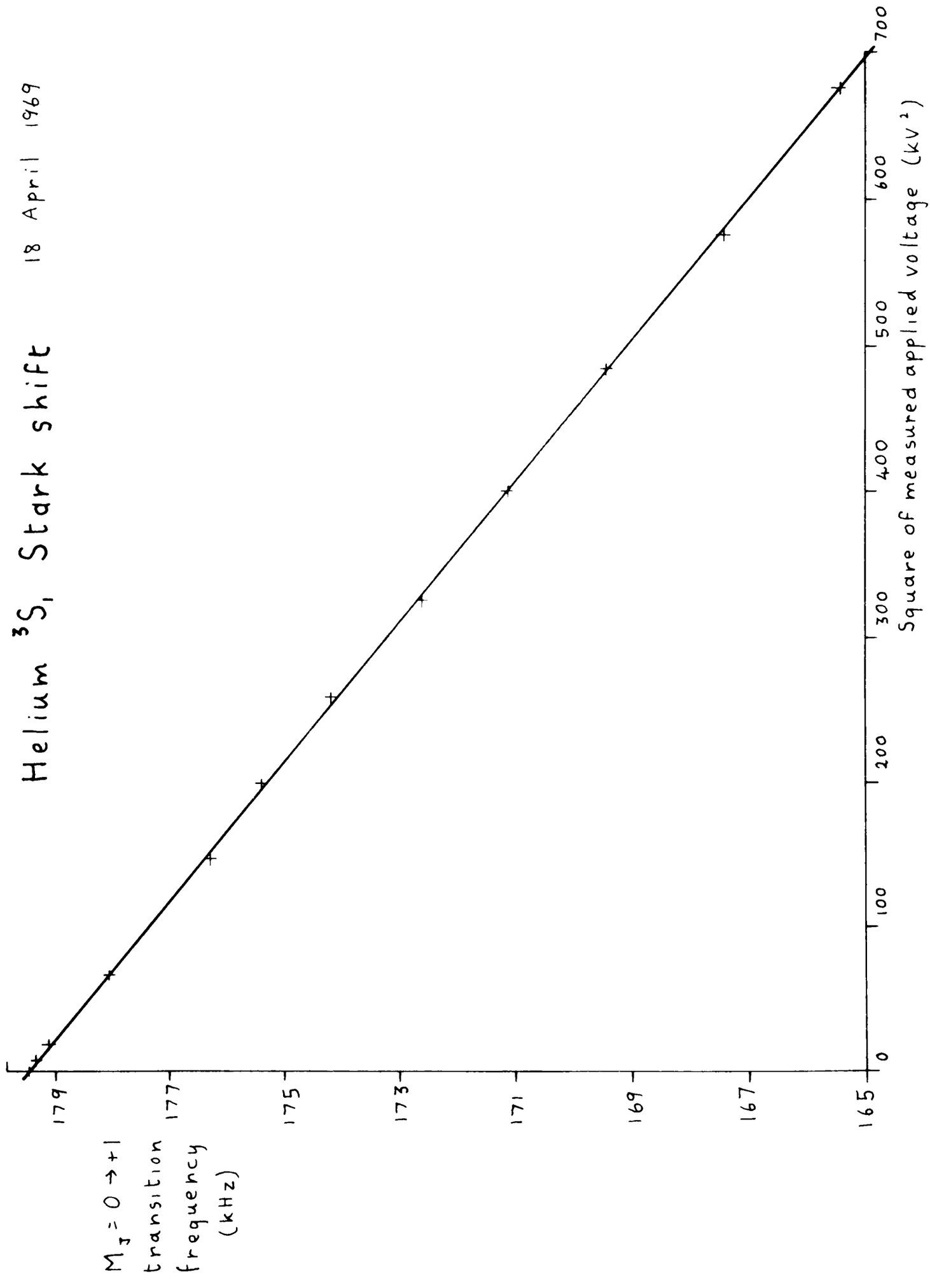
$$E_\perp / E_{||} \simeq 1/100$$

in an obvious notation. Rewriting the electric field dependence of the Stark shift as

$$3E_{\parallel}^2 - E^2 = 2E^2 \left(1 - \frac{3}{2}\left(\frac{E_\perp}{E}\right)^2\right)$$

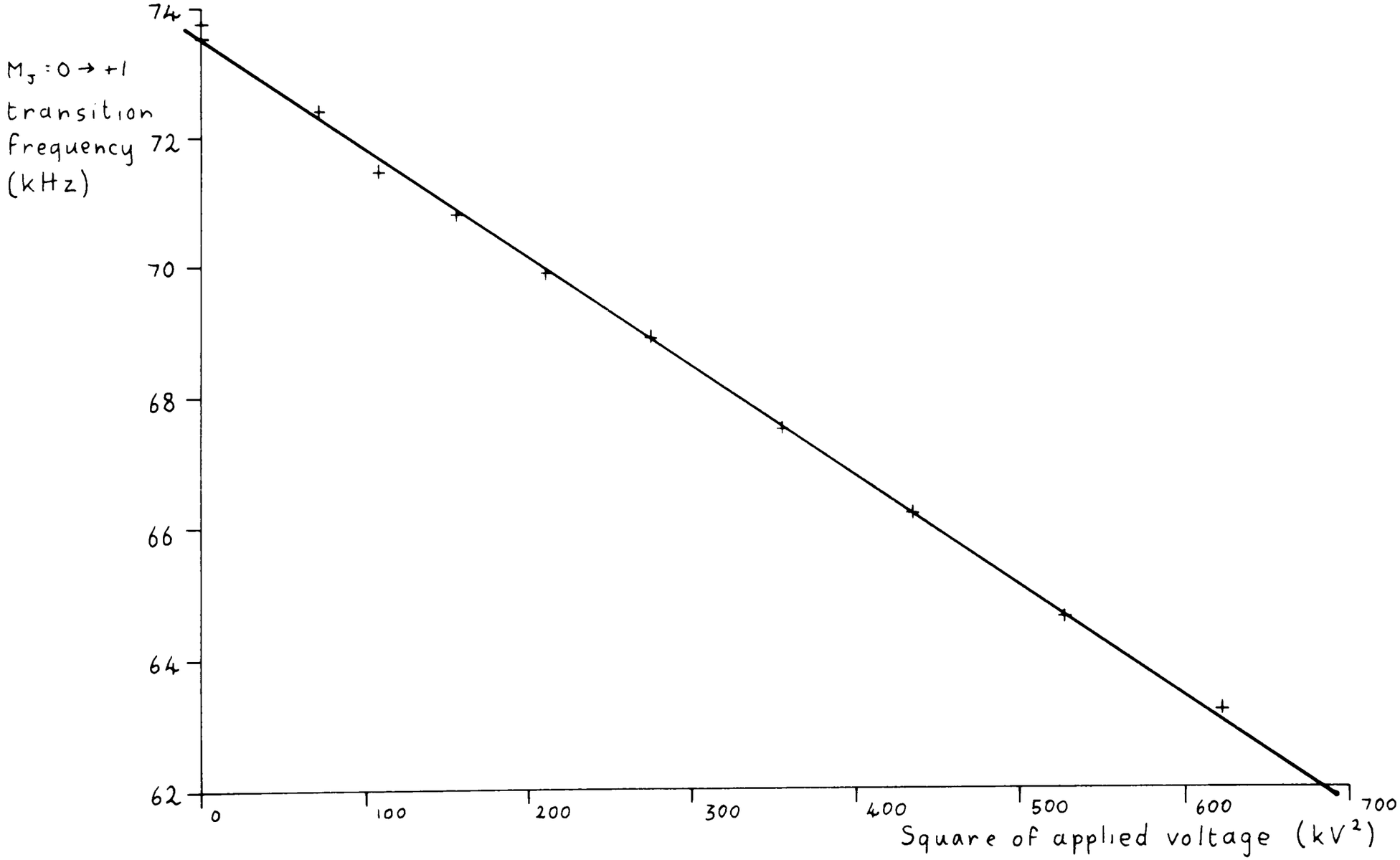
we see that this error is not likely to be troublesome even at far higher precisions than at present.

Fig 91


Helium $^3S_1$ Stark shift
18 April 1969
$M_J = 0 \rightarrow +1$ transition frequency (kHz)
179
177
175
173
171
169
167
165
0
100
200
300
400
500
600
700
Square of measured applied voltage (kV^2)

Helium $^3S_1$ Stark shift 30 Oct 1969

Fig 92



9.3 Helium

The results obtained for the Stark shift of the frequency of the transition $M_J = 0 \rightarrow +1$ are plotted in figs. 9.1 and 9.2.

The runs were performed at resonance frequencies of 180 k Hz and 70 k Hz respectively. A more important difference is that the field plates were removed and reassembled between the two runs.

Results for run 1 (18 April 1969) are plotted against applied potential as measured on the Brandenburg meters. It is observed that measured values of $+9.15 \pm .05$ kV and $-9.00 \pm .05$ kV on these meters correspond to values of $9.474 \pm .002$ and $-9.474 \pm .002$ as measured by a Fluke potential divider and a DVM. The measured effective plate separation is $a_{eff} = 2.608 \pm .05$ mm. The slope of measured shift vs. square of observed applied voltage, as determined by (equally weighted) least squares fitting to the points, is $-0.02078 \pm .00008$ k Hz/$(kV)^2$. From these figures we obtain the Stark shift

$$\delta \nu_{01} = -12.97 \pm 0.7 \text{ k Hz at } 10^5 \text{ V/cm.}$$

In the second run (30 Oct. 1969) we measured the applied voltage V directly with the Fluke dividers and DVM. The plate separation a_{eff} was $2.695 \pm .05$ mm, and the slope of shift vs. V^2 was $(-0.01686 \pm .00018)$ k Hz/$(kV)^2$. We obtain

$$\delta \nu_{01} = -12.25 \pm 0.7 \text{ k Hz at } 10^5 \text{ V/cm.}$$

We feel that since the field plate separation, and its variation along the length of the plates, were quite different for the two runs, the results may be taken as independent. Combining them, we find

$$\delta \nu_{01} = -12.61 \pm 0.5 \text{ k Hz}$$

from which

$$\alpha_t = +(3.38 \pm 0.13) \times 10^{-3} \text{ a.u.}$$

This is in excellent agreement with the value of Ramsey and Petrasso (1969, published since our result was obtained):

$$\alpha_t = +(3.42 \pm 0.11) \times 10^{-3} \text{ a.u.},$$

and with the theoretical values.

Stark shift in Ne $^3P_2$ state ν_{01} (low E)

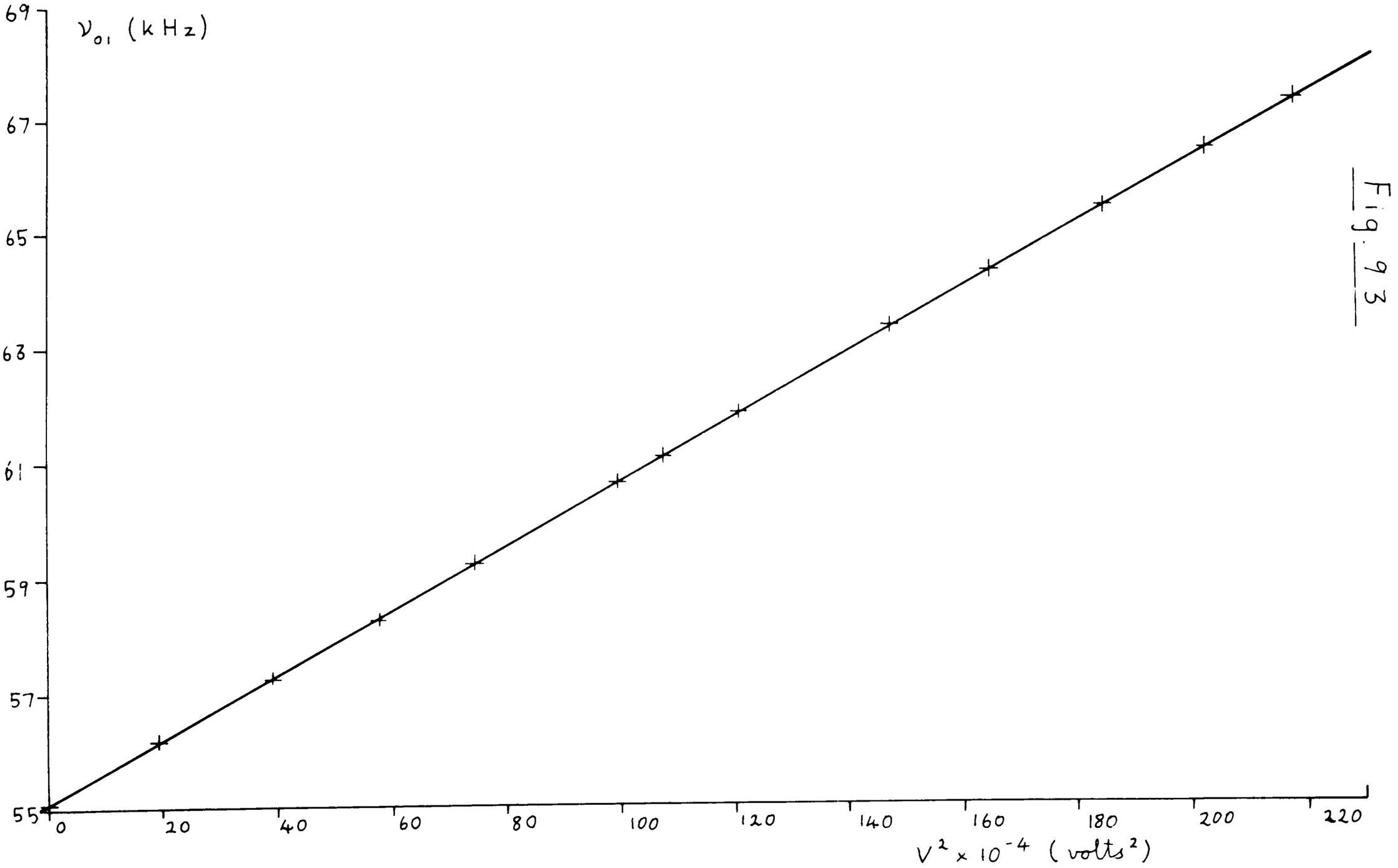


Fig. 93

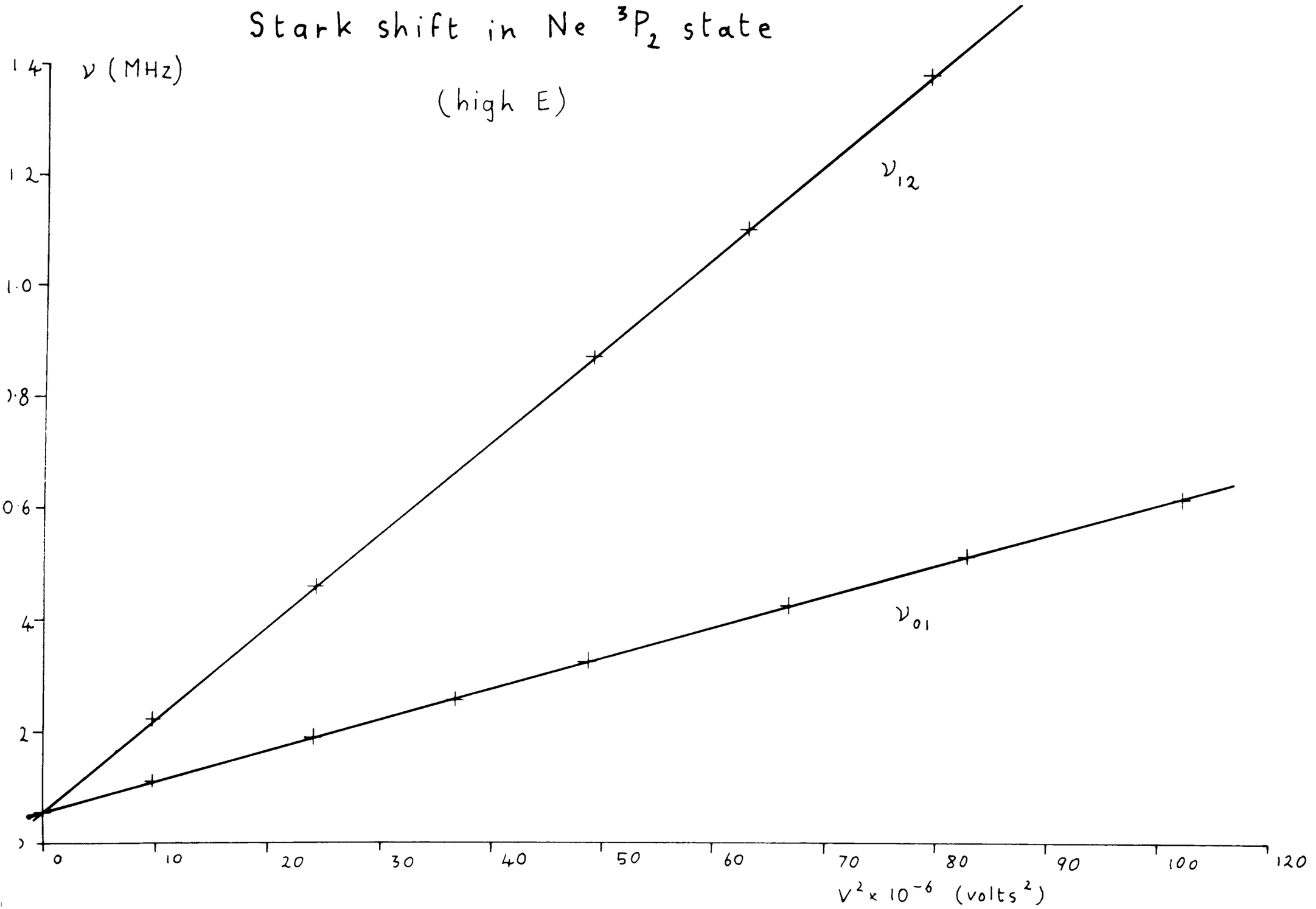

Stark shift in Ne $^3P_2$ state
(high E)
ν (MHz)
1·4
1·2
1·0
0·8
0·6
4
2
0
10
20
30
40
50
60
70
80
90
100
120
$V^2 \times 10^{-6}$ (volts^2)
ν_{12}
ν_{01}

Fig 94

Table 91

Stark shifts in rare gas $^3P_2$ states

	$\delta\nu_{10}$ (at low E) Hz/V^2	$\delta\nu_{10}$ (at high E) Hz/V^2	$\delta\nu_{12}$ (at high E) Hz/V^2
Ne	$(0.5568 \pm 0.0007) \times 10^{-2}$	$(0\,5481 \pm 0\,002) \times 10^{-2}$	$(1655 \pm 0\,005) \times 10^{-2}$
A	$(1\,706 \pm 0.002) \times 10^{-2}$	$(1.703 \pm 0\,008) \times 10^{-2}$	$(5\,128 \pm 0\,033) \times 10^{-2}$
Kr	$(2\,227 \pm 0\,005) \times 10^{-2}$	$(2\,205 \pm 0\,008) \times 10^{-2}$	$(6\,607 \pm 0\,08) \times 10^{-2}$
Xe	$(3\,466 \pm 0\,01) \times 10^{-2}$	$(3\,427 \pm 0\,01) \times 10^{-2}$	$(10\,28 \pm 0\,03) \times 10^{-2}$

Table 92

Tensor polarizability of rare gas $^3P_2$ states

	α_t (a.u)	$\delta\nu_{10}$ at 10^5 V/cm (MHz)
Ne	6·501 ± 0·26	4 044 ± 0 16
A	19 92 ± 0 80	12 39 ± 0 50
Kr	25 99 ± 1 2	16 17 ± 0 73
Xe	40 46 ± 1 8	25·17 ± 1·1

9.4 The rare gases

We give in figs. 9.3 and 9.4 plots of the Stark shifts in the $^3P_2$ state of Ne. These are representative of the results in all the rare gases, though Ne in fact has the poorest signal, widest resonance, and smallest differential polarizability. The high electric field data, fig. 9.4, were obtained by observing resonances as "flop-outs" from the $M_J = +1$ state, so that the $M_J = +1 \rightarrow 0$ and $M_J = +1 \rightarrow +2$ transitions could both be measured.

In table 9.1 we give the observed values of the Stark shifts, in Hz/V^2, for all the rare gases, as found by least squares fitting. The errors quoted are standard deviations as obtained from the least squares procedure. It will be seen that in no case is there any significant departure from the expected ratio of 3 to 1 for the shifts of the $M_J = +1 \rightarrow 0$ and $M_J = +1 \rightarrow +2$ transitions. All the data was taken with $a_{eff} = 2.695 \pm .05$ mm, as for the second helium run. We may use this value, together with the observed ratio of high field to low field measurements of the Stark shift $\delta\nu_{01}$ in the $M_J = +1 \rightarrow 0$ line, to obtain the expected value of a_{shp}, the gapwidth at the r.f. coil used in the high field measurements. We find in this way $a_{shp} = 2.71 \pm .06$ mm; the directly measured value is $2.77 \pm .03$ mm.

In table 9.2 we give the values of $\delta\nu_{01}$ at 10^5 V/cm, and α_t, for all the rare gases. We have used the low field measurements and a_{eff}. This may seem unwise as the quoted error on a_{shp} is lower; however, the value of a_{eff} is obtained from several independent measurements of gapwidth and this gives us greater confidence in the quoted size of its error. The ratio of the values of α_t should of course be as accurate as the values of observed shifts in table 9.1. The values of α_t are in good agreement with the deflection measurements of Robinson et al., 1966, to within the errors of the latter.

9.5 Future work

We now consider a little further the requirements for a high precision measurement of the helium tensor polarizability.

We envisage the use of more sophisticated data collection with computer controlled switching of the applied EHT and simultaneous modulation of the r.f. oscillator to follow the resonance. Similar techniques have been used previously (see e.g. Angel 1968) and in helium a precision of 1 part in 10^5 in resonance shift measurement should be straightforward to achieve. The magnitude of the EHT could also be controlled by the computer if required. Continuous monitoring of the "$\underline{v} \times \underline{E}$ effect" to ensure adequate alignment of B and E fields would be possible, though probably unnecessary.

Resonance distortions due to the $M_J = 0 \longrightarrow -1$ transition might be important at the level of 1 part in 10^4 precision. If this is so, they may be allowed for by taking data with varying r.f. amplitude and extrapolating to zero; this might be expected to reduce the effects by a factor 10. We have seen that power shifts contribute less than 1% of the shift observed at 10^5 V/cm in the present experiment and, using the theory of Ramsey (1959), they are probably of order 0.1% of the Stark shift. Further improvements are possible by working at higher electric field. We therefore expect the effects may be reduced below 1 part in 10^4.

There remains the problem of the determination of the electric field. The measurement of applied potential presents relatively little problem. The Fluke potential dividers at present used by us have a long term division accuracy of 1 part in 10^4 at 10 kV, and this may presumably be improved with careful setting up of the resistors. On the other hand, it seems impossible to improve on the present accuracy of gapwidth determination by more than an order of magnitude with the length of plate and gapwidth required for the helium measurement. We have already mentioned the possibility of the use of a rare gas Stark effect to

set up a secondary standard for electric field measurement; as far as we are aware no such standard exists at present. Field plates constructed sufficiently well to allow interferometric measurement of their spacing over a 10 cm length do not seem out of the question; with such plates a linewidth of about 4 k Hz would be available in Xe, allowing a determination of its Stark shift at 10^5 V/cm to be made to at least 1 part in 10^5. The use of such a secondary standard could introduce error if the calibrating Xe beam and the He beam traverse different trajectories. Unfortunately we have no direct data on this; however, the results of Ramsey and Petrasso, who measured the Stark shifts for various detector positions, lead us to believe the effects are small.

We conclude that a determination of the $^3S_1$ tensor polarizability to 1 part in 10^4 is quite feasible.

Appendix A. Effective Hamiltonians

We wish to study a system with a Hamiltonian

$$\hat{H} = \hat{H}_o + \hat{H}_{pert}$$

where

$$\hat{H}_o \, | i \rangle = E_i \, | i \rangle$$

and where there exists a group of levels $i = 1, \ldots, n$ which are nearly degenerate and well separated from all other levels. We wish to construct an effective Hamiltonian $H_{(eff)}$ which, operating in the nearly degenerate manifold, will give an approximation to the energy levels and which will also be useful in time dependent problems.

It is convenient to use a matrix representation based on the states $| i \rangle$. We want to approximately block-diagonalise the matrix of H so that a submatrix corresponding to the manifold of interest can be separated; this submatrix will be $\hat{H}_{(eff)}$. We therefore wish to eliminate by some unitary transformation those elements

$$\langle p | H | q \rangle = H_{pq}$$
$$= \langle p | H_{pert} | q \rangle$$

where $| p \rangle$ is a member of the manifold of interest and $| q \rangle$ is not. Now, the Jacobi method of matrix diagonalisation utilises a set of "rotations" each constructed to reduce some particular off-diagonal element to zero (see e.g. Fox (1964)). We shall show that these provide a suitable basis for our approximate reduction. For simplicity, we shall specialise to real matrices; the results obtained are rather clearly independent of this restriction.

Let $\underline{H}^{(r)}$ denote the Hamiltonian matrix after r rotations. Then

$$\underline{H}^{(r)} = \underline{T}^{(r)} \, \underline{H}^{(r-1)} \, \underline{\tilde{T}}^{(r)}$$

$\underline{T}^{(r)}$ is defined as having all elements equal to those of the unit matrix except

$$T^{(r)}_{pp} = T^{(r)}_{qq} = \cos\theta_r = C_r$$

$$T^{(r)}_{qp} = \sin\theta_r = S_r$$

$$T^{(r)}_{pq} = -S_r$$

Then $\underline{H}^{(r)}$ is identical to $\underline{H}^{(r-1)}$ except in the p and q rows and columns. For these, we have

$$H^{(r)}_{pp} = H^{(r-1)}_{pp} + (H^{(r-1)}_{qq} - H^{(r-1)}_{pp})\, S_r^2 + 2\, C_r S_r\, H^{(r-1)}_{pq}$$

$$H^{(r)}_{qq} = H^{(r-1)}_{qq} + (H^{(r-1)}_{pp} - H^{(r-1)}_{qq})\, S_r^2 + 2\, C_r S_r\, H^{(r-1)}_{pq}$$

$$H^{(r)}_{pq} = C_r S_r\, (H^{(r-1)}_{qq} - H^{(r-1)}_{pp}) + (C_r^2 - S_r^2)\, H^{(r-1)}_{pq} = H^{(r)}_{qp}$$

$$H^{(r)}_{mq} = H^{(r-1)}_{mq}\, C_r - H^{(r-1)}_{mp}\, S_r = H^{(r)}_{qm} \qquad m \neq p,q$$

$$H^{(r)}_{mp} = H^{(r-1)}_{mp}\, C_r + H^{(r-1)}_{mq}\, S_r = H^{(r)}_{pm} \qquad m \neq p,q$$

Now, if we set

$$\tan 2\theta_r = \frac{2H^{(r-1)}_{pq}}{H^{(r-1)}_{pp} - H^{(r-1)}_{qq}}$$

we ensure

$$H^{(r)}_{pq} = 0$$

We note that for all p,q such that $|p\rangle$ is in the manifold of interest and $|q\rangle$ outside it, $\tan\theta$ is a small quantity if the manifold is sufficiently well separated from all other levels. We therefore write

$$C_1 = 1 + 0(\theta^2)$$

$$S_1 = \theta_1 + 0(\theta^3)$$

$$= \frac{H^{(0)}_{pq}}{H^{(0)}_{pp} - H^{(0)}_{qq}} + 0(\theta^3)$$

So that

$$H^{(1)}_{pp} = H_{pp} + H_{pq}\,\theta_1 + 0(\theta^3)$$

$$H^{(1)}_{qq} = H_{qq} - H_{pq}\,\theta_1 + 0(\theta^3)$$

$$H^{(1)}_{pq} = 0$$

$$H^{(1)}_{mq} = H_{mq} - H_{mp}\,\theta_1 + 0(\theta^2) \quad m \neq p,q$$

$$H^{(1)}_{mp} = H_{mp} + H_{mq}\,\theta_1 + 0(\theta^2) \quad m \neq p,q$$

From these transformation relations, it is clear that, apart from H_{pq}, elements in the region of the matrix to be eliminated are unaltered except by terms of order θ. Thus to this order, we may eliminate all such elements by successive rotations defined by

$$\theta_r = \frac{H^{(0)}_{ts}}{H^{(0)}_{tt} - H^{(0)}_{ss}}$$

where t spans all values for which $|t\rangle$ is in the manifold of interest, and s all those for which $|s\rangle$ is outside the manifold. This elimination by successive small rotations is possible, in other words, because small rotations approximately commute. From the transformation equations, we may write as the first approximation to $\underline{H}_{(eff)}$

$$H_{(eff)\,ll} = H_{ll} + \sum_i{}' \frac{H_{li}\,H_{il}}{H_{ll} - H_{ii}} + 0\left\{\frac{H_{li}^3}{(H_{ll} - H_{ii})^2}\right\}$$

$$H_{(eff)\,ml} = H_{ml} + \sum_i{}' \frac{H_{mi}\,H_{il}}{H_{ll} - H_{ii}} + 0\left\{\frac{H_{li}^3}{(H_{ll} - H_{ii})^2}\right\} \quad m \neq l .$$

where the sums span all states $|i\rangle$ outside the manifold of interest.

We may in principle use a second set of rotations, defined by angles ϕ, to eliminate the residual elements connecting the manifold to other levels. We have to eliminate elements of typical size

$$H_{il}\,\theta$$

so that typically

$$\phi \simeq \frac{H_{il}\,\theta}{H_{ii} - H_{ll}}$$

$$\simeq \theta^2$$

Hence the new approximate $\underline{H}_{(eff)}$ will be modified on and off the diagonal by terms of order

$$H_{il}\,\theta\,\phi$$

$$\simeq H_{il}\,\theta^3$$

Thus $\underline{H}_{(eff)}$ is correct to the order quoted above. We note that $\underline{H}_{(eff)}$ is only approximately Hermitian; however, this is consistent with the order of accuracy quoted.

This is the form of Hamiltonian required for the discussion of the $|M_J| = 1$ sublevel in high electric field. The form used to obtain the complete $J = 2$ effective Hamiltonian comes from neglecting in the energy denominators the energy differences between the nearly degenerate levels of the manifold.

We proceed to consider, with somewhat less precision, some aspects of the time dependent problem. We suppose that we can write

$$\hat{H}(t) = \hat{H}_o + \hat{H}_{(pert)}(t)$$

$$\hat{H}_{(pert)} = \hat{h}_{(pert)} \sin \omega t$$

We consider the effect of a transformation $T(t)$ on the time dependent Schrödinger equation

$$\hat{H}(t)\,\Psi(t) = i\hbar \frac{\partial}{\partial t}\Psi(t)$$

We have

$$\hat{T}\hat{H}\hat{T}^{\dagger}\hat{T}\,\Psi(t) = i\hbar\hat{T}\frac{\partial}{\partial t}\Psi(t)$$

$$\therefore \quad \hat{H}'\Psi' = i\hbar\left[\frac{\partial}{\partial t}(\hat{T}\Psi) - \left(\frac{\partial}{\partial t}\hat{T}\right)\Psi\right]$$

$$= i\hbar\frac{\partial}{\partial t}\Psi' - i\hbar\frac{\partial\hat{T}}{\partial t}\hat{T}^{\dagger}\hat{T}\Psi$$

$$= i\hbar\frac{\partial}{\partial t}\Psi' - i\hbar\left[\frac{\partial\hat{T}}{\partial t}\hat{T}^{\dagger}\right]\Psi'$$

$$\therefore \left\{\hat{H}' + i\hbar\left[\frac{\partial\hat{T}}{\partial t}\hat{T}^{\dagger}\right]\right\}\Psi' = i\hbar\frac{\partial}{\partial t}\Psi'$$

or

$$\hat{H}''\Psi' = i\hbar\frac{\partial}{\partial t}\Psi'$$

If we now take a matrix representation and use for $\underline{T}$ a product of rotations defined as before, we shall have for a typical rotation $\underline{R}(\theta)$

$$\theta \simeq \frac{H_{pq}}{H_{pp} - H_{qq}} \simeq \frac{h_{pq}}{H_{pp} - H_{qq}} \sin \omega t$$

and

$$\left[\frac{\partial R}{\partial t} R^{\dagger} \right]_{pq} = - \left[\frac{\partial R}{\partial t} R^{\dagger} \right]^{*}_{qp}$$

$$= \frac{\omega h_{pq}}{H_{pp} - H_{qq}} \cos \omega t$$

with all other elements zero to order θ.

Thus the rotation leaves a term of order $\omega \theta$ in $\underline{H}''$ in the position where $\underline{H}'$ contained a zero. However, if we are interested in inducing transitions within the nearly degenerate manifold, $\hbar \omega$ will be small compared with $H_{pp} - H_{qq}$ and these elements are negligible. Thus for such problems an effective Hamiltonian can be set up as before, and it will have the same form as the time-independent $H_{(eff)}$.

To complete the discussion of the problem, we now have to consider the explicit effect of the transformation T(t) on the wavefunction Ψ (t). We write

$$\Psi (t) = \sum_i a_i (t) \, | i \rangle$$

We are interested in the time dependence of the a_i. We make the usual assumption that at t = 0 the atom is in a well defined eigenstate e.g. $| 1 \rangle$:

$$\Psi (0) = | 1 \rangle$$

$$a_i (0) = \delta (1, i)$$

This assumption implies a sudden application of the perturbation. Now, if we write

$$\Psi'(t) = \hat{T}(t) \sum_i a_i |i\rangle$$

$$= \sum_i b_i |i\rangle$$

we see that for our choice of $T(t)$, and within the manifold of interest,

$$a_i = b_i + 0(\theta^2)$$

This represents an admixture of states one order in θ smaller than taken into account in constructing $H_{(eff)}$, and it is non-resonant in nature.

Thus the Schrödinger equation

$$H_{(eff)}(t)\ \Psi(t) = i\hbar \frac{\partial}{\partial t} \Psi(t)$$

is adequate for discussion of resonant behaviour in the manifold of interest, if $H_{(eff)}$ is formally identical to that derived for the time independent problem.

Appendix B. Stark shift symmetry properties

a) General

We wish to study the effect of the Stark operator

$$-e\sum_i \underline{r}_i \cdot \underline{E} = -\underline{P}\cdot\underline{E} = \sum_q (-1)^q P_{-q} E_q$$

where $\underline{P}$ is a vector in orbital space. We shall study interactions quadratic in E, using the form of effective operator given in chap. 2, and discussing angular integrals by diagrammatic methods following the conventions of Brink and Satchler (1968). We shall take the case where the energy denominators are independent of all magnetic quantum numbers.

Our expressions for matrix elements of the effective Stark interaction will then have the general form

$$\langle JM \mid \hat{H}^{eff} \mid J'M'\rangle = \sum_{\substack{\text{intermediate}\\ \text{states}}} \sum_{qq} \quad \begin{array}{c} JM \qquad\qquad J'M' \\ \square \\ 1\,-q \qquad 1\,-q' \end{array} \quad \times (-1)^q E_q (-1)^{q'} E_{q'},$$

x (reduced matrix elements)

x (energy denominators) B(1)

The block diagram will contain 3-j symbols introduced by use of the Wigner-Eckart theorem. It may also contain 3-j symbols uncoupling the JM_J representation to $LM_L\,SM_S$, for instance. Summation over the magnetic quantum numbers of the intermediate states is implied in the construction of the block; this is possible because of the assumed independence of the energy denominators from all magnetic quantum numbers.

As an example, suppose we have

$$\langle JM|\hat{H}^{eff}|J'M'\rangle = \sum_{\gamma' J'' M''} \frac{\langle \gamma JM|-\underline{P}.\underline{E}|\gamma' J''M''\rangle\langle \gamma' J''M''|-\underline{P}.\underline{E}|\gamma JM\rangle}{(W_{\gamma J} - W_{\gamma' J''})}$$

then this will be rewritten as

$$\sum_{\gamma' J''} \sum_{qq'} \quad \begin{array}{ccccc} JM & + & J'' & + & J'M' \\ \rightarrow & & \rightarrow & & \\ | & & | & & | \\ 1 & -q & 1 & -q' & \end{array} \quad \times (-1)^q E_q \, (-1)^{q'} E_{q'}$$

$$\times \quad \frac{\langle \gamma J \| P \| \gamma' J''\rangle\langle \gamma' J'' \| P \| \gamma J\rangle}{(W_{\gamma J} - W_{\gamma' J''})}$$

We note that with the block in normal form, the JM line carries an arrow; this can be seen directly for the example above, and follows more generally by induction or by the requirements on the form of the block with no external interaction lines.

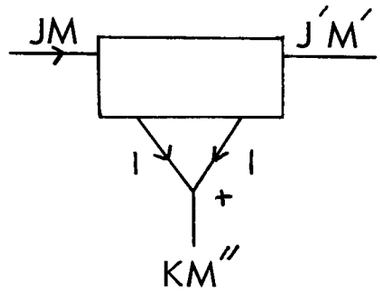
All angular dependence is expressed in the free lines of the block, and the components of $\underline{E}$. We may perform similar manipulations on these for all members of the series. We therefore consider the angular dependence of a typical member

$$X = \sum_{qq'} \quad \begin{array}{ccc} JM & \rightarrow & J'M' \\ & \square & \\ 1 & -q \quad 1 & -q \end{array} \quad \times (-1)^q E_q \, (-1)^q E_q \qquad B(2)$$

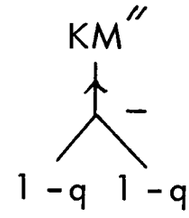
where the block is considered to be reduced to normal form. We recouple the Stark interaction lines and split off a Clebsch-Gordon coefficient; we use

this to recouple the field components to form a tensor:

$$X = \sum_{\substack{qq' \\ KM''}}$$

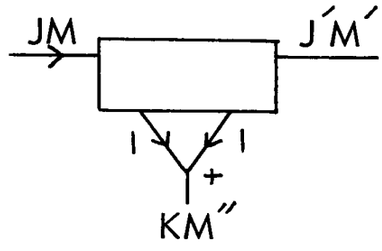


$\times$



$$\times (2K+1) \times (-1)^{q} E_{q} (-1)^{q'} E_{q'}$$

$$X = \sum_{KM''}$$



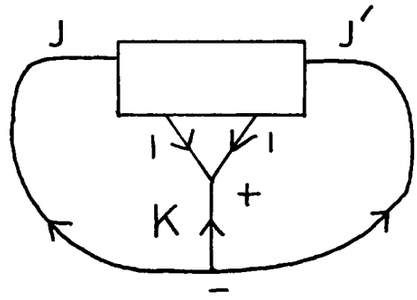
$$\times (2K+1)(-1)^{K}$$

$$\times (-1)^{M''} \left\{ \underline{E}\,\underline{E} \right\}^{(K)}_{-M''}$$

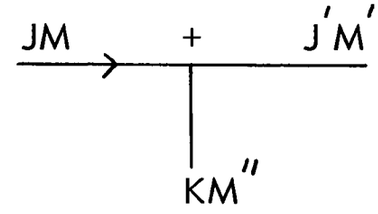
B(3)

Now we reduce the block, which is still in normal form:

$$X = \sum_{KM''}$$



$\times$



$\times$

$$\times (2K+1)(-1)^{K} \times (-1)^{M''} \left\{ \underline{E}\,\underline{E} \right\}^{(K)}_{-M''}$$

B(4)

This form for X at once allows us to write

$$\langle JM \mid \hat{H}^{eff} \mid J'M' \rangle = \left\langle JM \left| \sum_{K} T^{(K)} \cdot \left\{ \underline{E}\,\underline{E} \right\}^{(K)} \right| J'M' \right\rangle$$

Since $\left\{ \underline{E}\,\underline{E} \right\}^{(1)} = 0$, the allowed values of K are 0 and 2. These are the required results.

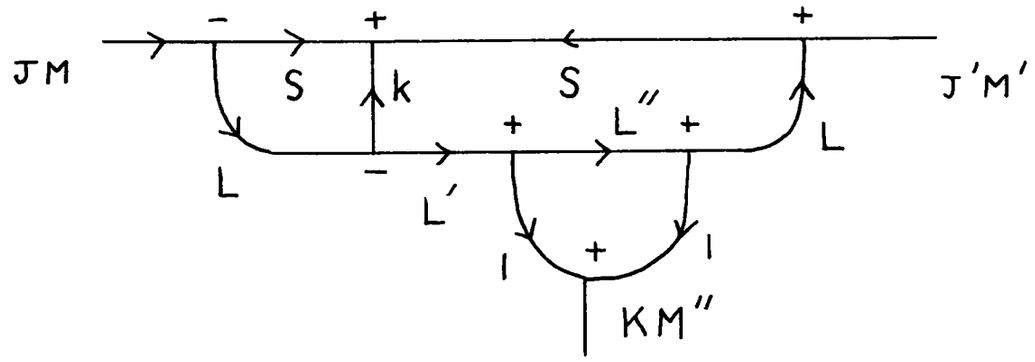
b) The helium 2^3S_1 state

We now consider the case of metastable helium. We shall use the LS coupling approximation, including relativistic interactions as perturbations:

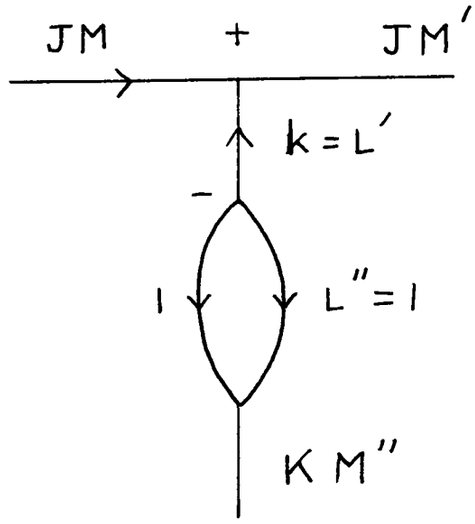
$$\hat{H}_{rel} = \sum_k T^{(k)}\,(\text{spin}) \;.\; T^{(k)}\,(\text{orbit})$$

The effects we shall be interested in are first order in relativistic interactions, second order in Stark interaction; therefore we cannot use the simple second order form for the effective Hamiltonian. However, we may still use the general form B(1) if the effective Hamiltonian is free of "renormalisation" terms; this will be true for the cases we study. The actual form of the Hamiltonian, which we use in chap.8, may be obtained by almost any perturbation technique.

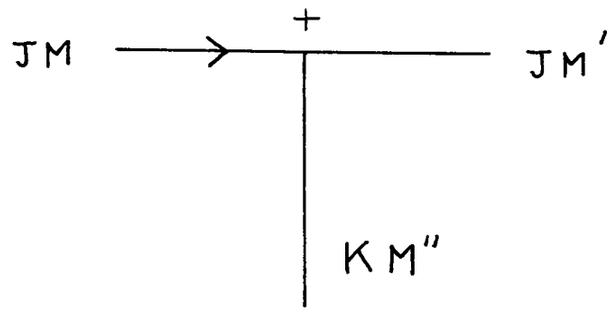
A typical diagram, after recoupling to the form of B(3), is



Here k is the relativistic interaction line. Setting L = 0 and omitting factors independent of magnetic quantum numbers gives



which immediately reduces to



with k = K. This is the angular part of the Wigner-Eckart theorem, as expected.

For the class of terms represented by this diagram, a tensor Stark effect requires a k = 2 relativistic interaction. Moreover a pure k = 2 interaction implies the vanishing of the K = 0 scalar Stark interaction. H^{ss} is pure tensor so that the required results hold for this class of terms.

Clearly, the diagram discussed corresponds to the D-state perturbations of chap.8. The P-state diagram is topologically identical when L = 0, and so gives the same result. These are the only two possibilities.

Appendix C. Time reversal, spectra, and electric dipole moments

We consider some aspects of time reversal violation.

Consider the system of interest subject to external fields $\underline{E}$ and $\underline{B}$. We describe the system by a Hamiltonian $H(\underline{E},\underline{B})$ and write

$$H(\underline{E},\underline{B})\,\psi(\underline{E},\underline{B}) = W(\underline{E},\underline{B})\,\psi(\underline{E},\underline{B}) \qquad C.1$$

Now consider the action of time reversal on the total system, that is the system of interest and the fields. We represent this by an operator θ_T. If and only if the system is invariant under time reversal, we may write

$$\theta_T\, H(\underline{E},\underline{B})\, \theta_T^{-1} = H(\underline{E},\underline{B})$$

In general, we set

$$H(\underline{E},\underline{B}) = H_o(\underline{E},\underline{B}) + H_v(\underline{E},\underline{B})$$

where H_v is time reversal violating:

$$\theta_T \left[H_o(\underline{E},\underline{B}) + H_v(\underline{E},\underline{B}) \right] \theta_T^{-1} = H_o(\underline{E},\underline{B}) - H_v(\underline{E},\underline{B})$$
$$= H^T(\underline{E},\underline{B}) \qquad C.2$$

Now we set

$$\theta_T = \theta_F \theta_S \qquad C.3$$

where θ_F and θ_S respectively act only on the external fields and on the system of interest. Clearly $\left[\theta_F,\theta_S\right] = 0$. It is well known (see e.g. Sakurai 1964) that the action of time reversal on the fields is

$$\underline{E} \longrightarrow \underline{E}$$
$$\underline{B} \longrightarrow -\underline{B}$$

Hence

$$\theta_F\, H(\underline{E},\underline{B})\, \theta_F^{-1} = H(\underline{E},-\underline{B})$$
$$\therefore\quad \theta_T\, H(\underline{E},\underline{B})\, \theta_T^{-1} = \theta_S\, H(\underline{E},-\underline{B})\, \theta_S^{-1}$$
$$\therefore\quad \theta_S\, H(\underline{E},\underline{B})\, \theta_S^{-1} = H^T(\underline{E},-\underline{B}) \qquad C.4$$

We now use this in C.1 :

$$\theta_S \, H(\underline{E}, \underline{B}) \, \theta_S^{-1} \, \theta_S \, \psi \, (\underline{E}, \underline{B}) = W(\underline{E}, \underline{B}) \, \theta_S \, \psi \, (\underline{E}, \underline{B})$$

(the form of the right-hand side assumes W is real)

$$\therefore \quad H^T \, (\underline{E}, -\underline{B}) \, \theta_S \, \psi \, (\underline{E}, \underline{B}) = W(\underline{E}, \underline{B}) \, \theta_S \, \psi \, (\underline{E}, \underline{B}) \qquad \text{C.5}$$

But by direct replacement in C.1

$$H \, (\underline{E}, -\underline{B}) \, \psi \, (\underline{E}, -\underline{B}) = W(\underline{E}, -\underline{B}) \, \psi \, (\underline{E}, -\underline{B}) \qquad \text{C.6}$$

Hence if and only if $H_v = 0$, we may assert

$$W \, (\underline{E}, \underline{B}) = W(\underline{E}, -\underline{B}) \qquad \text{C.7}$$

This means that if the spectrum of energy levels for fields $\underline{E}$, $\underline{B}$ is different from that for $\underline{E}$, $-\underline{B}$, we conclude that time reversal is not a symmetry of the system.

To extend this result, we introduce the operator R_T which rotates system and fields through π about an axis parallel to $\underline{B} \times \underline{E}$. This is a symmetry operation if the universe is isotropic; its effect on the fields is

$$\underline{E} \longrightarrow -E$$
$$\underline{B} \longrightarrow -\underline{B}$$

Carrying through a process parallel to that used above, we find

$$W(\underline{E}, \underline{B}) = W(-\underline{E}, -\underline{B}) \qquad \text{C.8}$$

We therefore conclude

$$W(\underline{E}, -\underline{B}) = W(-\underline{E}, \underline{B})$$
$$= W(\underline{E}, \underline{B}) \quad \text{iff} \quad H_v = 0 \qquad \text{C.9}$$

We now specialise to the case where $W(\underline{E},\underline{B})$ is nondegenerate, and suppose $H_v = 0$. Then we may write from C.5, C.6 and their analogs involving R_S

$$R_S \psi(\underline{E},-\underline{B}) = e^{i\delta_1} \psi(-\underline{E},\underline{B}) \qquad \text{C.10}$$

$$\theta_S \psi(\underline{E},\underline{B}) = e^{i\delta_2} \psi(+\underline{E},-\underline{B}) \qquad \text{C.11}$$

Suppose our system has an electric dipole moment $\underline{D}$ in the state $\psi(\underline{E},\underline{B})$:

$$\underline{D} = \langle \psi(\underline{E},\underline{B}) | \hat{\underline{D}} | \psi(\underline{E},\underline{B}) \rangle \qquad \text{C.12}$$

Now, it is known (Harrison 1969) that

$$\theta_S \hat{\underline{D}} \theta_S^{-1} = \hat{\underline{D}}$$

$$R_S \hat{\underline{D}} R_S^{-1} = -\hat{\underline{D}}$$

We may write from C.12

$$\underline{D} = \langle \theta_S R_S \psi(\underline{E},\underline{B}) | \theta_S R_S \hat{\underline{D}} R_S^{-1} \theta_S^{-1} | \theta_S R_S \psi(\underline{E},\underline{B}) \rangle$$

$$= -\langle \psi(-\underline{E},\underline{B}) | \hat{\underline{D}} | \psi(-\underline{E},\underline{B}) \rangle \qquad \text{C.13}$$

from C.10, 11. We define $\underline{D}$ as a permanent dipole if it has a nonzero value at $E = 0$. But then, comparing C.12, 13, we see

$$\underline{D}(\text{permanent}) = -\underline{D}(\text{permanent})$$

$$= 0$$

if $\psi(0,\underline{B})$ remains nondegenerate. We may also show this result by consideration of the effect of $\underline{D}$ on the spectrum, using C.9.

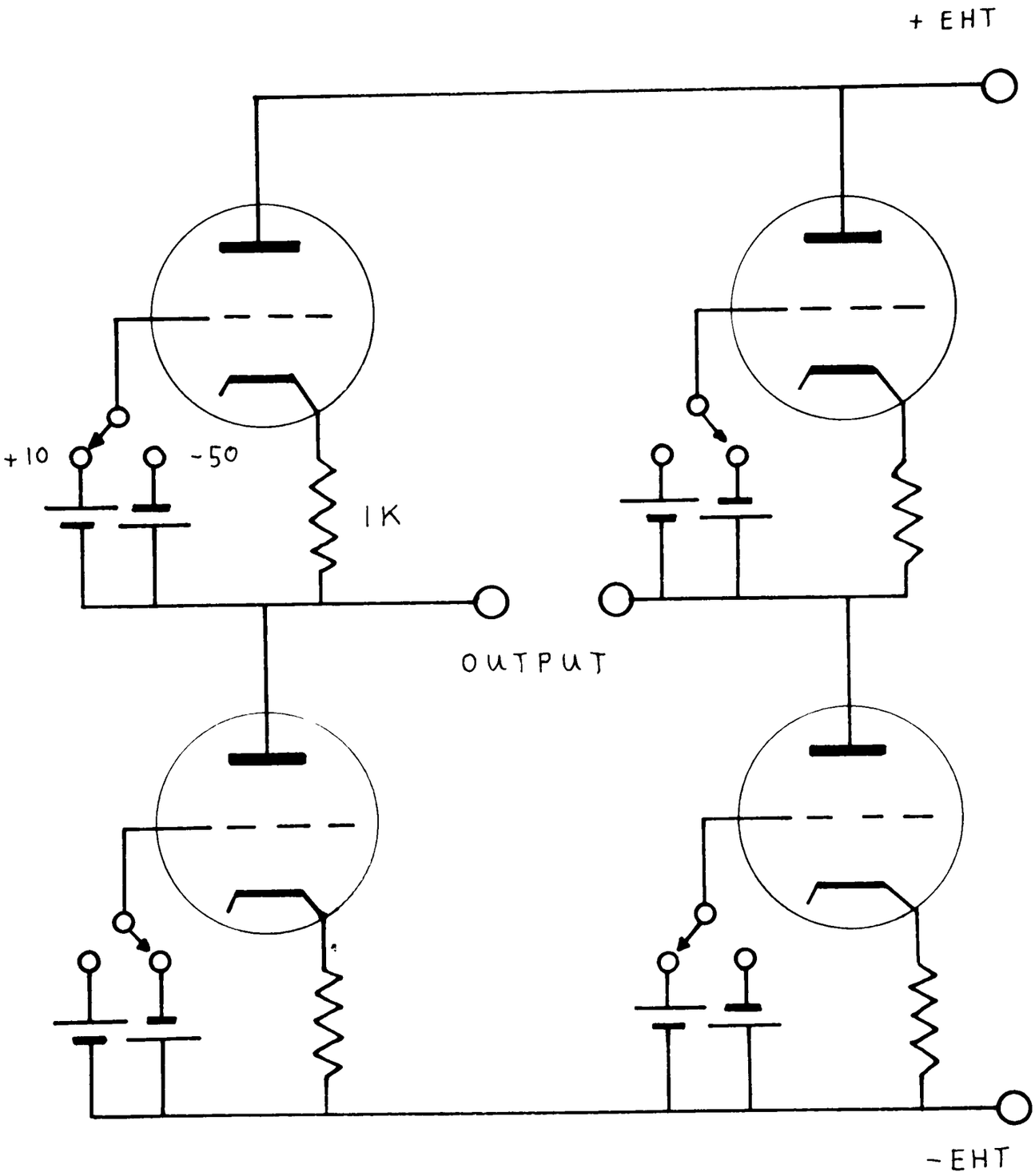
This result may be applied to any system. Applied to a classical particle, it is uninteresting because of degeneracy. Applied to an electron, it states that if time reversal is a symmetry, the electron cannot have an edm because there

exists but a single (nondegenerate) type of electron.

We note that the proof assumes that stationary states may be written down. This may not be the case (e.g. for an atom in a nonuniform magnetic field) in which event the results do not apply.

Simplified electronic EHT switch

Fig D·1



For implementation of grid switching, see text

Appendix D. Assorted electronics

a) Electronic EHT switching

We have constructed two EHT reversing switches using thermionic valves. The basic circuit is given in fig. D-1.

The first version used CV73 tubes; these are high current tetrodes with a 12.5 kV anode rating. The screen grids were held at about +10V w.r.t. cathode, and control grids switched between -50V and +10V. This switching was implemented by opto-electronic coupling to a transistor invertor floating at cathode potential. The circuit used out-of-date techniques (a neon tube light source and discrete component photo-preamplifier) and we do not reproduce it; the salient feature was the use of a simple Perspex light pipe, about 3 inches long. With the floating circuitry well enclosed in a box tied to cathode potential, the switching worked excellently. The circuit reversed ± 5 kV within 2V, and worked well up to switching rates of a few hundred Hz, essentially limited by the optoelectronics. No unpleasant switching transients were produced, possibly as a result of the inclusion of the cathode resistors.

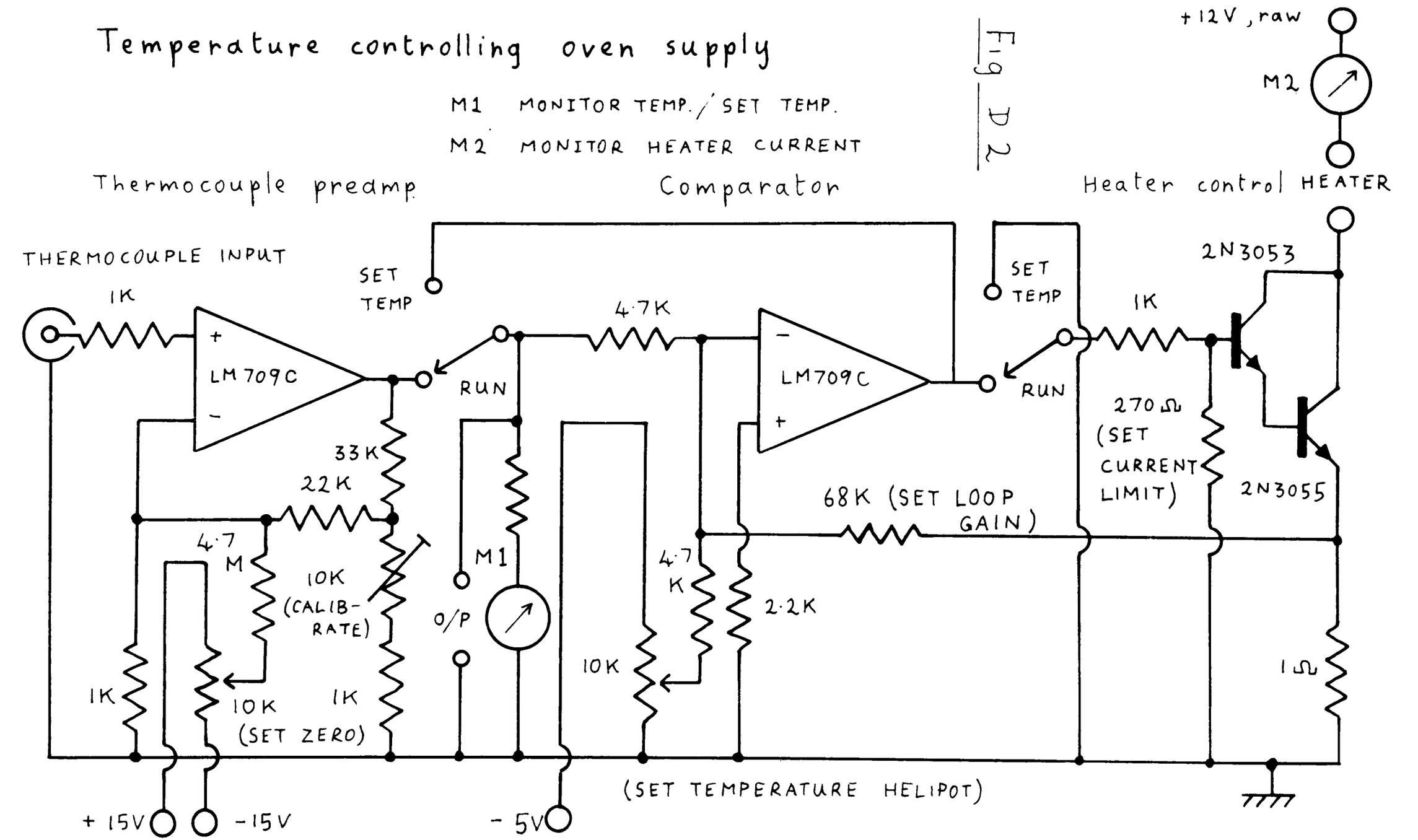
The second version used Ferranti HL22 tubes which are triodes with a 25 kV anode rating. The switching to the top valves was now controlled by current flowing through 200 M Ω resistors connected to the outputs, but this was due simply to a lack of suitable floating power supplies for optoelectronic switches. The grids were again switched between + 10 V and - 50 V. The HL22 is a low current device ($\simeq$ 2mA) with unusual planar geometry, and we found it impossible to achieve good switch-on voltage drops, apparently because of static charges on the glass envelope. Values of 50 V were obtained, subject to drift with time. Switching rates up to about 100 Hz were achieved, limited by the permissible tube current and the 10^{-9} F load. The setup was compatible with the computer, and extremely high reliability was obtained under computer control.

Temperature controlling oven supply

Fig. A2

M1 MONITOR TEMP./SET TEMP.

M2 MONITOR HEATER CURRENT



b) Temperature controlled oven supply

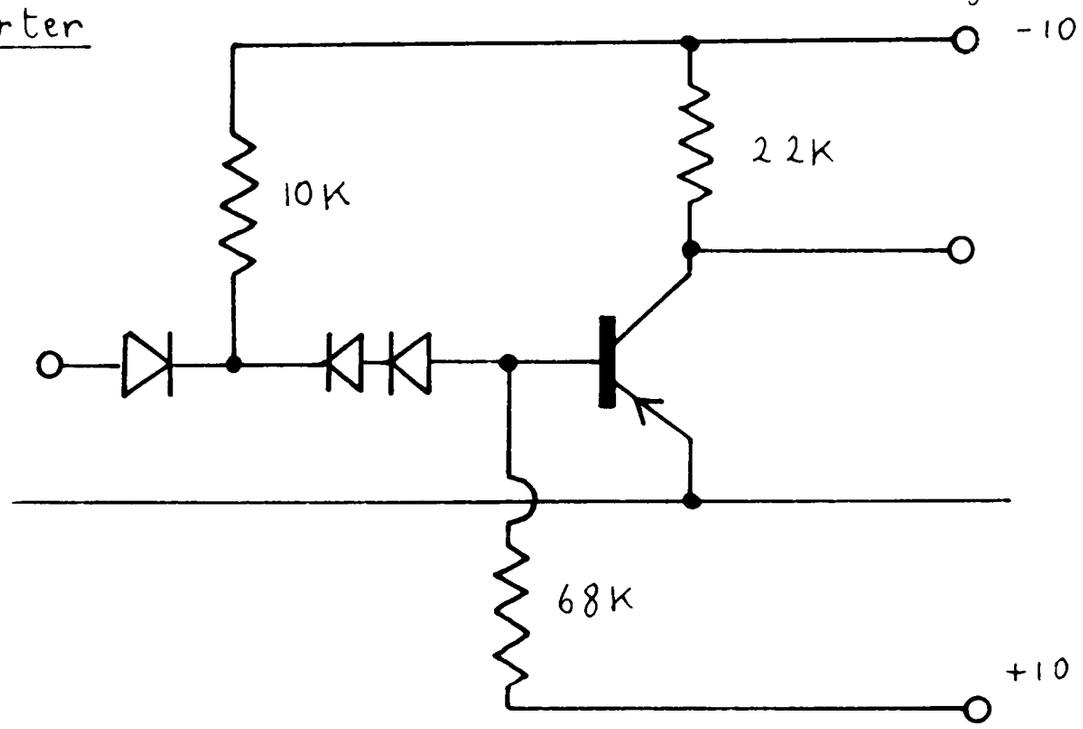
We give in fig. D-2 the circuit of the supply used with our alkali oven. Omitted from the diagram are all stabilisation components, since it is envisaged that these will change with layout. We initially experienced difficulty with r.f. oscillation, which gave strange D.C. behaviour; this was cured by careful earthing, decoupling of power rails, and slowing down the amplifiers.

The range of "proportional" control is about 10°C below the set temperature, and stability is certainly better than 1°C. The settling temperature is a few degrees below the temperature set. All these parameters depend on the chosen loop gain.

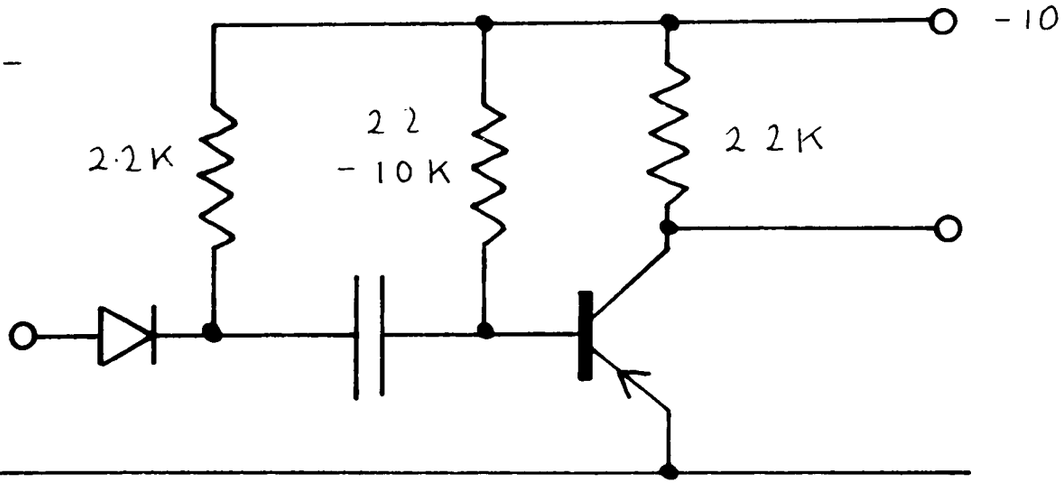
EHT switching logic circuits Fig D 3

All semiconductors silicon general purpose

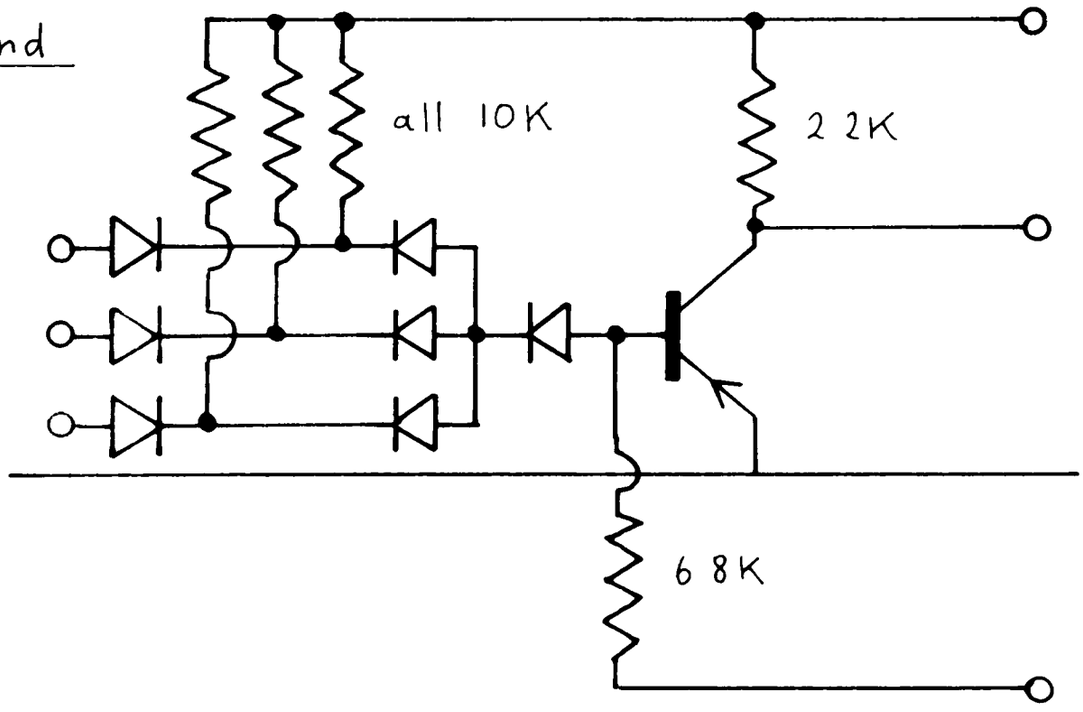
Inverter



Delay



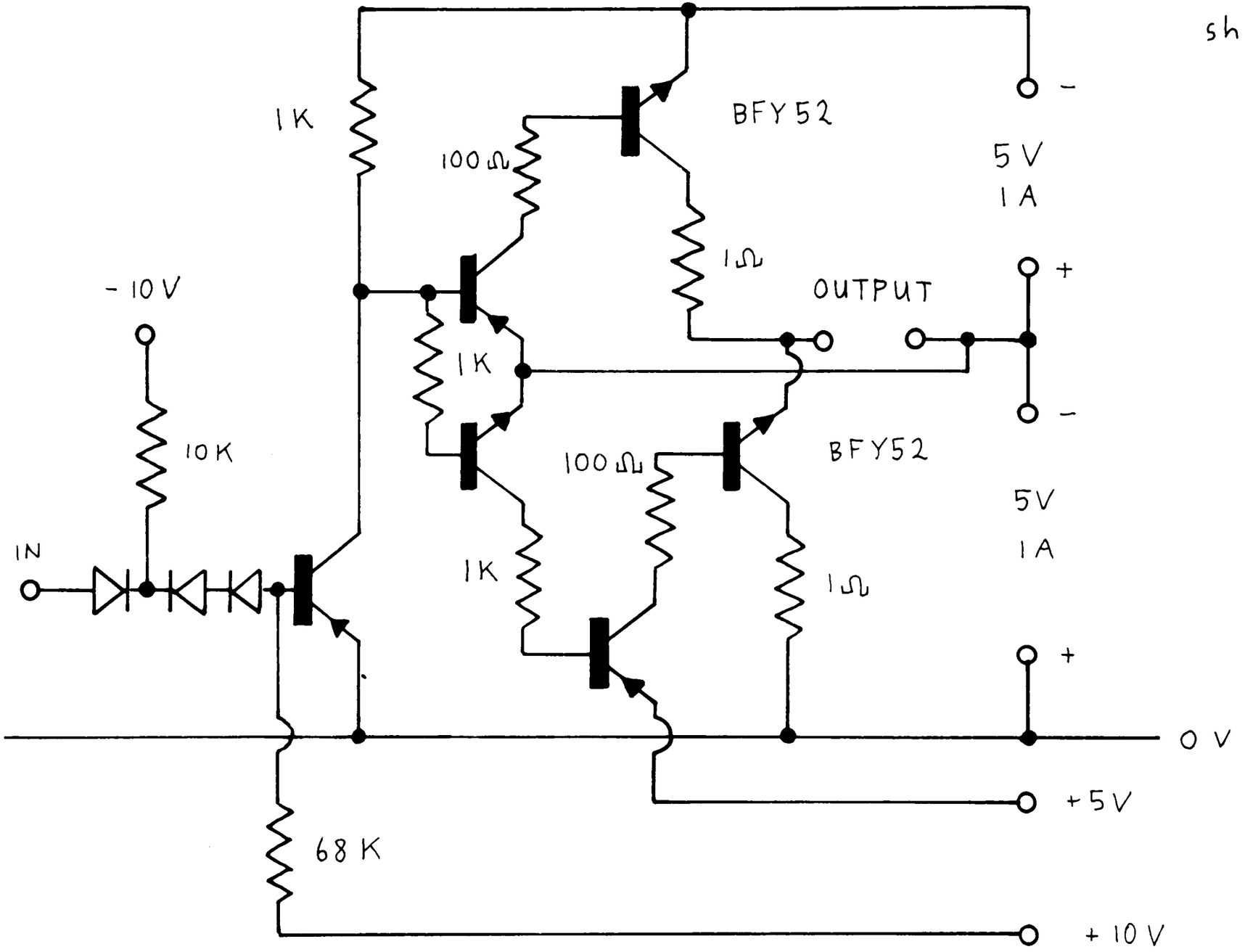
And



Bipolar relay driver

All semiconductors silicon general purpose except where shown.

Fig D4

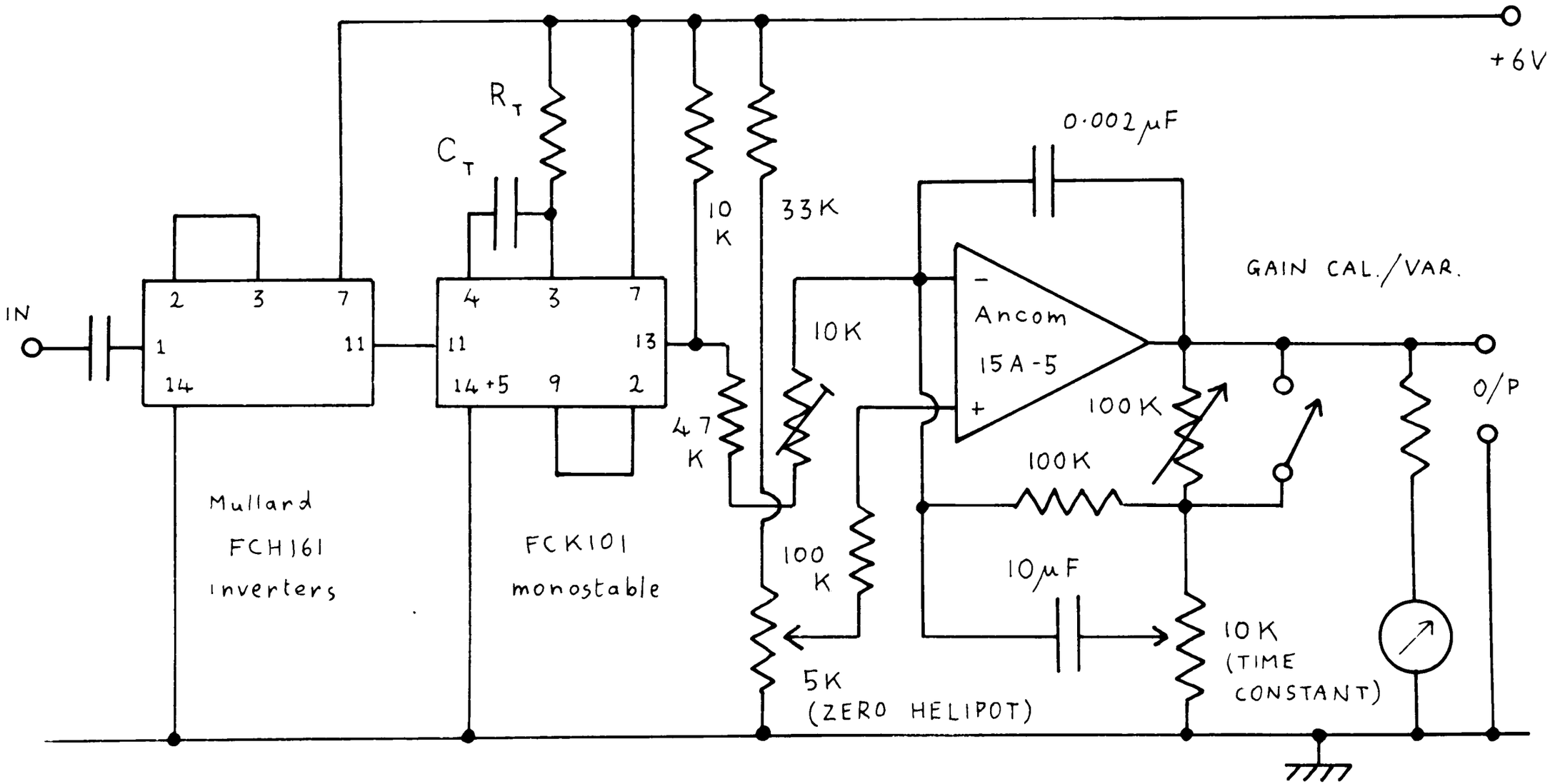


c) Logic for mechanical EHT switching

We give in figs. D-3 and D-4 the circuits used in the switching logic of the mechanical EHT system described in chap. 4. The delay circuit has behaviour less well defined than a monostable, though by and large it is compatible with a DTL system; its advantage in the present case is its extreme noise immunity, which greatly improves the overall reliability of the system.

Fig D5

Pulse rate meter



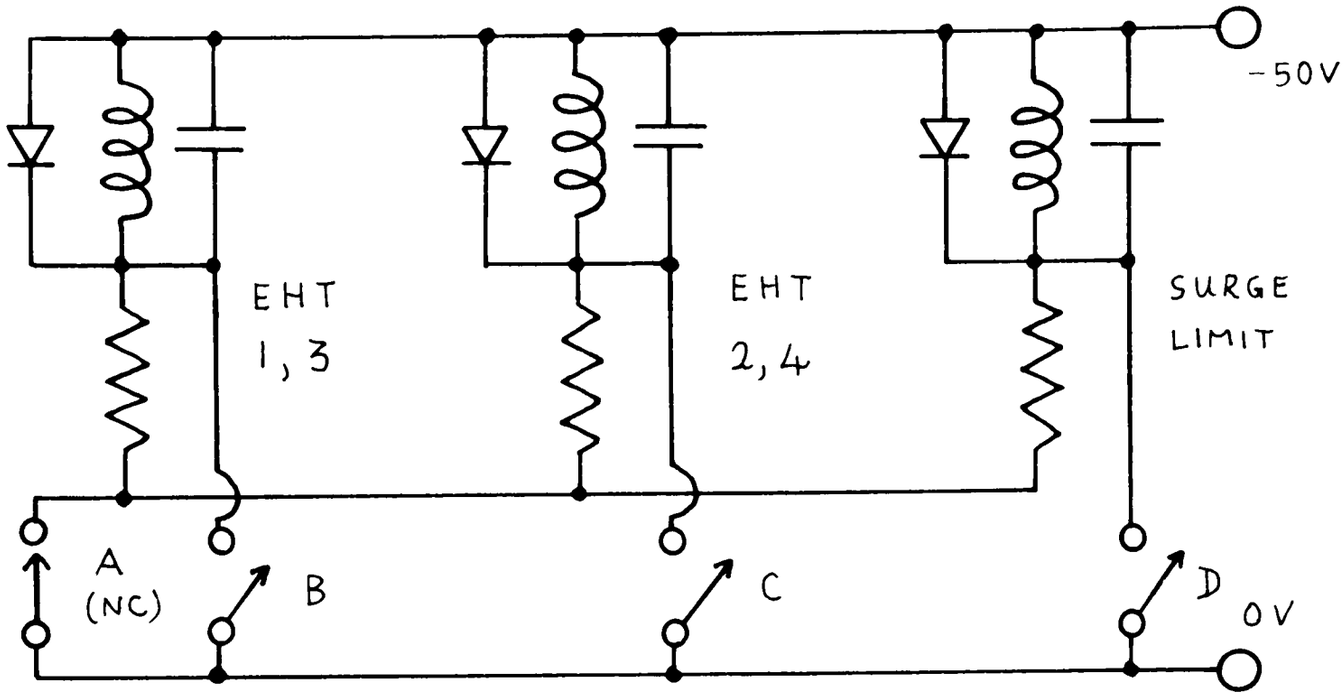
R_T, C_T switched For each range R_T separately adjustable on each

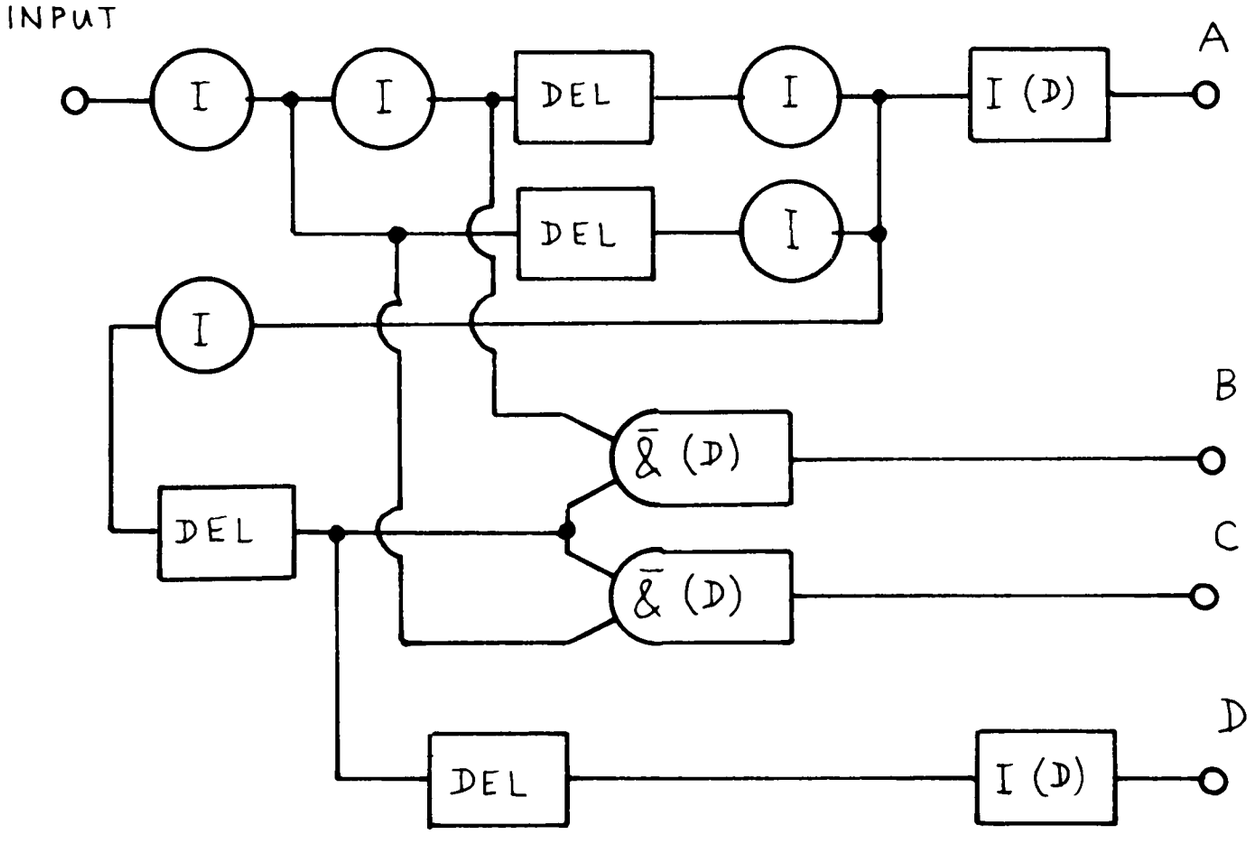
d) Pulse rate meter

This circuit is shown in fig. D.5. It follows the usual pattern but uses DTL integrated circuits and an encapsulated operational amplifier to achieve compactness, reliability, and stability of operation. It gives about 10% accuracy at 10^6 c.p.s. random count rate, and most of this is probably due to the slow discriminator used to drive it. With steady pulse rates the accuracy and linearity are about 2%. A feature is the continuously variable output time constant.

Reed relay EHT system

Fig D·6





Modules (D) have relay driving output.

e) Reed relay EHT switching

Our reed relay EHT switch was arranged in the usual bridge fashion, with the addition of switchable surge limiting resistors and 1K suppressor resistors physically close to the DRVT 25 reeds. We did not implement the plate discharging facility of the later mechanical switch.

We have mentioned already the problem of electrostatic sticking in these reeds; partly in an attempt to overcome this, and partly to cut down changes in stray magnetic field on reversal, we used the reeds in a bistable mode with switching accomplished by pulsing.

Referring to fig. D-6, switch A (another vacuum reed relay) is normally held closed and B, C, D normally open. The values of the resistors in series with the EHT switch driver coils are chosen so that the coils are energised between pull in and drop out for the EHT switches; therefore any of these that are open stay open, any closed stay closed. The switching cycle, controlled by the logic shown in D-6, begins with the opening of A; all EHT reeds now open. Next, either B or C is closed, and A also closes again. According to whether B or C is closed, one diagonal pair or the other of the EHT switches of the bridge are pulsed closed (in theory!) and the new EHT sign established. The driving switch B or C reopens, the surge limiter shorting switches are pulsed closed by the closure of D, and finally D opens to end the cycle.

The electronic part of the circuit worked well using the logic circuitry described in appendix D(c). The driving reeds were less reliable than hoped. The EHT switches were pulse energised with up to 1 kA turn and still stuck open. Even when they did operate, they were disappointingly slow; the complete switching cycle took about 100 msec. The bistable mode of operation reduced stray field changes by about a factor 10, and was surprisingly stable and easy to set up. Selection of switches was not required.

EHT stabiliser

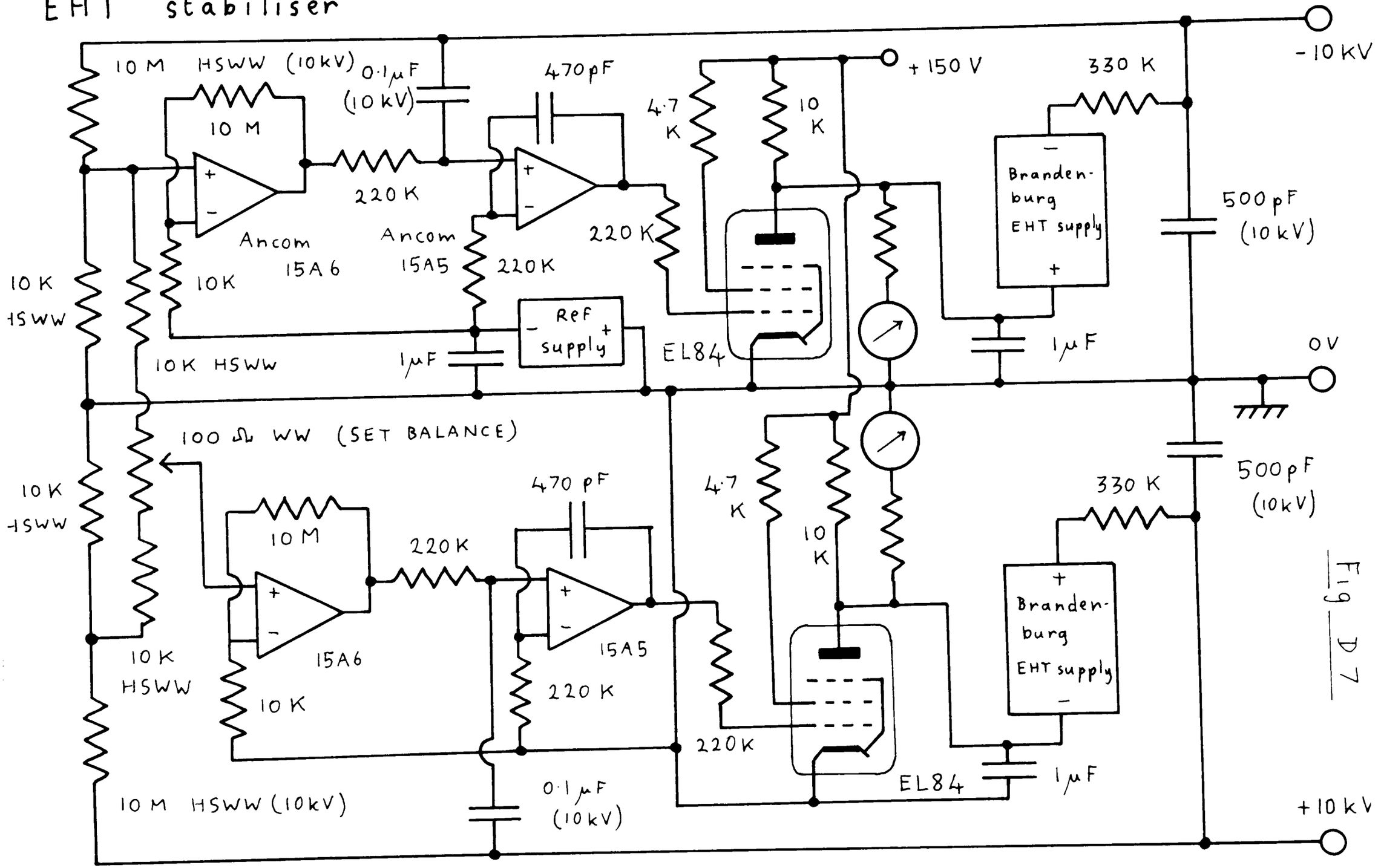


Fig 4A7

f) EHT stabiliser

At an early stage in the dipole experiment it appeared we should need greater EHT stability, and equality of positive and negative supplies, than was in fact ultimately called for. We designed and built the circuit of fig. D-7 in an attempt to achieve stabilities of a few p.p.m. The circuit operates, but was in fact never tested to this level of precision.

It will be observed that the overall gain from one EHT rail to the output of the first operational amplifier is unity, and it is at this point that AC feedback from the EHT rail is coupled in. This arrangement, suggested by Mr. D.T. Smith, gives improved l.f. stability.

The input potential dividers are the Fluke instruments mentioned previously. The reference supply is based on a Mullard BZX47 precision Zener, but construction of this was not completed.

Appendix E. "Up-down counter" program.

We give below a listing of the program.

```
/NEW UPDOWN COUNTER. 15 FEB 69


*400

CSERVS,0
SOF
JMP CK
CLA
TAD CB1
TAD CKFLG
DCA CKFLG
CK,CLA
TAD CKFLG
SNA
JMP OK
IAC
DCA CKFLG
CBF
JMP I CSERVS

OK,TAD MD
LAB
CLA CLL
RIB
DCA TPAC
CBF
DCA TPAC+1
DCA TPAC+2
TAD PMD
RAL
DCA PMD
TAD AST
SZL
TAD C3
DCA TPPNT
TPACC
CLA
TAD SJO
DCA JO3
TAD STS
RILP,DCA STADR
TAD PMD
RAL CLL
DCA PMD
TAD STADR
SNL
TAD C17
DCA TPPNT
TPACC
TAD STADR
TAD C3
ISZ JO3
JMP RILP
TAD C17
DCA TPPNT
TPACC
JMS I CTRLP
ISZ RO
SKP
JMS I RORP
SCF
SKP
HLT
ISZ TOL
SKP
ISZ TOH
JMP I CSERVS
JMP I TOP

CB1,-2
C3,3
RORP,ROR
JO3,0
C6,6
STADR,0
C17,17
C44,44
CTRLP,CTRL
TOP,TO

TPACCS,0
CLA CLL
TAD I TPPNT
TAD TPAC
DCA I TPPNT
SNL
JMP I TPACCS
ISZ TPPNT
ISZ I TPPNT
JMP I TPACCS
ISZ TPPNT
ISZ I TPPNT
JMP I TPACCS
JMP I TPACCS

*600

ROR,0
CLA CLL
TAD ROS
DCA RO
TAD CB3
TAD CKFLG
DCA CKFLG
TAD AST
DCA TPPNT
TAD I TPPNT
DCA TPAC
ISZ TPPNT
TAD I TPPNT
ISZ TPPNT
DCA TPAC+1
TAD I TPPNT
ISZ TPPNT
DCA TPAC+2
TPNEG
TPADD
JMS TSFT
TAD TPAC+2
TAD RC4000
LCB
JMP I ROR

CB3,-2
RC4000,4000

TPNEGS,0
CLA CLL
TAD TPAC
CIA
DCA TPAC
TAD TPAC+1
CMA
SZL
IAC CLL
DCA TPAC+1
TAD TPAC+2
CMA
SZL
IAC CLL
DCA TPAC+2
JMP I TPNEGS

TPADDS,0
CLA CLL
TAD TPACST
DCA TPACP
TAD CM3
DCA LPC
ALP,TAD I TPPNT
TAD I TPACP
```

```
DCA I TPACP
ISZ TPPNT
ISZ TPACP
RAL
ISZ LPC
JMP ALP
CLA CLL
JMP I TPADDS

LPC,Ø
TPACP,Ø
TPACST,TPAC
CM3,-3

TSFT,Ø
CLA
TAD ASFT
DCA ATEMP
TAD ATEMP
SNA
JMP I TSFT
TAD CM14
SMA SZA
JMP RED
STA
TAD ATEMP
DCA ASFT1
TAD TPAC+1
MQL
TAD TPAC+2
SHL
ASFT1,Ø
DCA TPAC+2
JMP I TSFT
RED,DCA ATEMP
TAD TPAC
DCA ATEMP1
DCA TPAC
TAD TPAC+1
DCA ATEMP2
TAD ATEMP1
DCA TPAC+1
TAD ATEMP2
DCA TPAC+2
JMP TSFT+4
ASFT,Ø
ATEMP,Ø
ATEMP1,Ø
ATEMP2,Ø
CM14,-14
```

```
*1ØØØ

CTRL,Ø
CLA
TAD MD
DCA PMD
TAD MC
AND MMSK1
SNA
JMP CONT1
CLA
TAD CB2
TAD CKFLG
DCA CKFLG
CONT1,TAD XL
DCA XAL
TAD XH
DCA XAH
ISZ XL
SKP
ISZ XH
NOP
TAD XAL
CMA
AND XL
SZA
JMP LO
TAD XAH
CMA
AND XH
LSR
Ø
NMI
CLA
SCA
JMP CONT
LO,LSR
Ø
NMI
CLA
SCA
TAD C14
CONT,TAD MCOGPT
DCA MCP
TAD I MCP
DCA MC
TAD MC
CMA
DCA TEMP1
```

```
TAD MD
CMA
DCA TEMP2
TAD MC
AND TEMP2
DCA TEMP2
TAD MD
AND TEMP1
TAD TEMP2
DCA MD
JMP I CTRL

XAL,Ø
XAH,Ø
C14,14
MCOGPT,MCOG
MCP,Ø
TEMP1,Ø
TEMP2,Ø
MMSK1,4Ø
CB2,-2Ø

*12ØØ

TO,CLA CLL
TAD TOHS
DCA TOH
TAD TOLS
DCA TOL
TAD OGSFT
TAD STOG
DCA STS
ION
TAD OGSFT
CIA
DCA OGSFT
TAD OGSFT
TAD STOG
DCA TSTP
TAD FS
DCA F
TAD FSTS
DCA FSTP
TAD SJO
DCA JO4
TTLP,TAD TSTP
TAD CT17
DCA TSTP+1
TPFP
TSTP
```

```
JMS I 7
FADD I FSTP
FPUT I FSTP
FEXT
TPFP
TSTP+1
JMS I 7
FPUT FTEMP
FGET I FSTP
FSUB FTEMP
FPUT I FSTP
FEXT
CLA
DCA 55
TAD SPC
ITYP
ISZ F
JMP .+5
STA
DCA 55
TAD FS
DCA F
JMS I 6
CLA
TAD TSTP
TAD CT3
DCA TSTP
TAD FSTP
TAD CT3
DCA FSTP
ISZ JO4
JMP TTLP
CLA
TAD TSTP
TAD CT17
DCA TSTP
TPFP
TSTP
JMS I 7
FADD FTL
FPUT FTL
FEXT
CLA
TAD SPC
ITYP
JMS I 6
JMS I 7
FGET FTL
SQROOT
FEXT
CLA
TAD SPC
ITYP
STA
DCA 55
JMS I 6
CLA
TAD LFC
ITYP
NOP
JMP .-1

TSTP,Ø
Ø
LFC,212
FS,-4
F,Ø
JO4,Ø
FSTP,Ø
CT17,17
FTEMP,Ø
Ø
Ø
SPC,240
CT3,3
FTL,Ø
Ø
Ø

*1600

TPFPS,Ø
CLA
TAD I TPFPS
ISZ TPFPS
DCA INPT
TAD I INPT
DCA INPT
TAD I INPT
DCA TL
DCA I INPT
ISZ INPT
TAD I INPT
DCA TM
DCA I INPT
ISZ INPT
TAD I INPT
DCA TH
DCA I INPT
TAD TH
TAD TM
TAD TL
SZA
JMP CC
DCA 45
DCA 46
DCA 44
JMP I TPFPS
CC,CLA
TAD TH
CIA
TAD TM
SZA
JMP AA
TAD TH
SPA
CMA
SZA
JMP AA
CLA
TAD TL
MQL
TAD TM
IOF
NMI
DCA 45
MQA
DCA 46
SCA
ION
CIA
TAD TC27
DCA 44
JMP I TPFPS
AA,CLA
TAD TM
MQL
TAD TH
IOF
NMI
DCA 45
MQA
DCA 46
SCA
ION
CIA
DCA SCST
TAD SCST
TAD TC43
DCA 44
```

```
TAD SCST
TAD TC27
DCA SFTH
TAD TL
LSR
SFTH,0
TAD 45
DCA 45
MQA
TAD 46
DCA 46
JMP I TPFPS

INPT,0
TC27,27
TC43,43
SCST,0
TL,0
TM,0
TH,0
```

```
*0
0
JMP I ISPT
ISPT,IS

*2200

IS,DCA IST
MQA
DCA MIST
RAL
DCA LIST
SCF
SKP
JMS I CSERVP
TSF
SKP
JMS PTION
KSF
SKP
JMS KION
CLA CLL
TAD LIST
RAR
TAD MIST
MQL
TAD IST
ION
JMP I 0

CSERVP,CSERVS
IST,0
MIST,0
LIST,0

PTION,0
TCF
STA
DCA PTFLG
JMP I PTION

KION,0
KRB
DCA KBUFF
ACT
261
INIT
JMP I KION

ITYPS,0
DCA PTBUFF
TAD PTFLG
SNA
JMP .-2
CLA
DCA PTFLG
TAD PTBUFF
TLS
CLA
JMP I ITYPS

PTBUFF,0

ACTS,0
CLA
TAD KBUFF
CIA
TAD I ACTS
ISZ ACTS
SNA
JMP .+4
CLA
ISZ ACTS
JMP I ACTS
TAD I ACTS
DCA ACTS
JMP I ACTS

CHECKS,0
DCA CBUFF
TAD CHECKS
DCA EXST
TAD I CHECKS
CIA
TAD CBUFF
SPA CLA
JMP CEX1
TAD CBUFF
CIA
ISZ CHECKS
TAD I CHECKS
SPA CLA
JMP CEX1
ISZ CHECKS
ISZ CHECKS
TAD CBUFF
JMP I CHECKS
CEX1,CLA
TAD EXST
TAD EXC2
DCA EXST
TAD I EXST
DCA CHECKS
TAD CBUFF
JMP I CHECKS

EXST,0
EXC2,2
CBUFF,0

KACCS,0
KSF
JMP .-1
KRB
DCA KBUFF
JMP I KACCS

PTS,0
TSF
JMP .-1
TLS
CLA
JMP I PTS

DPTS,0
TAD DC260
JMS PTS
JMP I DPTS
DC260,260

*200

INIT,CLA
TLS
TAD C215
TYPE
TAD C212
TYPE
LAB
LBB
TAD CA4000
LCB
INIT1,OCACC;257
ACT;20;INCON1
ACT;17;INCON2
ACT;16;INCON3
ACT;15;INCON4
ACT;14;INCON5
TAD KBUFF
CHECK;0;13;INIT1
```

```
JMP I .+1
INCON6

OCACCS,0
CLA
DCA INBUFF
STA
DCA LPFLG
TAD I OCACCS
ISZ OCACCS
DCA ACARG
OCLP,KACC
ACT
ACARG,0
OCTERM
TAD KBUFF
TAD ACM260
DCA KBUFF
TAD KBUFF
CHECK;0;9;OCLP
DTYPE
TAD INBUFF
CLL RAL
RTL
TAD KBUFF
DCA INBUFF
ISZ LPFLG
NOP
JMP OCLP
OCTERM,ISZ LPFLG
JMP .+4
STA
DCA LPFLG
JMP OCLP
TAD KBUFF
TYPE
TAD INBUFF
DCA KBUFF
JMP I OCACCS

INBUFF,0
LPFLG,0
ACM260,-260
CA4000,4000

C212,212
C215,215

INCON6,DCA I MNUMP
MDACC
JMS I MILP
JMP INIT1
MILP,MIL
MNUMP,MNUM

INCON5,MDACC
CLA CLL
TAD YL
CIA
DCA TOLS
TAD YH
CMA
SZL
CLL IAC
DCA TOHS
JMP INIT1

INCON4,MDACC
CLA
TAD YL
CIA
DCA ROS
JMP INIT1

INCON3,OCACC;215
TAD IC212
TYPE
TAD KBUFF
DCA I ASFTPT
JMP INIT1
IC212,212
ASFTPT,ASFT

INCON2,MDACC
CLA
TAD YL
DCA PH
JMP INIT1

*2400

MDACCS,0
CLA
DCA YL
DCA YH
MDLP,KACC
ACT;273;MDSFT
ACT;215;.+2
JMP .+6
TAD KBUFF
TYPE
TAD MDC212
TYPE
JMP I MDACCS
TAD KBUFF
TAD MCM260
DCA KBUFF
TAD KBUFF
CHECK;0;1;MDLP
DTYPE
TAD YL
MQL
TAD YH
SHL
0
DCA YH
MQA
TAD KBUFF
DCA YL
JMP MDLP
MDSFT,TAD KBUFF
TYPE
OCACC
215
TAD MDC212
TYPE
TAD KBUFF
SNA
JMP I MDACCS
TAD ACM1
DCA MSFT
TAD YL
MQL
TAD YH
SHL
MSFT,0
DCA YH
MQA
DCA YL
JMP I MDACCS

MDC212,212
MCM260,-260
ACM1,-1

INCON1,CLA
TAD INC215
TYPE
TAD INC212
TYPE
```

```
TSF
JMP .-1
CLA
DCA XL
DCA XH
TAD PH
DCA MD
TAD MD
DCA MC
TAD MD
LAB
JMS I CTRLI
CLA
TAD OGSFTS
TAD STOG
DCA STS
TAD OGSFTS
CIA
DCA OGSFT
TAD TOLS
DCA TOL
TAD TOHS
DCA TOH
DCA I FTLI
DCA I FTLI+1
DCA I FTLI+2
DCA CKFLG
TAD C2000
DCA CLRPNT
TAD CM200
DCA CLRCT
DCA I Z CLRPNT
ISZ CLRCT
JMP .-2
CBF
SCF
JMP .-1
CLA
DCA PTFLG
TLS
CBF
JMS I RORI
ION
JMP .-1

INC215,215
INC212,212
CTRLI,CTRL
FTLI,FTL
FTL+1
FTL+2
C2000,1777
CM200,-200
CLRCT,0
RORI,ROR

*2600

MIL,0
CLA
DCA NO
TAD MCM2
DCA HA
TAD YLADD
DCA YPT
TAD MDPOG
DCA MDPPT
MDPL,CLA
DCA I MDPPT
TAD MCM14
DCA HB
DCA SFL
MLP,CLA MQL
TAD I YPT
CLL RAR
DCA I YPT
GLK
TAD NO
DCA NO
TAD NO
CLL RAR
GLK
LSR
0
SHL
SFL,0
TAD I MDPPT
DCA I MDPPT
ISZ SFL
ISZ HB
JMP MLP
ISZ YPT
ISZ MDPPT
ISZ HA
JMP MDPL

CLA
TAD MNUM
DCA SFR
TAD MDC4000
LSR
SFR,0
SHL
0
DCA CNUMB
TAD CNUMB
CMA
DCA MCNUMB
TAD MCOGP
DCA MCPT
IAC
TAD MDPOG
DCA MDPPT
TAD MCM2
DCA HA
TDPL,CLA
TAD I MDPPT
MQL
TAD MCM14
DCA HB
TLP,CLA CLL
SHL
0
RAR
TAD MCNUMB
AND I MCPT
SZL
TAD CNUMB
DCA I MCPT
ISZ MCPT
ISZ HB
JMP TLP
STA
TAD MDPPT
DCA MDPPT
ISZ HA
JMP TDPL
JMP I MIL

NO,0
MCM2,-2
HA,0
YLADD,YL
YPT,0
MDPOG,.+1
0
0
MDPPT,0
MCM14,-14
HB,0
```

```
MNUM,0
CNUMB,0
MCNUMB,0
MCOGP,MCOG
MCPT,0
MDC4000,4000

MCOG,0

*17

CLRPNT,0

*100

CKFLG,0
MD,0
PMD,0
MC,0
TPAC,0
0
0
STS,0
FSTS,2115
TPPNT,0
TOLS,0
TOL,0
TOHS,0
TOH,0
ROS,0
RO,0
XL,0
XH,0
OGSFTS,21
OGSFT,0
STOG,2027
AST,2000
SJO,-5
PTFLG,0
KBUFF,0
YL,0
YH,0
PH,0

ITYPP,ITYPS
ACTP,ACTS
CHECKP,CHECKS
KACCP,KACCS
PTP,PTS
DPTP,DPTS
OCACCP,OCACCS
MDACCP,MDACCS
TPACCP,TPACCS
TPNEGP,TPNEGS
TPADDP,TPADDS
TPFPP,TPFPS

*5
7400
7200
5600

*7345
ITYP
NOP
NOP
NOP

*6636
JMP EX

*6630
JMS NM

*6642
JMS SC

*62
NM,0
IOF
NMI
JMP I NM

SC,0
SCA
ION
JMP I SC

EX,ION
JMP I .+1
6655

LAB=6434
LBB=6444
SQROOT=0002
LCB=6464
SCF=6451
SOF=6442
RIB=6452
CBF=6454
ITYP=JMS I ITYPP
ACT=JMS I ACTP
CHECK=JMS I CHECKP
KACC=JMS I KACCP
TYPE=JMS I PTP
DTYPE=JMS I DPTP
OCACC=JMS I OCACCP
MDACC=JMS I MDACCP
TPACC=JMS I TPACCP
TPNEG=JMS I TPNEGP
TPADD=JMS I TPADDP
TPFP=JMS I TPFPP

$
```

```
/ERROR PATCH FOR ROR.

*600

ROR,0
CLA CLL
TAD ROS
DCA RO
TAD CB3
TAD CKFLG
DCA CKFLG
TAD AST
DCA TPPNT
TAD I TPPNT
DCA TPAC
DCA I TPPNT
ISZ TPPNT
TAD I TPPNT
DCA TPAC+1
DCA I TPPNT
ISZ TPPNT
TAD I TPPNT
DCA TPAC+2
DCA I TPPNT
ISZ TPPNT
TPNEG
TPADD
JMS TSFT
TAD TPAC+2
TAD I FBSTP
DCA I FBSTP
TAD I FBSTP
TAD RC4000
LCB
JMP I ROR

CB3,-2
FBSTP,FBST
RC4000,4000

TPNEGS,0
CLA CLL
TAD TPAC
CIA
DCA TPAC
TAD TPAC+1
CMA
SZL
IAC CLL
DCA TPAC+1
TAD TPAC+2
CMA
SZL
IAC CLL
DCA TPAC+2
JMP I TPNEGS

TPADDS,0
CLA CLL
TAD TPACST
DCA TPACP
TAD CM3
DCA LPC
ALP,TAD I TPPNT
TAD I TPACP
DCA I TPACP
DCA I TPPNT
ISZ TPPNT
ISZ TPACP
RAL
ISZ LPC
JMP ALP
CLA CLL
JMP I TPADDS

LPC,0
TPACP,0
TPACST,TPAC
CM3,-3

TSFT,0
CLA
TAD ASFT
DCA ATEMP
TAD ATEMP
SNA
JMP I TSFT
TAD CM14
SMA SZA
JMP RED
STA
TAD ATEMP
DCA ASFT1
TAD TPAC+1
MQL
TAD TPAC+2
SHL
ASFT1,0
DCA TPAC+2
JMP I TSFT
RED,DCA ATEMP
TAD TPAC
DCA ATEMP1
DCA TPAC
TAD TPAC+1
DCA ATEMP2
TAD ATEMP1
DCA TPAC+1
TAD ATEMP2
DCA TPAC+2
JMP TSFT+4

ASFT,0
ATEMP,0
ATEMP1,0
ATEMP2,0
CM14,-14
TPNEG=JMS TPNEGS
TPADD=JMS TPADDS

*356

ASFTP,ASFT

ROS=116
RO=117
CKFLG=100
AST=125
TPPNT=111
TPAC=104
FBST=2170
LCB=6464
MQL=7421
SHL=7413

$
```

```
/MAGNETIC FIELD REVERSAL PATCH. 9 OCT 69


                        DCA LP
*1004                   TAD AST
                        DCA PNT
JMS I ELCKPT            DCA I PNT
JMS I MGCKPT            ISZ PNT
CLA                     ISZ LP
JMP .+5                 JMP .-3
                        JMP I MGCK
*1103                   C4000,4000
                        CM6,-6
ELCKPT,ELCK             LP,0
MGCKPT,MGCK             MMSK2,20
                        FBMMP,FBMM
*3000                   FBSTP,FBST
                        PNT,0
ELCK,0                  CB4,-40
CLA                     TEMP,0
TAD MC
AND MMSK1               MC=103
SNA                     CKFLG=100
JMP I ELCK              FBST=2170
CLA                     FBMM=2171
TAD CB2                 AST=125
TAD CKFLG               LCB=6464
DCA CKFLG
JMP I ELCK              $
CB2,-20
MMSK1,50

MGCK,0
CLA
TAD MC
AND MMSK2
SNA
JMP I MGCK
CLA
TAD CB4
TAD CKFLG
DCA CKFLG
TAD I FBSTP
DCA TEMP
TAD I FBMMP
DCA I FBSTP
TAD TEMP
DCA I FBMMP
TAD I FBSTP
TAD C4000
LCB
CLA
TAD CM6
```

Bibliography

Akhiezer A.I. and Berestetskii V.B. (1965) "Quantum Electrodynamics" Interscience.

Angel J.R.P. (1967) Thesis, Oxford University.

Angel J.R.P. and Sandars P.G.H. (1968) Proc.Roy.Soc. A305 , 125.

Barut A.O. (1967) "The Theory of the Scattering Matrix" McMillan.

Bég M.A.B. (1969) Ann.Phys. 52, 577.

Bernstein J., Feinberg G., Lee T.D. (1965) Phys.Rev. 139, B1650.

Bleaney B.I. and Bleaney B. (1957) "Electricity and Magnetism" O.U.P.

Bloch F. (1946) Phys.Rev. 70, 460.

Block F., Hansen W.W. and Packard M. (1946) Phys.Rev. 70, 474.

Brink D.M. and Satchler G.R. (1969) "Angular Momentum" (2nd ed.) O.U.P.

Brooker G.A. (1969) Private communication.

Carrico J.P., Lipworth E., Sandars P.G.H., Stein T.S. and Weisskopf M.C. (1968) Phys.Rev. 174, 125.

Casella R.C. (1968) Phys.Rev.Lett. 21, 1128.

Casella R.C. (1969) Phys.Rev.Lett. 22, 554.

Christenson J.H., Cronin J.W., Fitch V.L. and Turlay R. (1964) Phys.Rev.Lett. 13, 138.

Cooley J.W. and Tukey J.W. (1965) Math. Computation 19, 296.

Dalgarno A. and Kingston A.E. (1958) Proc.Phys.Soc. 72, 1053.

Daniels J.M. (1964) Can.J.Phys. 42, 1687.

Davydov A.S. (1965) "Quantum Mechanics" Pergamon Press.

Drake G.W.F. (1970) Phys.Rev.Lett. 24, 765.

Foldy L.L. (1952) Phys.Rev. 87, 688.

Foley H.M. (1969) Private communication to P.G.H. Sandars.

Fox L. (1964) "Numerical Linear Algebra" O.U.P.

Fraser L.J. (1968) Thesis, Yale University.

Hagstrum H.D. (1956) Phys.Rev. 104, 317.

Harrison G.E. (1969) Thesis, Oxford University.

Hasted J.B. (1964) "Physics of Atomic Collisions" Butterworths.

Heil H. (1944) Z.Phys. 120, 212.

Hiida K. (1965) Prog.Theor.Phys. 33, 264.

Hoel P.G. (1954) "Introduction to Mathematical Statistics" J. Wiley and Sons.

Hughes V.W. and Schultz H.L. (1967) "Atomic Sources and Detectors" Academic Press.

Ignatovich V.K. (1968) Dubna preprint P4-4142 (to be published)

Jackson J.D. (1962) "Classical Electrodynamics" J. Wiley and Sons.

Judd B.R. (1963) "Operator Techniques in Atomic Spectroscopy" McGraw-Hill.

Kabir P.K. (1968) "The CP Puzzle" Academic Press.

Kaminsky M. (1965) "Atomic and Ionic Impact Phenomena on Metal Surfaces" Academic Press.

Lee T.D. and Yang C.N. (1957) Brookhaven report BNL 443 (T91).

Lurio A. (1969) Private communication.

MacDonald D.K.C. (1949) Phil.Mag. 40, 561.

MacDonald D.K.C. (1962) "Noise and Fluctuations" J. Wiley and Sons.

"Modern Computing Methods"(1961) H.M.S.O.

Moore C.E. (1949) "Atomic Energy Levels" NBS Washington.

Okun' L.B. (1967) Sov.Phys.Uspekhi 9, 574.

Parzen E. (1960) "Modern Probability Theory and its Applications" J. Wiley and Sons.

Phillips E.G. "Functions of a Complex Variable" Oliver and Boyd (1940).

Pichanick F.M.J., Swift R.D., Johnson C.E., and Hughes V.W. (1968) Phys.Rev. 169, 55.

Player M.A. and Sandars P.G.H. (1966) Clarendon Lab. report (unpublished).

Player M.A. and Sandars P.G.H. (1969) Phys.Lett. 30A , 475.

Ramsey A.T. and Petrasso R. (1969) Phys.Rev. Lett. 23, 1478.

Ramsey N.F. (1956) "Molecular Beams" O.U.P.

Ramsey N.F. (1959) in "Recent Research in Molecular Beams" ed. I. Estermann, Academic Press.

Robinson E.J., Levine J. and Bederson B. (1966) Phys.Rev. 146, 95.

Robinson F.N.H. (1962) "Noise in Electrical Circuits" O.U.P.

Rothman J. (1968) "Decus" program library no. 8-144 Digital Equipment Corp.

Sakurai J.J. (1964) "Invariance Principles and Elementary Particles" Princeton University Press.

Salpeter E.E. (1958) Phys.Rev. 112, 1642.

Salwen H. (1955) Phys.Rev. 99, 1274.

Salzman F. and Salzman G. (1965) Phys.Lett. 15, 91.

Salzman F. and Salzman G. (1966) Nuov.Cim. 41A , 711.

Sandars P.G.H. (1965) Phys.Lett. 14, 194.

Sandars P.G.H. (1966a) Phys.Lett. 22, 290.

Sandars P.G.H. (1966b) Clarendon Laboratory report (unpublished).

Sandars P.G.H. (1968) J.Phys. B 1, 499.

Sandars P.G.H. and Lipworth E. (1964) Phys.Rev.Lett. 13, 718.

Schiff B. and Pekeris C.L. (1968) Phys.Rev. 134, A638.

Schiff L.I. (1955) "Quantum Mechanics" McGraw-Hill.

Schiff L.I. (1963) Phys.Rev. 132, 2194.

Schweber S.S. (1961) "An Introduction to Relativistic Quantum Field Theory" Row, Peterson and Co.

Shapiro F.L. (1968) Sov.Phys. Uspekhi 11, 345.

Sternheimer R.M. (1951) Phys.Rev. 84, 244.

Sternheimer R.M. (1969) to be published.

Streater R.F. and Wightman A.S. (1964) "PCT, Spin and Statistics and All That" Benjamin.

Tinker M.H. (1967) Thesis, Oxford University.

Varney R.N. (1968) Phys.Rev. 175, 98.

Warrington D.M. (1968) Thesis, Oxford University .

Wu C.S., Ambler E., Hayward R.W., Hoppes D.D. and Hudson R.P. (1957) Phys.Rev. 105, 1413.

Weisskopf M.C., Carrico J.P., Gould H., Lipworth E., and Stein T.S. (1968) Phys.Rev.Lett. 21, 1645.

Wiese W.L., Smith M.W. and Glennon B.M. (1966) "Atomic Transition Probabilities" NBS, Washington.